Sofia Pereira das Neves

Exploring the role of astrocytes in the pathophysiology of multiple sclerosis

UMinho | 2020

Universidade do Minho
Escola de Medicina

Sofia Pereira das Neves

Exploring the role of astrocytes in the pathophysiology of multiple sclerosis

junho de 2020

Universidade do Minho
Escola de Medicina

Sofia Pereira das Neves

Exploring the role of astrocytes in the pathophysiology of multiple sclerosis

Tese de Doutoramento
Doutoramento em Envelhecimento e Doenças Crónicas

Trabalho efetuado sob a orientação da
Doutora Fernanda Marques
e da
Doutora Rita Teodoro

junho de 2020

DIREITOS DE AUTOR E CONDIÇÕES DE UTILIZAÇÃO DO TRABALHO POR TERCEIROS

Este é um trabalho académico que pode ser utilizado por terceiros desde que respeitadas as regras e boas práticas internacionalmente aceites, no que concerne aos direitos de autor e direitos conexos.

Assim, o presente trabalho pode ser utilizado nos termos previstos na licença abaixo indicada.

Caso o utilizador necessite de permissão para poder fazer um uso do trabalho em condições não previstas no licenciamento indicado, deverá contactar o autor, através do RepositóriUM da Universidade do Minho.

Licença concedida aos utilizadores deste trabalho

Atribuição-NãoComercial-SemDerivações

CC BY-NC-ND

https://creativecommons.org/licenses/by-nc-nd/4.0/

Agradecimentos

"Look up... and climb the steps for what you want to achieve" (Charlie Chaplin)

Começo por agradecer a orientação, o apoio e ajuda que a minha orientadora Fernanda me deu durante a realização deste trabalho. Agradeço também o apoio da minha orientadora Rita.

De seguida, este trabalho não poderia ter sido realizado sem o apoio incondicional das pessoas mais importantes na minha vida – Ricardo, Carla, mãe e pai.

Agradeço também toda a ajuda laboratorial do Joe DeYoung, Fuying Gao, Giovanni Coppola, Ana Falcão, Cláudia Nóbrega, Carlos Bessa, João Cerqueira, Liliana Santos, Goreti Pinto, Eduarda Correia, Cláudia Pereira, Joana Palha, Nuno Sousa, Margarida Correia-Neves, João Sousa, Cláudia Miranda, Patrício Costa, João Oliveira, Gisela Santos, Catarina Barros, Diana Pereira, Ricardo Ferreira, Cristina Mota, Susana Monteiro, Adelaide Fernandes, toda a equipa do biotério.

Aos meus (ex-)companheiros de bancada: Sandro, Vítor, Inês, Marta, Joana, e em especial, Catarina, aprendi muito convosco, o vosso apoio foi muito importante e vou guardar-vos sempre no meu coração.

Aos meus companheiros e amigos para a vida Margarida, Madalena e Eduardo.

À Sónia Gomes, que para além de colega de bancada, foi uma parceira de grandes aventuras. Aos grandes amigos que levo do ICVS: Teresa, Dinis, Bárbara, Sónia Borges, Fátima, Liliana Amorim, Gabriela, Francisca, Belina.

Aos colegas do PhDOC, e seus orientadores, pelas discussões científicas em todos os retiros. Em especial à Raquel, à Rita e ao Marco pelo companheirismo durante estes anos.

A todos os NeRDs em geral pela ajuda e discussão científica, e em especial à Sara Silva pelo sorriso constante e disponibilidade para com os outros.

This work was supported by Foundation for Science and Technology (FCT) and COMPETE through the project EXPL/NEU-OSD/2196/2013 and by The Clinical Academic Center (2CA-Braga) through the project EXPL/001/2016. The work at ICVS/3B's has been developed under the scope of the project NORTE-01-0145-FEDER-000013, supported by the Northern Portugal Regional Operational Programme (NORTE 2020), under the Portugal 2020 Partnership Agreement, through the European Regional Development Fund (FEDER), and funded by FEDER funds through the Competitiveness Factors Operational Programme (COMPETE), and by National funds, through the Foundation for Science and Technology (FCT), under the scope of the project POCI-01-0145-FEDER-007038. FM is an assistant researcher and recipient of an FCT Investigator grant with the reference CEECIND/01084/2017. SN is a recipient of a Ph.D. fellowship with the reference PD/BD/114120/2015 from MCTES national funds.

STATEMENT OF INTEGRITY

I hereby declare having conducted this academic work with integrity. I confirm that I have not used plagiarism or any form of undue use of information or falsification of results along the process leading to its elaboration.

I further declare that I have fully acknowledged the Code of Ethical Conduct of the University of Minho.

Exploring the role of astrocytes in the pathophysiology of multiple sclerosis

Abstract

The presence of reactive astrocytes in multiple sclerosis (MS), a chronic inflammatory disease of the central nervous system, has been described for a long time, however its contribution for disease pathophysiology is still not fully understood. Therefore, in this work we proposed to further explore the contribution of astrocytes in MS using different experimental approaches. We started by performing a temporal transcriptomic analysis of astrocytes in the chronic experimental autoimmune encephalomyelitis (EAE) MS animal model. For that we isolated astrocytes from the cerebellum in 3 disease time points: before the symptom's appearance (pre-symptomatic phase), at the onset/peak of the disease and at the chronic phase of EAE. Particularly at the onset phase of disease, astrocytes overexpressed genes associated with a neurotoxic phenotype (known as A1 phenotype), along with the overexpression of genes involved in metabolic pathways, like glycolysis and tricarboxylic acid cycle. This suggested that astrocytes could be undergoing metabolic reprogramming, similarly to what happens in macrophages/microglia in response to different inflammatory stimuli. On the second part of this work, we induced EAE in a model that presents "silent" astrocytes, i.e. astrocytes that present minimal calcium elevations in the soma and main processes, due to the ablation of the inositol 1,4,5-triphosphate receptor type 2 (IP_3R2-null). IP_3R2-null mice and wild-type littermates presented similar disease clinical scores, however IP_3R2-null mice had decreased lesion burden in the cerebellum white matter, which could be associated with the increased astrocyte reactivity observed in these mice near the lesions, compared to the normal appearing white matter. Next, we studied the effects of a neuroprotective drug, dimethyl fumarate (DMF), on astrocyte activation and on the cognitive function in the EAE model. DMF treatment, started at the symptomatic phase of disease, was able to reduce astrocyte reactivity, evaluated by a decrease in the number of cells, and demyelination in the fimbria, which is the most important white matter pathway in the hippocampus, possibly contributing to the prevention of cognitive deficits observed in DMF-treated EAE animals. Finally, we focused our attention on a protein produced by astrocytes during EAE, lipocalin-2 (LCN2), an acute phase protein that was previously suggested as a possible disease biomarker. After the quantification of LCN2 concentration in cerebrospinal fluid samples from MS patients, we observed that increased LCN2 levels were associated with faster disease progression. However, this association was no longer statistically significant after controlling for the patients' age and the presence of oligoclonal bands.

Keywords: astrocytes; dimethyl fumarate; lipocalin-2; metabolic reprogramming; multiple sclerosis.

Investigação do papel dos astrócitos na patofisiologia da esclerose múltipla

Resumo

A presença de astrócitos reativos na esclerose múltipla (EM), uma doença inflamatória crónica do sistema nervoso central, já é conhecida há muito tempo, porém a sua contribuição para a patofisiologia da doença não está totalmente esclarecida. Assim, neste trabalho propomos explorar a contribuição dos astrócitos na EM usando diferentes abordagens experimentais. Começámos por fazer uma análise temporal do transcriptoma dos astrócitos no modelo animal crónico de EM de encefalomielite autoimune experimental (EAE). Para isso, isolámos astrócitos do cerebelo em 3 momentos experimentais: antes do aparecimento de sintomas (fase pré-sintomática), no pico da doença e na fase crónica. Em particular no pico da doença, os astrócitos sobre-expressaram genes associados a um fenótipo neurotóxico (conhecido como fenótipo A1), e genes envolvidos em diferentes vias metabólicas, tais como a glicólise e o ciclo dos ácidos tricarboxílicos. Estas alterações sugeriram que os astrócitos poderiam estar a passar por um processo de reprogramação metabólica, semelhante ao que acontece com macrófagos/microglia em resposta a diferentes estímulos inflamatórios. Na segunda parte deste trabalho, induzimos EAE num modelo de astrócitos "silenciados", i.e. astrócitos que apresentam elevações de cálcio mínimas no soma e processos principais, devido à deleção do recetor tipo 2 do inositol 1,4,5-trifosfato (IP_3R2-null). Os animais IP_3R2-null e do tipo selvagem das mesmas ninhadas desenvolveram a doença de modo semelhante, no entanto os animais IP_3R2-null apresentaram uma diminuição da carga de lesão na substância branca do cerebelo, que poderá estar associada ao aumento da reatividade dos astrócitos observada perto destas regiões de lesão, comparativamente à substância branca aparentemente normal. De seguida, estudámos os efeitos de um fármaco neuroprotetor, o dimetil fumarato (DMF), na ativação dos astrócitos e na função cognitiva no modelo de EAE. O tratamento com DMF, iniciado na fase sintomática da doença, reduziu a reatividade dos astrócitos, avaliada através de uma diminuição do seu número, e a desmielinização na fimbria, que é o feixe de substância branca mais importante no hipocampo, o que poderá ter contribuído para a prevenção de défices cognitivos nos animais EAE tratados com DMF. Por último, focámos a nossa atenção numa proteína produzida pelos astrócitos em resposta à EAE, a lipocalina-2 (LCN2), uma proteína de fase aguda que foi anteriormente sugerida como um possível marcador de doença. Após a quantificação dos níveis de LCN2 no líquido cefalorraquidiano de doentes com EM, observámos que níveis elevados de LCN2 estavam associados a uma progressão mais rápida da doença. Porém, esta associação perdeu a significância estatística após controlar para a idade dos doentes e para a presença de bandas oligoclonais.

Palavras-chave: astrócitos; dimetil fumarato; esclerose múltipla; lipocalina-2; reprogramação metabólica.

Table of contents

Abbreviations list

#

17-AAG - 17-allylamino-17-demehtoxygeldanamycin

24p3R - 24p3 cell receptor

3D - Three-dimensional

4-AP - 4-aminopyridine

A

ACM - Astrocyte-conditioned medium

ACSA-2 - Astrocyte cell surface antigen 2

Act1 - Actin related gene 1

AKT - Protein kinase B

Aldh1l1 - Aldehyde dehydrogenase 1 family member L1

Aldoc - Fructose-biphosphate aldolase C

ALS - Amyotrophic lateral sclerosis

Amigo2 - Adhesion molecule with Ig like domain 2

APCs - Antigen-presenting cells

AQP4 - Aquaporin 4

Atp - Adenosine triphosphate

Atp1b2 - ATPase Na+/K+ Transporting Subunit Beta 2

Atp5b - Adenosine Triphosphate subunit 5 beta

B

B4galt6 - Beta-1,4-galactosyltransferase 6

BBB - Blood-brain barrier

BDNF - Brain-derived neurotrophic factor

BM-hMSC - Bone marrow derived human mesenchymal stem cell

C

C - Chronic phase

C1q - Complement component 1q

C3 - Complement component 3

C5a - Complement component 5a

CA - Cornu amonis

Ca^{2+} - Calcium

cAMP - Cyclic adenosine monophosphate

CCL - Chemokine C-C motif ligand

CCR - Chemokine (C-C motif) receptor

CD - Cluster of differentiation

Cers - Ceramide synthase

CFA - Complete Freund's adjuvant

cGMP-PKG - Cyclic guanosine monophosphate dependent protein kinase G

CHI3L1 - Chitinase-3-like-1

CI - Confidence interval

CIS - Clinically isolated syndrome

CNS - Central nervous system

CP - Choroid plexus

CPM - Counts per million

CREB - cAMP-response element binding protein

CSF - Cerebrospinal fluid

CSPGs - Chondroitin sulfate proteoglycans

CTL - Cytotoxic T cell

Cx - Connexin

CXCL - Chemokine C-X-C motif ligand

CYM-5442 - 2-(4-(5-(3,4-diethoxyphenyl)-1,2,4-oxadiazol-3-yl)-2,3-dihydro-1H-inden-1-yl amino) ethanol

D

DAPI - 4′,6-diamidino-2-phenylindole

DARPP32 - Dopamine- and cAMP-regulated neuronal phosphoprotein

DCX - Doublecortin

DG - Dentate gyrus

DMF - Dimethyl fumarate

E

EAE - Experimental autoimmune encephalomyelitis or Encefalomielite autoimune experimental

EBV - Epstein-Barr virus

ECM - Extracellular matrix

EDSS - Expanded disability status scale

EM - Esclerose múltipla

EP - Ethyl pyruvate

ER - Endoplasmic reticulum

ERK - Extracellular-signal-regulated kinase

ET-1 - Endothelin-1

F

FasL - Fas ligand

Fbln5 - Fibulin 5

FGF-2 - Basic fibroblast growth factor

Fkbp5 - FK506 binding protein 5

FKPM - Fragments per kilobase of exon per million fragments mapped

G

GA - Glatiramer acetate

GABA - Gamma-aminobutyric acid

Gd - Gadolinium

GDP - Guanosine dih«phosphate

GFAP - Glial acidic fibrillary protein

GL - Granular layer

GLAST - Glutamate/aspartate transporter

GLT-1 - Glutamate transporter solute carrier family 1 member 2

GLUL - Glutamate synthetase

GM - Gray matter

GM-CSF - Granulocyte-macrophage colony-stimulating factor

GPCR - G protein-coupled receptor

gp-MBP - Guinea pig myelin basic protein

H

h - hours

HBEGF - Heparin-binding EGF-like growth factor

HGF - Hepatocyte growth factor

HLA - Human leukocyte antigen

HR - Hazard ratio

Hspcb - Heat Shock Protein 90 alpha family class B member 1

min - Minutes

ML - Molecular layer

MMF - Monomethyl fumarate

I

Iba1 - Ionized calcium-binding adaptor molecule 1

ICAM-1 - Intercellular adhesion molecule 1

ICOL - Inducible costimulator ligand

ICOS - Inducible costimulator

Idh3g - Isocitrate dehydrogenase 3 (NAD+) gamma

IFNβ - Interferon beta

IFNγ - Interferon gamma

Ig - Immunoglobulin

IkB - Inhibitory proteins of kB family

IL - Interleukin

iNOS - Inducible nitric oxide synthase

IP_3 - Inositol 1,4,5-triphosphate

IP_3R - Inositol 1,4,5-triphosphate receptor

IP_3R2 - Inositol 1,4,5-triphosphate receptor type 2 or Recetor tipo 2 do inositol 1,4,5-trifosfato

IQR - Interquartile range

K

K^+ - Potassium

L

L - Lesion

LCN2 - Lipocalin-2

LDH - Lactate dehydrogenase

LFA-1 - Leukocyte function-associated antigen-1

LFB - Luxol fast blue

LP - Lumbar puncture

LPC - Lysolecithin

LPS - Lipopolysaccharide

LXR - Liver X receptor

M

MACS - Magnetic-activated cell sorting

MAPK - Mitogen activated protein kinase

MBP - Myelin basic protein

MCT - Monocarboxylate transporter

MHC - Major histocompatibility complex

MOG - Myelin oligodendrocyte glycoprotein

MRI - Magnetic resonance imaging

MS - Multiple sclerosis

MSCs - Mesenchymal stem cells

MWM - Morris water maze

N

NAWM - Normal appearing white matter

NF-L - Neurofilament light chain

NF-κB - Nuclear factor kappa B

NMO - Neuromyelitis optica

NO - Nitric oxide

Nrf2 - Nuclear factor erythroid 2-related factor 2

O

O - Onset phase

OCBs - Oligoclonal bands

OPCs - Oligodendrocyte precursor cells

P

P - Pre-symptomatic phase

p.i. - Post-immunization

PBS - Phosphate buffered saline

PFA - Paraformaldehyde

Pfkm - Phosphofructokinase muscle

Pi3K - Phosphoinositide 3-kinase

PLC - Phospholipase C

PLP - Proteolipid protein

PML - Progressive multifocal leukoencephalopathy

PPMS - Primary progressive multiple sclerosis

PTX - Pertussis toxin

R

RANK - Receptor activator of NF-κB

RANKL - RANK ligand

RNAseq - RNA-sequencing

RNS - Reactive nitrogen species

ROS - Reactive oxygen species

RRMS - Relapsing-remitting multiple sclerosis

RT - Room temperature

RXR - Retinoid X receptor

S

s - seconds

S100β - S100 calcium-binding protein B

S1P - Sphingosine-1-phosphate

SD - Standard deviation

Sdha - Succinate dehydrogenase complex subunit A flavoprotein

SEM - Standard error of the mean

SGZ - Sub-granular zone

SPMS - Secondary progressive multiple sclerosis

STAT - Signal transducer and activator of transcription

SUR1 - Sulfonylurea receptor 1

T

Tbp - TATA binding protein

TCA - Tricarboxylic acid

TCR - T cell receptor

Th - T helper

TIMP - Tissue inhibitor of metalloproteinase

TMEV - Theiler's encephalomyelitis virus

TNFα - Tumor necrosis factor alpha

Treg - Regulatory T cells

TREM - Triggering receptor expressed on myeloid cells

V

VCAM-1 - Vascular cell adhesion molecule-1

VEGF - Vascular endothelial growth factor

VLA-4 - Very late antigen-4

W

WM - White matter

Wt - Wild-type

Figures list

Chapter 1

Chapter 2

Chapter 3

Chapter 4

Chapter 5

Tables list

Chapter 1

Chapter 2

Chapter 4

Chapter 5

Annex 1

Thesis layout

CHAPTER 1 comprises a general introduction that covers general aspects of multiple sclerosis (MS). An overview of the main functions of astrocytes both in physiological and pathological conditions is also performed.

CHAPTER 2 includes the transcriptomic and morphological study performed in astrocytes from EAE animals, at different disease time points. In this work, we observed that astrocytes overexpressed genes associated with a neurotoxic phenotype (A1 phenotype) and also genes involved in metabolic pathways, including glycolysis and tricarboxylic acid (TCA) cycle, particularly in the onset/peak phase of disease. Also, astrocytes near lesion regions, in EAE animals, presented increased length and complexity, compared to astrocytes from the white matter of non-induced animals.

CHAPTER 3 presents the results obtained after EAE induction in a model of impaired global astrocytic calcium signaling, the type 2 inositol 1,4,5-triphosphate receptor (IP_3R2)-null mice. Even tough no differences were found between genotypes regarding clinical score, the IP_3R2-null animals presented a decreased lesion burden in the cerebellum white matter, at the onset phase of disease. Moreover, cerebellum' astrocytes from IP_3R2-null mice, but not wild-type animals, presented increased length and complexity near lesion sites compared to the normal appearing white matter, which could be associated with an increased ability to limit immune cell spreading in the IP_3R2-null mice.

CHAPTER 4 comprises the results obtained after the symptomatic treatment of EAE animals with dimethyl fumarate (DMF). DMF treatment was able to reduce astrocytic activation in the fimbria of the animals and revert the cognitive deficits observed in vehicle-treated animals, which was accompanied by a decrease in demyelination.

Lipocalin-2 (LCN2) is highly expressed by astrocytes in both MS and EAE and it was suggested as a possible disease biomarker. In **CHAPTER 5** we performed a follow-up study to explore the prognostic value of LCN2 in MS patients, and found that higher cerebrospinal levels of this protein were associated with a faster disease progression. However, this association was no longer significant after controlling for the age of the patients and presence of oligoclonal bands. Nevertheless, and considering the confidence intervals, we suggest that LCN2 could be useful for disease prognosis if used in a wider biomarker panel.

CHAPTER 6 presents a general discussion of the results and future experiments that would help to further explore the findings obtained in this work.

CHAPTER 1

General introduction

1. Multiple sclerosis

Multiple sclerosis (MS) clinical and pathological characteristics were first described more than 100 years ago by Charcot, Carswell, Cruveilhier and others (Lucchinetti et al., 2005; Noseworthy et al., 2000). Nowadays, it is defined as a chronic immune-mediated disorder of the central nervous system (CNS), that occurs in genetically susceptible people, associated with an environmental stimulus, however its etiopathology remains largely unknown (Compston and Coles, 2008; Nicholas and Rashid, 2013; Noseworthy et al., 2000; Nylander and Hafler, 2012).

Approximately 80-85% of MS patients initially present with a relapsing-remitting (RR) disease course, characterized by the appearance of clinical symptoms followed by a recovery period, spontaneous or in response to treatment. After a variable period of time irreversible damage accumulates and patients begin to experience a steady state of deterioration in neurologic functions, independently of any acute attack. This stage of disease is termed secondary progressive MS (SPMS) (Faissner et al., 2019; Goodin, 2014; Lassmann, 2014; Noseworthy et al., 2000; Nylander and Hafler, 2012). The remaining 15-20% of MS patients develop a progressive clinical course from the beginning of disease [primary progressive MS (PPMS)], experiencing neurologic decline without ever presenting acute clinical attacks (Faissner et al., 2019; Goodin, 2014; Noseworthy et al., 2000; Nylander and Hafler, 2012).

MS is the most common cause of neurologic disability in young adults (Duffy et al., 2014; Nicholas and Rashid, 2013; Stys et al., 2012), with the appearance of symptoms occurring between 15 and 45 years of age, in the majority of cases (Goodin, 2014; Nicholas and Rashid, 2013). RRMS presents a female:male ratio of approximately 2:1, while PPMS presents similar incidence among men and women (Correale et al., 2017; Goodin, 2014; Noseworthy et al., 2000). The world prevalence of MS varies considerably, however there is a strong correlation between prevalence and distance from the equator (Figure 1. 1), which is believed to be associated with sunlight exposure and vitamin D levels (Azary et al., 2018; Kearns et al., 2018; Reich et al., 2018). In the district of Braga in Portugal, the incidence of MS was reported to be 2.74/100.000 inhabitants and the prevalence 39.82/100.000 inhabitants (Figure 1. 1) (Figueiredo et al., 2015).

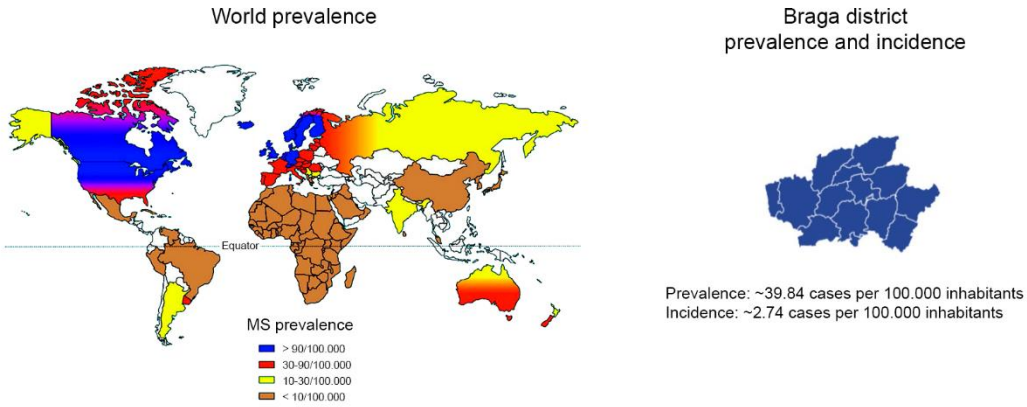

Figure 1. 1 – Epidemiology of multiple sclerosis.

Estimated MS prevalence worldwide and in the district of Braga. Data obtained or adapted from (Figueiredo et al., 2015; Goodin, 2014).

1.1. Pathophysiology of MS

There are two main hypothesis that try to explain the pathophysiology of MS. On one hand, MS is believed to be caused by the activation of peripheral autoreactive T cells that migrate into the CNS and initiate the disease process ("outside-in" hypothesis) (Baecher-Allan et al., 2018). On the other hand, the "inside-out" hypothesis proposes that MS occurs within the CNS, as a primary neurodegenerative disorder. Namely, cytodegeneration, possibly focused on the oligodendrocyte-myelin complex, can be the initial event, leading to the release of highly antigenic constituents and, consequently, to an inflammatory and autoimmune response, in a predisposed host (Duffy et al., 2014; Stys et al., 2012). In this case, what distinguishes MS from other progressive neurodegenerative disorders is the propensity of the hosts' immune cells to react against the highly autoantigenic components, released after cytodegeneration (Stys et al., 2012).

In contrast, the "outside-in" hypothesis suggests that mechanisms of molecular mimicry, meaning cross-reactivity between self and non-self antigens, are responsible for the development of the autoimmune response in MS patients (Nylander and Hafler, 2012; Rojas et al., 2018). Of interest, potential cross-reactivity between myelin epitopes with microbial antigens has been demonstrated (Wucherpfennig et al., 1997). Nevertheless, the antigen specificity of the immune response in MS is unresolved (Compston and Coles, 2008), but the general consensus is that several pathological antigens are involved in the disease (Nylander and Hafler, 2012). The search for candidate autoantigens has concentrated on myelin components, since demyelination is a hallmark of MS lesions. In fact, myelin-specific antibodies and reactive cells have been found in MS patients (Berger et al., 2003; Cruz et al., 1987; Navikas et al., 1995;

O'Connor et al., 2005). However, a recent study has identified a possible non-myelin target antigen, the guanosine diphosphate (GDP)-L-fucose synthase (Planas et al., 2018). Interestingly, human and bacterial GDP-L-fucose synthase peptides present high similarity. Moreover, a significant association was found between the recognition of GDP-L-fucose synthase peptides and myelin basic protein (MBP) peptides, however it remains unclear if there is cross-recognition between these two peptides, whether the recognition of one of the peptides facilitates the exposure of the other one and the *de novo* activation of autoreactive T cells against this last one, or if the two responses occur simultaneously (Planas et al., 2018). Likewise, post-translational modifications, such as citrullination (namely MBP citrullination), glycosylation and glycation, have been suggested to have an impact on the generation of autoimmune antigens (Opdenakker et al., 2016; Stys et al., 2012).

The MS pathological process includes increased BBB permeability, multifocal inflammation, demyelination, oligodendrocyte death, reactive gliosis, axonal degeneration and neuronal death (Baecher-Allan et al., 2018). Of relevance, immune cell migration to the CNS can occur through the brain barriers. There are two main barriers that protect the brain: the well-known blood-brain barrier (BBB), which is formed by the presence of tight junctions between the brain endothelial cells and by the astrocytic end-feet, and the blood-cerebrospinal fluid (CSF) barrier which is composed by the choroid plexus (CP) epithelial cells. The CP is the brain structure responsible for CSF production, and the presence of tight junctions between CP epithelial cells form the blood-CSF barrier. This barrier prevents leukocyte entry into the CSF, even tough they can easily pass the fenestrated blood vessels of the CP parenchyma (Lopes Pinheiro et al., 2016). However, in MS, this barrier was found to be compromised by the specific loss of epithelial tight junction proteins, like claudin-3 (Kooij et al., 2014). Moreover, CP epithelial cells may express high levels of adhesion molecules and chemokines. After crossing this barrier, leukocytes now have access to the CSF, where they interact with resident dendritic cells (epiplexus cells), triggering the release of large amounts of inflammatory mediators, like pro-inflammatory cytokines. These mediators are believed to induce the expression of adhesion molecules and chemokines in brain endothelial cells. In turn, this will induce a massive entry of immune cells into the brain parenchyma through the BBB (Figure 1. 2) (Lopes Pinheiro et al., 2016).

The migration process across the endothelial cells of the BBB is better understood than the one across CP epithelial cells. The first point of contact occurs between lymphocyte selectin ligands (e.g. P selectin glycoprotein ligand-1) and endothelial cell selectins (e.g. E- and P-selectin). These interactions allow the tethering and rolling of lymphocytes along the vascular wall, where they will encounter chemokines, upregulated by endothelial cells during neuroinflammation. The binding to these chemokines deliver a

signal to very late antigen-4 (VLA-4) and leukocyte function-associated antigen-1 (LFA-1) integrins, on the lymphocyte surface, that induces their conformational change and clustering, increasing their affinity for the endothelial ligands intercellular adhesion molecule 1 (ICAM-1) and vascular cell adhesion molecule-1 (VCAM-1) (Lopes Pinheiro et al., 2016). During the inflammatory response, tumor necrosis factor alpha (TNFα) and interferon gamma (IFNγ) promote VCAM-1 expression by endothelial cells (Steinman, 2001). Interestingly, reactive astrocytes can also express VCAM-1 (Gimenez et al., 2004; Lee and Benveniste, 1999; Ponath et al., 2018), and this expression is important for lymphocytes to effectively enter the CNS parenchyma (Gimenez et al., 2004). Lymphocytes are then arrested on the vessel wall, and may begin to polarize and crawl, migrating to the brain parenchyma by diapedesis. Lymphocyte diapedesis can occur in two different ways: migration across adjacent endothelial cells (paracellular route) or migration through a single endothelial cell (transcellular route), in which case a channel or pore has to be formed (Lopes Pinheiro et al., 2016).

After leukocytes have extravasated, they do not enter directly in the CNS parenchyma, but are first trapped in perivascular spaces formed by the parenchyma basement membrane, that surrounds blood vessels, and by retracted astrocytic end-feet. Passage beyond this barrier into the parenchyma requires active recruitment and degradation of extracellular matrix (ECM) proteins (Sofroniew, 2015; Steinman, 2001). Both astrocytes and immune cells are sources of matrix metalloproteinases (MMPs; family of enzymes involved in the degradation of the ECM), which are important for this migration (Gerwien et al., 2016; Miljkovic et al., 2011; Song et al., 2015).

Once inside the CNS, myelin-specific T cells are reactivated through an interaction with antigen-presenting cells (APCs), in the presence of the antigen and adequate co-stimulation (Chastain et al., 2011; Lucchinetti et al., 2005; Noseworthy et al., 2000). Microglial cells, infiltrating macrophages, B cells and astrocytes may function as APCs (Lucchinetti et al., 2005). Then, T cell start producing cytokines that induce the activation of macrophages, microglia and astrocytes, that then produce nitric oxide (NO), osteopontin, oxygen free radicals, among others (Ortiz et al., 2014; Steinman, 2001). B cells will start producing not only antibodies against proteins and lipids of the myelin sheath, but also pro-inflammatory and regulatory cytokines (Kasper and Shoemaker, 2010; Steinman, 2001). The combined effect of antibodies, complement, NO and pro-inflammatory cytokines induces myelin phagocytosis by macrophages, leading to demyelination and axonal and neuronal damage (Figure 1. 2) (Ortiz et al., 2014; Steinman, 2001). Importantly, B cells can also play a protective role in the CNS, via downregulation of inflammation and opsonization of myelin debris, facilitating their clearance by phagocytosis (Duffy et al., 2014).

Even tough MS is viewed as a T cell-mediated disease, it has become increasingly clear that several other innate and adaptive immune cells, as well as glial cells, like microglia and astrocytes, are also relevant in the disease context (Duffy et al., 2014). Microglial activation occurs not only in lesions, but also in the normal appearing white matter (NAWM) and gray matter. Moreover, these cells are able to produce reactive oxygen and nitrogen species (ROS and RNS, respectively), that induce direct neuronal damage, via mitochondrial dysfunction. However, microglia is also involved in debris phagocytosis and clearance, and can also produce growth factors (Correale et al., 2017; Reich et al., 2018). Astrocytes proliferate and become activated within demyelinating lesions, suggesting these CNS cells can also play critical roles in oligodendrocyte injury and axonal degeneration (Correale et al., 2017). The main physiological and pathological roles of astrocytes will be further discussed in a following section.

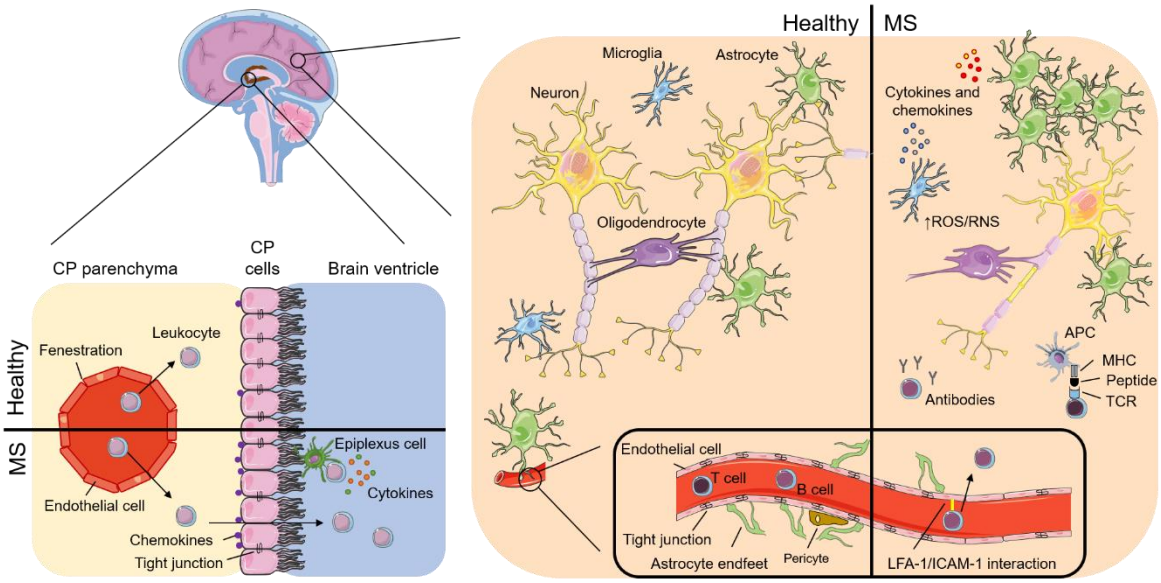

Figure 1. 2 – Immune cell entry to the CNS during MS.

Immune cells enter the CNS of MS patients after the blood-CSF and blood-brain barriers have been compromised. Images obtained and adapted from Servier Medical Art and (Lopes Pinheiro et al., 2016). CNS – central nervous system; CP – choroid plexus; ICAM-1 – intercellular adhesion molecule 1; LFA-1 – lymphocyte function-associated antigen 1; MHC – major histocompatibility complex; RNS – reactive nitrogen species; ROS – reactive oxygen species; TCR – T cell receptor.

1.2. Genetic and environmental susceptibility factors

As mentioned before, MS can arise in environmentally and genetically susceptible individuals. Regarding the genetic susceptibility, human leukocyte antigen (HLA) genes exert the largest contribution for MS susceptibility, however it is not fully clear how it affects the risk of developing MS (Alcina et al., 2012).

The HLA system is a cluster of gene complex, encoding the major histocompatibility complex (MHC) proteins in humans, which are involved in antigen presentation. Disease associated MHC alleles may confer susceptibility by interfering with the T cell repertoire selection in the thymus and peripheral immune system and/or by presenting self-peptides against which an autoimmune response is developed (Smith et al., 1998). The specific allele that presents the higher genetic risk for MS patients is the HLA-DRB1*1501 (increased risk, odds ratio ≈ 3) (Baecher-Allan et al., 2018; Goodin, 2014; Hafler et al., 2005; Kearns et al., 2018; Paul et al., 2019; Reich et al., 2018), which explains between 14-50% of the genetic risk (Hafler et al., 2005). Nevertheless, only a very small fraction of HLA-DRB1*1501 carriers (<5%) are susceptible to develop MS (Goodin, 2014). Genome wide association studies have revealed other polymorphisms associated with higher risk for developing MS, most of them related to immune pathway genes, although most of them showed only a modest effect. In this regard, polymorphisms in the *interleukin-2 receptor subunit alpha* and *interleukin-7 receptor* genes seem to be the most commonly associated with MS, after MHC (Baecher-Allan et al., 2018; Nylander and Hafler, 2012; Paul et al., 2019).

Epidemiologic data has identified several infectious and non-infectious factors associated with increased risk to develop MS. Potential environmental triggers include trauma, stress, vaccinations, typhoid, smallpox, chickenpox, Epstein-Barr virus (EBV) and human herpesvirus 6 infection, tobacco, vitamin deficiencies, low sunlight exposure, living with domesticated animals, occupational hazards, dietary habits and toxic exposure (Celarain and Tomas-Roig, 2020; Goodin, 2014; Reich et al., 2018). Alterations in gut microbiota composition have also been identified not only in MS patients compared to healthy controls, but also among RRMS patients during the remission or active states of disease (Chen et al., 2016), and were shown to possibly play a role in T helper (Th) 17 cell differentiation (Cosorich et al., 2017). Interestingly, recent publications from the Quintana lab have demonstrated that different environmental factors, like commensal bacteria metabolites and environmental chemicals (e.g. herbicide linuron), are able to modulate CNS-resident cells, contributing to disease pathogenesis in a MS animal model, the experimental autoimmune encephalomyelitis (EAE) model (Rothhammer et al., 2018; Rothhammer et al., 2016; Wheeler et al., 2019).

Furthermore, epigenetic alterations have been described in MS patients. The hypermethylation of E-cadherin and ICAM-1 in MS patients may contribute to increased BBB permeability and leukocyte invasion, respectively (Celarain and Tomas-Roig, 2020), contributing to the CNS invasion by peripheral immune cells.

Besides the association of genetic and environmental factors with the risk of developing MS, they can also be associated with the likelihood of RRMS patients presenting acute attacks. These factors include pregnancy, occurrence of non-specific infections, trauma or psychological stress (Goodin, 2014).

1.3. Pathological hallmarks of disease

The pathological hallmark of MS is the sclerotic plaque, characterized by focal demyelination, inflammation, oligodendrocyte depletion, scar formation and varying axonal destruction (Compston and Coles, 2008; Lassmann, 2018; Lucchinetti et al., 2005; Popescu et al., 2013). Some of the demyelinated areas are able to be remyelinated. This remyelination is possible due to the presence of oligodendrocyte precursor cells (OPCs) in the adult CNS, that migrate to the lesions and presumably act as the source of cells having the potential to remyelinate naked axons (Compston and Coles, 2008; Duffy et al., 2014). While patients generally return to near normal neurological function, repeated episodes of disease activity are associated with irreversible axonal injury, gliotic scarring and exhaustion of the OPCs pool, leading to the progressive loss of neurological function (Compston and Coles, 2008; Noseworthy et al., 2000; Nylander and Hafler, 2012; Steinman, 2001). At the progressive phase of disease, chronic axonal injury could be explained by several mechanisms: repeated demyelination/remyelination cycles in the same region, lack of trophic support from myelin and oligodendrocytes, increased energy demand that causes chronic mitochondrial failure, increased oxidative stress, alterations in the expression or activity of axonal ion channels and Wallerian degeneration (Correale et al., 2017; Lassmann, 2014; Popescu et al., 2013; Reich et al., 2018).

Even tough MS is generally considered a white matter disease, the gray matter is also affected. Demyelination also occurs in deep cerebral nuclei and the cerebral cortex (Lucchinetti et al., 2005; Popescu et al., 2013). The main differences between cortical and white matter lesions are a decreased inflammatory component and overall decreased tissue injury, making it more difficult to evaluate the full extent of damage in cortical regions, by magnetic resonance imaging (MRI) or post-mortem analysis (Lucchinetti et al., 2005; Reich et al., 2018). Importantly, cortical demyelination can affect neuronal function, viability and survival, and thus have an impact on neurologic and cognitive disability in MS patients (Lucchinetti et al., 2005; Popescu et al., 2013).

Moreover, there are MRI and pathological evidences that the NAWM in MS patients already presents alterations. The NAWM pathology is characterized by diffuse T cell infiltrates (mainly cluster of differentiation (CD)8+ T cells), astrogliosis, microglial activation, diffuse axonal injury and nerve fiber

degeneration (Allen et al., 2001; Cambron et al., 2012; Ceccarelli et al., 2007; Evangelou et al., 2000; Hafler et al., 2005; Kutzelnigg et al., 2005; Lassmann, 2018; Lucchinetti et al., 2005; Vercellino et al., 2017). Gene expression studies of the NAWM have found an overexpression of genes involved in different levels of the inflammatory response (e.g. signaling, transcription, cell adhesion and antigen presentation), genes known to be induced upon oxidative stress, and genes involved in energy metabolism (Graumann et al., 2003; Zeis et al., 2008). It is unclear, however, whether these alterations represent reactive changes or if they are reflecting an inherent abnormality within the white matter of MS patients (Lucchinetti et al., 2005).

1.4. MS symptoms

The injury to the myelin membrane results in the exposure of axons, that are no longer able to efficiently transmit action potentials due to the loss of saltatory conduction. This slowing or blocking of the action potential propagation is ultimately responsible for the neurological symptoms presented by MS patients (Noseworthy et al., 2000). The clinical symptoms are associated with the site of neurologic lesions (Nylander and Hafler, 2012), that are scattered throughout the CNS, with a predilection for the optic nerve, periventricular white matter, brain stem, cerebellum and spinal cord white matter (Lucchinetti et al., 2005; Noseworthy et al., 2000; Nylander and Hafler, 2012; Popescu et al., 2013). MS symptoms include fatigue, continence problems (bladder incontinence and constipation), pain, sensory disturbances (paresthesia), lack of coordination, visual impairment and neuropsychological symptoms (depression, anxiety, cognitive impairment) (Figure 1. 3A) (Celarain and Tomas-Roig, 2020; Duffy et al., 2014; Marrie, 2017; Nicholas and Rashid, 2013; Steinman, 2001). Ultimately, patients lose the ability to walk on their own and become confined to bed. Importantly, early in the disease course, a high percentage of patients have reported fatigue (95%) and cognitive difficulties (71%), and these were often associated with decreased work productivity (Kobelt et al., 2017; Sa et al., 2017). In the specific case of neuropsychological symptoms, it is important to evaluate and follow MS patients, since some studies reported a higher suicide risk in these patients compared to a control population (Goodin, 2014).

The most widely used instrument to evaluate the degree of disability in MS patients is the 10-point expanded disability status scale (EDSS) (Figure 1. 3B). Unfortunately, even considering the modifications performed on this scale throughout the years, it is complicated to score patients, the scale is highly subjective at lower degrees of disability, and it presents poor inter-rate and test-retest reliability. Moreover, it places a big emphasis on ambulation status compared to other neurologic functions (Goodin, 2014).

MS has a massive impact on the patients quality of life and presents a substantial economic burden (Celarain and Tomas-Roig, 2020), even compared to more prevalent neurological conditions (Figure 1. 3C). Not surprisingly, the costs associated with MS increase with the disability degree (Figure 1. 3D). Patients eventually present serious disabilities and impairments, that require a comprehensive care that includes access to physical and occupational therapy, neuropsychology and other health-care professionals (Compston and Coles, 2008). Additional costs, not health related, are associated with MS, since only around 50% of patients below retirement age are still employed, and this percentage decreases with increased EDSS (Figure 1. 3C-D) (Kobelt et al., 2017; Sa et al., 2017).

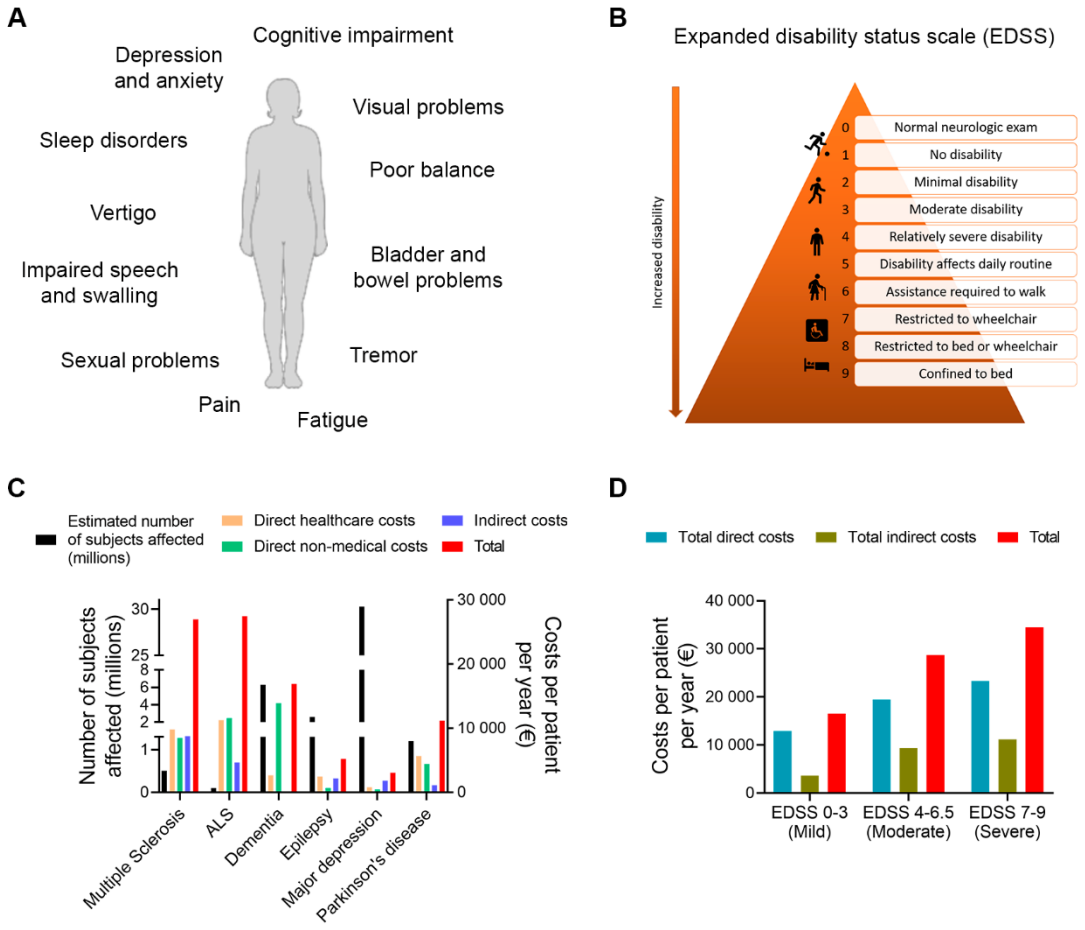

Figure 1. 3 – MS symptoms, disease severity scale and disease-associated costs.

(A) Symptoms of MS. (B) Expanded disability status scale (EDSS) used to evaluate disability in MS. (C) Estimated number of subjects affected and mean annual cost per patient in Europe by diagnostic group. (D) Estimated mean annual cost per patient by disease severity, in Portugal. Data obtained or adapted from (Giovannoni et al., 2016; Kurtzke, 1983; Olesen et al., 2012; Sa et al., 2017).

1.4.1. Cognitive deficits in MS patients

As already mentioned, cognitive problems present a high prevalence in MS patients (Kobelt et al., 2017; Sa et al., 2017). Notably, cognitive impairment is associated with a high impact on social integration, employability and in the ability to perform everyday tasks, independently of disease severity (Chiaravalloti and DeLuca, 2008). Studies have shown that memory, attention, information processing speed, executive functions and visual spatial perception are impaired with disease progression (Branco et al., 2019; Chiaravalloti and DeLuca, 2008; Ifantopoulou et al., 2019; Prokopova et al., 2017). The prevalence of cognitive impairment was found to increase with age (Branco et al., 2019), however, cognitive impairment seems to already be present at initial stages of disease, in which patients present no disability and minimal neurological signs (Prokopova et al., 2017). Cognitive deficits were also found in animal models of MS, before the onset of motor symptoms (Dutra et al., 2013).

While cognitive disturbances affect a large number of MS patients, the responsible mechanisms are not fully understood. Habbas and colleagues (2015) have suggested that increased levels of TNFα, which are believed to be associated with cognitive alterations (Bjugstad et al., 1998; Matsumoto et al., 2002) and are present in MS patients (Maimone et al., 1991; Rossi et al., 2014), in the hippocampal dentate gyrus activates TNF receptors in astrocytes, which in turn triggers an astrocyte-neuron signaling cascade that induces persistent functional modifications of hippocampal excitatory synapses. Interestingly, these results suggest that the mechanism responsible for cognitive dysfunction is distinct from the one causing motor symptoms (Habbas et al., 2015).

Cognitive dysfunction is thought to be more associated with pathological processes in the gray matter, than with white matter demyelination (Geurts and Barkhof, 2008; Lycke and Zetterberg, 2017). This was supported by the fact that MS patients with cognitive decline presented more cortical damage than cognitively preserved patients (Calabrese et al., 2009). Thus, treatments able to improve neuroprotection may have a beneficial impact on cognition.

Cognitive deficits are often neglected or not taken into consideration in randomized clinical trials and in the neurology outpatient clinic (Lycke and Zetterberg, 2017). Since most trials have not been powered or planned to demonstrate positive effects on cognition, few disease modifying treatments have demonstrated beneficial effects on the cognitive performance of MS patients (Muckschel et al., 2016). Mattioli and co-workers (2011, 2015) reported a significant improvement in the neuropsychological performance (memory, attention and executive function) of MS patients treated with natalizumab (see "Current therapeutic approaches" sub-section for more information), after 1-3 years of follow-up (Mattioli et al., 2015; Mattioli et al., 2011). Of notice, after three years of natalizumab treatment patients presented

a significant increase in the mean cortical volume of prefrontal and parahippocampal regions, compared to baseline, suggesting a reduction in brain atrophy that could be involved in improved cognitive function (Mattioli et al., 2015). In addition, interferon beta (IFNβ) (see "Current therapeutic approaches" sub-section for more information) seemed to present beneficial effects on several cognitive domains (attention, concentration, visual-spatial learning, recall) after 1-2 years of treatment (Barak and Achiron, 2002; Fischer et al., 2000). The beneficial effects of IFNβ on cognitive function could be associated with both short-term (inhibition of anti-inflammatory mediators) and long-term (prevention of CNS tissue injury) mechanisms (Fischer et al., 2000). Contrarily to these drugs, glatiramer acetate (GA) (see "Current therapeutic approaches" sub-section for more information) treatment for two years did not seem to alter the cognitive performance of RRMS patients (Weinstein et al., 1999).

1.5. MS diagnosis

There are no clinical features or diagnostic tests specific of MS. Hence, clinical, laboratory and imaging findings were integrated to develop the McDonald criteria for MS diagnosis (Table 1. 1). Using these criteria, the outcome of the diagnostic evaluation can be: (1) MS, if the criteria are fulfilled and there is no better explanation for the clinical presentation; (2) possible MS, in the case of a clinically isolated syndrome (CIS) without complete fulfillment of the criteria; or (3) not MS, if another diagnosis arises during follow-up that better explains the clinical presentation of the patient (Thompson et al., 2018). In these McDonald criteria, needed for the final diagnosis of MS, there has to be evidence of lesions in a minimum of two CNS regions, along with evidence that the insult occurred spaced in time, either by MRI or clinical history (Noseworthy et al., 2000; Nylander and Hafler, 2012; Paul et al., 2019). A progressive disease course that lasts longer than one year is suggestive of PPMS (Thompson et al., 2018). Table 1. 1 presents the 2017 revisions of the McDonald criteria.

Table 1. 1 – 2017 McDonald criteria for diagnosis of MS.

Criteria for diagnosis of MS in patients with an attack at onset		
Number of clinical attacks	**Number of lesions with objective clinical evidence**	**Additional data**
≥2	≥2	Not required
≥2	1 (and historical evidence of a previous attack involving a lesion in a distinct anatomical region)	Not required
≥2	1	Dissemination in space demonstrated by an additional clinical attack implicating a different CNS region OR by MRI*
1	≥2	Dissemination in time demonstrated by an additional clinical attack OR by MRI* OR by the presence of CSF-specific OCBs‡
1	1	Dissemination in space demonstrated by an additional clinical attack implicating a different CNS region OR by MRI* AND Dissemination in time demonstrated by an additional clinical attack OR by MRI* OR by the presence of CSF-specific OCBs‡

Criteria for diagnosis of MS in patients with a progressive disease course from onset	
Required criteria	**Additional criteria (two of the following)**
1 year of disability progression independent of clinical relapse	Dissemination in space demonstrated by MRI*
	Two or more T2-hyperintense lesions in the spinal cord
	Presence of CSF-specific OCBs

* The MRI criteria for dissemination in space and time are described in the "MS biomarkers" sub-section of this introduction. ‡ The presence of CSF-specific OCBs does not demonstrate dissemination in time *per se*, but can substitute for the requirement of its demonstration. Adapted from (Thompson et al., 2018). CNS – central nervous system; CSF – cerebrospinal fluid; MRI – magnetic resonance imaging; OCBs – oligoclonal bands.

1.6. MS biomarkers

As already mentioned, MS is a heterogeneous disease regarding clinical appearance and progression, histopathological alterations, as well as response to therapy. So, it is of the most utter importance to identify specific features of the disease that facilitate the diagnosis, prognosis and evaluation of

therapeutic response in MS patients (Harris et al., 2017; Paul et al., 2019; Ziemssen et al., 2019). The identification of disease biomarkers is important for all these steps. A biomarker is a characteristic that can be objectively measured and assessed, and that can be used as an indicator of normal biological processes, pathological processes or pharmacologic response to therapies (Comabella and Montalban, 2014; Lycke and Zetterberg, 2017; Paul et al., 2019; Ziemssen et al., 2019). Ideally, this characteristic should be present in patients with a specific disease and absent in other patients or healthy people, or vice-versa. Sample collection for biomarker analysis should be performed using a safe procedure for the patient, and its detection should be performed accurately and reproducibly, while also being fast, simple and cost-effective to ensure wide implementation (Paul et al., 2019; Ziemssen et al., 2019). Hence, the detection methods used should be reliable enough to not be influenced by factors like sample collection, sample processing and sample storage (Ziemssen et al., 2019). In addition, good biomarkers should correlate with the disease biology or pathogenesis, such as inflammatory activity, degree of neurodegeneration, demyelination or remyelination (Paul et al., 2019). It is also important to take into consideration that the usage of a biomarker in clinical practice should include multiple validations using independent cohorts of patient (Paul et al., 2019).

Currently, MRI acquisitions provide important information regarding the size, number, age and development of CNS lesions, and play an important role in MS diagnosis and therapy monitoring. Namely, in the case of CIS patients, those that present an abnormal MRI have a long term risk of progression to clinically definite MS of 60-82%, compared to a 8-25% risk in CIS patients with a normal MRI (Brownlee and Miller, 2014). The usage of gadolinium (Gd) as a contrast agent in MRI is useful to detect acute lesions characterized by BBB disruption (Lycke and Zetterberg, 2017). In the recent 2017 revisions of the McDonald criteria, dissemination in time can be demonstrated in MRI by the simultaneous presence of Gd-enhancing and non-enhancing lesions at a given time point, or by the presence of a new T2-hyperintense or Gd-enhancing lesion on a follow-up MRI, having as baseline a scan taken previously. Dissemination in space can be demonstrated by the presence of one or more T2-hyperintense lesions characteristic of MS in at least two of the following areas of the CNS: periventricular, cortical or juxtacortical and infratentorial brain regions, and spinal cord (Thompson et al., 2018). Importantly, Gd-enhancing lesions are rarely identified in progressive MS, suggesting a reduced breakdown of the BBB in these patients (Baecher-Allan et al., 2018; Lassmann, 2018).

As for molecular biomarkers, the existence of oligoclonal bands (OCBs) in the patients' CSF, but not in the serum, is an indicator of intrathecal antibody synthesis and is present in more than 87% of MS patients (Dobson et al., 2013; Ziemssen et al., 2019). OCBs are defined as at least two immunoglobulin (Ig) bands

present in the CSF, with no corresponding band present in the serum (Wahed, 2019). Agarose gel electrophoresis with isoelectric focusing, followed by immunoblotting or immunofixation for IgG, is the most sensitive approach, at present, to demonstrate the presence of CSF-specific OCBs. Importantly, CSF and serum samples always have to be processed together, to confirm CSF specificity (Thompson et al., 2018). Even tough OCBs are not specific of MS, and can be found in several other disorders, such as systemic lupus erythematosus and neurosyphilis, their presence presents a strong prognostic value for conversion from CIS to clinically definite MS (Deisenhammer et al., 2019; Harris et al., 2017; Reich et al., 2018; Ziemssen et al., 2019). The IgG index can also be used as a marker of intrathecal production of Igs (Ziemssen et al., 2019), but this method is less reliable (Thompson et al., 2018).

Besides the presence of OCBs, other biomarkers have also been suggested to present prognostic value for CIS conversion to clinically definite MS. High chitinase-3-like-1 (CHI3L1) concentration in the CSF is an independent risk factor for this conversion (Harris et al., 2017; Lycke and Zetterberg, 2017; Ziemssen et al., 2019), and is also associated with a faster disease progression in MS patients (Martinez et al., 2015). CHI3L1 is a glycosidase secreted by monocytes, microglia and activated astrocytes, whose physiological role in the CNS in unknown (Ziemssen et al., 2019). Moreover, the presence of antibodies against measles, rubella and varicella-zoster in the CSF was found to be significantly more frequent in CIS patients that converted to clinically definite MS (Brettschneider et al., 2009).

Maveskar and co-workers (2019) have recently reported the overexpression of two clusters of proteins in MS patients compared to controls, one enriched in astrocytes and the other in microglia (astrocyte cluster 8: MMP7, Serpin Family A Member 3, granzyme A and chloride intracellular channel 1; microglia cluster 2: desmoglein-2 and TNF receptor superfamily member 25). Moreover, these clusters were significantly correlated with disease severity scales (Masvekar et al., 2019).

Considering MS is an inflammatory disease, the cytokine and chemokine profile of these patients has also been studied. Compared to controls, MS patients presented increased serum levels of interleukin (IL)-6, IL-12, IL-17, IL-23, IL-4 and IFNγ (Kallaur et al., 2013; Li et al., 2017), and CSF levels of IL-6, IL-4, IL-12, chemokine C-C motif ligand (CCL) 2, CCL5 and chemokine C-X-C motif ligand (CXCL) 13 (Alvarez et al., 2013; Bartosik-Psujek and Stelmasiak, 2005; Deisenhammer et al., 2019; Domingues et al., 2017; Malmestrom et al., 2006). Moreover, increased CSF CXCL13 levels were found in CIS patients converting to clinically definite MS compared to non-converters (Lycke and Zetterberg, 2017; Paul et al., 2019). On the other hand, Tejera-Alhambra and colleagues (2015) observed a decreased serum concentration of CCL11, CCL2 and CCL5 in RRMS, compared with progressive MS patients and healthy controls (Tejera-Alhambra et al., 2015). Complement system activation has also been demonstrated in MS, having

increased complement component 1q (C1q) and complement component 3 (C3) levels been found in the CSF of MS patients (Hakansson et al., 2020; Lindblom et al., 2016). In addition, CSF C3a presented prognostic value, since patients who developed new T2 MRI lesions during follow-up presented significantly higher levels of this protein at baseline (Hakansson et al., 2020). However, increased CSF cytokine levels are also found in other neuroinflammatory disorders (Komori et al., 2015; Lepennetier et al., 2019; Lycke and Zetterberg, 2017), so their quantification alone does not present good diagnostic or prognostic value in MS, but their inclusion in a broader biomarkers panel could be useful.

Biomarkers associated with neurodegeneration, that reflect different pathological processes like axonal or glial degeneration, astrogliosis and oxidative stress, have also been measured in the MS context (Lycke and Zetterberg, 2017). Namely, MS patients presented increased CSF levels of neurofilament light chain (NF-L), compared to controls, and its levels were found to be a good prognostic biomarker for CIS conversion to clinically definite MS, and RRMS conversion to SPMS (Hakansson et al., 2017; 2018; Harris et al., 2017; Lycke and Zetterberg, 2017; Martinez et al., 2015; Paul et al., 2019; Ziemssen et al., 2019). NFs are the major structural components of the axonal and dendritic cytoskeleton, and during axonal injury they are released into the extracellular space (Harris et al., 2017). In addition, total Tau protein levels were increased in MS patients compared to controls (Bartosik-Psujek et al., 2011). Nevertheless, these biomarkers are not diagnosis-specific, since higher levels of NF-L and total Tau are a general marker of axonal injury, and are present in other neurological disorders associated with this process (Deisenhammer et al., 2019).

As for markers associated with glial degeneration, studies have found increased CSF glial acidic fibrillary protein (GFAP) levels, an intermediate filament of the astrocytic cytoskeleton, in MS patients compared to controls (Domingues et al., 2017; Lycke and Zetterberg, 2017), and high levels of this protein were associated with earlier disability progression and more severe disability (Comabella and Montalban, 2014; Martinez et al., 2015; Petzold et al., 2002). Recently, GFAP levels were found to be increased in the serum of SPMS patients, compared to controls and RRMS, and the levels of this protein were positively correlated with the serum NF-L levels, even tough no significant differences were found between groups regarding NF-L levels. Moreover, elevated serum GFAP and NF-L levels were associated with increased disability, evaluated by higher EDSS score, and disease duration (Hogel et al., 2020). Similarly, the CSF and serum levels of S100 calcium-binding protein β (S100β), a commonly used astrocytic marker (Wang and Bordey, 2008), were found increased in MS patients (Barateiro et al., 2016; Bartosik-Psujek et al., 2011; Petzold et al., 2002; Rejdak et al., 2007).

Other biomarkers could be useful for differential diagnosis, since they are indicative of other demyelinating diseases. This is the case of anti-aquaporin 4 (AQP4) antibodies, that are detectable in approximately 75% of neuromyelitis optica (NMO) patients but not in MS patients (Ziemssen et al., 2019).
Additional biomarkers have been used to monitor therapy response. Namely, the presence of neutralizing antibodies against IFNβ and natalizumab is used to identify patients non-responders to treatment (Ziemssen et al., 2019). The presence of John Cunningham virus antibodies is also monitored in patients treated with Natalizumab, since the reactivation of this virus could cause progressive multifocal leukoencephalopathy (PML) (Paul et al., 2019).

In conclusion, a single biomarker will most likely not be effective in the diagnosis of such a complex and heterogeneous disease like MS, and future efforts must be done to integrate different types of data, including clinical, radiological and biological, into predictive models for diagnosis, prognosis and treatment response (Comabella and Montalban, 2014; Paul et al., 2019). In an attempt to find novel disease biomarkers, several studies have used samples of MS patients and animal models to identify differentially expressed genes and proteins, along with their biological functions and signaling pathways (Table 1. 2).

Table 1. 2 – Biological function or pathway correspondent to differentially expressed genes in MS or EAE samples.

Sample	Analysis performed	Biological function of altered genes/ Altered pathways	Reference
Peripheral blood of MS patients	Microarray	T- and B-cell activation; degradation of extracellular matrix; chemokine receptors; apoptosis; humoral immune responses	(Ramanathan et al., 2001)
MS patients brain lesions	Microarray	Adhesion/structure/transport; growth factor-related; myelin formation; signaling; cell cycle/homeostasis/unknown; immune-related	(Whitney et al., 1999)
MS patients brain lesions	Microarray	Immune response genes; adhesion molecules; macrophage-related genes; complement activation; pro-inflammatory response; stress related genes; myelin proteins; neuron-specific genes	(Lock et al., 2002)
MS patients brain lesions	Microarray	Differences between lesion margin and center: cytokines; growth factors; receptors/surface molecules; signalling molecules; transcription factors; cell cycle proteins	(Mycko et al., 2003)
Endothelial cells from MS patients	Laser capture microdissection and microarray analysis	Endothelial cell activation; permeability and vessel tone; cell injury; matrix metalloproteinases	(Cunnea et al., 2010)

(Continues)

Table 1. 2 (Continued).

Sample	Analysis performed	Biological function of altered genes/ Altered pathways	Reference
Astrocytes from the NAWM of MS patients	Immunoguided laser capture microdissection	RNA processing; immunity and defense; intracellular signaling cascade; protein metabolism and modification; cytoskeleton; neuronal development; response to metal ions; cellular cation homeostasis; response to hypoxia	(Waller et al., 2016)
MS patients brain lesions	Laser capture microdissection and proteomics	Active plaque: oxidative phosphorylation; regulation of actin cytoskeleton; IL-4, IL-6, IL-2 signaling pathways; transcriptional regulation by STAT; catenin signaling pathway; calcium signaling; oxidative phosphorylation Chronic-active plaque: focal adhesion; cell communication; ECM-receptor interaction; purine metabolism; inflammation mediated by chemokine and cytokine signaling pathway; integrin signaling pathway; muscarinic acetylcholine receptor 1 and 3 signaling pathway; nicotinic acetylcholine receptor signaling pathway; PI3K signaling pathway; IL-4, IL-6, IFNα/β signaling pathways; transcriptional regulation by STAT; calcium signaling; hepatic fibrosis and hepatic stellate cell activation; urine metabolism; actin cytoskeleton signaling; oxidative phosphorylation Chronic plaque: focal adhesion; regulation of actin cytoskeleton; oxidative phosphorylation; cell communication; integrin signaling pathway; IL-4, HGF, TCRα/β, IL-6 signaling pathways; biosynthesis of steroids; actin cytoskeleton signaling; ubiquinone biosynthesis; axonal guidance signaling; integrin signaling	(Han et al., 2008) (Satoh et al., 2009)
CSF from RRMS patients	Proteomics	Cell adhesion; ECM proteins; complement factors; ephrins and other proteins involved in synaptic plasticity; aminoglycan processes; coagulation and inflammation	(Kroksveen et al., 2017)
Spinal cord of C57BL/6 mice immunized with MOG_{35-55}	Microarray	Antigen processing and presentation; immune-related; extracellular matrix; cell adhesion and matrix degradation; signal transduction; transcription; cell structure; movement and secretion; CNS-related; cell division and death	(Ibrahim et al., 2001)
Spinal cord of C57BL/6 mice immunized with MOG_{38-50}	Microarray	Acute phase: injury response factors; inducers of neurite outgrowth and differentiation; ion channels and ion transporters; regulators of synaptic vesicle targeting/fusion; synapse structure/formation Recovery phase: growth factors; regeneration-related proteins; immunoglobulins; myelin genes	(Carmody et al., 2002)
Spinal cord of Lewis rats immunized with gp-MBP	Microarray	Ion homeostasis; Ca^{2+} homeostasis; vesicular function; exocitosis; mitochondrial function; impulse conduction	(Nicot et al., 2003)

(Continues)

Table 1. 2 (Continued).

Sample	Analysis performed	Biological function of altered genes/ Altered pathways	Reference
Spinal cord of Dark Agouti rats immunized with MOG_{1-125}	Microarray	Ion channel and transporter proteins; regulators of synaptic transmission; myelin genes; cholesterol biosynthesis pathway	(Mueller et al., 2008)
Spinal cord of SJL/J mice immunized with MOG_{35-55}	Microarray	Immune/defense responses; cytokine signaling; antiviral response; extracellular matrix organization; iron metabolism; arginine and proline metabolism.	(Gresle et al., 2014)
Spinal cord of Lewis rats immunized with recombinant MBP	Microarray	Immune-related: antigen presentation; Th cell differentiation; CTL-mediated apoptosis of target cells; Fcγ-mediated phagocytosis in macrophages; interferon signaling; dendritic cell maturation; B cell development; TREM signaling; innate/adaptive immune cells; complement system; pathogenesis of MS CNS-related: synaptic long-term potentiation; dopamine-DARPP32 in cAMP signaling; ALS signaling; CREB signaling in neurons; endothelin-1 signaling; biosynthesis of steroids; taurine/hypotaurine metabolism	(Inglis et al., 2012)
Spinal cord of SJL/J mice immunized with PLP and TMEV-IDD mice	Microarray	Downregulated only in EAE: myelination; brain development; axogenesis1 Upregulated only in EAE: chemotaxis; leukocyte migration; cellular response to interleukin-1; T cell differentiation involved in immune response; T helper 1 cell differentiation; adaptive immune response Upregulated only in TMEV-IDD: positive regulation of B cell activation; B cell receptor signaling pathway; complement activation-classical pathway; innate immune response Upregulated in both models: antigen processing and presentation; Myd88-dependent toll-like receptor signaling pathway; microglial cell activation; response to interferon-beta; Toll-like receptors signaling pathways; astrocytes development	(DiSano et al., 2019)
Brain of C57BL/6 mice immunized with MOG_{35-55}	LncRNA microarray	Glutamatergic synapses; calcium signaling pathways; retrograde endocannabinoid signaling; adherens junctions; leukocyte transendothelial migration; salivary secretion; insulin signaling pathway; gastric acid secretion; amphetamine addiction; long-term potentiation; renin-angiotensin system; african trypanosomiasis; malaria; neuroactive ligand-receptor interaction; complement and coagulation cascades; basal cell carcinoma; glutathione metabolism; GABAergic synapse	(Liu et al., 2018)

(Continues)

Table 1. 2 (Continued).

Sample	Analysis performed	Biological function of altered genes/ Altered pathways	Reference
Spinal cord of Lewis rats immunized with gp-MBP	Proteomics	Energy metabolism; cell growth and/or maintenance; transport; protein metabolism; cell communication and signaling; regulation of nucleobase; nucleoside; nucleotide; and nucleic acid metabolism	(Farias et al., 2012)
CSF from Lewis rats immunized with gp-MBP	Proteomics	Class I acute phase proteins; components of the complement system; serine protease inhibitor; antioxidant enzymes; iron metabolism; immunoglobulins; calcium homeostasis	(Rosenling et al., 2012)
Astrocytes from spinal cord and cerebellum of GFAP-Cre RiboTag mice immunized with MOG_{35-55}	High throughput sequencing	Spinal cord: superpathway of cholesterol biosynthesis; cholesterol biosynthesis I; cholesterol biosynthesis II (via 24;25- dihydrolanosterol); cholesterol biosynthesis III (via desmosterol); hepatic fibrosis/hepatic stellate cell activation; clathrin-mediated endocytosis signaling; superpathway of geranylgeranyldiphosphate iosynthesis I (via mevalonate); axonal guidance signaling; antigen presentation pathway; IFN signaling; IL-8 signaling Cerebellum: superpathway of cholesterol biosynthesis; cholesterol biosynthesis I; cholesterol biosynthesis II (via 24;25- dihydrolanosterol); cholesterol biosynthesis III (via Desmosterol); LXR/RXR activation; antigen presentation pathway; IFN signaling; complement system; epoxysqualene biosynthesis; mevalonate pathway I; superpathway of geranylgeranyldiphosphate biosynthesis I (via mevalonate)	(Itoh et al., 2018)
Astrocytes from spinal cord of C57BL/6 mice immunized with MOG_{35-55}	FACS and RNAseq	Signal transduction; interferome type I interferon responsive genes; reactome interferon signaling; interferon-beta response up; interferon-beta 1 targets; IkB-kinase-NF-κB cascade; positive regulation of cell proliferation; regulation of cellular metabolic processes; cytokine activity; cell migration; chemokine activity; inflammatory response	(Rothhammer et al., 2016)
Astrocytes form the optic nerve of GFAP-Cre RiboTag mice immunized with MOG_{35-55}	RNAseq	Complement system; antigen presentation; Th cell differentiation; Th1 and Th1 activation; OX40 signaling; Ca^{2+}-induced T lymphocytes apoptosis; ICOS-ICOSL signaling in Th cells; communication between innate and adaptive immune system; dendritic cell maturation; autoimmune thyroid disease signaling; superpathway of cholesterol biosynthesis; cholesterol biosynthesis I; cholesterol biosynthesis II; cholesterol biosynthesis III; LXR/RXR activation; neuropathic pain signaling; oxidative ethanol degradation III; TCA cycle II (eukaryotic); ethanol degradation IV; epoxysqualene biosynthesis	(Tassoni et al., 2019)

(Continues)

Table 1. 2 (Continued).

Sample	Analysis performed	Biological function of altered genes/ Altered pathways	Reference
Endothelial cells of Rosa-tdTomato; VE-Cadherin-Cre^{ERT2} mice immunized with MOG_{35-55}	FACS and RNAseq	Acute phase: immune response; inflammatory response; cellular response to interferon beta; TNF signaling pathway; malaria; cytokine-cytokine receptor interaction; cell adhesion; cellular response to extracellular stimulus; positive regulation of endothelial cell proliferation; ECM-receptor interaction; protein digestion and absorption; focal adhesion Subacute phase: cell adhesion; cell division; mitotic nuclear division; ECM-receptor interaction; Pi3K-AKT signaling pathway; focal adhesion; negative regulation of transcription from RNA polymerase II prmtr; negative regulation of sequence-specific DNA binding transcription factor activity; cell differentiation; MAPK signaling pathway; amphetamine addiction; pathways in cancer Chronic phase: cell adhesion; ossification; collagen fibril organization; ECM-receptor interaction; PI3K-AKT signaling pathway; focal adhesion; muscle organ development negative regulation of ERK1 and ERK2 cascade; intracellular signal transduction; cGMP-PKG signaling pathway; thyroid hormone signaling pathway; oxytocin signaling pathway	(Munji et al., 2019)
Spinal cord of Biozzi ABH mice immunized with spinal cord homogenate	RNAseq	Superpathway of cholesterol biosynthesis; dendritic cell maturation; T helper cell differentiation; hepatic fibrosis/hepatic stellate cell activation; altered T cell and B cells signaling in rheumatoid arthritis; acute phase response signaling; antigen presentation pathway; LXR/RXR activation; complement system; role of pattern recognition receptors in recognition of bacteria and viruses; iron transport; cell chemotaxis; cell adhesion; cell differentiation; proliferation	(Sevastou et al., 2016)

AKT – Protein kinase B; ALS – amyotrophic lateral sclerosis; Ca^{2+} – calcium; cAMP – cyclic adenosine monophosphate; cGMP-PKG – cyclic guanosine monophosphate dependent protein kinase G; CNS – central nervous system; CREB – cAMP-response element binding protein; CTL – cytotoxic T cell; DARPP32 – dopamine- and cAMP-regulated neuronal phosphoprotein; ECM – extracellular matrix; ERK – extracellular-signal-regulated kinase; GABA - gamma-aminobutyric acid; gp-MBP – guinea pig myelin basic protein; HGF – hepatocyte growth factor; ICOS – inducible costimulator; ICOL – ICOS ligand ; IFN – interferon; IkB – inhibitory proteins of kB family; IL – interleukin; LXR – liver X receptor; MAPK – mitogen activated protein kinase; MBP – myelin basic protein; MOG – myelin oligodendrocyte glycoprotein; NF-κB – factor nuclear kappa B; Pi3K – phosphoinositide 3-kinase; PLP – proteolipid protein; RXR – retinoid X receptor; STAT – signal transducer and activator of transcription; TCA – tricarboxylic acid cycle; TCR – T cell receptor; Th – T helper; TMEV-IDD - Theiler's murine encephalomyelitis

(Continues)

virus-induced demyelinating disease; TNF – tumor necrosis factor; TREM – triggering receptor expressed on myeloid cells.

Of interest, recently our group has identified one astrocytic protein with potential as an additional MS biomarker, which is lipocalin-2 (LCN2), that we will further explore.

1.6.1. Lipocalin-2

LCN2 levels were found to be increased in serum and CSF samples of MS patients, compared to controls (Al-Temaimi et al., 2017; Al Nimer et al., 2016; Berard et al., 2012; Marques et al., 2012). One study, however, reported decreased LCN2 CSF and serum levels in MS patients compared to controls (Khalil et al., 2016). However, these authors identified high LCN2 CSF levels as an independent factor predicting CIS conversion to clinically definite MS, during the follow-up period (Khalil et al., 2016). In addition, Al Nimer and co-workers (2016) reported higher LCN2 CSF levels in PPMS and SPMS patients compared to RRMS (Al Nimer et al., 2016). Interestingly, in the SPMS patients, LCN2 index was positively correlated with the NF-L levels in the CSF (Al Nimer et al., 2016). As for animal studies, *Lcn2* was found to be highly upregulated in the CP and spinal cord of two different EAE mice models, at the onset phase of disease (Berard et al., 2012; Marques et al., 2012; Nam et al., 2014). Of interest, LCN2 levels were shown to decrease after natalizumab treatment, both in the EAE model (Marques et al., 2012) and in MS patients (Al Nimer et al., 2016).

LCN2 is an acute phase protein that acts as a potent bacteriostatic agent. More specifically, during an infection, bacteria acquire iron, that is important for its replication and growth, from the host by secreting and re-uptaking iron chelators, called siderophores. Siderophores present higher affinity for iron than the mammalian proteins involved in their transport, like lactoferrin, transferrin, and ferritin. LCN2 released by neutrophils at sites of infection and inflammation bind to bacterial siderophores with high specificity and affinity, thus preventing iron sequestering by bacteria (Flo et al., 2004; Goetz et al., 2002). Moreover, the ability of LCN2 to deliver or withdraw iron from cells is important for the regulation of cell apoptosis or proliferation, respectively (Devireddy et al., 2005). The modulation of the homeostatic functions of LCN2 is highly dependent on its interaction with cell-surface receptors, namely the 24p3 cell receptor (24p3R) and megalin (Devireddy et al., 2005; Ferreira et al., 2015).

In the CNS, LCN2 is probably involved in similar mechanisms as those described in the periphery, like the modulation of the innate immune response, through siderophore binding, the balance between pro- and anti-inflammatory responses, cellular activation and migration. Of interest, previous work from our

lab has demonstrated that LCN2 is a key modulator of neurogenesis, and that LCN2-null mice present impaired hippocampal-dependent memory and anxious-like behavior (Ferreira et al., 2013; Ferreira et al., 2018).

LCN2 expression in the CNS is described to occur mainly in response to an injury or inflammation, while in physiological conditions it was observed by some authors but not by others (Ferreira et al., 2015). LCN2 was shown to be highly expressed in astrocytes, but not in microglia, neurons or oligodendrocytes (Marques et al., 2012; Nam et al., 2014), while the 24p3R is expressed in almost all CNS cell types (Ferreira et al., 2015).

Cell culture studies have demonstrated that *Lcn2* expression was strongly enhanced in astrocytes stimulated by lipopolysaccharide (LPS) and TNFα (Jang et al., 2013; Lee et al., 2009). Peripheral injection of LPS also increased LCN2 expression in astrocytes and CP cells of wild-type (Wt) mice (Jang et al., 2013; Marques et al., 2008). In addition, cultured astrocytes exposed to LCN2 became reactive, demonstrating hypertrophy of cellular processes, increased GFAP expression, increased NO production, and increased expression of *Il-1b*, *Tnfa*, *inducible nitric oxide synthase* (*Inos*) and *Cxcl10* (Jang et al., 2013; Lee et al., 2009). Since astrocytes express the 24p3R, the LCN2 secreted by these cells under inflammatory conditions can act in an autocrine manner to induce morphological alterations (Lee et al., 2009).

Two studies so far have used LCN2-null animals to induce EAE, however the results are contradictory. Berard and colleagues (2012) reported that some LCN2-null and Wt animals developed RR EAE, while others presented with chronic disease. For the animals with RR EAE, LCN2-null mice presented increased disease severity, evaluated by a higher mean clinical score at disease peak and delayed mean day of disease remission. However, LCN2-null animals with chronic EAE only presented a significantly higher mean clinical score at the end-stage of disease. Moreover, LCN2-null mice presented an increase in total lesioned area and number of immune cells per spinal cord section, and increased expression levels of TFNα and IFNγ in the spinal cord (Berard et al., 2012). Overall, this study suggests that LCN2 plays a protective role in EAE. On the other hand, Nam and co-workers (2014) observed a decreased disease severity in LCN2-null mice immunized with 200 μg of myelin oligodendrocyte glycoprotein 35-55 (MOG_{35-55}), compared to Wt mice, while disease symptoms were not significantly different in the two genotypes under mild disease conditions (50 μg of MOG_{35-55}). LCN2-null animals, immunized with the highest MOG dosage, presented a decrease in infiltration of inflammatory cells, histological score and demyelination area percentage in their spinal cord, in accordance with the lowest disease score observed. Moreover, the increase observed in the number of GFAP+ astrocytes and ionized calcium (Ca^{2+})-binding adaptor

molecule 1 (Iba1)+ microglia was attenuated in LCN2-null mice, that also presented a reduction in the expression levels of Il-*17a*, *Ifng*, *Tnfa*, *Il-12*, *Il-6*, *Il-1b*, *Ccl2* and *Cxcl10* (Nam et al., 2014). Hence, this study points to a detrimental effect of LCN2 in EAE.

1.7. Current therapeutic approaches

Presently, MS has no cure, however, in the recent decades, different disease-modifying therapies have been developed, allowing the reduction of disease severity and the frequency of relapses, by altering or suppressing the immune system (Table 1. 3) (Correale et al., 2017; Lassmann, 2014). However, progressive MS has limited treatment options (Correale et al., 2017; Faissner et al., 2019), with the exception of the monoclonal antibody ocrelizumab, which presented positive results in clinical trials with PPMS patients (Wolinsky et al., 2018). Of relevance, corticosteroids, such as methylprednisolone, are often used to treat clinically significant relapses, but there is no evidence that it prevents new relapses or influences long-term disability (Myhr and Mellgren, 2009; Noseworthy et al., 2000).

Table 1. 3 – Therapeutic agents approved in the European Union for the treatment of MS.

Active compound (brand name)	Therapeutic action	Type of administration
IFNβ1a (Avonex®, Rebif®)	Anti-inflammatory; effects on the endothelial cells of the BBB	Intramuscular or subcutaneous
IFNβ1b (Betaferon®, Extavia®)	Anti-inflammatory; effects on the endothelial cells of the BBB	Subcutaneous
Peginterferon beta 1a (Plegridy®)	Similar to IFNβ, but presents increased half-life with extended activity, allowing a reduction in dose frequency, and presents reduced immunogenecity	Subcutaneous
Glatiramer acetate (Copaxone®, Glatiramer Mylan)	Random mixture of synthetic polypeptides composed of four amino acids (L-glutamic acid, L-lysine, L-alanine and L-tyrosine) that probably competes with myelin peptides for binding to MHC on APCs	Subcutaneous
Dimethyl fumarate (Tecfidera®)	Anti-inflammatory and cytoprotective properties, mediated via activation of Nrf2	Oral
Teriflunomide (Aubagio®)	Non-competitive and reversible inhibition of mitochondrial enzyme dihydroorotate dehydrogenase, which is essential for *de novo* pyrimidine biosynthesis	Oral
Ocrelizumab (Ocrevus®)	CD20 monoclonal antibody – near-complete ablation of CD20+ B cells mainly in the periphery, since it presents limited penetration across the BBB	Intravenous

(Continues)

Table 1. 3 (Continued).

Active compound (brand name)	Therapeutic action	Type of administration
Fingolimod (Gilenya®)	Sphingosine 1-phosphate receptor modulator – decreases immune cell trafficking out of secondary lymphoid organs	Oral
Alemtuzumab (Lemtrada®)	CD52 monoclonal antibody – lymphocyte depletion	Intravenous
Natalizumab (Tysabri®)	VLA-4 monoclonal antibody – prevents leukocyte migration to the CNS, via BBB	Intravenous
Cladribine (Mavenclad®)	CD4+ and CD8+ T cell depletion through interference with cell metabolism of DNA repair processes	Oral
Mitoxantrone (Novantrone ®)	Anti-neoplastic drug with immunosuppressive and immunomodulatory effects – intercalation with DNA repair and topoisomerase II inhibition	Intravenous

Data obtained from (Burness and Deeks, 2014; Colombo et al., 2014; Dorr and Paul, 2015; European Multiple Sclerosis Platform; Huwiler and Zangemeister-Wittke, 2018; Rafiee Zadeh et al., 2019a; Rafiee Zadeh et al., 2019b; Sabatino et al., 2019; Schrempf and Ziemssen, 2007). APCs – antigen presenting cells; BBB – blood-brain barrier; CD – cluster of differentiation; IFNβ – interferon beta; MHC – major histocompatibility complex; Nrf2 - nuclear factor erythroid 2-related factor 2; VLA-4 – very late antigen-4.

Apart from the use of therapeutic drugs, there are also other life-style alterations that can help improve the health status of MS patients, even tough they cannot replace conventional MS treatments. As mentioned before, some of the proposed environmental risk factors include tobacco, dietary habits, like high salt consumption, and vitamin deficiencies, more importantly, deficiency of vitamin D. So, quitting smoking, adopting a healthy diet, engaging in exercise, and vitamin D supplementation could present beneficial effects in these patients (Celarain and Tomas-Roig, 2020). As an example, vitamin D administration presented protective effects in EAE animals (Colotta et al., 2017) and seemed to improve cognitive performance in MS patients (Darwish et al., 2017).

Considering that MS is a heterogenous disease with both an inflammatory and a neurodegenerative phase, it requires the development of therapies against not only the different immune effector mechanisms, but that can also confer protection to other targets of the disease, namely oligodendrocytes and neurons. Moreover, the therapeutic approach should be adapted to the disease stage (Lucchinetti et al., 2005).

1.7.1. Dimethyl fumarate

Dimethyl fumarate (DMF) is the di-methylester of fumaric acid. Fumaric acid esters were initially used to treat psoriasis, but were introduced in MS because of their potent anti-inflammatory effects (Salmen and Gold, 2014). Namely, DMF is suggested to present effects on the innate and adaptive immune systems, by the modulation of APCs and T cell differentiation (Dubey et al., 2015). Moreover, it also presents neuroprotective effects (Dubey et al., 2015; Salmen and Gold, 2014).

After oral administration, DMF is rapidly hydrolyzed to its active metabolite monomethyl fumarate (MMF) by intestinal esterases (Dubey et al., 2015). MMF is then absorbed and distributed, being able to cross the BBB (Salmen and Gold, 2014). *In vitro* studies have shown that MMF protects murine neurons and astrocytes from hydrogen peroxide-induced oxidative stress (Linker et al., 2011). Moreover, *in vivo* studies observed an improvement in the clinical course of EAE after preventive or symptomatic DMF treatment, (Linker et al., 2011; Schilling et al., 2006). These effects were found to be nuclear factor erythroid 2-related factor (Nrf2)-dependent (Linker et al., 2011; Scannevin et al., 2012). DMF/MMF is able to induce intranuclear translocation of Nrf2, increasing the transcription of several anti-oxidative genes (Brennan et al., 2015; Salmen and Gold, 2014). Considering that oxidative stress may be involved in the pathogenesis of axonal damage and tissue injury in MS, DMF poses as an interesting therapy to confer neuroprotection, and is a good candidate drug to prevent cognitive decline.

DMF also inhibits the translocation of nuclear factor kappa B (NF-κB), suppressing NF-κB-dependent transcription. This results in both anti-inflammatory and anti-oxidative effects. The first are related with a reduction of pro-inflammatory cytokines and adhesion molecules synthesis, and with apoptosis induction. The anti-oxidant effects result from a decreased activity of iNOS, which diminishes nitrite accumulation (Salmen and Gold, 2014; Treumer et al., 2003).

The randomized double-blind phase III DEFINE trial showed a significant reduction in the proportions of patients with relapse, in the annualized relapse rate, in disability progression, measured by EDSS, and in the number of new/enlarging T2 and Gd-enhancing T1 lesions on MRI, after 2 years of treatment. The randomized phase III CONFIRM trial presented similar results (Salmen and Gold, 2014). The main side effects of DMF treatment are gastrointestinal symptoms, such as flushing, diarrhea, nausea and vomiting. Proteinuria, pruritus and upper respiratory tract infections and erythema were also reported. In addition, lymphocyte counts decrease around 30% in the first year of DMF treatment, hence it is important to perform a complete blood count before treatment initiation (Dubey et al., 2015; Linker and Gold, 2013; Salmen and Gold, 2014).

2. Astrocytes in the pathophysiology of MS

It is known that the adaptive immune system is extremely important during the RR phase of MS, however at the progressive phase of disease the BBB breakdown is less prominent, and the oligodendrocyte damage and neurodegeneration occurring are believed to be driven by chronic innate immune response involving CNS-resident cells, namely microglia and astrocytes (Correale and Farez, 2015; Nylander and Hafler, 2012; Wheeler and Quintana, 2019). Furthermore, several studies in MS patients and EAE animals have reported significant alterations in astrocytes and their functions, that could contribute to the disease pathophysiology (D'Amelio et al., 1990; Eng et al., 1989; Lee et al., 1990; Villarroya et al., 2001; Wang et al., 2005). Namely, astrocytes proliferate and become reactive in active MS lesions, presenting with eosinophilic hypertrophic cell bodies and numerous fibrillary processes (Brambilla, 2019; Ciccarelli et al., 2014; Correale et al., 2017; Popescu et al., 2013). Accumulation of hypertrophic GFAP-positive astrocytes is also evident in the spinal cord of EAE animals (Duffy et al., 2014). Moreover, reactive astrocytes are already present in early pre-lesions, identified by focal mild perivascular lymphocyte infiltration and BBB breakdown, in the NAWM and in the brain parenchyma before immune cell infiltration, suggesting these cells could be early and active contributors to lesion development (Alvarez et al., 2015; Brambilla, 2019; Broux et al., 2015; Luo et al., 2008). Of notice, already in 1863 Rindfleisch described the presence of abnormal multinucleated process bearing cells, later identified as astrocytes, in a CNS pathology called “grey degeneration”, before the identification of MS as a disease (Williams et al., 2007).

Astrocytes can be distinguished from other glial cells, like microglia and oligodendrocytes, by the expression of GFAP, vimentin, S100β, glutamine synthetase, glutamate/aspartate transporter (GLAST) (Correale and Farez, 2015) and aldehyde dehydrogenase 1 family member L1 (Aldh1L1) (Sofroniew and Vinters, 2010). Importantly, astrocytes participate in several aspects of CNS development and homeostasis, such as physical structuring of the brain, synapse maintenance and refinement, regulation of extracellular concentrations of ions and neurotransmitters, synthesis of metabolic substrates for neurons, formation and maintenance of BBB integrity and regulation of blood flow (Figure 1. 4) (Correale and Farez, 2015; Duffy et al., 2014; Kimelberg and Nedergaard, 2010; Pekny and Pekna, 2016; Sofroniew and Vinters, 2010; Wheeler and Quintana, 2019; Williams et al., 2007). Some of these functions, and how they are altered during MS, will be discussed in more detail in the next chapter sub-sections.

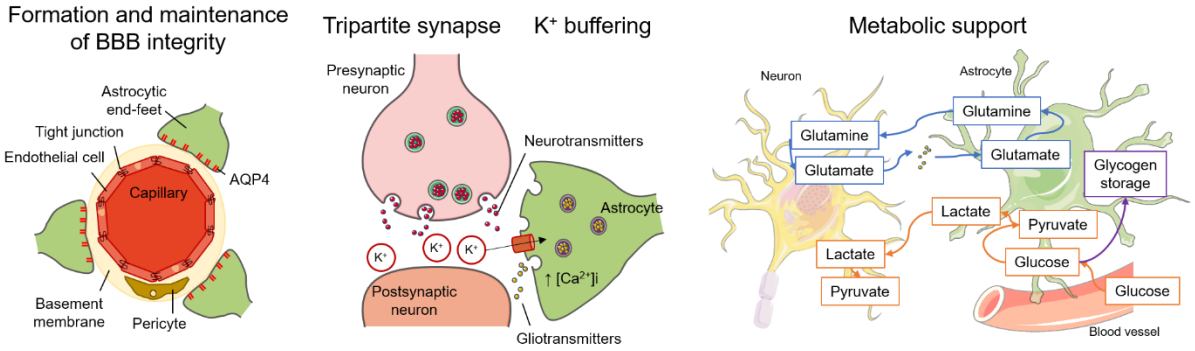

Figure 1. 4 – Functions performed by astrocytes in physiological conditions.

Astrocytes participate in several homeostatic functions, including formation and maintenance of the BBB; as a member of the tripartite synapse, they regulate synaptogenesis, synaptic plasticity and stability, uptake glutamate and buffer extracellular K^+; and they are involved in neuronal metabolic support, via the glucose-lactate shuttle, glutamate-glutamine cycle and by storing glycogen, for example. Images obtained and adapted from Servier Medical Art. AQP4 – aquaporin-4; Ca^{2+} - calcium; K^+ - potassium.

In response to different brain insults, such as inflammation, trauma or infection, astrocytes become reactive (reactive astrogliosis), and suffer morphological and molecular changes, that can range from reversible alterations in gene expression (e.g. GFAP overexpression) and cell hypertrophy to long-lasting gliotic scar formation (Broux et al., 2015; Hamby and Sofroniew, 2010; Nair et al., 2008). Reactive astrocytes exert several protective but also detrimental functions. Some of the protective functions performed are the uptake of excessive extracellular glutamate, protection from oxidative stress, neuroprotection via adenosine release, facilitation of BBB repair and limitation of inflammatory cell spreading into healthy CNS parenchyma (Hamby and Sofroniew, 2010). As for the detrimental effects, these include, but are not limited to, production of cytokines, chemokines, and neurotoxic levels of ROS and RNS, and contribution for increased BBB permeability (Figure 1. 5) (Sofroniew and Vinters, 2010). Following acute inflammation and demyelination, hypertrophic astrocytes are involved in the formation of the gliotic scar. Astrocyte structural proteins, like GFAP, were found to be required for the process of reactive astrogliosis and glial scar formation (Sofroniew, 2015; Sofroniew and Vinters, 2010). The glial scar plays both detrimental and beneficial roles. On one hand, it presents has a physical barrier that prevents axonal regeneration and remyelination (Correale and Farez, 2015; Nair et al., 2008; Ponath et al., 2018). After injury, astrocytes rapidly upregulate chondroitin sulfate proteoglycans (CSPGs) expression that inhibit neurite outgrowth and axonal regeneration (Brosnan and Raine, 2013; Galloway et al., 2020; Nair et al., 2008; Wiese et al., 2012). Moreover, even tough the overexpression of basic fibroblast growth factor (FGF-2) by astrocytes promotes OPC proliferation and survival, it also prevents OPC maturation, thus being detrimental for remyelination (Correale and Farez, 2015; Nair et al., 2008).

Other molecules produced by astrocytes that were shown to inhibit OPC maturation or suppress axonal growth are hyaluronan, insulin-like growth factor-binding proteins 7, and ephrins (Correale and Farez, 2015; Tan et al., 2015). In addition, calpain, which is involved in the degradation of axonal and myelin proteins, including MBP, myelin-associated glycoprotein and neurofilament proteins, was overexpressed by reactive astrocytes located in or near inflammatory foci, during EAE (Shields et al., 1998). On the other hand, the gliotic scar confines the inflamed region, thus preventing the spread of immune cells into the healthy surrounding tissue (Correale and Farez, 2015; Pekny and Pekna, 2016; Ponath et al., 2018; Sofroniew, 2015). Reactive astrocytes also contribute to the clearance of myelin debris in sites of demyelination, through both myelin phagocytosis and recruitment of macrophages and microglia. This clearance is a critical step in promoting repair, since myelin debris are detrimental to remyelination (Figure 1. 5) (Galloway et al., 2020).

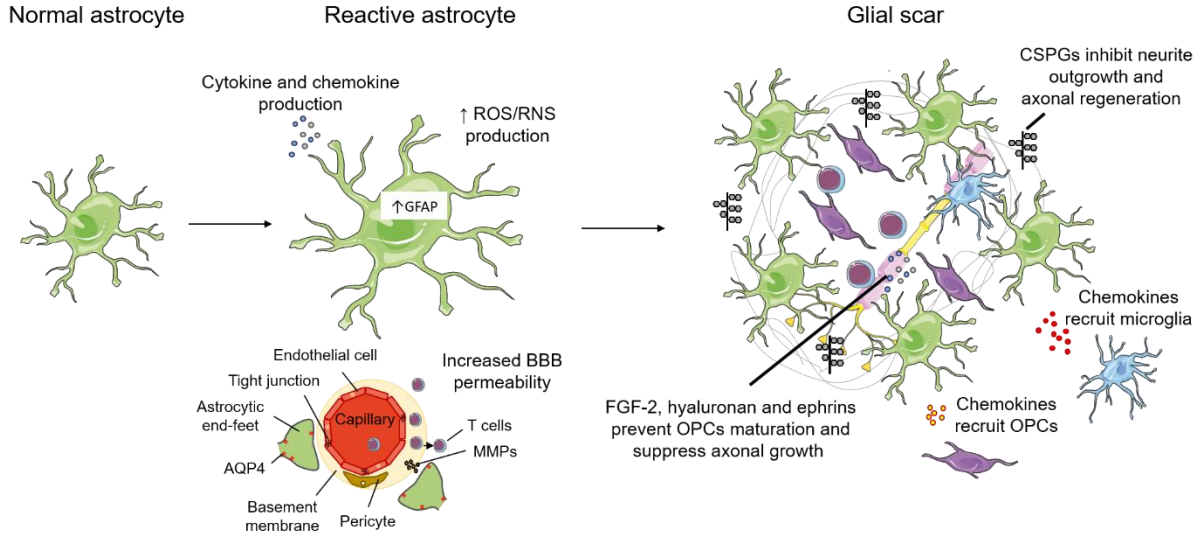

Figure 1. 5 – Functions performed by reactive astrocytes in MS and EAE.

In the disease context, astrocytes become reactive and are involved in the formation of the gliotic scar. Hypertrophic reactive astrocytes overexpress GFAP, produce cytokines and chemokines, increase the production of ROS and RNS, and contribute to increase the BBB permeability. Astrocytes from the glial scar produce CSPGs, FGF-2, hyaluronan and ephrins, that inhibit axonal growth and prevent OPCs maturation. However, these astrocytes also recruit microglial cells, that are important for myelin debris removal, and also OPCs, involved in remyelination. The glial scar confines the damaged tissue and prevents the spread of immune cells into the healthy surrounding tissue. Images obtained and adapted from Servier Medical Art. AQP4 – aquaporin-4; BBB – blood-brain barrier; CSPGs – chondroitin sulfate proteoglycans; FGF-2 – basic fibroblast growth factor; GFAP – glial fibrillary acidic protein; MMPs – matrix metalloproteinases; OPCs – oligodendrocyte precursor cells; RNS – reactive nitrogen species; ROS – reactive oxygen species.

The beneficial roles of reactive astrocytes and the glial scar are evidenced by several studies in EAE animals, in which reactive astrogliosis has been prevented, resulting in increased disease severity associated with increased parenchymal immune-cell infiltration (Haroon et al., 2011; Liedtke et al., 1998; Toft-Hansen et al., 2011; Voskuhl et al., 2009). Hence, ablating astrocyte reactivity completely seems to be detrimental for CNS repair, as astrocytes are important for the confinement of lesions and the restoration of CNS homeostasis (Nair et al., 2008).

Astrocytic reactivity is regulated by key canonical signaling cascades, among which the NF-κB pathway is essential for the establishment of neuroinflammation. This signaling pathway is directly activated by stimulation with pro-inflammatory cytokines, among them TNFα and IL-1β (Ponath et al., 2018). Accordingly, EAE animals with selective ablation or inactivation of NF-κB in astrocytes presented a reduced clinical score, usually associated with reduced demyelination, inflammation and neuronal loss (Brambilla et al., 2014; Brambilla et al., 2009; Brosnan and Raine, 2013; Gupta et al., 2019; Sofroniew, 2014).

2.1. Synthesis of metabolic substrates

Astrocytes present several metabolic functions essential for brain homeostasis, including the transport of nutrients and metabolic precursors to neurons via the malate-aspartate shuttle; the transport of extracellular glutamate and conversion to glutamine, that can be shuttled back to neurons (glutamate-glutamine cycle); the uptake of glucose and synthesis of lactate (glucose-lactate shuttle); glycogen storage; and cholesterol synthesis (Brambilla, 2019; Eilam et al., 2018; Maragakis and Rothstein, 2006; Ponath et al., 2018; Sofroniew and Vinters, 2010). Interestingly, transcriptomic analysis of astrocytes revealed an enriched expression of genes involved in several metabolic pathways (Cahoy et al., 2008; Lovatt et al., 2007). Moreover, Lovatt and colleagues (2007) found that both neurons and astrocytes expressed enzymes mediating aerobic metabolism, however, many pathways entering or exiting glycolysis and the tricarboxylic acid cycle (TCA) cycle, such as those involved in lactate and glutamate metabolism, were compartmentalized, with some reactions being more catalyzed in neurons and others in astrocytes (Lovatt et al., 2007). Specifically, astrocytes were found to overexpress, relatively to neurons, enzymes involved in glycolysis and the TCA cycle (Cahoy et al., 2008; Lovatt et al., 2007). However, in pathological conditions, the stimulation with cytokines for example, can impair the astrocytic metabolic functions (Ponath et al., 2018).

The astrocytic location at the interface between blood vessels and neurons, allows them to uptake glucose from circulation and use it to provide energy supply to neurons (glucose-lactate shuttle) (Brambilla, 2019; Ponath et al., 2018; Sofroniew and Vinters, 2010). More specifically, astrocytes degrade glucose to pyruvate which is then converted to lactate and released via astrocytic monocarboxylate transporters (MCT1 and 4) into the extracellular space. Once there, neurons uptake the lactate, via MCT2 and use it as energy substrate, following its intracellular conversion to pyruvate (Zeis et al., 2015). Interestingly, the expression levels of lactate dehydrogenases (Ldh) in astrocytes and neurons support a compartmentalized relationship of lactate metabolism between the two cell types. Namely, Ldhb catalyzes the conversion of pyruvate to lactate and is enriched in astrocytes, while Ldha that catalyzes the reverse reaction is enriched in neurons (Lovatt et al., 2007).

Lactate levels were found to be increased in the CSF of CIS and MS patients, in comparison to control subjects, and positively correlated with the number of inflammatory plaques and number of CSF mononuclear cells (Lutz et al., 2007; Simone et al., 1996). Importantly, it is well established that cerebral lactate concentration is directly dependent on its rate of production in the brain, and, in accordance with this, no correlation was found between serum and CSF lactate levels. However the authors hypothesize that the main source of lactate production are the infiltrating macrophages (Lutz et al., 2007; Simone et al., 1996), and not astrocytes. In fact, the astrocytic lactate production seems to be decreased in MS. Microarray analyses of MS brains detected a downregulation of genes involved in the glucose-lactate shuttle, such as *MCT1*, while *LDHA* was increased (Zeis et al., 2015). Moreover, the activation of cultured murine astrocytes with TNFα/IFNγ or TNFα/IL-1β decreased lactate release (Chao et al., 2019; Gavillet et al., 2008).

Another source of energy supply to neurons, especially during hypoglycemia or during periods of high neuronal activity, results from glycogenolysis in astrocytes, since these cells are the main storage site of glycogen in the CNS (Brambilla, 2019; Santello et al., 2019; Sofroniew and Vinters, 2010). Actually, astrocytes express enriched levels of all glycogen-metabolizing enzymes, in comparison to neurons (Lovatt et al., 2007).

Through the glutamate-glutamine cycle, astrocytes uptake glutamate from the synaptic cleft and convert it to glutamine, that is released back to synapses for reconversion into active neurotransmitters by neurons (Sofroniew and Vinters, 2010). In fact, antisense knock-down studies have shown that the astrocytic glutamate transporters GLAST and glutamate transporter solute carrier family 1 member 2 (SLC1A2/GLT-1) are responsible for over 80% of glutamate uptake in the brain (Maragakis and Rothstein, 2006). Similarly to what is observed for Ldh expression, astrocytes express glutamate synthetase (GLUL),

that catalyzes the conversion of glutamate into glutamine, whereas neurons express glutaminase and glutamate decarboxylase 1, involved in glutamate and gamma-aminobutyric acid (GABA) synthesis from glutamine (Lovatt et al., 2007).

Following injury, astrocytes initially upregulate the expression of glutamate transporters, like GLT-1, and glutamine synthetase, as a protective mechanism activated by the increased glutamate levels (Kostic et al., 2013; Nair et al., 2008). However, in the case of MS and EAE, in the next phase of disease this protective mechanism seems to be inactivated, since GLT-1 protein levels decrease below control levels (Kostic et al., 2013). Actually, increased CSF glutamate levels were reported to occur in MS patients, compared to individuals lacking objective signs of neurological disorders (Stover et al., 1997a; Stover et al., 1997b), and GLUL expression levels were found to be decreased in the brain of MS patients (Zeis et al., 2015). *In vitro* studies have shown that inflammatory mediators, like TNFα and IL-1β, can potentiate glutamate neurotoxicity by inhibiting its uptake by astrocytes (Kostic et al., 2013; Musella et al., 2016; Tilleux and Hermans, 2007). Moreover, glutamate excitotoxicity causes damage to both neurons and oligodendrocytes (Pitt et al., 2000).

In order to maintain membrane homeostasis and myelin synthesis, neurons and oligodendrocytes are dependent on the cholesterol synthesized by astrocytes, which are the main cells producing cholesterols (Brambilla, 2019; Itoh et al., 2018). However, cholesterol synthesis seems to be impaired in MS and EAE, since the expression of genes involved in this pathway were found to be decreased in both conditions (Itoh et al., 2018; Lavrnja et al., 2017; Lock et al., 2002; Mueller et al., 2008; Sevastou et al., 2016; Tassoni et al., 2019).

2.2. Formation and maintenance of BBB integrity

It was already mentioned that the BBB integrity is compromised during MS (Baecher-Allan et al., 2018). In physiological conditions, the BBB separates the brain tissue from the circulating blood, and is constituted by epithelial cells with tight junctions, pericytes, the basement membrane, and astrocytic end-feet (Ortiz et al., 2014; Prat et al., 2001; Sofroniew and Vinters, 2010). This barrier is responsible for the regulation of the import and export of key substances between the peripheral blood and the CNS, including gases, glucose, water, metabolites and cells (Abbott et al., 2006; Broux et al., 2015; Prat et al., 2001). More importantly, the BBB protects the brain from fluctuations in ionic composition, that occur after meals and exercise, for example, and that could disturb the synaptic and axonal signaling (Abbott et al., 2006). Some of the functions performed by astrocytes at the BBB are the production of vasoactive

molecules, including prostaglandins and NO, that regulate CNS blood flow. Furthermore, they present specialized water and ion channels, like AQP4, that control the composition of extracellular fluid and the pH (Brambilla, 2019; Ludwin et al., 2016; Ponath et al., 2018; Sofroniew, 2015).

It was shown that, during EAE, astrocytes retract their processes, thereby decreasing perivascular coverage (Figure 1. 5) (Eilam et al., 2018). In addition, the distribution of AQP4 channels is described to be highly polarized towards astrocytic foot processes, however this polarization is loss in astrocytes located near EAE lesions (Figure 1. 5) (Wolburg-Buchholz et al., 2009).

IL-6, TNFα, IL-1β, immunity-related GTPase family M member 1, vascular endothelial growth factor (VEGF), and CCL2 released by astrocytes during inflammation increase BBB permeability, by acting on endothelial cells and their tight junctions (Brosnan and Raine, 2013; Broux et al., 2015; Nair et al., 2008; Wang et al., 2013a). VEGF has the additional characteristic of being chemotactic for monocytes, so its release by astrocytes also increases leukocyte extravasation (Brosnan and Raine, 2013; Proescholdt et al., 2002; Sofroniew, 2015). Of notice, a high number of VEGF+ astrocytes were found in or adjacent to MS lesions, while no VEGF+ cells were observed in control brains or unaffected regions of MS brains (Proescholdt et al., 2002). In accordance with these deleterious functions, the conditional deletion of VEGF-A in astrocytes (Gfap-Cre:Vegfa$^{fl/fl}$) improved the clinical signs of EAE, associated with the maintenance of claudin-5 expression (tight junction protein) and a restriction in BBB breakdown (Argaw et al., 2012). Endothelin-1 (ET-1) is a potent vasoconstrictor predominantly produced by endothelial cells and also by reactive astrocytes. ET-1 overexpression both in endothelial cells and astrocytes, and posterior EAE induction, resulted in more severe disease, increased demyelination and increased inflammatory cell infiltration. Furthermore, plasma and CSF levels of ET-1 are increased in MS patients (Guo et al., 2014).

Other proteins released by reactive astrocytes during EAE have an opposite effect, being involved in the BBB repair and inhibition of leukocyte migration. These include annexin-1, retinoic acid and sonic hedgehog synthesis (Brambilla, 2019; Huitinga et al., 1998; Mizee et al., 2014; Sofroniew, 2015).

The basement membrane is composed of ECM proteins, including glycoproteins and fibrous proteins, that are synthetized by endothelial cells and astrocytes (Miljkovic et al., 2011). As mentioned before, MMPs produced by astrocytes, namely MMP2 and MMP9, are able to degrade these ECM proteins (Figure 1. 5) (Miljkovic et al., 2011; Song et al., 2015). However, astrocytes also have the ability to produce tissue inhibitors of MMPs (TIMPs), namely TIMP-1, which inhibit the action of MMPs (Miljkovic et al., 2011; Pagenstecher et al., 1998; Teesalu et al., 2001).

Remarkably, studies performed in GFAP-luciferase animals showed bioluminescence, indicative of GFAP transcriptional response, in the CNS of mice before CD4+ T cell infiltration and the presence of clinical manifestations, suggesting that astrocytes become reactive before CNS inflammation and could contribute to BBB destabilization and permeability (Broux et al., 2015; Luo et al., 2008).

2.3. Synapse maintenance and refinement

The ramified processes of astrocytes make contact with pre- and post-synaptic terminals, forming the tripartite synapse. Within this structure, astrocytes are involved in different processes, like regulation of synaptogenesis, synaptic plasticity and stability, uptake of glutamate and buffering of extracellular potassium (K^+) (Brambilla, 2019; Ponath et al., 2018; Santello et al., 2019).

There is now accumulating evidence that astrocytes directly participate in synaptic transmission. More specifically, alterations in neuronal synaptic activity induce the release of neurotransmitters, such as glutamate and GABA, that are sensed by astrocytes. Astrocytes respond by increasing its intracellular Ca^{2+} concentration, and posteriorly releasing synaptically active molecules (gliotransmitters), like glutamate, adenosine triphosphate (ATP), adenosine and D-serine (Barres, 2008; Sofroniew and Vinters, 2010).

2.4. Synthesis of immunomodulatory molecules and growth factors

In EAE and MS, astrocytes can synthesize several immunomodulatory factors: chemokines involved in increased BBB permeability and immune cell migration, including CCL2, CCL3, CCL4, CCL5, CCL8, CCL20, CCL19, CX3CL1, CXCL8, CXCL10, CXCL12 and CXCL1; pro- and anti-inflammatory cytokines, such as TNFα, IL-1β, IL-6, IL-10, IL-12, IL-23, IL-27, IL-15, IL-33, IFNα and TGFβ; complement proteins, like complement component 5a (C5a), C3a, C1q; B-cell activation factor, involved in B cell survival and proliferation; and ROS and RNS involved in oxidative stress (Ambrosini et al., 2005; Berman et al., 1996; Brambilla, 2019; Chastain et al., 2011; Columba-Cabezas et al., 2003; Correale and Farez, 2015; Glabinski et al., 1997; Glabinski et al., 1995; Lopes Pinheiro et al., 2016; Miljkovic et al., 2011; Miyagishi et al., 1997; Nair et al., 2008; Nataf et al., 1998; Ponath et al., 2018; Ransohoff et al., 1993; Shrestha et al., 2014; Sunnemark et al., 2005; Villarroya et al., 1996; Williams et al., 2007).

The astrocytic targeted deletion of some of the immunomodulatory factors mentioned was able to improve disease symptoms in EAE animals. Namely, the conditional deletion of IL-6 in astrocytes was able to significantly decrease the clinical score in EAE female mice. Moreover, these mice presented a significant

decrease in the number of infiltrates and in astrocyte reactivity, and an increased percentage of myelinated area (Erta et al., 2016). The deletion of CXCL10 in astrocytes delayed EAE onset and decreased the severity of cumulative clinical deficits, compared to control animals. However, during the chronic phase of disease there were no differences between the experimental groups, indicating that the effect of astrocyte-derived CXCL10 is exerted during the initial phases of disease (Mills Ko et al., 2014). The conditional deletion of CCL2 decreased the severity of EAE clinical neurological deficits (Moreno et al., 2014; Paul et al., 2014). This was accompanied by a significant decrease of CNS leukocyte accumulation (Moreno et al., 2014; Paul et al., 2014) and by a higher preservation of claudin-5 staining (Paul et al., 2014). Similarly, the astrocytic targeted expression of a complement inhibitor, complement receptor-related protein y, improved the clinical scores of EAE animals, that presented decreased immune cell infiltration in the CNS (Davoust et al., 1999). On the contrary, the overexpression of C3a in astrocytes increased the EAE severity and mortality rate. This was associated with an increased CNS infiltration with macrophages and CD4+ T cells (Boos et al., 2004). The overexpression of C5a in astrocytes did not affect disease development (Reiman et al., 2005). IFNγ signaling in astrocytes was described as being important for protection against autoimmune-mediated neurological disability, since EAE induction in mice expressing a signaling deficient dominant negative IFNγ receptor I specifically in astrocytes presented increased disease severity, associated with higher expression levels of CCL5, IL-1 and TNF, loss of axons and increased demyelination (Hindinger et al., 2012).

Some of the chemokines produced by astrocytes are also chemoattractants for OPCs, including CXCL1, CXCL8 and CXCL10, allowing them to migrate towards the demyelinated plaques (Williams et al., 2007). Surprisingly, CXCL12 and CCL2 also seemed to be involved in the attraction of transplanted neural precursor cells, in the EAE model, suggesting that, besides attracting inflammatory cells, they could also play a role in the migration of precursor cells to lesions (Cohen et al., 2014).

Astrocytes were found to be central contributors for oxidative stress in EAE (Mossakowski et al., 2015). iNOS, endothelial nitric oxide synthase and neuronal nitric oxide synthase expression was found to be upregulated in astrocytes during EAE, contributing to NO production (Brambilla, 2019; Cross et al., 1997; Kim et al., 2000; Shin, 1999; 2001; Tran et al., 1997). In addition, *in situ* hybridization and immunohistochemistry studies have shown extensive iNOS reactivity in hypertrophic astrocytes in acute but not chronic MS lesions (Brosnan and Raine, 2013). ROS and RNS cause oxidative stress and have been implicated in mechanisms underlying lesion pathogenesis (Brambilla, 2019; Emerson and LeVine, 2000). They are produced not only by microglia and immune cells, but also by astrocytes (Brambilla, 2019). The main local effects of increased ROS and RNS are the modulation of BBB function and

oligodendrocyte damage (Brambilla, 2019; Miljkovic et al., 2011). Oligodendrocytes are particularly vulnerable to oxidative stress possibly because their antioxidant levels are low (Miljkovic et al., 2011). Contrariwise, and in an attempt to decrease oxidative-mediated cellular damage, astrocytes overexpress heme-oxygenase 1, involved in the protection against oxidant-mediated injury (Emerson and LeVine, 2000), and antioxidant enzymes, like superoxide dismutase 2, NAD(P)H Quinone Dehydrogenase 1, and peroxiredoxins (Brambilla, 2019; Qi et al., 1997; Yun et al., 2015). Reactive astrocytes also protect neurons from oxidative stress via glutathione dependent mechanisms (Gavillet et al., 2008; Pekny and Nilsson, 2005). Of interest, a possible beneficial role has also been suggested for increased NO levels, namely in the apoptosis of inflammatory cells (Kim et al., 2000).

Besides immunomodulator molecules, astrocytes also increase the production of growth factors in the disease context, like brain-derived neurotrophic factor (BDNF) and nerve growth factor (Brambilla, 2019; Chastain et al., 2011; Micera et al., 1998; Nair et al., 2008; Ponath et al., 2018; Stadelmann et al., 2002). The increased levels of these growth factors could represent an attempt to prevent or reduce neurite damage in the lesioned regions (Micera et al., 1998). In accordance with these protective properties, a worsening of EAE symptoms could be observed in GFAP-Cre:BDNF$^{fl/fl}$ mice, which present a specific deletion of BDNF in astrocytes. These animals additionally presented increased mortality and axonal damage (Linker et al., 2010).

2.5. Interaction between astrocytes and T cells

Activated anti-myelin T cells that have infiltrated the CNS will not induce injury unless they are reactivated against their specific antigen, through its presentation by APCs (De Keyser et al., 2003). Astrocytes have been pointed as possible APCs of myelin antigens to T cells, in the context of EAE and MS (Correale and Farez, 2015; De Keyser et al., 2003; Ponath et al., 2018). Namely, astrocytes have been shown to process and present myelin-related antigens, such as MBP, proteolipid protein (PLP) and MOG, to encephalitogenic CD4+ T cells (Miljkovic et al., 2011; Myers et al., 1993). Importantly, the necessary molecules for efficient antigen presentation to and activation of CD4+ T cells, including MHC class II and co-stimulator molecules, like B7-1 (CD80) and B7-2 (CD86), have been shown to be present on astrocytes (Issazadeh et al., 1998; Lee et al., 1990; Miljkovic et al., 2011; Nair et al., 2008; Nikcevich et al., 1997; Ponath et al., 2018; Villarroya et al., 2001).

The astrocytic interaction with T cells is also important for T-cell infiltration in the CNS. More specifically, receptor activator of NF-κB (RANK) ligand (RANKL) expression on T cells was shown to induce the

expression of CCL20 on astrocytes, and both the T-cell-specific inactivation of RANKL and the astrocyte-specific deletion of RANK decreased the infiltration of T cells into the CNS of EAE animals, significantly improving their clinical score (Guerrini et al., 2015).

Furthermore, T cell apoptosis can be induced by astrocytes, for example via Fas ligand (FasL) (Correale and Farez, 2015; Hara et al., 2011; Wang et al., 2013b; Xie and Yang, 2015). FasL is expressed in astrocytes and increases in response to cytokines, like IL-1, IL-6, TNFα and IFNγ (Xie and Yang, 2015). A previous study has demonstrated that astrocytic FasL is crucial for the termination of the autoimmune T cell response in the CNS, which allows clinical recovery of symptoms in EAE. Specifically, GFAP-Cre:FasL$^{fl/fl}$ mice induced with EAE presented a similar day of first symptoms and peak of disease, however control mice recovered after the peak while the conditional knock-outs did not. Furthermore, these animals presented more widespread inflammation, characterized by an increased number of CD4+ and CD8+ T cells, and more severe demyelination, compared to controls. they also presented a decreased percentage of 7-Aminoactinomycin D positive CD4+ T cell, suggesting that the elimination of these cells by apoptosis was impaired (Wang et al., 2013b).

2.6. Astrocyte subpopulations

Astrocytes are a very heterogenous population of cells in terms of gene expression profile, physiological properties and response to injury (Batiuk et al., 2020; Bribian et al., 2018; Zhang and Barres, 2010). Differences have even been observed between astrocytic subpopulations regarding spontaneous and behavior-evoked Ca^{2+} activities. Being such a diverse group of cells, it is not surprising that different astrocytic subpopulations respond to disease and injury in different manners (Zhang and Barres, 2010). In order to better understand astrocyte heterogeneity, several laboratories have recently taken advantage of transcriptomic tools to perform molecular classifications of astrocyte subpopulations, both under physiological and pathological conditions (Boisvert et al., 2018; Chai et al., 2017; Clarke et al., 2018; John Lin et al., 2017; Pekny and Pekna, 2016). Interestingly, these studies have shown that astrocytes exhibit broad and diverse changes in gene expression profiles in response to different types of stimulation (Sofroniew, 2014), however, common altered pathways induced in reactive astrocytes include antigen presentation and regulation of inflammatory-mediators production.

In vitro studies have shown major differences in the gene expression profile of astrocytes stimulated with different mediators of reactive astrogliosis, such as LPS, IL-1β, TNFα, IFNγ or TGFβ (Anderson et al., 2014; Hamby et al., 2012). *In vivo* studies comparing neuroinflammation and ischemia models found

two different types of reactive astrocytes, which were recently termed "A1" and "A2", in parallel to the "M1" and "M2" macrophage nomenclature (Liddelow and Barres, 2017; Liddelow et al., 2017). A1 astrocytes were found to lose the ability to promote neuronal survival, outgrowth and synaptogenesis. Instead, A1 astrocytes highly upregulate classical complement cascades previously shown to be destructive to synapses, thus acquiring neurotoxic functions, inducing the death of neurons and oligodendrocytes. By contrast, A2 astrocytes, present in ischemia models, upregulate the expression of genes involved in repair and protective functions, such as neurotrophic factors, therefore presenting a neuroprotective phenotype (Anderson et al., 2014; Liddelow et al., 2017; Zamanian et al., 2012). Of interest, C3+ A1 astrocytes were observed in MS demyelinating lesions (Liddelow et al., 2017). It should be noted that this nomenclature is too simplistic, and more than two polarization states have been described for macrophages (M1, M2a, M2b, M2c) (Liddelow and Barres, 2017). The same is probably true in the case of astrocytes, since recent studies have identified several astrocytic clusters both in MS and EAE (Table 1. 4).

Table 1. 4 – Identification of astrocytic sub-populations by single cell analysis of samples from EAE animals or MS patients.

Samples	Methodology	Results	Pathway analysis	Reference
Brain and spinal cord of C57BL/6 mice immunized with MOG_{35-55}	Single-cell RNAseq	Identification of 8 clusters of astrocytes, being cluster 4 the most expanded in EAE	Cluster 4: mitochondrial dysfunction; NRF2 oxidative stress response; unfolded protein response; production of NO and ROS; IL-6 signaling; neuroinflammation signaling; leukocyte extravasation signaling; GM-CSF signaling; NF-κB signaling; pathogenesis of MS; DNA methylation signaling	(Wheeler et al., 2020)
Brain and spinal cord of $TdTomato^{Gfap}$ mice immunized with MOG_{35-55}	Single-cell RNAseq	Identification of 17 clusters of astrocytes, being cluster 5 the most expanded in EAE	Cluster 5: mitochondrial function; NRF2 oxidative stress response; unfolded protein response; hypoxia signaling; chemokine signaling; S1P signaling; ceramide signaling; ER stress pathway; IL-6 signaling; GM-CSF signaling	(Wheeler et al., 2020)
MS patients brain lesions	Single-cell RNAseq	Identification of 16 clusters of astrocytes, being cluster 1 the most expanded in MS	Cluster 1: neuroinflammation signaling; chemokine signaling; mitochondrial dysfunction; NRF2 oxidative stress response; GM-CSF signaling; IL-6 signaling; iNOS signaling; NF-κB signaling	(Wheeler et al., 2020)

(Continues)

Table 1. 4 (Continued).

Samples	Methodology	Results	Pathway analysis	Reference
One demyelinating lesion and one post-demyelinating lesion from two MS patients	Imaging mass cytometry and single-cell RNAseq	Identification of 5 clusters in the demyelinating lesion and 2 clusters in the post-demyelinating lesion	Not performed	(Park et al., 2019)
Cortical gray matter and adjacent subcortical white matter from lesions of MS patients	Single-nucleus RNA-sequencing	Differentiation between protoplasmic and fibrous/reactive astrocytes	Glutamate homeostasis; potassium homeostasis	(Schirmer et al., 2019)

ER – endoplasmic reticulum; GM-CSF – granulocyte-macrophage colony-stimulating factor; IL – interleukin; iNOS – inducible nitric oxide synthase; MS – multiple sclerosis; NF-κB - Nuclear factor kappa B; NO – nitric oxide; NRF2 – nuclear factor erythroid 2-related factor 2; ROS – reactive oxygen species; S1P – sphingosine-1-phosphate.

Future studies, that help to define astroglial subtypes based on their molecular, functional and structural properties will greatly improve our understanding of their specific roles in MS pathophysiology (Correale and Farez, 2015).

2.7. Astrocyte Ca^{2+} signaling

Astrocytes do not elicit or propagate action potentials along their processes. Instead, they exhibit regulated increases in intracellular Ca^{2+} concentrations, that represent a form of astrocyte excitability (Scemes and Giaume, 2006; Sofroniew and Vinters, 2010). Ca^{2+} waves are defined as localized intracellular Ca^{2+} increases, that are followed by a succession of similar events in a wave-like fashion, and they can be restricted to one cell (intracellular) or transmitted to neighboring cells (intercellular) (Scemes and Giaume, 2006). Intercellular Ca^{2+} waves can propagate by cell-to-cell diffusion, through gap junction channels, or by the release of factors like ATP (Abbott et al., 2006; Scemes and Giaume, 2006; Volterra and Meldolesi, 2005).

Astrocytes are linked and communicate with each other by gap junctions, formed by connexin (Cx) 43 and Cx30 (Correale and Farez, 2015), thus allowing the transfer of ions and metabolites throughout the astrocytic network (Brand-Schieber et al., 2005), including K^+ dissipation and intercellular Ca^{2+} waves

propagation (Correale and Farez, 2015). This astrocytic connectivity seems to be important for coordinated activation and bursting synchronization of neuronal networks (Santello et al., 2019).

Astrocyte excitation can occur in response to or independently of chemical signals released in neural circuits (neuron-dependent and spontaneous excitation, respectively) (Cornell-Bell et al., 1990; Jensen and Chiu, 1990; Volterra and Meldolesi, 2005). Of relevance, it is currently known that the modulation of intracellular Ca^{2+} concentration present functional significance in both astrocyte-astrocyte and astrocyte-neuron intercellular communication (Araque et al., 1998; Sofroniew and Vinters, 2010). In fact, astrocyte intracellular Ca^{2+} elevations can be triggered by transmitters, including glutamate and purines released during neuronal activity, eliciting also the release of gliotransmitters (e.g. glutamate, ATP, adenosine and D-serine) by astrocytes (Barres, 2008; Guerra-Gomes et al., 2017; Sofroniew and Vinters, 2010; Volterra et al., 2014; Volterra and Meldolesi, 2005).

The most widely accepted mechanism for astrocytic Ca^{2+} increases is the canonical phospholipase C (PLC)/inositol 1,4,5-triphosphate (IP_3) pathway (Agulhon et al., 2008; Scemes and Giaume, 2006). PLC hydrolyses phosphatidylinositol 4,5-biphosphate to diacylglycerol and IP_3, in response to G_q G protein-coupled receptor (GPCR) activation, thereby activating IP_3 receptors (IP_3Rs), resulting in Ca^{2+} release from the endoplasmic reticulum (Agulhon et al., 2008; Petravicz et al., 2008; Vardjan and Zorec, 2015).

Of importance, astrocyte hyperactivation, associated with enhanced astrocytic Ca^{2+} signaling, has been observed to occur in some disease models (Ding et al., 2007; Kuchibhotla et al., 2009; Nedergaard et al., 2010; Reichenbach et al., 2018), while others presented decreased astrocytic spontaneous Ca^{2+} signaling (Jiang et al., 2016). Moreover, astrocyte stimulation with cytokines and other inflammatory mediators induced changes in the expression levels of several GPCRs and their intracellular G protein effectors (Anderson et al., 2014; Hamby et al., 2012; Sofroniew, 2014), consequently altering intracellular Ca^{2+} concentrations (Anderson et al., 2014; Hamby et al., 2012). It has also been shown that IP_3-dependent Ca^{2+} signaling and the downstream functions of N-cadherin are required for reactive astrogliosis (Correale and Farez, 2015; Kanemaru et al., 2013; Pekny and Pekna, 2016). Thus, astrocytic Ca^{2+} signaling seems to be involved not only in physiological functions, but also appears to be altered in pathological conditions.

Immunohistochemistry studies have revealed that, in the CNS, the IP_3R2 is primarily expressed in astrocytes (Hertle and Yeckel, 2007; Sharp et al., 1999). Accordingly, in the IP_3R2-null mouse model, G_q GPCR-dependent intracellular Ca^{2+} elevations are absent in the soma and main processes of astrocytes, but not in neurons (Agulhon et al., 2008; Li et al., 2015; Petravicz et al., 2008; Xie et al., 2015). However,

astrocytes from these animals still seem to present IP_3R2-independent Ca^{2+} fluctuations within their processes (Agarwal et al., 2017; Okubo et al., 2019; Rungta et al., 2016; Srinivasan et al., 2015).

Previous studies using pathological models demonstrated that Ca^{2+} signaling disruption, through constitutive IP_3R2 deletion, has beneficial effects in some of the models (Heuser et al., 2018; Li et al., 2015; Rakers and Petzold, 2017; Reichenbach et al., 2018) and deleterious effects on others (Staats et al., 2016; Zheng et al., 2013). Importantly, IP_3R2-null mice do not demonstrate neurodevelopmental alterations, nor motor or neurological reflexes alterations in adulthood, thus presenting as a reliable model to study the functional impact of impaired global IP_3R2-dependent astrocytic Ca^{2+} elevations in adult mice (Guerra-Gomes et al., 2020).

2.8. Role of currently approved MS drugs on astrocytes[1]

The studies previously mentioned have as main goal the identification of astrocytic-intrinsic pathways associated with the control of CNS inflammation, modulation of neuronal health and maintaining BBB integrity, which can guide the development of new therapeutic approaches, particularly for the progressive phase of disease, for which existing drugs offer limited benefit (Wheeler and Quintana, 2019). Even tough no astrocyte-specific therapy has been developed for the treatment of MS, beneficial effects of some of the approved MS drugs could be related to the modulation of astrocytic functions (Miljkovic et al., 2011).

As mentioned before, corticosteroids are used to treat clinical relapses (Noseworthy et al., 2000). Lee and co-workers (2014) used a liposomal encapsulated formula of methylprednisolone to treat EAE mice, after the appearance of clinical symptoms. A low dose of methylprednisolone was encapsulated in liposomes, and their efficacy was compared with the efficacy of low and high doses of free drug. They observed an amelioration of the clinical score in the groups treated with low dose liposomal methylprednisolone and high dose free methylprednisolone, in comparison with low dose free methylprednisolone and vehicle-treated animals. In addition, liposomal encapsulated methylprednisolone significantly reduced the number of GFAP positive astrocytes, in spinal cord lesions, similarly to the high dose free methylprednisolone (Lee et al., 2014). Regarding the effects of methylprednisolone in human astrocytes the knowledge is still very scarce.

Another drug that is used as an anti-symptomatic treatment for MS is 4-aminopyridine (4-AP), which is a potent inhibitor of voltage gated K^+ channels. However, its efficacy in improving the clinical symptoms of

[1] This subsection was adapted from a review manuscript in preparation and presented in Annex 1.

EAE animals was dependent on the model used (Moriguchi et al., 2018). Pre-symptomatic treatment, since the day of immunization, was able to improve disease severity in the RR EAE model (SJL/J females immunized with $PLP_{139-151}$) but not in the chronic EAE model (C57BL/6 females immunized with MOG_{35-55}). Moreover, in the SJL/J EAE mice, 4-AP was able to downregulate GFAP expression (Moriguchi et al., 2018).

Regarding disease modifying drugs, interferons (IFNs), GA, laquinimod and DMF are among the first line treatments used in MS patients. The mechanism of action of IFNs in MS is not fully understood, but they present several immune-mediating activities, and several clinical trials demonstrated that IFNβ1b treatment reduces the frequency of relapses (Noseworthy et al., 2000). Even tough with different biological activities, IFNβ demonstrated a good efficacy in long-term RRMS therapy, and also, to some extent, in SPMS therapy (Lubina-Dabrowska et al., 2017). Regarding animal model results, the pre-symptomatic treatment of EAE Lewis female rats with both IFNβ1a and IFNβ1b presented beneficial effects on the animals' clinical score, and a reduction in GFAP protein levels in the animals' cortex, when compared to non-treated animals (Lubina-Dabrowska et al., 2017). To improve the therapeutic effects of IFNs, Mastronardi and colleagues (2004) combined IFNβ therapy with vitamin B_{12} cyanocobalamin, since previous works had demonstrated beneficial effects of vitamin B_{12} treatment in reversing demyelination. The combinatorial treatment was able to reduce clinical disease and cell infiltration to near normal levels. Moreover, the amount of GFAP in whole brain homogenates was reduced to the levels of untreated mice, indicating a reduction in astrocytic activation (Mastronardi et al., 2004).

GA is a mixture of synthetic polypeptides resembling MBP, and composed of alanine, lysine, glutamic acid and tyrosine (Ure and Rodriguez, 2002). These types of polypeptides were initially used to simulate the ability of MBP to induce EAE, however they were not able to induce disease, and several of them were even shown to suppress EAE. Moreover, this suppressive capacity was independent of species, disease type or encephalitogen used for EAE induction (Ziemssen and Schrempf, 2007). In the Lewis rat EAE model, subcutaneous injections of GA, starting on the day of immunization, besides decreasing the clinical symptoms of disease, reduced GFAP immunofluorescence labelling in the spinal cord, compared to placebo-treated rats (Marques et al., 2009). Furthermore, GA treatment was able to revert the alterations occurring in the astrocyte association with cortical blood vessels and neuronal synapses. Under physiological conditions, the astrocytes' cell bodies are located close to penetrating blood vessels. However, in EAE animals, astrocytes presented an activated morphology, with retracted un-branched processes, and extensive decrease in the perivascular end-feet coverage as well as number of processes pointing towards neurons. In GA-treated animals, after preventive or suppressive treatment, most of the

astroglial cell bodies were lined along the blood vessels and their morphology resembled pre-inflammatory appearance with multiple astrocyte-blood vessels and astrocyte-neuronal contacts (Eilam et al., 2018). GA was also shown to modulate astrocytic reactivity *in vitro*. Namely, the IL-1β- and TNFα-induced production of CCL5 was inhibited by GA pre-treatment, in astrocytoma cell lines (Li and Bever, 2001; Li et al., 2001).

DMF treatment in astrocyte cultures, or microglia/astrocyte co-cultures, was shown to attenuate the LPS-induced increase of *Il-1b*, *Il-6* and *Tnfa* expression (Wierinckx et al., 2005; Wilms et al., 2010) and the IL-1β-induced increase of *Il-6*, *Cxcl10* and *Ccl2* (Galloway et al., 2017). However, no effect was observed regarding *Inos* expression (Wilms et al., 2010). Contrarily to these results, in the work by Lin and colleagues (2011), DMF treatment was able to suppress the LPS- and IFNγ-induced nitrite production, both in primary astrocyte cultures and rat C6 glioma cells (Lin et al., 2011). Both *in vitro* and *in vivo* studies have observed an increased expression of Nrf2 in astrocytes, after treatment with DMF or MMF (Brennan et al., 2015; Brennan et al., 2017; Linker et al., 2011).

A redox analogue of DMF, ethyl pyruvate (EP), was also tested in an EAE rat model. The intraperitoneal treatment with EP, starting on the day before appearance of clinical symptoms, significantly reduced the animals clinical score and seemed to reduce astrocyte activation at day 12 post-immunization (Djedovic et al., 2017). When tested *in vitro*, both DMF and EP suppressed IL-6 release and NF-κB activation in IFNγ- and IL-17-stimulated astrocytes (Miljkovic et al., 2015). Taking all this into account, both DMF and EP could target astrocytes and play a direct antioxidative protection in the context of EAE and MS.

Regarding second line treatments, natalizumab and fingolimod are widely used. Natalizumab is a humanized mouse monoclonal antibody against the integrin VLA-4 on leukocytes, which prevents leukocyte entry into the CNS. Previous work from our lab has shown that natalizumab treatment, after the appearance of clinical symptoms of disease, was able to improve the clinical manifestations of disease of a RR model of EAE (Marques et al., 2012). Moreover, treated animals presented a decrease in the CSF LCN2 levels and in the number of LCN2 GFAP double positive cells in the cerebellum (Marques et al., 2012). Hence, it seems that natalizumab treatment is able to reduce astrocyte activation, since LCN2 in the brain is described to occur mainly in astrocytes and in response to an injury or inflammatory stimulus (Ferreira et al., 2015). Still, it is possible that this improvement in astrocytic reactivity might just be related with natalizumab's ability to prevent immune cell infiltration into the brain (Marques et al., 2012).

The main immunomodulatory mechanism of action of fingolimod is related with its effects on lymphocyte homing. Fingolimod decreases immune cell trafficking out of secondary lymphoid organs, such as lymph

nodes, by acting on sphingosine-1-phosphate (S1P) receptors. Therefore, fingolimod prevents immune cell migration into the CNS (Colombo et al., 2014; Huwiler and Zangemeister-Wittke, 2018). Importantly, reactive astrocytes represent a direct target of fingolimod, since they overexpress sphingosine-1-phosphate (S1P) receptors and this drug is able to cross the BBB (Colombo et al., 2014; Van Doorn et al., 2010). Hence, several *in vitro* and *in vivo* studies have explored the effects of fingolimod on astrocytes. In what concerns the *in vitro* studies, fingolimod was shown to modulate the expression of genes associated with migratory pathways, antigen presentation, inflammasome activation, axonal guidance and fatty acid α-oxidation, when added to a primary astrocytic human culture (Rothhammer et al., 2017). Van Doorn and co-workers (2010) observed a decrease in TNFα-induced CCL2 release, in primary cultures of human astrocytes, in a concentration-dependent fashion, after fingolimod pre-treatment (Van Doorn et al., 2010). Furthermore, it was shown that the astrocyte-conditioned medium (ACM) of cells cultured in the presence of IL-1, IL-17 or S1P induced *in vitro* neuronal degeneration. However, when neurons were exposed to the same ACM in the presence of fingolimod, or to the ACM of astrocytes cultured in the presence of fingolimod, neurodegeneration was hampered or reduced (Colombo et al., 2014; Rothhammer et al., 2017). Further neuroprotective effects of fingolimod were shown by its ability to induce *leukemia inhibitory factor*, *IL-11* and *heparin-binding EGF-like growth factor (HBEGF)* expression in human astrocyte cell cultures, both in the presence and absence of the inflammatory cytokine TNF (Hoffmann et al., 2015).

As for the *in vivo* studies, C57BL/6 EAE animals treated with fingolimod, after the appearance of clinical signs of disease, presented clinical recovery at later time points (Colombo et al., 2014; Smith et al., 2018). Moreover, fingolimod-treated animals presented decreased astrocytic activation (Colombo et al., 2014; Smith et al., 2018) and reduced iNOS levels (Colombo et al., 2014). In another study, fingolimod was used to treat nonobese diabetic EAE mice, instead of using the chronic EAE model, since this resembles several aspects of secondary progressive MS (Rothhammer et al., 2017). In this case, treatment started at day 40 post-immunization, already at the chronic progressive phase of disease, and after the initial acute neurological event, followed by recovery. After 80 days of treatment, fingolimod-treated animals presented a decrease in the average clinical score, compared to vehicle-treated animals (Rothhammer et al., 2017). In what concerns astrocytes, fingolimod treatment downregulated the expression of pro-inflammatory cytokines and chemokines, including *Il-6*, *Ccl2*, *Ccl20*, *Ifng*, *Il-23a*, *Cxcl10* and *Il-1b*, and of neurotoxic factors, like *Inos* (Rothhammer et al., 2017). In addition, the conditional deletion of the $S1P_1$ receptor subtype in GFAP-expressing astrocytes, but not in synapsin-expressing neurons, ameliorated the clinical severity of EAE (Choi et al., 2011). Despite $S1P_1$ signaling in astrocytes

being a key mediator of fingolimod efficacy, conflicting results regarding $S1P_1$ signaling have been shown in the sense that both $S1P_1$ deletion in astrocytes and exposure to $S1P_1$ agonists, like fingolimod, ameliorate EAE (Choi et al., 2011). Other studies have targeted $S1P_1$ receptors using a different agonist, namely CYM-5442 (2-(4-(5-(3,4-diethoxyphenyl)-1,2,4-oxadiazol-3-yl)-2,3-dihydro-1H-inden-1-yl amino) ethanol). The treatment of MOG_{35-55}-induced EAE mice with this agonist, after the appearance of clinical symptoms, resulted in a significant attenuation of clinical signs and weight loss and astrogliosis inhibition, as evaluated by decreased GFAP immunostaining (Gonzalez-Cabrera et al., 2012).

In the cuprizone model, which is a T cell independent experimental model of toxic CNS demyelination, fingolimod treatment significantly suppressed the accumulation of reactive astrocytes, but only when treatment was initiated soon after the beginning of cuprizone diet (3 days later) (Kim et al., 2018), and not after demyelination was already established (Alme et al., 2015).

Thesis aims

The role of astrocytes in the pathophysiology of MS is not fully understood. Recent studies have provided information regarding astrocytic genes and pathways possibly altered at specific disease time points, however an analysis performed throughout disease development is still missing, which we propose to perform in this work. With this analysis we expect to unravel novel possible disease biomarkers or therapeutic targets. One protein that was found to be overexpressed by astrocytes in the EAE context, and that is increased in samples from MS patients, is LCN2. Nevertheless, LCN2 is also increased in the context of other diseases, so its diagnostic value alone is poor, but its prognostic value in MS is currently unknown.

As already mentioned, alterations in intracellular Ca^{2+} levels are important for astrocytic function, and represent a form of astrocyte excitability. "Silencing" astrocytes, by impairing global astrocytic Ca^{2+} signaling, is beneficial in some disease animal models, but detrimental in others, but its impact on EAE remains to be addressed.

A growing body of data indicates that astrocytes are a good therapeutic target to treat many neurological conditions. In the case of MS, it could be particularly important for progressive forms of disease, since astrocytes seem to play an important role during this stage of the disease. Moreover, astrocytes also seem to play a role in the mechanisms leading to cognitive deficits in MS patients. In this regard, DMF could be a good drug to target astrocytes and improve cognition in MS, since it presents immunomodulatory and neuroprotective effects, and was shown to modulate the inflammatory response of astrocytes.

Taking all this into consideration, in this work we intended to:

- Explore the transcriptomic and morphological alterations occurring in astrocytes during EAE, at distinct time points along disease development;
- Assess the impact of "silencing" astrocytes for EAE development and progression;
- Study the impact of dimethyl fumarate on the cognitive performance of EAE animals and its effect on astrocytes;
- Evaluate the prognostic value of LCN2 for MS progression.

References

Abbott NJ, Ronnback L, Hansson E. Astrocyte-endothelial interactions at the blood-brain barrier. Nature Reviews Neuroscience. 2006;7:41-53.

Agarwal A, Wu PH, Hughes EG, Fukaya M, Tischfield MA, Langseth AJ, et al. Transient opening of the mitochondrial permeability transition pore induces microdomain calcium transients in astrocyte processes. Neuron. 2017;93:587-605 e587.

Agulhon C, Petravicz J, McMullen AB, Sweger EJ, Minton SK, Taves SR, et al. What is the role of astrocyte calcium in neurophysiology? Neuron. 2008;59:932-946.

Al-Temaimi R, AbuBaker J, Al-Khairi I, Alroughani R. Remyelination modulators in multiple sclerosis patients. Experimental and Molecular Pathology. 2017;103:237-241.

Al Nimer F, Elliott C, Bergman J, Khademi M, Dring AM, Aeinehband S, et al. Lipocalin-2 is increased in progressive multiple sclerosis and inhibits remyelination. Neurology: Neuroimmunology and NeuroInflammation. 2016;3:e191.

Alcina A, Abad-Grau Mdel M, Fedetz M, Izquierdo G, Lucas M, Fernandez O, et al. Multiple sclerosis risk variant HLA-DRB1*1501 associates with high expression of DRB1 gene in different human populations. PloS One. 2012;7:e29819.

Allen IV, McQuaid S, Mirakhur M, Nevin G. Pathological abnormalities in the normal-appearing white matter in multiple sclerosis. Neurological Sciences. 2001;22:141-144.

Alme MN, Nystad AE, Bo L, Myhr KM, Vedeler CA, Wergeland S, et al. Fingolimod does not enhance cerebellar remyelination in the cuprizone model. Journal of Neuroimmunology. 2015;285:180-186.

Alvarez E, Piccio L, Mikesell RJ, Klawiter EC, Parks BJ, Naismith RT, et al. CXCL13 is a biomarker of inflammation in multiple sclerosis, neuromyelitis optica, and other neurological conditions. Multiple Sclerosis. 2013;19:1204-1208.

Alvarez JI, Saint-Laurent O, Godschalk A, Terouz S, Briels C, Larouche S, et al. Focal disturbances in the blood-brain barrier are associated with formation of neuroinflammatory lesions. Neurobiology of Disease. 2015;74:14-24.

Ambrosini E, Remoli ME, Giacomini E, Rosicarelli B, Serafini B, Lande R, et al. Astrocytes produce dendritic cell-attracting chemokines in vitro and in multiple sclerosis lesions. Journal of Neuropathology and Experimental Neurology. 2005;64:706-715.

Anderson MA, Ao Y, Sofroniew MV. Heterogeneity of reactive astrocytes. Neuroscience Letters. 2014;565:23-29.

Araque A, Parpura V, Sanzgiri RP, Haydon PG. Glutamate-dependent astrocyte modulation of synaptic transmission between cultured hippocampal neurons. European Journal of Neuroscience. 1998;10:2129-2142.

Argaw AT, Asp L, Zhang J, Navrazhina K, Pham T, Mariani JN, et al. Astrocyte-derived VEGF-A drives blood-brain barrier disruption in CNS inflammatory disease. Journal of Clinical Investigation. 2012;122:2454-2468.

Azary S, Schreiner T, Graves J, Waldman A, Belman A, Guttman BW, et al. Contribution of dietary intake to relapse rate in early paediatric multiple sclerosis. Journal of Neurology, Neurosurgery and Psychiatry. 2018;89:28-33.

Baecher-Allan C, Kaskow BJ, Weiner HL. Multiple sclerosis: mechanisms and immunotherapy. Neuron. 2018;97:742-768.

Barak Y, Achiron A. Effect of interferon-beta-1b on cognitive functions in multiple sclerosis. European Neurology. 2002;47:11-14.

Barateiro A, Afonso V, Santos G, Cerqueira JJ, Brites D, van Horssen J, et al. S100B as a potential biomarker and therapeutic target in multiple sclerosis. Molecular Neurobiology. 2016;53:3976-3991.

Barres BA. The mystery and magic of glia: a perspective on their roles in health and disease. Neuron. 2008;60:430-440.

Bartosik-Psujek H, Psujek M, Jaworski J, Stelmasiak Z. Total tau and S100b proteins in different types of multiple sclerosis and during immunosuppressive treatment with mitoxantrone. Acta Neurologica Scandinavica. 2011;123:252-256.

Bartosik-Psujek H, Stelmasiak Z. Correlations between IL-4, IL-12 levels and CCL2, CCL5 levels in serum and cerebrospinal fluid of multiple sclerosis patients. Journal of Neural Transmission. 2005;112:797-803.

Batiuk MY, Martirosyan A, Wahis J, de Vin F, Marneffe C, Kusserow C, et al. Identification of region-specific astrocyte subtypes at single cell resolution. Nature Communications. 2020;11:1220.

Berard JL, Zarruk JG, Arbour N, Prat A, Yong VW, Jacques FH, et al. Lipocalin 2 is a novel immune mediator of experimental autoimmune encephalomyelitis pathogenesis and is modulated in multiple sclerosis. Glia. 2012;60:1145-1159.

Berger T, Rubner P, Schautzer F, Egg R, Ulmer H, Mayringer I, et al. Antimyelin antibodies as a predictor of clinically definite multiple sclerosis after a first demyelinating event. The New England Journal of Medicine. 2003;349:139-145.

Berman JW, Guida MP, Warren J, Amat J, Brosnan CF. Localization of monocyte chemoattractant peptide-1 expression in the central nervous system in experimental autoimmune encephalomyelitis and trauma in the rat. Journal of Immunology. 1996;156:3017-3023.

Bjugstad KB, Flitter WD, Garland WA, Su GC, Arendash GW. Preventive actions of a synthetic antioxidant in a novel animal model of AIDS dementia. Brain Research. 1998;795:349-357.

Boisvert MM, Erikson GA, Shokhirev MN, Allen NJ. The aging astrocyte transcriptome from multiple regions of the mouse brain. Cell Reports. 2018;22:269-285.

Boos L, Campbell IL, Ames R, Wetsel RA, Barnum SR. Deletion of the complement anaphylatoxin C3a receptor attenuates, whereas ectopic expression of C3a in the brain exacerbates, experimental autoimmune encephalomyelitis. Journal of Immunology. 2004;173:4708-4714.

Brambilla R. The contribution of astrocytes to the neuroinflammatory response in multiple sclerosis and experimental autoimmune encephalomyelitis. Acta Neuropathologica. 2019;137:757-783.

Brambilla R, Morton PD, Ashbaugh JJ, Karmally S, Lambertsen KL, Bethea JR. Astrocytes play a key role in EAE pathophysiology by orchestrating in the CNS the inflammatory response of resident and peripheral immune cells and by suppressing remyelination. Glia. 2014;62:452-467.

Brambilla R, Persaud T, Hu X, Karmally S, Shestopalov VI, Dvoriantchikova G, et al. Transgenic inhibition of astroglial NF-kappa B improves functional outcome in experimental autoimmune encephalomyelitis by suppressing chronic central nervous system inflammation. Journal of Immunology. 2009;182:2628-2640.

Branco M, Ruano L, Portaccio E, Goretti B, Niccolai C, Patti F, et al. Aging with multiple sclerosis: prevalence and profile of cognitive impairment. Neurological Sciences. 2019;40:1651-1657.

Brand-Schieber E, Werner P, Iacobas DA, Iacobas S, Beelitz M, Lowery SL, et al. Connexin43, the major gap junction protein of astrocytes, is down-regulated in inflamed white matter in an animal model of multiple sclerosis. Journal of Neuroscience Research. 2005;80:798-808.

Brennan MS, Matos MF, Li B, Hronowski X, Gao B, Juhasz P, et al. Dimethyl fumarate and monoethyl fumarate exhibit differential effects on KEAP1, NRF2 activation, and glutathione depletion in vitro. PloS One. 2015;10:e0120254.

Brennan MS, Matos MF, Richter KE, Li B, Scannevin RH. The NRF2 transcriptional target, OSGIN1, contributes to monomethyl fumarate-mediated cytoprotection in human astrocytes. Scientific Reports. 2017;7:42054.

Brettschneider J, Tumani H, Kiechle U, Muche R, Richards G, Lehmensiek V, et al. IgG antibodies against measles, rubella, and varicella zoster virus predict conversion to multiple sclerosis in clinically isolated syndrome. PloS One. 2009;4:e7638.

Bribian A, Perez-Cerda F, Matute C, Lopez-Mascaraque L. Clonal glial response in a multiple sclerosis mouse model. Frontiers in Cellular Neuroscience. 2018;12:375.

Brosnan CF, Raine CS. The astrocyte in multiple sclerosis revisited. Glia. 2013;61:453-465.

Broux B, Gowing E, Prat A. Glial regulation of the blood-brain barrier in health and disease. Seminars in Immunopathology. 2015;37:577-590.

Brownlee WJ, Miller DH. Clinically isolated syndromes and the relationship to multiple sclerosis. Journal of Clinical Neuroscience. 2014;21:2065-2071.

Burness CB, Deeks ED. Dimethyl fumarate: a review of its use in patients with relapsing-remitting multiple sclerosis. CNS Drugs. 2014;28:373-387.

Cahoy JD, Emery B, Kaushal A, Foo LC, Zamanian JL, Christopherson KS, et al. A transcriptome database for astrocytes, neurons, and oligodendrocytes: a new resource for understanding brain development and function. Journal of Neuroscience. 2008;28:264-278.

Calabrese M, Agosta F, Rinaldi F, Mattisi I, Grossi P, Favaretto A, et al. Cortical lesions and atrophy associated with cognitive impairment in relapsing-remitting multiple sclerosis. Archives of neurology. 2009;66:1144-1150.

Cambron M, D'Haeseleer M, Laureys G, Clinckers R, Debruyne J, De Keyser J. White-matter astrocytes, axonal energy metabolism, and axonal degeneration in multiple sclerosis. Journal of Cerebral Blood Flow and Metabolism. 2012;32:413-424.

Carmody RJ, Hilliard B, Maguschak K, Chodosh LA, Chen YH. Genomic scale profiling of autoimmune inflammation in the central nervous system: the nervous response to inflammation. Journal of Neuroimmunology. 2002;133:95-107.

Ceccarelli A, Rocca MA, Falini A, Tortorella P, Pagani E, Rodegher M, et al. Normal-appearing white and grey matter damage in MS. A volumetric and diffusion tensor MRI study at 3.0 Tesla. Journal of Neurology. 2007;254:513-518.

Celarain N, Tomas-Roig J. Aberrant DNA methylation profile exacerbates inflammation and neurodegeneration in multiple sclerosis patients. Journal of Neuroinflammation. 2020;17:21.

Chai H, Diaz-Castro B, Shigetomi E, Monte E, Octeau JC, Yu X, et al. Neural circuit-specialized astrocytes: transcriptomic, proteomic, morphological, and functional evidence. Neuron. 2017;95:531-549 e539.

Chao CC, Gutierrez-Vazquez C, Rothhammer V, Mayo L, Wheeler MA, Tjon EC, et al. Metabolic control of astrocyte pathogenic activity via cPLA2-MAVS. Cell. 2019;179:1483-1498 e1422.

Chastain EM, Duncan DS, Rodgers JM, Miller SD. The role of antigen presenting cells in multiple sclerosis. Biochimica et Biophysica Acta. 2011;1812:265-274.

Chen J, Chia N, Kalari KR, Yao JZ, Novotna M, Paz Soldan MM, et al. Multiple sclerosis patients have a distinct gut microbiota compared to healthy controls. Scientific Reports. 2016;6:28484.

Chiaravalloti ND, DeLuca J. Cognitive impairment in multiple sclerosis. Lancet Neurology. 2008;7:1139-1151.

Choi JW, Gardell SE, Herr DR, Rivera R, Lee CW, Noguchi K, et al. FTY720 (fingolimod) efficacy in an animal model of multiple sclerosis requires astrocyte sphingosine 1-phosphate receptor 1 (S1P1) modulation. Proceedings of the National Academy of Sciences of the United States of America. 2011;108:751-756.

Ciccarelli O, Barkhof F, Bodini B, De Stefano N, Golay X, Nicolay K, et al. Pathogenesis of multiple sclerosis: insights from molecular and metabolic imaging. Lancet Neurology. 2014;13:807-822.

Clarke LE, Liddelow SA, Chakraborty C, Munch AE, Heiman M, Barres BA. Normal aging induces A1-like astrocyte reactivity. Proceedings of the National Academy of Sciences of the United States of America. 2018;115:E1896-E1905.

Cohen ME, Fainstein N, Lavon I, Ben-Hur T. Signaling through three chemokine receptors triggers the migration of transplanted neural precursor cells in a model of multiple sclerosis. Stem Cell Research. 2014;13:227-239.

Colombo E, Di Dario M, Capitolo E, Chaabane L, Newcombe J, Martino G, et al. Fingolimod may support neuroprotection via blockade of astrocyte nitric oxide. Annals of Neurology. 2014;76:325-337.

Colotta F, Jansson B, Bonelli F. Modulation of inflammatory and immune responses by vitamin D. Journal of Autoimmunity. 2017;85:78-97.

Columba-Cabezas S, Serafini B, Ambrosini E, Aloisi F. Lymphoid chemokines CCL19 and CCL21 are expressed in the central nervous system during experimental autoimmune encephalomyelitis: implications for the maintenance of chronic neuroinflammation. Brain Pathology. 2003;13:38-51.

Comabella M, Montalban X. Body fluid biomarkers in multiple sclerosis. Lancet Neurology. 2014;13:113-126.

Compston A, Coles A. Multiple sclerosis. Lancet. 2008;372:1502-1517.

Cornell-Bell AH, Finkbeiner SM, Cooper MS, Smith SJ. Glutamate induces calcium waves in cultured astrocytes: long-range glial signaling. Science. 1990;247:470-473.

Correale J, Farez MF. The role of astrocytes in multiple sclerosis progression. Frontiers in neurology. 2015;6:180.

Correale J, Gaitan MI, Ysrraelit MC, Fiol MP. Progressive multiple sclerosis: from pathogenic mechanisms to treatment. Brain. 2017;140:527-546.

Cosorich I, Dalla-Costa G, Sorini C, Ferrarese R, Messina MJ, Dolpady J, et al. High frequency of intestinal TH17 cells correlates with microbiota alterations and disease activity in multiple sclerosis. Science Advances. 2017;3:e1700492.

Cross AH, Manning PT, Stern MK, Misko TP. Evidence for the production of peroxynitrite in inflammatory CNS demyelination. Journal of Neuroimmunology. 1997;80:121-130.

Cruz M, Olsson T, Ernerudh J, Hojeberg B, Link H. Immunoblot detection of oligoclonal anti-myelin basic protein IgG antibodies in cerebrospinal fluid in multiple sclerosis. Neurology. 1987;37:1515-1519.

Cunnea P, McMahon J, O'Connell E, Mashayekhi K, Fitzgerald U, McQuaid S. Gene expression analysis of the microvascular compartment in multiple sclerosis using laser microdissected blood vessels. Acta Neuropathologica. 2010;119:601-615.

D'Amelio FE, Smith ME, Eng LF. Sequence of tissue responses in the early stages of experimental allergic encephalomyelitis (EAE): immunohistochemical, light microscopic, and ultrastructural observations in the spinal cord. Glia. 1990;3:229-240.

Darwish H, Haddad R, Osman S, Ghassan S, Yamout B, Tamim H, et al. Effect of vitamin D replacement on cognition in multiple sclerosis patients. Scientific Reports. 2017;7:45926.

Davoust N, Nataf S, Reiman R, Holers MV, Campbell IL, Barnum SR. Central nervous system-targeted expression of the complement inhibitor sCrry prevents experimental allergic encephalomyelitis. Journal of Immunology. 1999;163:6551-6556.

De Keyser J, Zeinstra E, Frohman E. Are astrocytes central players in the pathophysiology of multiple sclerosis? Archives of neurology. 2003;60:132-136.

Deisenhammer F, Zetterberg H, Fitzner B, Zettl UK. The cerebrospinal fluid in multiple sclerosis. Frontiers in Immunology. 2019;10:726.

Devireddy LR, Gazin C, Zhu X, Green MR. A cell-surface receptor for lipocalin 24p3 selectively mediates apoptosis and iron uptake. Cell. 2005;123:1293-1305.

Ding S, Fellin T, Zhu Y, Lee SY, Auberson YP, Meaney DF, et al. Enhanced astrocytic Ca2+ signals contribute to neuronal excitotoxicity after status epilepticus. Journal of Neuroscience. 2007;27:10674-10684.

DiSano KD, Linzey MR, Royce DB, Pachner AR, Gilli F. Differential neuro-immune patterns in two clinically relevant murine models of multiple sclerosis. Journal of Neuroinflammation. 2019;16:109.

Djedovic N, Stanisavljevic S, Jevtic B, Momcilovic M, Lavrnja I, Miljkovic D. Anti-encephalitogenic effects of ethyl pyruvate are reflected in the central nervous system and the gut. Biomedicine and Pharmacotherapy. 2017;96:78-85.

Dobson R, Ramagopalan S, Davis A, Giovannoni G. Cerebrospinal fluid oligoclonal bands in multiple sclerosis and clinically isolated syndromes: a meta-analysis of prevalence, prognosis and effect of latitude. Journal of Neurology, Neurosurgery and Psychiatry. 2013;84:909-914.

Domingues RB, Fernandes GBP, Leite F, Tilbery CP, Thomaz RB, Silva GS, et al. The cerebrospinal fluid in multiple sclerosis: far beyond the bands. Einstein (Sao Paulo). 2017;15:100-104.

Dorr J, Paul F. The transition from first-line to second-line therapy in multiple sclerosis. Current Treatment Options in Neurology. 2015;17:354.

Dubey D, Kieseier BC, Hartung HP, Hemmer B, Warnke C, Menge T, et al. Dimethyl fumarate in relapsing-remitting multiple sclerosis: rationale, mechanisms of action, pharmacokinetics, efficacy and safety. Expert Review of Neurotherapeutics. 2015;15:339-346.

Duffy SS, Lees JG, Moalem-Taylor G. The contribution of immune and glial cell types in experimental autoimmune encephalomyelitis and multiple sclerosis. Multiple Sclerosis International. 2014;2014:285245.

Dutra RC, Moreira EL, Alberti TB, Marcon R, Prediger RD, Calixto JB. Spatial reference memory deficits precede motor dysfunction in an experimental autoimmune encephalomyelitis model: the role of kallikrein-kinin system. Brain, Behavior, and Immunity. 2013;33:90-101.

Eilam R, Segal M, Malach R, Sela M, Arnon R, Aharoni R. Astrocyte disruption of neurovascular communication is linked to cortical damage in an animal model of multiple sclerosis. Glia. 2018;66:1098-1117.

Emerson MR, LeVine SM. Heme oxygenase-1 and NADPH cytochrome P450 reductase expression in experimental allergic encephalomyelitis: an expanded view of the stress response. Journal of Neurochemistry. 2000;75:2555-2562.

Eng LF, D'Amelio FE, Smith ME. Dissociation of GFAP intermediate filaments in EAE: observations in the lumbar spinal cord. Glia. 1989;2:308-317.

Erta M, Giralt M, Jimenez S, Molinero A, Comes G, Hidalgo J. Astrocytic IL-6 influences the clinical symptoms of EAE in mice. Brain Sciences. 2016;6.

European Multiple Sclerosis Platform. MS Facts | MS Treatments. 11/03/2020. http://www.emsp.org/about-ms/ms-treatments/.

Evangelou N, Esiri MM, Smith S, Palace J, Matthews PM. Quantitative pathological evidence for axonal loss in normal appearing white matter in multiple sclerosis. Annals of Neurology. 2000;47:391-395.

Faissner S, Plemel JR, Gold R, Yong VW. Progressive multiple sclerosis: from pathophysiology to therapeutic strategies. Nature Reviews: Drug Discovery. 2019;18:905-922.

Farias AS, Martins-de-Souza D, Guimaraes L, Pradella F, Moraes AS, Facchini G, et al. Proteome analysis of spinal cord during the clinical course of monophasic experimental autoimmune encephalomyelitis. Proteomics. 2012;12:2656-2662.

Ferreira AC, Da Mesquita S, Sousa JC, Correia-Neves M, Sousa N, Palha JA, et al. From the periphery to the brain: lipocalin-2, a friend or foe? Progress in Neurobiology. 2015;131:120-136.

Ferreira AC, Pinto V, Da Mesquita S, Novais A, Sousa JC, Correia-Neves M, et al. Lipocalin-2 is involved in emotional behaviors and cognitive function. Frontiers in Cellular Neuroscience. 2013;7:122.

Ferreira AC, Santos T, Sampaio-Marques B, Novais A, Mesquita SD, Ludovico P, et al. Lipocalin-2 regulates adult neurogenesis and contextual discriminative behaviours. Molecular Psychiatry. 2018;23:1031-1039.

Figueiredo J, Silva A, Cerqueira JJ, Fonseca J, Pereira PA. MS prevalence and patients' characteristics in the district of Braga, Portugal. Neurology Research International. 2015;2015:895163.

Fischer JS, Priore RL, Jacobs LD, Cookfair DL, Rudick RA, Herndon RM, et al. Neuropsychological effects of interferon beta-1a in relapsing multiple sclerosis. Multiple Sclerosis Collaborative Research Group. Annals of Neurology. 2000;48:885-892.

Flo TH, Smith KD, Sato S, Rodriguez DJ, Holmes MA, Strong RK, et al. Lipocalin 2 mediates an innate immune response to bacterial infection by sequestrating iron. Nature. 2004;432:917-921.

Galloway DA, Gowing E, Setayeshgar S, Kothary R. Inhibitory milieu at the multiple sclerosis lesion site and the challenges for remyelination. Glia. 2020;68:859-877.

Galloway DA, Williams JB, Moore CS. Effects of fumarates on inflammatory human astrocyte responses and oligodendrocyte differentiation. Annals of Clinical and Translational Neurology. 2017;4:381-391.

Gavillet M, Allaman I, Magistretti PJ. Modulation of astrocytic metabolic phenotype by proinflammatory cytokines. Glia. 2008;56:975-989.

Gerwien H, Hermann S, Zhang X, Korpos E, Song J, Kopka K, et al. Imaging matrix metalloproteinase activity in multiple sclerosis as a specific marker of leukocyte penetration of the blood-brain barrier. Science Translational Medicine. 2016;8:364ra152.

Geurts JJ, Barkhof F. Grey matter pathology in multiple sclerosis. Lancet Neurology. 2008;7:841-851.

Gimenez MA, Sim JE, Russell JH. TNFR1-dependent VCAM-1 expression by astrocytes exposes the CNS to destructive inflammation. Journal of Neuroimmunology. 2004;151:116-125.

Giovannoni G, Butzkueven H, Dhib-Jalbut S, Hobart J, Kobelt G, Pepper G, et al. Brain health: time matters in multiple sclerosis. Multiple Sclerosis and Related Disorders. 2016;9 Suppl 1:S5-S48.

Glabinski AR, Tani M, Strieter RM, Tuohy VK, Ransohoff RM. Synchronous synthesis of alpha- and beta-chemokines by cells of diverse lineage in the central nervous system of mice with relapses of chronic experimental autoimmune encephalomyelitis. The American Journal of Pathology. 1997;150:617-630.

Glabinski AR, Tani M, Tuohy VK, Tuthill RJ, Ransohoff RM. Central nervous system chemokine mRNA accumulation follows initial leukocyte entry at the onset of acute murine experimental autoimmune encephalomyelitis. Brain, Behavior, and Immunity. 1995;9:315-330.

Goetz DH, Holmes MA, Borregaard N, Bluhm ME, Raymond KN, Strong RK. The neutrophil lipocalin NGAL is a bacteriostatic agent that interferes with siderophore-mediated iron acquisition. Molecular Cell. 2002;10:1033-1043.

Gonzalez-Cabrera PJ, Cahalan SM, Nguyen N, Sarkisyan G, Leaf NB, Cameron MD, et al. S1P(1) receptor modulation with cyclical recovery from lymphopenia ameliorates mouse model of multiple sclerosis. Molecular Pharmacology. 2012;81:166-174.

Goodin DS. The epidemiology of multiple sclerosis: insights to disease pathogenesis. Handbook of Clinical Neurology. 2014;122:231-266.

Graumann U, Reynolds R, Steck AJ, Schaeren-Wiemers N. Molecular changes in normal appearing white matter in multiple sclerosis are characteristic of neuroprotective mechanisms against hypoxic insult. Brain Pathology. 2003;13:554-573.

Gresle MM, Schulz K, Jonas A, Perreau VM, Cipriani T, Baxter AG, et al. Ceruloplasmin gene-deficient mice with experimental autoimmune encephalomyelitis show attenuated early disease evolution. Journal of Neuroscience Research. 2014;92:732-742.

Guerra-Gomes S, Cunha-Garcia D, Marques Nascimento DS, Duarte-Silva S, Loureiro-Campos E, Morais Sardinha V, et al. IP3 R2 null mice display a normal acquisition of somatic and neurological development milestones. European Journal of Neuroscience. 2020.

Guerra-Gomes S, Sousa N, Pinto L, Oliveira JF. Functional roles of astrocyte calcium elevations: from synapses to behavior. Frontiers in Cellular Neuroscience. 2017;11:427.

Guerrini MM, Okamoto K, Komatsu N, Sawa S, Danks L, Penninger JM, et al. Inhibition of the TNF family cytokine RANKL prevents autoimmune inflammation in the central nervous system. Immunity. 2015;43:1174-1185.

Guo Y, Chung SK, Siu CW, Kwan SC, Ho PW, Yeung PK, et al. Endothelin-1 overexpression exacerbate experimental allergic encephalomyelitis. Journal of Neuroimmunology. 2014;276:64-70.

Gupta AS, Biswas DD, Brown SN, Mockenhaupt K, Marone M, Hoskins A, et al. A detrimental role of RelB in mature oligodendrocytes during experimental acute encephalomyelitis. Journal of Neuroinflammation. 2019;16:161.

Habbas S, Santello M, Becker D, Stubbe H, Zappia G, Liaudet N, et al. Neuroinflammatory TNFalpha impairs memory via astrocyte signaling. Cell. 2015;163:1730-1741.

Hafler DA, Slavik JM, Anderson DE, O'Connor KC, De Jager P, Baecher-Allan C. Multiple sclerosis. Immunological Reviews. 2005;204:208-231.

Hakansson I, Ernerudh J, Vrethem M, Dahle C, Ekdahl KN. Complement activation in cerebrospinal fluid in clinically isolated syndrome and early stages of relapsing remitting multiple sclerosis. Journal of Neuroimmunology. 2020;340:577147.

Hakansson I, Tisell A, Cassel P, Blennow K, Zetterberg H, Lundberg P, et al. Neurofilament light chain in cerebrospinal fluid and prediction of disease activity in clinically isolated syndrome and relapsing-remitting multiple sclerosis. European Journal of Neurology. 2017;24:703-712.

Hakansson I, Tisell A, Cassel P, Blennow K, Zetterberg H, Lundberg P, et al. Neurofilament levels, disease activity and brain volume during follow-up in multiple sclerosis. Journal of Neuroinflammation. 2018;15:209.

Hamby ME, Coppola G, Ao Y, Geschwind DH, Khakh BS, Sofroniew MV. Inflammatory mediators alter the astrocyte transcriptome and calcium signaling elicited by multiple G-protein-coupled receptors. Journal of Neuroscience. 2012;32:14489-14510.

Hamby ME, Sofroniew MV. Reactive astrocytes as therapeutic targets for CNS disorders. Neurotherapeutics. 2010;7:494-506.

Han MH, Hwang SI, Roy DB, Lundgren DH, Price JV, Ousman SS, et al. Proteomic analysis of active multiple sclerosis lesions reveals therapeutic targets. Nature. 2008;451:1076-1081.

Hara H, Nanri Y, Tabata E, Mitsutake S, Tabira T. Identification of astrocyte-derived immune suppressor factor that induces apoptosis of autoreactive T cells. Journal of Neuroimmunology. 2011;233:135-146.

Haroon F, Drogemuller K, Handel U, Brunn A, Reinhold D, Nishanth G, et al. Gp130-dependent astrocytic survival is critical for the control of autoimmune central nervous system inflammation. Journal of Immunology. 2011;186:6521-6531.

Harris VK, Tuddenham JF, Sadiq SA. Biomarkers of multiple sclerosis: current findings. Degenerative Neurological and Neuromuscular Disease. 2017;7:19-29.

Hertle DN, Yeckel MF. Distribution of inositol-1,4,5-trisphosphate receptor isotypes and ryanodine receptor isotypes during maturation of the rat hippocampus. Neuroscience. 2007;150:625-638.

Heuser K, Nome CG, Pettersen KH, Abjorsbraten KS, Jensen V, Tang W, et al. Ca2+ signals in astrocytes facilitate spread of epileptiform activity. Cerebral Cortex. 2018;28:4036-4048.

Hindinger C, Bergmann CC, Hinton DR, Phares TW, Parra GI, Hussain S, et al. IFN-gamma signaling to astrocytes protects from autoimmune mediated neurological disability. PloS One. 2012;7:e42088.

Hoffmann FS, Hofereiter J, Rubsamen H, Melms J, Schwarz S, Faber H, et al. Fingolimod induces neuroprotective factors in human astrocytes. Journal of Neuroinflammation. 2015;12:184.

Hogel H, Rissanen E, Barro C, Matilainen M, Nylund M, Kuhle J, et al. Serum glial fibrillary acidic protein correlates with multiple sclerosis disease severity. Multiple Sclerosis. 2020;26:210-219.

Huitinga I, Bauer J, Strijbos PJ, Rothwell NJ, Dijkstra CD, Tilders FJ. Effect of annexin-1 on experimental autoimmune encephalomyelitis (EAE) in the rat. Clinical and Experimental Immunology. 1998;111:198-204.

Huwiler A, Zangemeister-Wittke U. The sphingosine 1-phosphate receptor modulator fingolimod as a therapeutic agent: recent findings and new perspectives. Pharmacology and Therapeutics. 2018;185:34-49.

Ibrahim SM, Mix E, Bottcher T, Koczan D, Gold R, Rolfs A, et al. Gene expression profiling of the nervous system in murine experimental autoimmune encephalomyelitis. Brain. 2001;124:1927-1938.

Ifantopoulou P, Artemiadis AK, Bakirtzis C, Zekiou K, Papadopoulos TS, Diakogiannis I, et al. Cognitive and brain reserve in multiple sclerosis–A cross-sectional study. Multiple Sclerosis and Related Disorders. 2019;35:128-134.

Inglis HR, Greer JM, McCombe PA. Gene expression in the spinal cord in female lewis rats with experimental autoimmune encephalomyelitis induced with myelin basic protein. PloS One. 2012;7:e48555.

Issazadeh S, Navikas V, Schaub M, Sayegh M, Khoury S. Kinetics of expression of costimulatory molecules and their ligands in murine relapsing experimental autoimmune encephalomyelitis in vivo. Journal of Immunology. 1998;161:1104-1112.

Itoh N, Itoh Y, Tassoni A, Ren E, Kaito M, Ohno A, et al. Cell-specific and region-specific transcriptomics in the multiple sclerosis model: Focus on astrocytes. Proceedings of the National Academy of Sciences of the United States of America. 2018;115:E302-E309.

Jang E, Kim JH, Lee S, Kim JH, Seo JW, Jin M, et al. Phenotypic polarization of activated astrocytes: the critical role of lipocalin-2 in the classical inflammatory activation of astrocytes. Journal of Immunology. 2013;191:5204-5219.

Jensen AM, Chiu SY. Fluorescence measurement of changes in intracellular calcium induced by excitatory amino acids in cultured cortical astrocytes. Journal of Neuroscience. 1990;10:1165-1175.

Jiang R, Diaz-Castro B, Looger LL, Khakh BS. Dysfunctional calcium and glutamate signaling in striatal astrocytes from Huntington's disease model mice. Journal of Neuroscience. 2016;36:3453-3470.

John Lin CC, Yu K, Hatcher A, Huang TW, Lee HK, Carlson J, et al. Identification of diverse astrocyte populations and their malignant analogs. Nature Neuroscience. 2017;20:396-405.

Kallaur AP, Oliveira SR, Colado Simao AN, Delicato de Almeida ER, Kaminami Morimoto H, Lopes J, et al. Cytokine profile in relapsingremitting multiple sclerosis patients and the association between progression and activity of the disease. Molecular Medicine Reports. 2013;7:1010-1020.

Kanemaru K, Kubota J, Sekiya H, Hirose K, Okubo Y, Iino M. Calcium-dependent N-cadherin up-regulation mediates reactive astrogliosis and neuroprotection after brain injury. Proceedings of the National Academy of Sciences of the United States of America. 2013;110:11612-11617.

Kasper LH, Shoemaker J. Multiple sclerosis immunology: the healthy immune system vs the MS immune system. Neurology. 2010;74 Suppl 1:S2-8.

Kearns PKA, Casey HA, Leach JP. Hypothesis: Multiple sclerosis is caused by three-hits, strictly in order, in genetically susceptible persons. Multiple Sclerosis and Related Disorders. 2018;24:157-174.

Khalil M, Renner A, Langkammer C, Enzinger C, Ropele S, Stojakovic T, et al. Cerebrospinal fluid lipocalin 2 in patients with clinically isolated syndromes and early multiple sclerosis. Multiple Sclerosis. 2016;22:1560-1568.

Kim S, Bielawski J, Yang H, Kong Y, Zhou B, Li J. Functional antagonism of sphingosine-1-phosphate receptor 1 prevents cuprizone-induced demyelination. Glia. 2018;66:654-669.

Kim S, Moon C, Wie MB, Kim H, Tanuma N, Matsumoto Y, et al. Enhanced expression of constitutive and inducible forms of nitric oxide synthase in autoimmune encephalomyelitis. Journal of Veterinary Science. 2000;1:11-17.

Kimelberg HK, Nedergaard M. Functions of astrocytes and their potential as therapeutic targets. Neurotherapeutics. 2010;7:338-353.

Kobelt G, Thompson A, Berg J, Gannedahl M, Eriksson J, Group MS, et al. New insights into the burden and costs of multiple sclerosis in Europe. Multiple Sclerosis. 2017;23:1123-1136.

Komori M, Blake A, Greenwood M, Lin YC, Kosa P, Ghazali D, et al. Cerebrospinal fluid markers reveal intrathecal inflammation in progressive multiple sclerosis. Annals of Neurology. 2015;78:3-20.

Kooij G, Kopplin K, Blasig R, Stuiver M, Koning N, Goverse G, et al. Disturbed function of the blood-cerebrospinal fluid barrier aggravates neuro-inflammation. Acta Neuropathologica. 2014;128:267-277.

Kostic M, Zivkovic N, Stojanovic I. Multiple sclerosis and glutamate excitotoxicity. Reviews in the Neurosciences. 2013;24:71-88.

Kroksveen AC, Guldbrandsen A, Vaudel M, Lereim RR, Barsnes H, Myhr KM, et al. In-depth cerebrospinal fluid quantitative proteome and deglycoproteome analysis: presenting a comprehensive picture of pathways and processes affected by multiple sclerosis. Journal of Proteome Research. 2017;16:179-194.

Kuchibhotla KV, Lattarulo CR, Hyman BT, Bacskai BJ. Synchronous hyperactivity and intercellular calcium waves in astrocytes in Alzheimer mice. Science. 2009;323:1211-1215.

Kurtzke JF. Rating neurologic impairment in multiple sclerosis: an expanded disability status scale (EDSS). Neurology. 1983;33:1444-1452.

Kutzelnigg A, Lucchinetti CF, Stadelmann C, Bruck W, Rauschka H, Bergmann M, et al. Cortical demyelination and diffuse white matter injury in multiple sclerosis. Brain. 2005;128:2705-2712.

Lassmann H. Multiple sclerosis: lessons from molecular neuropathology. Experimental Neurology. 2014;262 Pt A:2-7.

Lassmann H. Multiple sclerosis pathology. Cold Spring Harbor Perspectives in Medicine. 2018;8.

Lavrnja I, Smiljanic K, Savic D, Mladenovic-Djordjevic A, Tesovic K, Kanazir S, et al. Expression profiles of cholesterol metabolism-related genes are altered during development of experimental autoimmune encephalomyelitis in the rat spinal cord. Scientific Reports. 2017;7:2702.

Lee DH, Rotger C, Appeldoorn CC, Reijerkerk A, Gladdines W, Gaillard PJ, et al. Glutathione PEGylated liposomal methylprednisolone (2B3-201) attenuates CNS inflammation and degeneration in murine

myelin oligodendrocyte glycoprotein induced experimental autoimmune encephalomyelitis. Journal of Neuroimmunology. 2014;274:96-101.

Lee S, Park JY, Lee WH, Kim H, Park HC, Mori K, et al. Lipocalin-2 is an autocrine mediator of reactive astrocytosis. Journal of Neuroscience. 2009;29:234-249.

Lee SC, Moore GR, Golenwsky G, Raine CS. Multiple sclerosis: a role for astroglia in active demyelination suggested by class II MHC expression and ultrastructural study. Journal of Neuropathology and Experimental Neurology. 1990;49:122-136.

Lee SJ, Benveniste EN. Adhesion molecule expression and regulation on cells of the central nervous system. Journal of Neuroimmunology. 1999;98:77-88.

Lepennetier G, Hracsko Z, Unger M, Van Griensven M, Grummel V, Krumbholz M, et al. Cytokine and immune cell profiling in the cerebrospinal fluid of patients with neuro-inflammatory diseases. Journal of Neuroinflammation. 2019;16:219.

Li H, Xie Y, Zhang N, Yu Y, Zhang Q, Ding S. Disruption of IP(3)R2-mediated Ca(2)(+) signaling pathway in astrocytes ameliorates neuronal death and brain damage while reducing behavioral deficits after focal ischemic stroke. Cell Calcium. 2015;58:565-576.

Li QQ, Bever CT. Glatiramer acetate blocks interleukin-1-dependent nuclear factor-kappaB activation and RANTES expression in human U-251 MG astroglial cells. Brain Research: Molecular Brain Research. 2001;87:48-60.

Li QQ, Burt DR, Bever CT. Glatiramer acetate inhibition of tumor necrosis factor-alpha-induced RANTES expression and release from U-251 MG human astrocytic cells. Journal of Neurochemistry. 2001;77:1208-1217.

Li YF, Zhang SX, Ma XW, Xue YL, Gao C, Li XY. Levels of peripheral Th17 cells and serum Th17-related cytokines in patients with multiple sclerosis: a meta-analysis. Multiple Sclerosis and Related Disorders. 2017;18:20-25.

Liddelow SA, Barres BA. Reactive astrocytes: production, function, and therapeutic potential. Immunity. 2017;46:957-967.

Liddelow SA, Guttenplan KA, Clarke LE, Bennett FC, Bohlen CJ, Schirmer L, et al. Neurotoxic reactive astrocytes are induced by activated microglia. Nature. 2017;541:481-487.

Liedtke W, Edelmann W, Chiu FC, Kucherlapati R, Raine CS. Experimental autoimmune encephalomyelitis in mice lacking glial fibrillary acidic protein is characterized by a more severe clinical course and an infiltrative central nervous system lesion. The American Journal of Pathology. 1998;152:251-259.

Lin SX, Lisi L, Dello Russo C, Polak PE, Sharp A, Weinberg G, et al. The anti-inflammatory effects of dimethyl fumarate in astrocytes involve glutathione and haem oxygenase-1. ASN Neuro. 2011;3.

Lindblom RP, Aeinehband S, Strom M, Al Nimer F, Sandholm K, Khademi M, et al. Complement receptor 2 is increased in cerebrospinal fluid of multiple sclerosis patients and regulates C3 function. Clinical Immunology. 2016;166-167:89-95.

Linker RA, Gold R. Dimethyl fumarate for treatment of multiple sclerosis: mechanism of action, effectiveness, and side effects. Current Neurology and Neuroscience Reports. 2013;13:394.

Linker RA, Lee DH, Demir S, Wiese S, Kruse N, Siglienti I, et al. Functional role of brain-derived neurotrophic factor in neuroprotective autoimmunity: therapeutic implications in a model of multiple sclerosis. Brain. 2010;133:2248-2263.

Linker RA, Lee DH, Ryan S, van Dam AM, Conrad R, Bista P, et al. Fumaric acid esters exert neuroprotective effects in neuroinflammation via activation of the Nrf2 antioxidant pathway. Brain. 2011;134:678-692.

Liu X, Zhang Q, Wang W, Zuo D, Wang J, Zhou F, et al. Analysis of Long Noncoding RNA and mRNA expression profiles in IL-9-activated astrocytes and EAE mice. Cellular Physiology and Biochemistry. 2018;45:1986-1998.

Lock C, Hermans G, Pedotti R, Brendolan A, Schadt E, Garren H, et al. Gene-microarray analysis of multiple sclerosis lesions yields new targets validated in autoimmune encephalomyelitis. Nature Medicine. 2002;8:500-508.

Lopes Pinheiro MA, Kooij G, Mizee MR, Kamermans A, Enzmann G, Lyck R, et al. Immune cell trafficking across the barriers of the central nervous system in multiple sclerosis and stroke. Biochimica et Biophysica Acta. 2016;1862:461-471.

Lovatt D, Sonnewald U, Waagepetersen HS, Schousboe A, He W, Lin JH, et al. The transcriptome and metabolic gene signature of protoplasmic astrocytes in the adult murine cortex. Journal of Neuroscience. 2007;27:12255-12266.

Lubina-Dabrowska N, Stepien A, Sulkowski G, Dabrowska-Bouta B, Langfort J, Chalimoniuk M. Effects of IFN-beta1a and IFN-beta1b treatment on the expression of cytokines, inducible NOS (NOS type II), and myelin proteins in animal model of multiple sclerosis. Archivum Immunologiae et Therapiae Experimentalis. 2017;65:325-338.

Lucchinetti CF, Parisi J, Bruck W. The pathology of multiple sclerosis. Neurologic Clinics. 2005;23:77-105.

Ludwin SK, Rao V, Moore CS, Antel JP. Astrocytes in multiple sclerosis. Multiple Sclerosis. 2016;22:1114-1124.

Luo J, Ho P, Steinman L, Wyss-Coray T. Bioluminescence in vivo imaging of autoimmune encephalomyelitis predicts disease. Journal of Neuroinflammation. 2008;5:6.

Lutz NW, Viola A, Malikova I, Confort-Gouny S, Audoin B, Ranjeva JP, et al. Inflammatory multiple-sclerosis plaques generate characteristic metabolic profiles in cerebrospinal fluid. PloS One. 2007;2:e595.

Lycke J, Zetterberg H. The role of blood and CSF biomarkers in the evaluation of new treatments against multiple sclerosis. Expert Review of Clinical Immunology. 2017;13:1143-1153.

Maimone D, Gregory S, Arnason BG, Reder AT. Cytokine levels in the cerebrospinal fluid and serum of patients with multiple sclerosis. Journal of Neuroimmunology. 1991;32:67-74.

Malmestrom C, Andersson BA, Haghighi S, Lycke J. IL-6 and CCL2 levels in CSF are associated with the clinical course of MS: implications for their possible immunopathogenic roles. Journal of Neuroimmunology. 2006;175:176-182.

Maragakis NJ, Rothstein JD. Mechanisms of Disease: astrocytes in neurodegenerative disease. Nature Clinical Practice: Neurology. 2006;2:679-689.

Marques F, Mesquita SD, Sousa JC, Coppola G, Gao F, Geschwind DH, et al. Lipocalin 2 is present in the EAE brain and is modulated by natalizumab. Frontiers in Cellular Neuroscience. 2012;6:33.

Marques F, Rodrigues AJ, Sousa JC, Coppola G, Geschwind DH, Sousa N, et al. Lipocalin 2 is a choroid plexus acute-phase protein. Journal of Cerebral Blood Flow and Metabolism. 2008;28:450-455.

Marques KB, Scorisa JM, Zanon R, Freria CM, Santos LM, Damasceno BP, et al. The immunomodulator glatiramer acetate influences spinal motoneuron plasticity during the course of multiple sclerosis in an animal model. Brazilian Journal of Medical and Biological Research. 2009;42:179-188.

Marrie RA. Comorbidity in multiple sclerosis: implications for patient care. Nature Reviews: Neurology. 2017;13:375-382.

Martinez MA, Olsson B, Bau L, Matas E, Cobo Calvo A, Andreasson U, et al. Glial and neuronal markers in cerebrospinal fluid predict progression in multiple sclerosis. Multiple Sclerosis. 2015;21:550-561.

Mastronardi FG, Min W, Wang H, Winer S, Dosch M, Boggs JM, et al. Attenuation of experimental autoimmune encephalomyelitis and nonimmune demyelination by IFN-beta plus vitamin B12: treatment to modify notch-1/sonic hedgehog balance. Journal of Immunology. 2004;172:6418-6426.

Masvekar R, Wu T, Kosa P, Barbour C, Fossati V, Bielekova B. Cerebrospinal fluid biomarkers link toxic astrogliosis and microglial activation to multiple sclerosis severity. Multiple Sclerosis and Related Disorders. 2019;28:34-43.

Matsumoto Y, Watanabe S, Suh YH, Yamamoto T. Effects of intrahippocampal CT105, a carboxyl terminal fragment of beta-amyloid precursor protein, alone/with inflammatory cytokines on working memory in rats. Journal of Neurochemistry. 2002;82:234-239.

Mattioli F, Stampatori C, Bellomi F, Scarpazza C, Capra R. Natalizumab significantly improves cognitive impairment over three years in MS: pattern of disability progression and preliminary MRI findings. PloS One. 2015;10:e0131803.

Mattioli F, Stampatori C, Capra R. The effect of natalizumab on cognitive function in patients with relapsing-remitting multiple sclerosis: preliminary results of a 1-year follow-up study. Neurological Sciences. 2011;32:83-88.

Micera A, Vigneti E, Aloe L. Changes of NGF presence in nonneuronal cells in response to experimental allergic encephalomyelitis in Lewis rats. Experimental Neurology. 1998;154:41-46.

Miljkovic D, Blazevski J, Petkovic F, Djedovic N, Momcilovic M, Stanisavljevic S, et al. A comparative analysis of multiple sclerosis-relevant anti-inflammatory properties of ethyl pyruvate and dimethyl fumarate. Journal of Immunology. 2015;194:2493-2503.

Miljkovic D, Timotijevic G, Mostarica Stojkovic M. Astrocytes in the tempest of multiple sclerosis. FEBS Letters. 2011;585:3781-3788.

Mills Ko E, Ma JH, Guo F, Miers L, Lee E, Bannerman P, et al. Deletion of astroglial CXCL10 delays clinical onset but does not affect progressive axon loss in a murine autoimmune multiple sclerosis model. Journal of Neuroinflammation. 2014;11:105.

Miyagishi R, Kikuchi S, Takayama C, Inoue Y, Tashiro K. Identification of cell types producing RANTES, MIP-1 alpha and MIP-1 beta in rat experimental autoimmune encephalomyelitis by in situ hybridization. Journal of Neuroimmunology. 1997;77:17-26.

Mizee MR, Nijland PG, van der Pol SM, Drexhage JA, van Het Hof B, Mebius R, et al. Astrocyte-derived retinoic acid: a novel regulator of blood-brain barrier function in multiple sclerosis. Acta Neuropathologica. 2014;128:691-703.

Moreno M, Bannerman P, Ma J, Guo F, Miers L, Soulika AM, et al. Conditional ablation of astroglial CCL2 suppresses CNS accumulation of M1 macrophages and preserves axons in mice with MOG peptide EAE. Journal of Neuroscience. 2014;34:8175-8185.

Moriguchi K, Miyamoto K, Fukumoto Y, Kusunoki S. 4-Aminopyridine ameliorates relapsing remitting experimental autoimmune encephalomyelitis in SJL/J mice. Journal of Neuroimmunology. 2018;323:131-135.

Mossakowski AA, Pohlan J, Bremer D, Lindquist R, Millward JM, Bock M, et al. Tracking CNS and systemic sources of oxidative stress during the course of chronic neuroinflammation. Acta Neuropathologica. 2015;130:799-814.

Muckschel M, Beste C, Ziemssen T. Immunomodulatory treatments and cognition in MS. Acta Neurologica Scandinavica. 2016;134 Suppl 200:55-59.

Mueller AM, Pedre X, Stempfl T, Kleiter I, Couillard-Despres S, Aigner L, et al. Novel role for SLPI in MOG-induced EAE revealed by spinal cord expression analysis. Journal of Neuroinflammation. 2008;5:20.

Munji RN, Soung AL, Weiner GA, Sohet F, Semple BD, Trivedi A, et al. Profiling the mouse brain endothelial transcriptome in health and disease models reveals a core blood-brain barrier dysfunction module. Nature Neuroscience. 2019;22:1892-1902.

Musella A, Mandolesi G, Mori F, Gentile A, Centonze D. Linking synaptopathy and gray matter damage in multiple sclerosis. Multiple Sclerosis. 2016;22:146-149.

Mycko MP, Papoian R, Boschert U, Raine CS, Selmaj KW. cDNA microarray analysis in multiple sclerosis lesions: detection of genes associated with disease activity. Brain. 2003;126:1048-1057.

Myers KJ, Dougherty JP, Ron Y. In vivo antigen presentation by both brain parenchymal cells and hematopoietically derived cells during the induction of experimental autoimmune encephalomyelitis. Journal of Immunology. 1993;151:2252-2260.

Myhr KM, Mellgren SI. Corticosteroids in the treatment of multiple sclerosis. Acta neurologica Scandinavica Supplementum. 2009:73-80.

Nair A, Frederick TJ, Miller SD. Astrocytes in multiple sclerosis: a product of their environment. Cellular and Molecular Life Sciences. 2008;65:2702-2720.

Nam Y, Kim JH, Seo M, Kim JH, Jin M, Jeon S, et al. Lipocalin-2 protein deficiency ameliorates experimental autoimmune encephalomyelitis: the pathogenic role of lipocalin-2 in the central nervous system and peripheral lymphoid tissues. Journal of Biological Chemistry. 2014;289:16773-16789.

Nataf S, Davoust N, Barnum SR. Kinetics of anaphylatoxin C5a receptor expression during experimental allergic encephalomyelitis. Journal of Neuroimmunology. 1998;91:147-155.

Navikas V, Link J, Palasik W, Soderstrom M, Fredrikson S, Olsson T, et al. Increased mRNA expression of IL-10 in mononuclear cells in multiple sclerosis and optic neuritis. Scandinavian Journal of Immunology. 1995;41:171-178.

Nedergaard M, Rodriguez JJ, Verkhratsky A. Glial calcium and diseases of the nervous system. Cell Calcium. 2010;47:140-149.

Nicholas R, Rashid W. Multiple sclerosis. American Family Physician. 2013;87:712-714.

Nicot A, Ratnakar PV, Ron Y, Chen CC, Elkabes S. Regulation of gene expression in experimental autoimmune encephalomyelitis indicates early neuronal dysfunction. Brain. 2003;126:398-412.

Nikcevich KM, Gordon KB, Tan L, Hurst SD, Kroepfl JF, Gardinier M, et al. IFN-gamma-activated primary murine astrocytes express B7 costimulatory molecules and prime naive antigen-specific T cells. Journal of Immunology. 1997;158:614-621.

Noseworthy JH, Lucchinetti C, Rodriguez M, Weinshenker BG. Multiple sclerosis. The New England Journal of Medicine. 2000;343:938-952.

Nylander A, Hafler DA. Multiple sclerosis. Journal of Clinical Investigation. 2012;122:1180-1188.

O'Connor KC, Appel H, Bregoli L, Call ME, Catz I, Chan JA, et al. Antibodies from inflamed central nervous system tissue recognize myelin oligodendrocyte glycoprotein. Journal of Immunology. 2005;175:1974-1982.

Okubo Y, Kanemaru K, Suzuki J, Kobayashi K, Hirose K, Iino M. Inositol 1,4,5-trisphosphate receptor type 2-independent Ca(2+) release from the endoplasmic reticulum in astrocytes. Glia. 2019;67:113-124.

Olesen J, Gustavsson A, Svensson M, Wittchen HU, Jonsson B, group Cs, et al. The economic cost of brain disorders in Europe. European Journal of Neurology. 2012;19:155-162.

Opdenakker G, Proost P, Van Damme J. Microbiomic and posttranslational modifications as preludes to autoimmune diseases. Trends in Molecular Medicine. 2016;22:746-757.

Ortiz GG, Pacheco-Moises FP, Macias-Islas MA, Flores-Alvarado LJ, Mireles-Ramirez MA, Gonzalez-Renovato ED, et al. Role of the blood-brain barrier in multiple sclerosis. Archives of Medical Research. 2014;45:687-697.

Pagenstecher A, Stalder AK, Kincaid CL, Shapiro SD, Campbell IL. Differential expression of matrix metalloproteinase and tissue inhibitor of matrix metalloproteinase genes in the mouse central nervous system in normal and inflammatory states. The American Journal of Pathology. 1998;152:729-741.

Park C, Ponath G, Levine-Ritterman M, Bull E, Swanson EC, De Jager PL, et al. The landscape of myeloid and astrocyte phenotypes in acute multiple sclerosis lesions. Acta Neuropathologica Communications. 2019;7:130.

Paul A, Comabella M, Gandhi R. Biomarkers in multiple sclerosis. Cold Spring Harbor Perspectives in Medicine. 2019;9.

Paul D, Ge S, Lemire Y, Jellison ER, Serwanski DR, Ruddle NH, et al. Cell-selective knockout and 3D confocal image analysis reveals separate roles for astrocyte-and endothelial-derived CCL2 in neuroinflammation. Journal of Neuroinflammation. 2014;11:10.

Pekny M, Nilsson M. Astrocyte activation and reactive gliosis. Glia. 2005;50:427-434.

Pekny M, Pekna M. Reactive gliosis in the pathogenesis of CNS diseases. Biochimica et Biophysica Acta. 2016;1862:483-491.

Petravicz J, Fiacco TA, McCarthy KD. Loss of IP3 receptor-dependent Ca2+ increases in hippocampal astrocytes does not affect baseline CA1 pyramidal neuron synaptic activity. Journal of Neuroscience. 2008;28:4967-4973.

Petzold A, Eikelenboom MJ, Gveric D, Keir G, Chapman M, Lazeron RH, et al. Markers for different glial cell responses in multiple sclerosis: clinical and pathological correlations. Brain. 2002;125:1462-1473.

Pitt D, Werner P, Raine CS. Glutamate excitotoxicity in a model of multiple sclerosis. Nature Medicine. 2000;6:67-70.

Planas R, Santos R, Tomas-Ojer P, Cruciani C, Lutterotti A, Faigle W, et al. GDP-l-fucose synthase is a CD4(+) T cell-specific autoantigen in DRB3*02:02 patients with multiple sclerosis. Science Translational Medicine. 2018;10.

Ponath G, Park C, Pitt D. The role of astrocytes in multiple sclerosis. Frontiers in Immunology. 2018;9:217.

Popescu BF, Pirko I, Lucchinetti CF. Pathology of multiple sclerosis: where do we stand? Continuum (Minneap Minn). 2013;19:901-921.

Prat A, Biernacki K, Wosik K, Antel JP. Glial cell influence on the human blood-brain barrier. Glia. 2001;36:145-155.

Proescholdt MA, Jacobson S, Tresser N, Oldfield EH, Merrill MJ. Vascular endothelial growth factor is expressed in multiple sclerosis plaques and can induce inflammatory lesions in experimental allergic encephalomyelitis rats. Journal of Neuropathology and Experimental Neurology. 2002;61:914-925.

Prokopova B, Hlavacova N, Vlcek M, Penesova A, Grunnerova L, Garafova A, et al. Early cognitive impairment along with decreased stress-induced BDNF in male and female patients with newly diagnosed multiple sclerosis. Journal of Neuroimmunology. 2017;302:34-40.

Qi X, Guy J, Nick H, Valentine J, Rao N. Increase of manganese superoxide dismutase, but not of Cu/Zn-SOD, in experimental optic neuritis. Investigative Ophthalmology and Visual Science. 1997;38:1203-1212.

Rafiee Zadeh A, Askari M, Azadani NN, Ataei A, Ghadimi K, Tavoosi N, et al. Mechanism and adverse effects of multiple sclerosis drugs: a review article. Part 1. International Journal of Physiology, Pathophysiology and Pharmacology. 2019a;11:95-104.

Rafiee Zadeh A, Ghadimi K, Ataei A, Askari M, Sheikhinia N, Tavoosi N, et al. Mechanism and adverse effects of multiple sclerosis drugs: a review article. Part 2. International Journal of Physiology, Pathophysiology and Pharmacology. 2019b;11:105-114.

Rakers C, Petzold GC. Astrocytic calcium release mediates peri-infarct depolarizations in a rodent stroke model. Journal of Clinical Investigation. 2017;127:511-516.

Ramanathan M, Weinstock-Guttman B, Nguyen LT, Badgett D, Miller C, Patrick K, et al. In vivo gene expression revealed by cDNA arrays: the pattern in relapsing-remitting multiple sclerosis patients compared with normal subjects. Journal of Neuroimmunology. 2001;116:213-219.

Ransohoff RM, Hamilton TA, Tani M, Stoler MH, Shick HE, Major JA, et al. Astrocyte expression of mRNA encoding cytokines IP-10 and JE/MCP-1 in experimental autoimmune encephalomyelitis. FASEB Journal. 1993;7:592-600.

Reich DS, Lucchinetti CF, Calabresi PA. Multiple sclerosis. The New England Journal of Medicine. 2018;378:169-180.

Reichenbach N, Delekate A, Breithausen B, Keppler K, Poll S, Schulte T, et al. P2Y1 receptor blockade normalizes network dysfunction and cognition in an Alzheimer's disease model. Journal of Experimental Medicine. 2018;215:1649-1663.

Reiman R, Campos Torres A, Martin BK, Ting JP, Campbell IL, Barnum SR. Expression of C5a in the brain does not exacerbate experimental autoimmune encephalomyelitis. Neuroscience Letters. 2005;390:134-138.

Rejdak K, Petzold A, Kocki T, Kurzepa J, Grieb P, Turski WA, et al. Astrocytic activation in relation to inflammatory markers during clinical exacerbation of relapsing-remitting multiple sclerosis. Journal of Neural Transmission. 2007;114:1011-1015.

Rojas M, Restrepo-Jimenez P, Monsalve DM, Pacheco Y, Acosta-Ampudia Y, Ramirez-Santana C, et al. Molecular mimicry and autoimmunity. Journal of Autoimmunity. 2018;95:100-123.

Rosenling T, Stoop MP, Attali A, van Aken H, Suidgeest E, Christin C, et al. Profiling and identification of cerebrospinal fluid proteins in a rat EAE model of multiple sclerosis. Journal of Proteome Research. 2012;11:2048-2060.

Rossi S, Motta C, Studer V, Barbieri F, Buttari F, Bergami A, et al. Tumor necrosis factor is elevated in progressive multiple sclerosis and causes excitotoxic neurodegeneration. Multiple Sclerosis. 2014;20:304-312.

Rothhammer V, Borucki DM, Tjon EC, Takenaka MC, Chao CC, Ardura-Fabregat A, et al. Microglial control of astrocytes in response to microbial metabolites. Nature. 2018;557:724-728.

Rothhammer V, Kenison JE, Tjon E, Takenaka MC, de Lima KA, Borucki DM, et al. Sphingosine 1-phosphate receptor modulation suppresses pathogenic astrocyte activation and chronic progressive CNS inflammation. Proceedings of the National Academy of Sciences of the United States of America. 2017;114:2012-2017.

Rothhammer V, Mascanfroni ID, Bunse L, Takenaka MC, Kenison JE, Mayo L, et al. Type I interferons and microbial metabolites of tryptophan modulate astrocyte activity and central nervous system inflammation via the aryl hydrocarbon receptor. Nature Medicine. 2016;22:586-597.

Rungta RL, Bernier LP, Dissing-Olesen L, Groten CJ, LeDue JM, Ko R, et al. Ca(2+) transients in astrocyte fine processes occur via Ca(2+) influx in the adult mouse hippocampus. Glia. 2016;64:2093-2103.

Sa MJ, Kobelt G, Berg J, Capsa D, Dalen J, European Multiple Sclerosis P. New insights into the burden and costs of multiple sclerosis in Europe: results for Portugal. Multiple Sclerosis. 2017;23:143-154.

Sabatino JJ, Jr., Probstel AK, Zamvil SS. B cells in autoimmune and neurodegenerative central nervous system diseases. Nature Reviews Neuroscience. 2019;20:728-745.

Salmen A, Gold R. Mode of action and clinical studies with fumarates in multiple sclerosis. Experimental Neurology. 2014;262 Pt A:52-56.

Santello M, Toni N, Volterra A. Astrocyte function from information processing to cognition and cognitive impairment. Nature Neuroscience. 2019;22:154-166.

Satoh JI, Tabunoki H, Yamamura T. Molecular network of the comprehensive multiple sclerosis brain-lesion proteome. Multiple Sclerosis. 2009;15:531-541.

Scannevin RH, Chollate S, Jung MY, Shackett M, Patel H, Bista P, et al. Fumarates promote cytoprotection of central nervous system cells against oxidative stress via the nuclear factor (erythroid-derived 2)-like 2 pathway. Journal of Pharmacology and Experimental Therapeutics. 2012;341:274-284.

Scemes E, Giaume C. Astrocyte calcium waves: what they are and what they do. Glia. 2006;54:716-725.

Schilling S, Goelz S, Linker R, Luehder F, Gold R. Fumaric acid esters are effective in chronic experimental autoimmune encephalomyelitis and suppress macrophage infiltration. Clinical and Experimental Immunology. 2006;145:101-107.

Schirmer L, Velmeshev D, Holmqvist S, Kaufmann M, Werneburg S, Jung D, et al. Neuronal vulnerability and multilineage diversity in multiple sclerosis. Nature. 2019;573:75-82.

Schrempf W, Ziemssen T. Glatiramer acetate: mechanisms of action in multiple sclerosis. Autoimmunity Reviews. 2007;6:469-475.

Sevastou I, Pryce G, Baker D, Selwood DL. Characterisation of transcriptional changes in the spinal cord of the progressive experimental autoimmune encephalomyelitis Biozzi ABH mouse model by RNA sequencing. PloS One. 2016;11:e0157754.

Sharp AH, Nucifora FC, Jr., Blondel O, Sheppard CA, Zhang C, Snyder SH, et al. Differential cellular expression of isoforms of inositol 1,4,5-triphosphate receptors in neurons and glia in brain. Journal of Comparative Neurology. 1999;406:207-220.

Shields DC, Tyor WR, Deibler GE, Banik NL. Increased calpain expression in experimental demyelinating optic neuritis: an immunocytochemical study. Brain Research. 1998;784:299-304.

Shin T. Enhanced expression of constitutive endothelial nitric oxide synthase by astrocytes in the spinal cords of rats with experimental autoimmune encephalomyelitis. Immunological Investigations. 1999;28:381-390.

Shin T. Increased expression of neuronal nitric oxide synthase in astrocytes and macrophages in the spinal cord of Lewis rats with autoimmune encephalomyelitis. Journal of Veterinary Science. 2001;2:195-199.

Shrestha B, Ge S, Pachter JS. Resolution of central nervous system astrocytic and endothelial sources of CCL2 gene expression during evolving neuroinflammation. Fluids and Barriers of the CNS. 2014;11:6.

Simone IL, Federico F, Trojano M, Tortorella C, Liguori M, Giannini P, et al. High resolution proton MR spectroscopy of cerebrospinal fluid in MS patients. Comparison with biochemical changes in demyelinating plaques. Journal of the Neurological Sciences. 1996;144:182-190.

Smith KJ, Pyrdol J, Gauthier L, Wiley DC, Wucherpfennig KW. Crystal structure of HLA-DR2 (DRA*0101, DRB1*1501) complexed with a peptide from human myelin basic protein. Journal of Experimental Medicine. 1998;188:1511-1520.

Smith PA, Schmid C, Zurbruegg S, Jivkov M, Doelemeyer A, Theil D, et al. Fingolimod inhibits brain atrophy and promotes brain-derived neurotrophic factor in an animal model of multiple sclerosis. Journal of Neuroimmunology. 2018;318:103-113.

Sofroniew MV. Multiple roles for astrocytes as effectors of cytokines and inflammatory mediators. Neuroscientist. 2014;20:160-172.

Sofroniew MV. Astrocyte barriers to neurotoxic inflammation. Nature Reviews Neuroscience. 2015;16:249-263.

Sofroniew MV, Vinters HV. Astrocytes: biology and pathology. Acta Neuropathologica. 2010;119:7-35.

Song J, Wu C, Korpos E, Zhang X, Agrawal SM, Wang Y, et al. Focal MMP-2 and MMP-9 activity at the blood-brain barrier promotes chemokine-induced leukocyte migration. Cell Reports. 2015;10:1040-1054.

Srinivasan R, Huang BS, Venugopal S, Johnston AD, Chai H, Zeng H, et al. Ca(2+) signaling in astrocytes from Ip3r2(-/-) mice in brain slices and during startle responses in vivo. Nature Neuroscience. 2015;18:708-717.

Staats KA, Humblet-Baron S, Bento-Abreu A, Scheveneels W, Nikolaou A, Deckers K, et al. Genetic ablation of IP3 receptor 2 increases cytokines and decreases survival of SOD1G93A mice. Human Molecular Genetics. 2016;25:3491-3499.

Stadelmann C, Kerschensteiner M, Misgeld T, Bruck W, Hohlfeld R, Lassmann H. BDNF and gp145trkB in multiple sclerosis brain lesions: neuroprotective interactions between immune and neuronal cells? Brain. 2002;125:75-85.

Steinman L. Multiple sclerosis: a two-stage disease. Nature Immunology. 2001;2:762-764.

Stover JF, Lowitzsch K, Kempski OS. Cerebrospinal fluid hypoxanthine, xanthine and uric acid levels may reflect glutamate-mediated excitotoxicity in different neurological diseases. Neuroscience Letters. 1997a;238:25-28.

Stover JF, Pleines UE, Morganti-Kossmann MC, Kossmann T, Lowitzsch K, Kempski OS. Neurotransmitters in cerebrospinal fluid reflect pathological activity. European Journal of Clinical Investigation. 1997b;27:1038-1043.

Stys PK, Zamponi GW, van Minnen J, Geurts JJ. Will the real multiple sclerosis please stand up? Nature Reviews Neuroscience. 2012;13:507-514.

Sunnemark D, Eltayeb S, Nilsson M, Wallstrom E, Lassmann H, Olsson T, et al. CX3CL1 (fractalkine) and CX3CR1 expression in myelin oligodendrocyte glycoprotein-induced experimental autoimmune encephalomyelitis: kinetics and cellular origin. Journal of Neuroinflammation. 2005;2:17.

Tan W, Pu Y, Shao Q, Fang X, Han D, Zhao M, et al. Insulin-like growth factor-binding protein 7 is up-regulated during EAE and inhibits the differentiation of oligodendrocyte precursor cells. Biochemical and Biophysical Research Communications. 2015;460:639-644.

Tassoni A, Farkhondeh V, Itoh Y, Itoh N, Sofroniew MV, Voskuhl RR. The astrocyte transcriptome in EAE optic neuritis shows complement activation and reveals a sex difference in astrocytic C3 expression. Scientific Reports. 2019;9:10010.

Teesalu T, Hinkkanen AE, Vaheri A. Coordinated induction of extracellular proteolysis systems during experimental autoimmune encephalomyelitis in mice. The American Journal of Pathology. 2001;159:2227-2237.

Tejera-Alhambra M, Casrouge A, de Andres C, Seyfferth A, Ramos-Medina R, Alonso B, et al. Plasma biomarkers discriminate clinical forms of multiple sclerosis. PloS One. 2015;10:e0128952.

Thompson AJ, Banwell BL, Barkhof F, Carroll WM, Coetzee T, Comi G, et al. Diagnosis of multiple sclerosis: 2017 revisions of the McDonald criteria. Lancet Neurology. 2018;17:162-173.

Tilleux S, Hermans E. Neuroinflammation and regulation of glial glutamate uptake in neurological disorders. Journal of Neuroscience Research. 2007;85:2059-2070.

Toft-Hansen H, Fuchtbauer L, Owens T. Inhibition of reactive astrocytosis in established experimental autoimmune encephalomyelitis favors infiltration by myeloid cells over T cells and enhances severity of disease. Glia. 2011;59:166-176.

Tran EH, Hardin-Pouzet H, Verge G, Owens T. Astrocytes and microglia express inducible nitric oxide synthase in mice with experimental allergic encephalomyelitis. Journal of Neuroimmunology. 1997;74:121-129.

Treumer F, Zhu K, Glaser R, Mrowietz U. Dimethylfumarate is a potent inducer of apoptosis in human T cells. Journal of Investigative Dermatology. 2003;121:1383-1388.

Ure DR, Rodriguez M. Polyreactive antibodies to glatiramer acetate promote myelin repair in murine model of demyelinating disease. FASEB Journal. 2002;16:1260-1262.

Van Doorn R, Van Horssen J, Verzijl D, Witte M, Ronken E, Van Het Hof B, et al. Sphingosine 1-phosphate receptor 1 and 3 are upregulated in multiple sclerosis lesions. Glia. 2010;58:1465-1476.

Vardjan N, Zorec R. Excitable astrocytes: Ca(2+)- and cAMP-regulated exocytosis. Neurochemical Research. 2015;40:2414-2424.

Vercellino M, Trebini C, Capello E, Mancardi GL, Giordana MT, Cavalla P. Inflammatory responses in multiple sclerosis normal-appearing white matter and in non-immune mediated neurological conditions with wallerian axonal degeneration: a comparative study. Journal of Neuroimmunology. 2017;312:49-58.

Villarroya H, Klein C, Thillaye-Goldenberg B, Eclancher F. Distribution in ocular structures and optic pathways of immunocompetent and glial cells in an experimental allergic encephalomyelitis (EAE) relapsing model. Journal of Neuroscience Research. 2001;63:525-535.

Villarroya H, Violleau K, Ben Younes-Chennoufi A, Baumann N. Myelin-induced experimental allergic encephalomyelitis in Lewis rats: tumor necrosis factor alpha levels in serum and cerebrospinal fluid immunohistochemical expression in glial cells and macrophages of optic nerve and spinal cord. Journal of Neuroimmunology. 1996;64:55-61.

Volterra A, Liaudet N, Savtchouk I. Astrocyte Ca(2)(+) signalling: an unexpected complexity. Nature Reviews Neuroscience. 2014;15:327-335.

Volterra A, Meldolesi J. Astrocytes, from brain glue to communication elements: the revolution continues. Nature Reviews Neuroscience. 2005;6:626-640.

Voskuhl RR, Peterson RS, Song B, Ao Y, Morales LB, Tiwari-Woodruff S, et al. Reactive astrocytes form scar-like perivascular barriers to leukocytes during adaptive immune inflammation of the CNS. Journal of Neuroscience. 2009;29:11511-11522.

Wahed A. Chapter 20 - Sources of errors in immunology and serology testing. In: Dasgupta A, Sepulveda JL, editors. Accurate Results in the Clinical Laboratory (Second Edition): Elsevier; 2019. p. 329-333.

Waller R, Woodroofe MN, Wharton SB, Ince PG, Francese S, Heath PR, et al. Gene expression profiling of the astrocyte transcriptome in multiple sclerosis normal appearing white matter reveals a neuroprotective role. Journal of Neuroimmunology. 2016;299:139-146.

Wang C, Wang C, Dong H, Wu XM, Wang C, Xia F, et al. Immune-related GTPase Irgm1 exacerbates experimental auto-immune encephalomyelitis by promoting the disruption of blood-brain barrier and blood-cerebrospinal fluid barrier. Molecular Immunology. 2013a;53:43-51.

Wang D, Ayers MM, Catmull DV, Hazelwood LJ, Bernard CC, Orian JM. Astrocyte-associated axonal damage in pre-onset stages of experimental autoimmune encephalomyelitis. Glia. 2005;51:235-240.

Wang DD, Bordey A. The astrocyte odyssey. Progress in Neurobiology. 2008;86:342-367.

Wang X, Haroon F, Karray S, Martina D, Schluter D. Astrocytic Fas ligand expression is required to induce T-cell apoptosis and recovery from experimental autoimmune encephalomyelitis. European Journal of Immunology. 2013b;43:115-124.

Weinstein A, Schwid SR, Schiffer RB, McDermott MP, Giang DW, Goodman AD. Neuropsychologic status in multiple sclerosis after treatment with glatiramer. Archives of neurology. 1999;56:319-324.

Wheeler MA, Clark IC, Tjon EC, Li Z, Zandee SEJ, Couturier CP, et al. MAFG-driven astrocytes promote CNS inflammation. Nature. 2020;578:593-599.

Wheeler MA, Jaronen M, Covacu R, Zandee SEJ, Scalisi G, Rothhammer V, et al. Environmental control of astrocyte pathogenic activities in CNS inflammation. Cell. 2019;176:581-596 e518.

Wheeler MA, Quintana FJ. Regulation of astrocyte functions in multiple sclerosis. Cold Spring Harbor Perspectives in Medicine. 2019;9.

Whitney LW, Becker KG, Tresser NJ, Caballero-Ramos CI, Munson PJ, Prabhu VV, et al. Analysis of gene expression in mutiple sclerosis lesions using cDNA microarrays. Annals of Neurology. 1999;46:425-428.

Wierinckx A, Breve J, Mercier D, Schultzberg M, Drukarch B, Van Dam AM. Detoxication enzyme inducers modify cytokine production in rat mixed glial cells. Journal of Neuroimmunology. 2005;166:132-143.

Wiese S, Karus M, Faissner A. Astrocytes as a source for extracellular matrix molecules and cytokines. Frontiers in Pharmacology. 2012;3:120.

Williams A, Piaton G, Lubetzki C. Astrocytes–friends or foes in multiple sclerosis? Glia. 2007;55:1300-1312.

Wilms H, Sievers J, Rickert U, Rostami-Yazdi M, Mrowietz U, Lucius R. Dimethylfumarate inhibits microglial and astrocytic inflammation by suppressing the synthesis of nitric oxide, IL-1beta, TNF-alpha and IL-6 in an in-vitro model of brain inflammation. Journal of Neuroinflammation. 2010;7:30.

Wolburg-Buchholz K, Mack AF, Steiner E, Pfeiffer F, Engelhardt B, Wolburg H. Loss of astrocyte polarity marks blood-brain barrier impairment during experimental autoimmune encephalomyelitis. Acta Neuropathologica. 2009;118:219-233.

Wolinsky JS, Montalban X, Hauser SL, Giovannoni G, Vermersch P, Bernasconi C, et al. Evaluation of no evidence of progression or active disease (NEPAD) in patients with primary progressive multiple sclerosis in the ORATORIO trial. Annals of Neurology. 2018;84:527-536.

Wucherpfennig KW, Catz I, Hausmann S, Strominger JL, Steinman L, Warren KG. Recognition of the immunodominant myelin basic protein peptide by autoantibodies and HLA-DR2-restricted T cell clones from multiple sclerosis patients. Identity of key contact residues in the B-cell and T-cell epitopes. Journal of Clinical Investigation. 1997;100:1114-1122.

Xie AX, Petravicz J, McCarthy KD. Molecular approaches for manipulating astrocytic signaling in vivo. Frontiers in Cellular Neuroscience. 2015;9:144.

Xie L, Yang SH. Interaction of astrocytes and T cells in physiological and pathological conditions. Brain Research. 2015;1623:63-73.

Yun HM, Park KR, Kim EC, Hong JT. PRDX6 controls multiple sclerosis by suppressing inflammation and blood brain barrier disruption. Oncotarget. 2015;6:20875-20884.

Zamanian JL, Xu L, Foo LC, Nouri N, Zhou L, Giffard RG, et al. Genomic analysis of reactive astrogliosis. Journal of Neuroscience. 2012;32:6391-6410.

Zeis T, Allaman I, Gentner M, Schroder K, Tschopp J, Magistretti PJ, et al. Metabolic gene expression changes in astrocytes in multiple sclerosis cerebral cortex are indicative of immune-mediated signaling. Brain, Behavior, and Immunity. 2015;48:313-325.

Zeis T, Graumann U, Reynolds R, Schaeren-Wiemers N. Normal-appearing white matter in multiple sclerosis is in a subtle balance between inflammation and neuroprotection. Brain. 2008;131:288-303.

Zhang Y, Barres BA. Astrocyte heterogeneity: an underappreciated topic in neurobiology. Current Opinion in Neurobiology. 2010;20:588-594.

Zheng W, Talley Watts L, Holstein DM, Wewer J, Lechleiter JD. P2Y1R-initiated, IP3R-dependent stimulation of astrocyte mitochondrial metabolism reduces and partially reverses ischemic neuronal damage in mouse. Journal of Cerebral Blood Flow and Metabolism. 2013;33:600-611.

Ziemssen T, Akgun K, Bruck W. Molecular biomarkers in multiple sclerosis. Journal of Neuroinflammation. 2019;16:272.

Ziemssen T, Schrempf W. Glatiramer acetate: mechanisms of action in multiple sclerosis. International Review of Neurobiology. 2007;79:537-570.

CHAPTER 2

Sofia Pereira das Neves, Fuying Gao, Joseph DeYoung, Giovanni Coppola, João Carlos Sousa, Nuno Sousa, Joana Almeida Palha, João José Cerqueira, Fernanda Marques

Astrocytes undergo metabolic reprogramming during the onset phase of EAE

(Manuscript in preparation)

(2020)

Title

Astrocytes undergo metabolic reprogramming during the onset phase of EAE

Authors

Sofia Pereira das Neves [a,b], Fuying Gao [c], Joseph DeYoung [c], Giovanni Coppola [c], João Carlos Sousa [a,b], Nuno Sousa [a,b,d], Joana Almeida Palha [a,b], João José Cerqueira [a,b,d], Fernanda Marques [a,b]

Affiliations

[a] Life and Health Sciences Research Institute (ICVS), School of Medicine, University of Minho, Campus Gualtar, 4710-057 Braga, Portugal.

[b] ICVS/3B's – PT Government Associate Laboratory, Braga/Guimarães, Portugal.

[c] Program in Neurogenetics, Department of Neurology, David Geffen School of Medicine – University of California, Los Angeles, CA, USA.

[d] Clinical Academic Center - Braga, Braga, Portugal.

Corresponding author

Fernanda Marques (PhD), Life and Health Sciences Research Institute (ICVS), School of Medicine, University of Minho, Campus Gualtar, 4710-057 Braga, Portugal.

Phone number: +351 253 604 839

E-mail: fmarques@med.uminho.pt

Abstract

Multiple sclerosis (MS) is a chronic inflammatory disease of the central nervous system that presents a largely unknown etiopathology. The presence of reactive astrocytes in MS lesions has been described for a long time, however the role that these cells play in the pathophysiology of MS are still not fully understood. Recent transcriptomic studies have suggested that different immune-related and metabolic pathways are altered in astrocytes of experimental autoimmune encephalomyelitis (EAE) animals, a model used to study MS, in comparison to control animals. However, few information is available regarding alterations occurring in astrocytes in different disease time points. So, in this study, we performed a transcriptomic analysis of astrocytes isolated from the cerebellum of EAE animals at three different disease time points: pre-symptomatic, onset/peak and chronic phases. We observed an upregulation of genes associated with a neurotoxic astrocytic phenotype (A1 astrocytes), concomitantly with an increased expression of genes involved in several metabolic pathways, including glycolysis and tricarboxylic acid cycle (TCA) cycle, and this was more pronounced at the onset phase of disease. These results suggest that astrocytes could be undergoing metabolic reprogramming, similarly to what occurs in microglia and macrophages. Furthermore, at each disease time point we also reconstructed the morphology of cerebellum' astrocytes in non-induced controls and in EAE animals, near lesion regions and in the normal appearing white mater (NAWM). We found that near lesions astrocytes presented increased length and complexity, compared to control astrocytes, while no significant alterations were observed in the NAWM.

Introduction

The term astrogliosis has been use for a long time and was first applied to designate pronounced structural changes occurring in astrocytes in response to CNS damage and disease (Sofroniew, 2014). Some astrogliosis features are transversal to several pathologies, like upregulation of glial fibrillary acidic protein (GFAP) and cellular hypertrophy, however these alterations can occur in different degrees, varying from small to very intense changes (Sofroniew, 2014). Of interest, the presence of highly abnormal astrocytes in multiple sclerosis (MS) lesions is known for a long time, namely, hypertrophic astrocytes were found both in acute and chronic active lesions, while chronic silent lesions display astroglial scar tissue (Correale and Farez, 2015; Frohman et al., 2006; Williams et al., 2007; Wu and Alvarez, 2011). MS is a chronic inflammatory neurodegenerative disease of the central nervous system (CNS) with unknown cause and diverse pathophysiological mechanisms (Negrotto and Correale, 2017; Noseworthy, 1999; Noseworthy et al., 2000). Several studies have also shown the presence of reactive astrocytes in the experimental autoimmune encephalomyelitis (EAE) model, which is an animal model of immune-mediated demyelination (Aquino et al., 1990; Luo et al., 2008; Smith and Eng, 1987; Smith et al., 1983; Tani et al., 1996). Still, the role of astrocytes, and the alterations occurring in these cells throughout disease development are not fully understood. Previous transcriptomic studies have demonstrated variability in astrocytic gene expression among different CNS regions in response to EAE induction, at the chronic phase of disease (days 45-50 post-disease induction) (Itoh et al., 2018; Tassoni et al., 2019). Nevertheless, commonly upregulated genes are associated with immune-related pathways, like antigen presentation and interferon (IFN) signaling pathways, while cholesterol synthesis pathways were downregulated, compared with control animals (Itoh et al., 2018; Tassoni et al., 2019). Moreover, Chao and colleagues (2019) recently described that alterations in immunometabolic pathways of astrocytes contribute to a pro-inflammatory profile of these cells in EAE animals (Chao et al., 2019).

In the present work, we studied the alterations occurring in astrocytes along disease development, by looking at different disease time points, namely the pre-symptomatic, the onset (peak of disease) and chronic phases. To do so, we studied the morphology and transcriptomic profile of astrocytes from the cerebellum, a CNS region widely affected in MS and EAE (das Neves et al., 2018; Du et al., 2019; Itoh et al., 2018; MacKenzie-Graham et al., 2006; Saab et al., 2004; Schreck et al., 2018). Interestingly, at the onset phase of disease, astrocytes presented a significant overexpression of genes associated with a neurotoxic phenotype (Liddelow et al., 2017) and others involved in metabolic pathways.

Methods

Animals and EAE induction

All experiments were reviewed and approved by the Portuguese national authority for animal experimentation, Direcção Geral de Veterinária (ID: DGV9458). Animals were housed and handled in accordance with the guidelines for the care and handling of laboratory animals in the Directive 2010/63/EU of the European Parliament and the Council.

Animals were housed under specific-pathogen-free conditions and maintained under standard laboratory settings: 12 h light/dark cycles (lights on at 8 a.m.), relative humidity of 55%, temperature between 22–24°C, and fed with regular rodent chow (4RF21, Mucedola SRL) and tap water *ad libitum*.

Disease was induced in 10-weeks old female C57BL/6J mice, purchased from Charles River Laboratories (France) using a commercial kit (EK-2110; Hooke Laboratories, Lawrence, MA, USA) according to the manufacturer's instructions. Briefly, animals were immunized subcutaneously with 200 μg of myelin oligodendrocyte glycoprotein $(MOG)_{35-55}$, emulsified in complete Freund's adjuvant (CFA), at the upper and lower back. Pertussis toxin (PTX) in phosphate buffered saline (PBS) was administered intraperitoneally 2 and 24 h after immunization [136 ng of PTX per injection (lot #1006)]. Non-induced age-matched littermate females were used as controls and were injected subcutaneously with a control emulsion and PTX (CK-2110; Hooke Laboratories) at the same concentration and time points as the EAE animals. Animals were daily weighted and monitored for clinical symptoms of disease.

Disease severity was assessed daily as follows: 0 = no clinical symptoms; 0.5 = partially limp tail; 1 = paralyzed tail; 1.5 = at least one hind limb falls through consistently when the animal is placed on a wire rack; 2 = loss in coordinated movement, wobbly walk; 2.5 = dragging of hind limbs; 3 = paralysis of both hind limbs; 3.5 = hind limbs paralyzed and weakness of forelimbs; 4 = complete hind limbs paralysis and partial forelimbs paralysis; 4.5 = animal is not alert, no movement; 5 = moribund state or death. Paralyzed mice, with clinical scores above 3, were offered easier access to food and water.

For biological sample collection, groups of EAE and non-induced animals were sacrificed, at the light phase of the diurnal cycle, at day 6 post-immunization (p.i.) (pre-symptomatic phase), on the first day of a clinical score of 3 (onset/peak phase; days 9-12), and on days 20-21 p.i. (chronic phase). Animals were anesthetized with an intraperitoneal injection of ketamine hydrochloride (150 mg/kg, Imalgene 1000) plus medetomidine hydrochloride (0.3 mg/kg, Dorben). Under deep anesthesia, mice were transcardially perfused with cold 0.9% saline solution, and the brain was dissected. For histological analysis, the brain was immediately embedded in Tissue-Tek O.C.T. compound (Sakura Finetek, Japan), snap-frozen and kept frozen (-20°C) until further sectioning.

Astrocyte isolation

The cerebellum was macrodissected for astrocyte isolation using magnetic-activated cell sorting (MACS) (Holt and Olsen, 2016). Briefly, the cerebellum was mechanically dissociated using a scalpel, followed by enzymatic dissociation using the Neural Tissue Dissociation kit (P) (Miltenyi Biotec, Cologne, Germany), according to the manufacturer's instructions. Myelin and cell debris were removed using the Myelin removal kit (Miltenyi Biotec), followed by microglia removal using Cd11b microbeads (Miltenyi Biotec). Finally, astrocytes were isolated using anti-astrocyte cell surface antigen (ACSA)-2 beads (Miltenyi Biotec). All the separation steps were performed using the AutoMACS Pro Separator equipment (Miltenyi Biotec).

Gene expression analysis by RNA-sequencing

Total RNA was extracted from isolated astrocytes using the RNeasy Plus Micro kit (Qiagen, Hilden, Germany) according to the manufacturer's instructions. RNA quality and quantification were performed using the Experion RNA HighSens Analysis kit (Bio-Rad, CA, USA) according to the manufacturer's instructions.

RNA samples were sequenced at the UCLA Neuroscience Genomics Core. RNA-sequencing (RNAseq) was carried out using Nugen Ovation RNA Ultra Low Input and Kapa Hyper. The RNA samples were made into barcoded cDNA library and then sequenced at 2x75bp paired end reads output with Illumina HiSeq 4000. No read trimming or filtering was done with this dataset, because the quality distribution and variance appeared normal. Short reads were aligned using STAR to the mouse (mm10), with default parameters. Differential expression analysis was performed using observation based-model (limma-voom). Genes with counts per million (CPM) > 0.5 in at least 3 non-induced samples and adjusted p-values < 0.05 were considered statistically significant and were used for differential expression analysis. Pathway analysis was performed using the ConsensusPathDB-mouse tool (Kamburov et al., 2011; Kamburov et al., 2009). A total of three non-induced and four EAE animals were sacrificed per experimental time point for the RNAseq experiments.

Gene expression analysis by qRT-PCR

Total RNA was extracted from isolated astrocytes using the RNeasy Plus Micro kit (Qiagen, Hilden, Germany) according to the manufacturer's instructions. RNA quality and quantification were performed using the Experion RNA HighSens Analysis kit (Bio-Rad, CA, USA) according to the manufacturer's instructions. 750 pg of total RNA from each sample were reverse transcribed into cDNA using the iScript cDNA synthesis kit (Bio-Rad), according to the manufacturer's instructions. qRT-PCR was performed on

a CFX96 real-time instrument (Bio-Rad) using the SsoFast EvaGreen Supermix (Bio-Rad). For each reaction, 5 µL of reaction mix, 0.5 µL of each primer (initial concentration 10 µM), 3 µL of RNase/DNase free water and 1 µL of cDNA were used. The cycling parameters were 1 cycle at 95°C, for 1 minute (min), followed by 40 cycles at 95°C for 15 seconds (s), annealing temperature (primer specific) for 20 s and 72°C for 20 s, finishing with 1 cycle at 65°C to 95°C for 5 s (melting curve). Product fluorescence was detected at the end of the elongation cycle. All melting curves exhibited a single sharp peak at the expected temperature. *Adenosine Triphosphate subunit 5 beta* (*Atp5b*), *Heat Shock Protein 90 alpha family class B member 1* (*Hspcb*) and *TATA binding protein* (*Tbp*) were used as reference genes. Primers used to measure the expression levels of selected mRNA transcripts by qRT-PCR were designed using the Primer-BLAST tool of NCBI (Bethesda, MD, USA) on the basis of the respective GenBank accession numbers, or were used as described by Liddelow and colleagues (2017) (Liddelow et al., 2017). Primers DNA sequences and annealing temperatures are provided in Supplementary table 2. 1.

GFAP immunofluorescence and 3-dimensional reconstruction of astrocytes

Serial 20 µm sections of cerebellum were fixed in 4% paraformaldehyde in PBS for 30 min at room temperature (RT). After antigen retrieval, with pre-heated citrate buffer (Sigma-Aldrich) in the microwave for 20 min, tissue slices were permeabilized with PBS-triton 0.3% at RT for 10 min, and subsequently blocked with 10% fetal bovine serum in PBS-triton 0.3% at RT for 30 min. Slides were incubated over-night with rabbit anti-mouse GFAP antibody (1:200; Dako, Denmark), diluted in blocking solution. Afterwards, slides were incubated with Alexa Fluor® 594 donkey anti-rabbit (1:500; Fisher Technologies, Thermo Fisher Scientific), diluted in PBS-triton 0.3%, for 2 h at RT. After incubation with 4′,6-diamidino-2-phenylindole (DAPI; 1:200; Invitrogen, Thermo Fisher Scientific), for 10 min at RT, slides were cover-slipped with Immumount (Fisher Scientific, Thermo Fisher Scientific) and examined under fluorescent light.

To perform the 3-dimensional reconstruction of astrocytes, 3-4 photographs per animal were taken from the cerebellum white matter, using a confocal microscope (FV1000, Olympus) and the following parameters: 40x objective, 1024x1024 resolution, 1 µm increment. In the case of EAE animals, photographs were acquired both near lesion regions and in regions of normal appearing white matter (NAWM), except for animals at the pre-symptomatic phase which did not present lesions. The confocal images were then used to performed the morphological reconstruction using the Fiji plugin "Simple Neurite Tracer" (Longair et al., 2011; Schindelin et al., 2012), as previously described (Tavares et al., 2017). For Sholl analysis, concentric circles were superimposed on astrocytes, with origin in the cell

soma and with 4 µm distance from each other. Results are presented as the average of 4-5 animals per experimental group, and 7-8 astrocytes were reconstructed per animal.

Statistical analysis

Statistical analysis was performed using SPSS software (version 23, IBM, USA) and GraphPad Prism (version 8, La Jolla, California, USA). The number of biological replicates (n) are specified in the legend of each figure. Results are presented as mean ± standard error of the mean (SEM), or only as mean for astrocytic sholl analysis. Statistical significance was considered for $p < 0.05$ (*), $p < 0.01$ (**), $p < 0.001$ (***), $p < 0.0001$ (****). The partial eta squared value (η_p^2) was calculated as a measure of effect size (Lakens, 2013).

Results

Altered astrocytic gene expression in EAE animals

To explore the alterations occurring in astrocytes throughout disease development, we performed transcriptomic analysis, by RNAseq, in astrocytes isolated from the cerebellum at different disease time points (Figure 2. 1A). The cerebellum is known to be affected both in the human disease and in the EAE model, and ACSA-2 was shown to be highly expressed in this region (Kantzer et al., 2017). To validate the specificity of our isolation protocol, in our RNAseq data we looked for the expression levels of genes associated with different CNS cell types and with different types of immune cells (Supplementary figure 2. 1 and Supplementary table 2. 2). We confirmed that this sorting method provided a cell population enriched in astrocytes, since the majority of astrocyte and Bergmann glia associated genes were highly expressed in our samples, while the majority of genes associated with other cell types were not expressed or presented low expression values. The *ATPase Na+/K+ Transporting Subunit Beta 2* (*Atp1b2*) gene, which was identified as being the ACSA-2 epitope (Batiuk et al., 2017), also presented high expression levels.

PTX has been suggested to facilitate EAE development by increasing the BBB permeability, thereby facilitating the migration of pathogenic T cells to the CNS, among other important biological effects (Hofstetter et al., 2002; Turley and Miller, 2007). Considering that astrocytes play an important role in the maintenance of BBB permeability (Abbott et al., 2006; Allen and Barres, 2009), and that non-induced animals were also injected with PTX, we also sacrificed a group of non-induced animals at each of the experimental time points. In fact, we observed that several astrocytic genes were significantly altered in non-induced animals, when comparing the animals of the three experimental time points (Supplementary figure 2. 2A).

Next, we compared gene expression values between EAE and non-induced animals, for each time point analyzed, and observed a total of 804 genes significantly altered at the pre-symptomatic phase, 470 genes altered at the onset phase and 296 genes altered at the chronic phase of disease (Figure 2. 1B). To explore the alterations occurring along disease development, we also compared the three EAE time points among each other (Supplementary figure 2. 2B). However, some of the differences found were also present in the comparison between time points in non-induced. For that reason, we next normalized each disease time point for the respective non-induced group, and verified which differences remained significant when comparing the EAE groups (Figure 2. 1C). Of interest, the chronic and pre-symptomatic phases of disease were more similar among each other than with the onset phase.

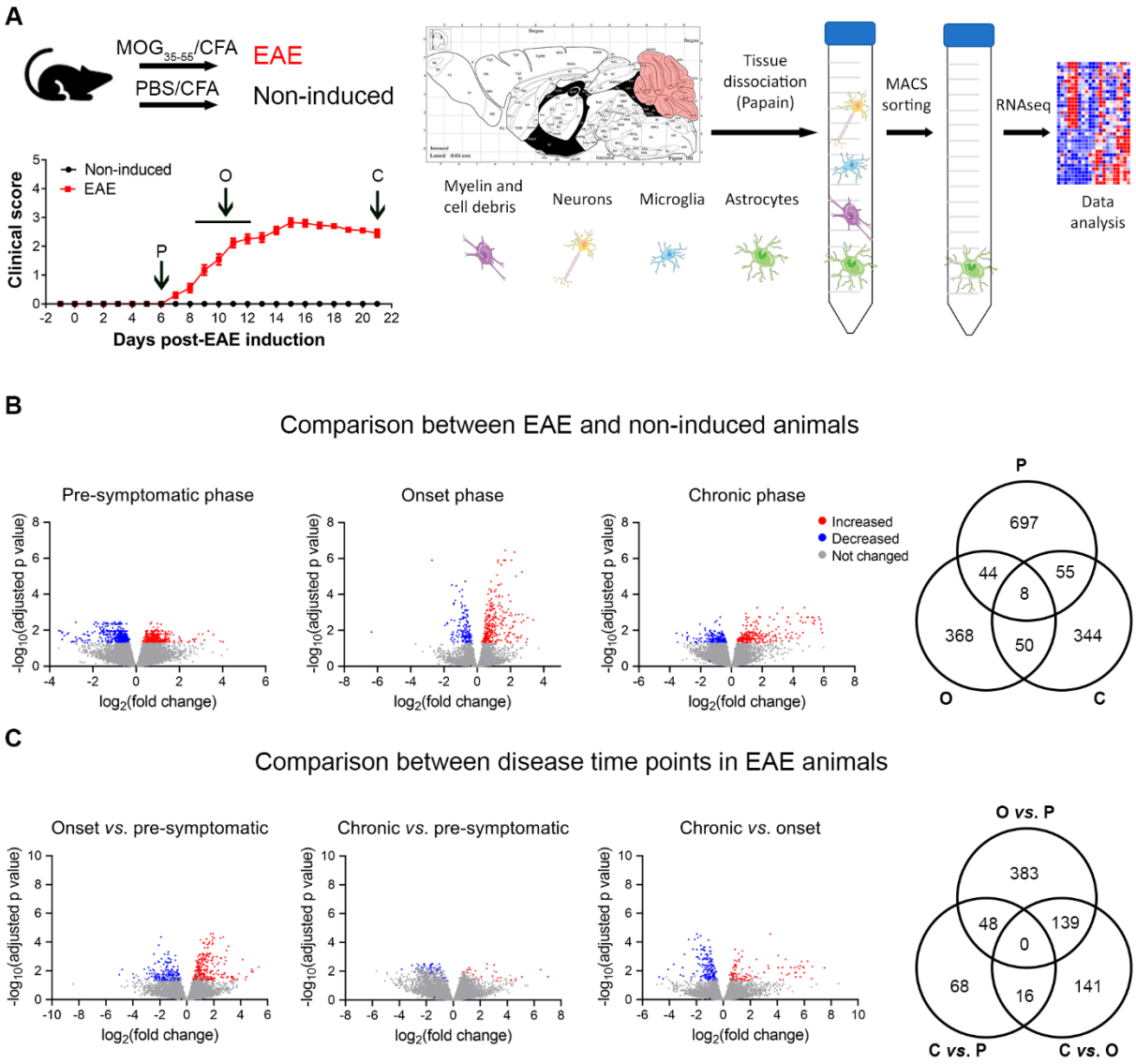

Figure 2. 1 – Sample collection for RNAseq analysis and differentially expressed genes.

(A) Schematic overview of the methodology used to isolate astrocytes from the cerebellum and posterior RNAseq analysis; average clinical score of the animals used in the study. (B) Volcano plot and Venn diagram depicting the differentially expressed astrocytic genes after comparing EAE and non-induced animals for each experimental time point. (C) Volcano plot and Venn diagram depicting the differentially expressed genes after comparison between disease time points in EAE animals, normalized for the respective non-induced group. In the Volcano plots, significant underexpessed genes are represented in blue; significant overexpressed genes are represented in red; genes whose expression was not significantly altered are represented in gray. Images obtained and adapted from Servier Medical Art. CFA – complete Freund's adjuvant; C – chronic time point; MACS – magnetic-activated cell sorting; MOG – myelin oligodendrocyte glycoprotein; O – onset time point; PBS – phosphate buffered saline; P – pre-symptomatic time point.

Over-representation pathway analysis was performed for the differentially expressed genes between EAE and non-induced animals (Figure 2. 2A-C, Supplementary table 2. 3, Supplementary table 2. 4,

Supplementary table 2. 5) and between EAE time points (Figure 2. 2D-F, Supplementary table 2. 6, Supplementary table 2. 7, Supplementary table 2. 8). Interestingly, several pathways related with extracellular matrix organization were significantly altered in EAE animals at the pre-symptomatic phase of disease, while at the onset phase, the mostly represented pathways were involved in metabolic pathways.

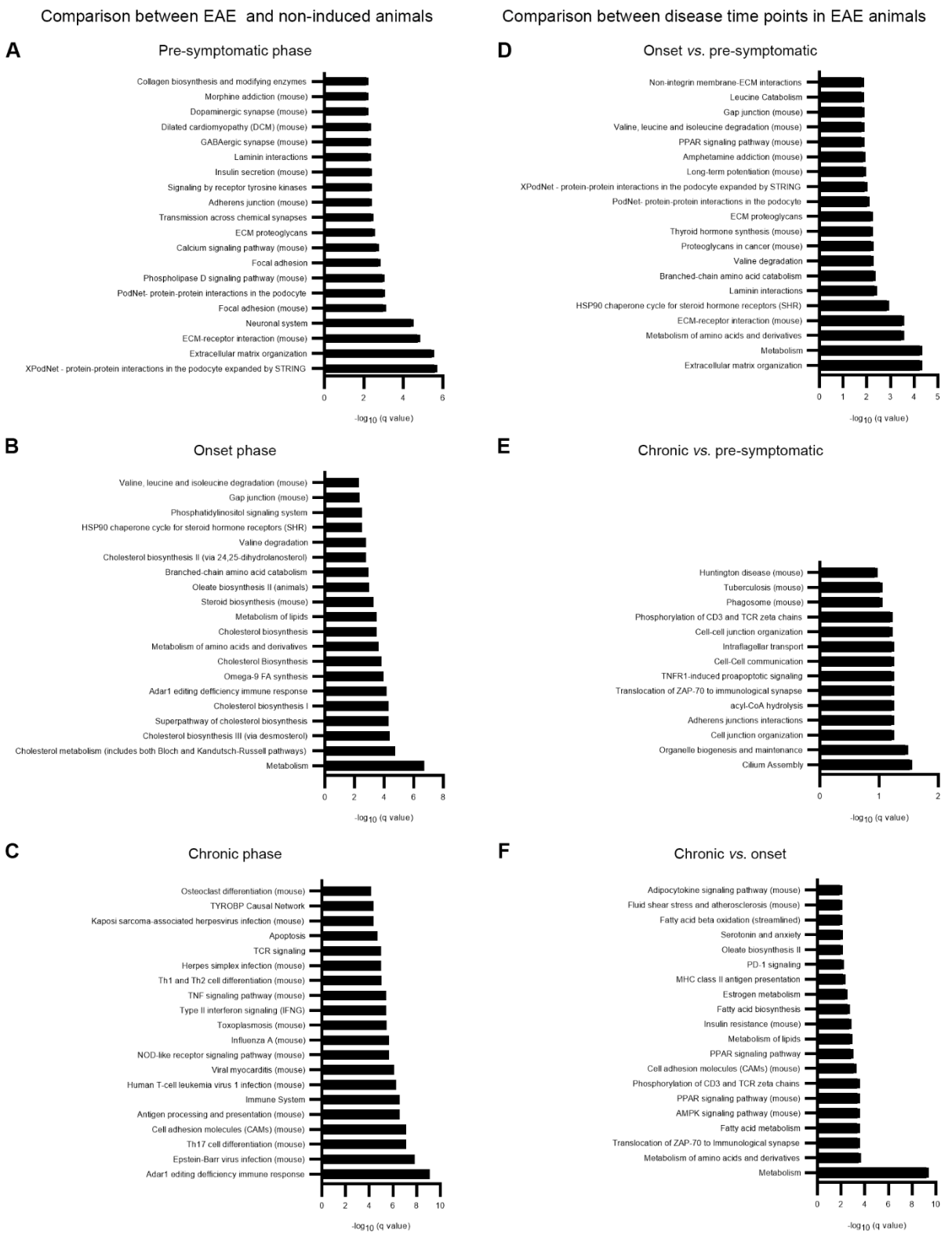

Figure 2. 2 – Pathway analysis results.

(A) Top 20 pathways altered in EAE animals at the pre-symptomatic, (B) onset and (C) chronic phases of disease, compared to non-induced animals. (D) Top 20 pathways altered at the onset *vs.* pre-symptomatic phases. (E) Top 20 pathways altered at the chronic *vs.* pre-symptomatic phases. (F) Top 20 pathways altered at the chronic *vs.* onset phases.

Astrocytic metabolic reprogramming at the onset phase of disease

As already mentioned, several metabolic pathways were significantly altered at the onset phase of disease. Among these were genes involved in glycolysis and the tricarboxylic acid cycle (TCA) cycle (Figure 2. 3A). The overexpression of some of these genes was confirmed by qRT-PCR, in a different group of animals (Figure 2. 3B. Two-Way ANOVA – between subject factors: disease and sacrifice time point. *Phosphofructokinase muscle* (*Pfkm*): disease – $F_{(1,22)} = 0.0212$, $p = 0.8854$; sacrifice time point – $F_{(2,22)} = 4.858$, $p = 0.0179$, $\eta^2 = 0.297$, Bonferroni's multiple comparison test – $p < 0.05$ for onset *vs*. chronic phase; interaction - $F_{(2,22)} = 0.4698$, $p = 0.6312$; *fructose-biphosphate aldolase C* (*Aldoc*): disease – $F_{(1,22)} = 0.3990$, $p = 0.5341$; sacrifice time point – $F_{(2,22)} = 2.832$, $p = 0.0805$; interaction - $F_{(2,22)} = 4.161$, $p = 0.0293$, $\eta^2 = 0.229$; *isocitrate dehydrogenase 3 (NAD+) gamma* (*Idh3g*): disease – $F_{(1,22)} = 6.639$, $p = 0.0172$, $\eta^2 = 0.089$; sacrifice time point – $F_{(2,22)} = 17.140$, $p < 0.0001$, $\eta^2 = 0.462$; interaction - $F_{(2,22)} = 5.664$, $p = 0.0104$, $\eta^2 = 0.153$; *succinate dehydrogenase complex subunit A flavoprotein* (*Sdha*): disease – $F_{(1,22)} = 0.9211$, $p = 0.3476$; sacrifice time point – $F_{(2,22)} = 5.358$, $p = 0.0127$, $\eta^2 = 0.309$, Bonferroni's multiple comparison test – $p < 0.05$ for onset *vs*. chronic phase; interaction - $F_{(2,22)} = 0.5214$, $p = 0.6009$).

Recently, Liddelow and colleagues (2017) characterized a population of reactive astrocytes, termed A1, induced by classically activated neuroinflammatory microglia (Liddelow et al., 2017). In our samples, we observed an overexpression of A1-specific genes in EAE animals, that was more evident at the onset phase of disease, while A2-specific genes did not present major alterations (Figure 2. 4A-B. Two-Way ANOVA – between subject factors: disease and sacrifice time point. *Fibulin 5* (*Fbln5*): disease – $F_{(1,22)} = 21.370$, $p = 0.0001$, $\eta^2 = 0.214$; sacrifice time point – $F_{(2,22)} = 12.670$, $p = 0.0002$, $\eta^2 = 0.253$; interaction - $F_{(2,22)} = 15.670$, $p < 0.0001$, $\eta^2 = 0.313$; *adhesion molecule with Ig like domain 2* (*Amigo2*): disease – $F_{(1,22)} = 15.070$, $p = 0.0008$, $\eta^2 = 0.209$; sacrifice time point – $F_{(2,22)} = 10.150$, $p = 0.0008$, $\eta^2 = 0.281$, $\eta^2 =$; interaction - $F_{(2,22)} = 7.406$, $p = 0.0035$, $\eta^2 = 0.205$; *FK506 binding protein 5* (*Fkbp5*): disease – $F_{(1,22)} = 34.860$, $p < 0.0001$, $\eta^2 = 0.326$; sacrifice time point – $F_{(2,22)} = 9.893$, $p = 0.0009$, $\eta^2 = 0.185$; interaction - $F_{(2,22)} = 15.170$, $p < 0.0001$, $\eta^2 = 0.284$).

Classically activated (M1) macrophages are characterized by an induction of aerobic glycolysis, that results in lactate production, and increased levels of TCA cycle intermediates (Galvan-Pena and O'Neill, 2014). Considering that similar metabolic alterations occur in astrocytes of EAE animals, and that these cells acquire a neurotoxic phenotype, it is possible that astrocytes could also undergo metabolic reprogramming in the EAE context.

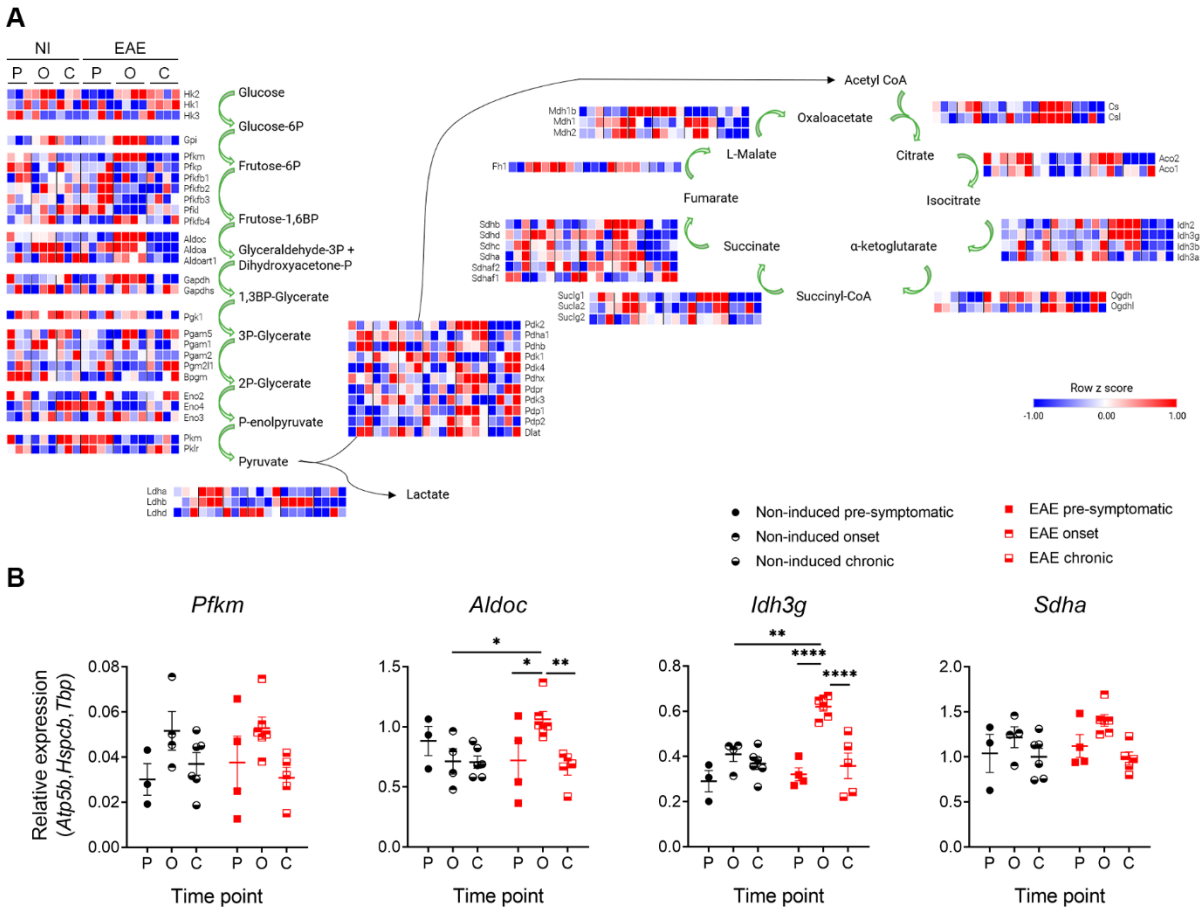

Figure 2. 3 – Increased expression of metabolic genes in astrocytes from EAE animals.

(A) Representation of the enzymes involved in glycolysis and the TCA cycle and respective RNAseq expression levels. (B) qRT-PCR expression levels of enzymes involved in glycolysis and the TCA cycle, namely *Pfkm*, *Aldoc*, *Idh3g* and *Sdha*. Data presented as mean ± SEM. n = 3-4 in (A) and n = 3-6 in (B). ** $p < 0.05$, ** $p < 0.01$, **** $p < 0.0001$. Heatmaps obtained using the Morpheus APP tool of CLUE, Broad Institute, Cambridge, MA, USA. C – chronic time point; NI – non-induced; O – onset time point; P – pre-symptomatic time point.

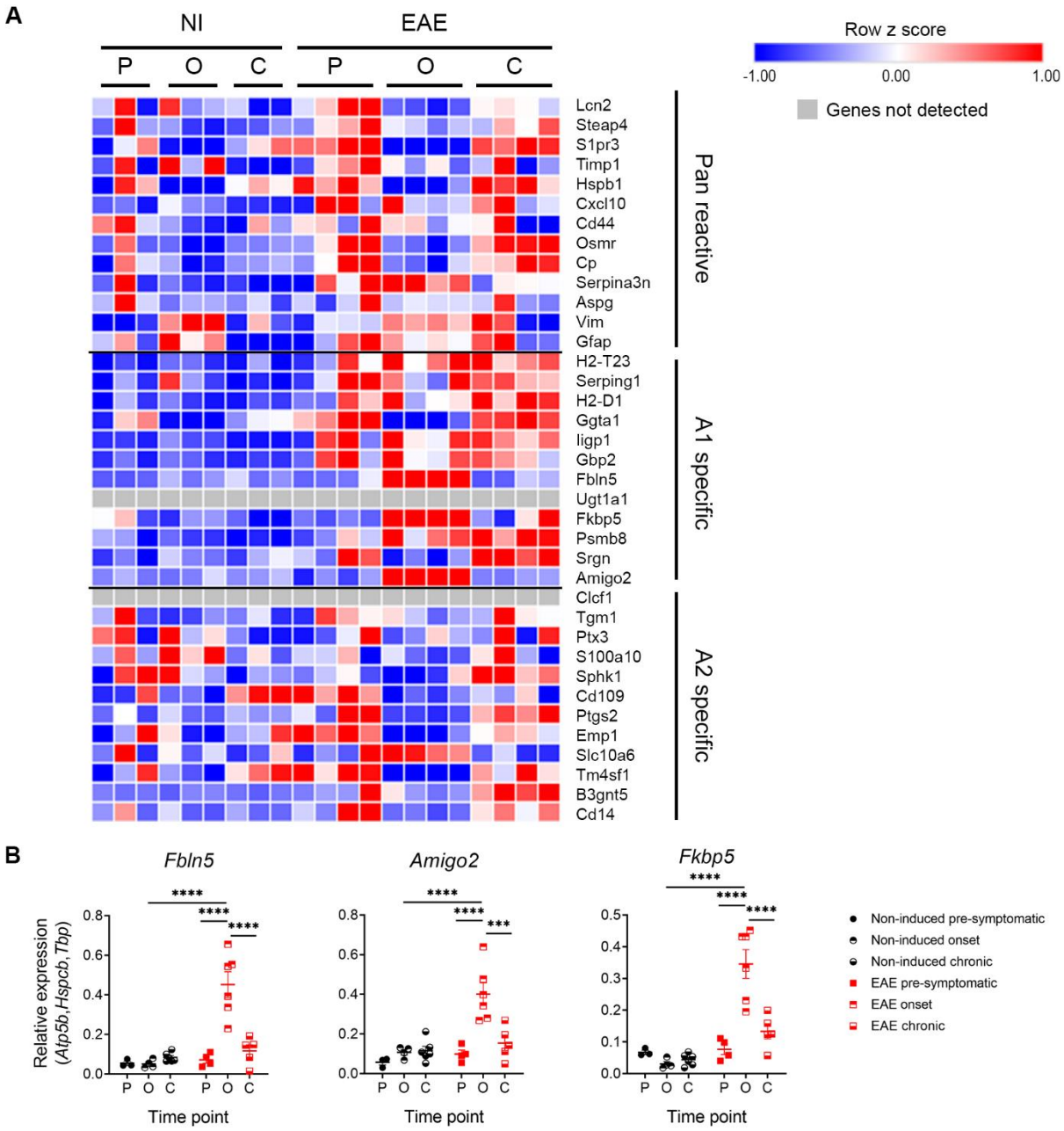

Figure 2. 4 – Astrocytes from EAE animals presented a neurotoxic phenotype.

(A) RNAseq expression levels of Pan reactive, A1 specific and A2 specific genes. (B) qRT-PCR expression levels of A1 specific genes. Data presented as mean ± SEM. n = 3-4 in (A) and n = 3-6 in (B). *** $p < 0.001$, **** $p < 0.0001$. Heatmaps obtained using the Morpheus APP tool of CLUE. C – chronic time point; NI – non-induced; O – onset time point; P – pre-symptomatic time point.

Increased astrocytic length and complexity in EAE animals near lesion regions

In EAE animals, at the onset and chronic phases, it was possible to observe focal perivascular lesions in the cerebellum white matter, absent in non-induced animals and at the pre-symptomatic phase of EAE. However, at those disease time points, animals also presented regions where the white matter appeared normal (NAWM regions). To explore the morphological alterations occurring in astrocytes after disease induction, we reconstructed their morphology in the cerebellum white matter of EAE animals, around lesion regions and also in NAWM regions, and compared them with astrocytes from non-induced animals. Figure 2. 5A shows representative images of the GFAP staining in non-induced animals, EAE animals sacrificed at the pre-symptomatic phase, and NAWM and lesion regions of EAE animals sacrificed at the onset and chronic phases. The stacked images were used to perform a 3-dimensional reconstruction of astrocytes, and the representative drawings for each experimental group are shown in Figure 2. 5B.

We started by comparing astrocytes from the NAWM of EAE animals with non-induced animals and no significant differences were observed in the total astrocytic length (Figure 2. 5C. Two-Way ANOVA – between subject factors: disease and sacrifice time point. Disease – $F_{(1,21)} = 1.158$, $p = 0.2941$; sacrifice time point – $F_{(2,21)} = 0.174$, $p = 0.8415$; interaction - $F_{(2,21)} = 0.637$, $p = 0.5389$). In addition, there were no differences in astrocytic ramification, as evaluated by the Sholl analysis, between the NAWM region of EAE animals and non-induced mice (Figure 2. 5F. Mixed ANOVA – between subject factors: disease, sacrifice time point; within subject factor: radius. Radius – $F_{(17,357)} = 354.805$, $p < 0.0001$, $\eta_p^2 = 0.944$; radius*disease interaction – $F_{(17,357)} = 1.049$, $p = 0.4034$; radius*sacrifice time point interaction – $F_{(34,357)} = 0.479$, $p = 0.9946$; radius*disease*sacrifice time point interaction – $F_{(34,357)} = 0.793$, $p = 0.7920$; disease – $F_{(1,21)} = 0.939$, $p = 0.3435$; sacrifice time point – $F_{(2,21)} = 0.159$, $p = 0.8544$; disease*sacrifice time point interaction – $F_{(2,21)} = 0.762$, $p = 0.4794$).

In lesioned areas of the EAE cerebellum, astrocytes were longer (Figure 2. 5D. Two-Way ANOVA – between subject factors: disease and sacrifice time point. Disease – $F_{(1,14)} = 9.548$, $p = 0.0080$, $\eta_p^2 = 0.405$; sacrifice time point – $F_{(1,14)} = 0.243$, $p = 0.6297$; interaction – $F_{(1,14)} = 0.149$, $p = 0.7050$), and more ramified, compared to non-induced controls (Figure 2. 5G. Mixed ANOVA – between subject factors: disease, sacrifice time point; within subject factor: radius. Radius - $F_{(15,210)} = 330.458$, $p < 0.0001$, $\eta_p^2 = 0.959$; radius*disease interaction – $F_{(15,210)} = 4.685$, $p < 0.0001$, $\eta_p^2 = 0.251$; radius*sacrifice time point interaction – $F_{(15,210)} = 0.903$, $p = 0.5613$; radius*disease*sacrifice time point interaction – $F_{(15,210)} = 1.061$, $p = 0.3949$; disease – $F_{(1,14)} = 9.201$, $p = 0.0089$, $\eta_p^2 = 0.397$; sacrifice time point – $F_{(1,14)} = 0.104$, $p = 0.7524$; disease*sacrifice time point interaction – $F_{(1,14)} = 0.490$, $p = 0.4952$).

We also observed an overall tendency for increased astrocytic length (Figure 2. 5E. Two-Way repeated measures ANOVA – between subject factor: sacrifice time point; within subject factor: cerebellum region. Cerebellum region – $F_{(1,8)} = 5.214$, $p = 0.0518$, $\eta_p^2 = 0.395$; sacrifice time point – $F_{(1,8)} = 0.182$, $p = 0.6809$; interaction – $F_{(1,8)} = 0.821$, $p = 0.3915$) and ramification, near lesion regions compared to NAWM regions (Figure 2. 5H. Mixed ANOVA – between subject factor: sacrifice time point; within subject factors: cerebellum region, radius. Cerebellum region – $F_{(1,8)} = 4.418$, $p = 0.0687$, $\eta_p^2 = 0.356$; Cerebellum region*sacrifice time point interaction – $F_{(1,8)} = 0.548$, $p = 0.4802$; radius – $F_{(17,136)} = 153.157$, $p < 0.0001$, $\eta_p^2 = 0.950$; radius*sacrifice time point interaction – $F_{(17,136)} = 0.299$, $p = 0.9969$; cerebellum region*radius interaction – $F_{(17,136)} = 2.991$, $p = 0.0002$, $\eta_p^2 = 0.272$; cerebellum region*radius*sacrifice time point interaction – $F_{(17,136)} = 1.673$, $p = 0.0550$, $\eta_p^2 = 0.173$; sacrifice time point – $F_{(1,8)} = 0.426$, $p = 0.5321$).

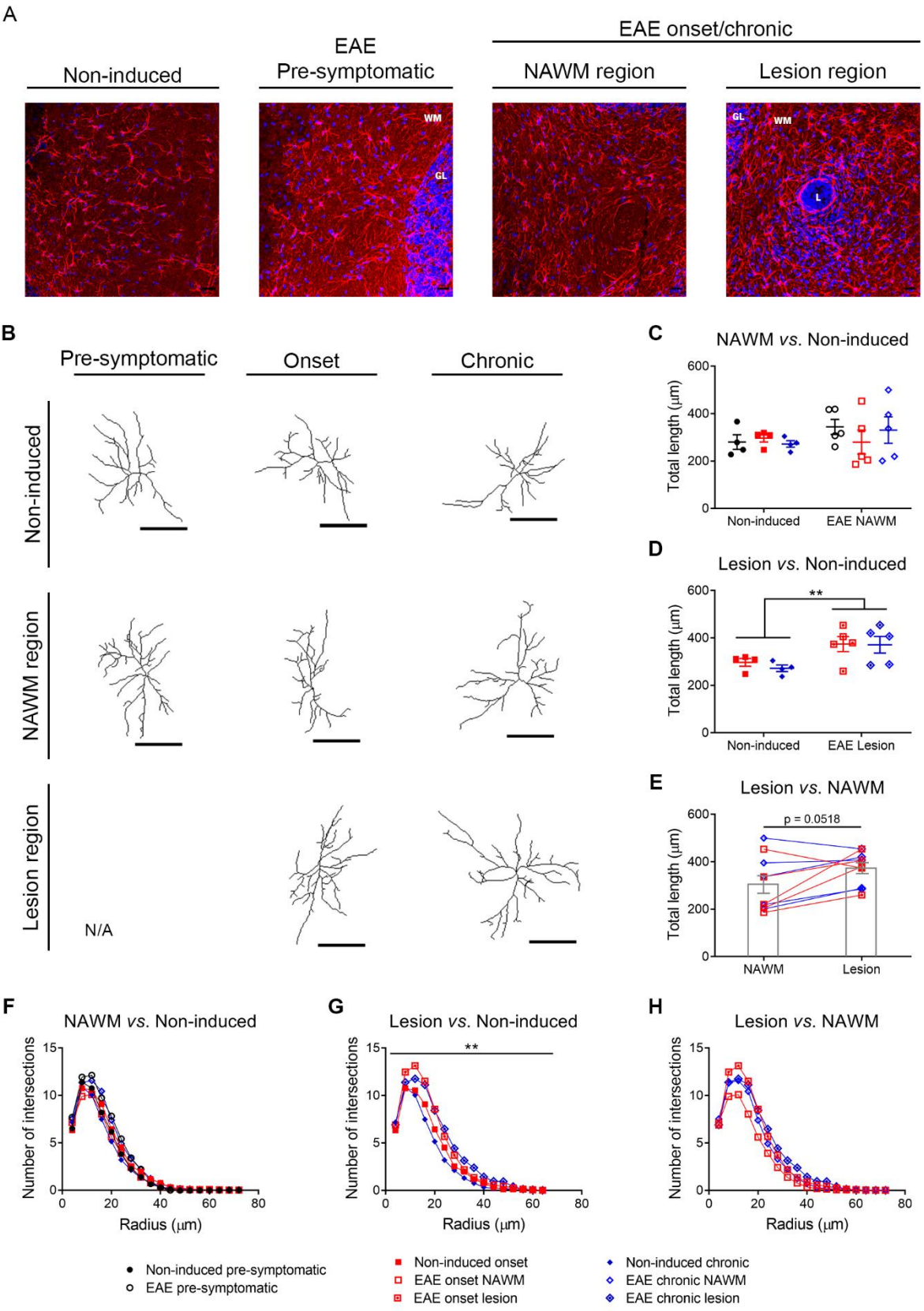

Figure 2. 6 – See next page for caption.

Figure 2. 5 – Astrocytes near lesion regions, in EAE animals, were longer and more complex compared to astrocytes from non-induced animals.

(A) Representative images of cerebellum sections from non-induced and EAE animals immunostained for GFAP (scale bar represents 20 μm). (B) Representative drawings of astrocytes reconstructed using the Simple Neurite Tracer plugin of Fiji (scale bar represents 20 μm). (C) Comparison between astrocytic total process length of non-induced and NAWM regions of EAE animals. (D) Comparison between astrocytic total process length of non-induced and lesion regions of EAE animals. (E) Comparison between total astrocytic process length of NAWM and lesion regions of EAE animals. (F) Comparison between number of intersections per radius in astrocytes from non-induced and from NAWM regions of EAE animals. (G) Comparison between number of intersections per radius in astrocytes from non-induced and from lesion regions of EAE animals. (H) Comparison between number of intersections per radius in astrocytes from NAWM and lesion regions of EAE animals. Data presented as mean ± SEM for total length or as mean for sholl analysis. n = 4-5, average of 7-8 astrocytes per animal. ** $p < 0.01$ for comparison between lesion region in EAE animals (onset and chronic phases) and non-induced groups (onset and chronic phases). GL – granular layer; L – lesion; N/A – not applicable; NAWM – normal appearing white matter; WM – white matter.

Discussion

Herein, we showed an astrocytic upregulation of glycolytic and TCA cycle regulatory genes in the MS animal model. Together with these alterations, we also detected an upregulation of genes associated with an astrocytic neurotoxic phenotype. How these metabolic alterations are linked with a pro-inflammatory and neurotoxic astrocytic phenotype and disease progression is unknown, but these results are in line with data from other fields, showing that a TCA cycle rate increase in monocytes is associated with a stronger immune response. Indeed, metabolic reprogramming is known to occur in macrophages and microglia in response to different stimuli. M1 (classically activated) macrophages/microglia are activated by bacterial-derived products, like LPS, and infection-associated signals, such as IFN gamma, and are usually part of the first line of defense of the innate immune system (Galvan-Pena and O'Neill, 2014; Orihuela et al., 2016). M1 polarized cells then produce pro-inflammatory cytokines and high levels of NO in order to kill the foreign pathogen and activate T cells to mount an adaptive immune response. A similar response can occur in the absence of microorganisms, as a result of trauma, ischemia-reperfusion injury or chemical exposure (Orihuela et al., 2016). On the other hand, M2 (alternatively activated) macrophages play an important role in the resolution phase of inflammation (Galvan-Pena and O'Neill, 2014; Orihuela et al., 2016), by producing anti-inflammatory factors that switch off pro-inflammatory cell phenotypes and re-establish homeostasis (Orihuela et al., 2016). Notably, the cells metabolic profile is a reflection of these functions. Namely, in M1 cells aerobic glycolysis is induced, to provide the cell with rapid energy, and the pentose phosphate pathway and respiratory chain functions are induced and attenuated, respectively, to increase the production of ROS and RNS (Galvan-Pena and O'Neill, 2014; Orihuela et al., 2016). M2 polarized cells need to be sustained for longer periods of time, so oxidative metabolism and fatty acid oxidation are induced (Galvan-Pena and O'Neill, 2014; Orihuela et al., 2016). Interestingly, the polarization for one of these phenotypes can be induced not only by the inflammatory factors already mentioned, but also by the modification of the cells metabolic state. Specifically, blocking oxidative metabolism drives macrophage polarization to an M1 state, while forcing it in M1 macrophages potentiates the M2 phenotype (Galvan-Pena and O'Neill, 2014).

Of relevance, astrocytes were recently classified into “A1” (neurotoxic) and “A2” (neuroprotective), in analogy to the M1/M2 macrophage nomenclature (Liddelow et al., 2017). Liddelow and colleagues (2017) showed that neuroinflammation induced an A1 phenotype, characterized by the loss of normal astrocytic functions and the gain of a neurotoxic role, which was deleterious for both neurons and oligodendrocytes. Conversely, A2 astrocytes were induced by ischemic conditions and presented a neuroprotective phenotype (Liddelow et al., 2017). Additionally, C3+ A1 astrocytes were found to be

present in demyelinating lesions of MS patients (Liddelow et al., 2017). In accordance, we observed that astrocytes isolated from the cerebellum of EAE animals presented an A1 phenotype, particularly at the onset phase of disease. Moreover, several genes involved in metabolic pathways were altered during this time point, including glycolytic and TCA cycle genes. Previous studies had also reported alterations in other metabolic pathways, namely sphingolipid metabolism and cholesterol biosynthesis, in astrocytes during EAE, which we also observed here (Chao et al., 2019; Itoh et al., 2018; Mayo et al., 2014; Mueller et al., 2008; Sevastou et al., 2016; Tassoni et al., 2019). Considering all these data, and the fact that metabolic alterations are associated with M1/M2 polarization, we hypothesize that similar metabolic alterations could occur in A1/A2 astrocytes.

To further explore this hypothesis, we are currently using primary astrocytic cultures, isolated by MACS from the cerebellum of P5-P7 pups, that are being stimulated with IL-1α, TNFα and C1q, to induce an A1 phenotype. Then, we will move to the characterization of their metabolic profile, focusing on the expression levels of genes involved in glycolysis and TCA cycle. Interestingly, a recent *in vitro* study has demonstrated differential metabolic profiles in astrocytes exposed to LPS for short or long periods of time. Namely, 30 min of LPS treatment increased the astrocytic glycolytic rate, but did not affect their oxidative phosphorylation rate, while treatment with LPS for 24 hours decreased the glycolytic capacity and increased the mitochondrial respiration of astrocytes (Robb et al., 2020). This study suggests that pro-inflammatory stimuli are able to modulate the metabolic profile of astrocytes, supporting the findings observed in our work.

In this work we also performed for the first time a morphological analysis of astrocytes of the cerebellum white matter in different disease time points. As already expected, astrocytes near lesion regions, at the onset and chronic phases of disease, were more reactive than astrocytes from non-induced animals, as evaluated by increased total length and number of ramifications. Regarding the NAWM, previous studies reported the presence of gliosis in MS patients (Allen and McKeown, 1979), however, Graumann and colleagues (2003) did not observe significant differences in GFAP expression between the NAWM of MS patients and control subjects (Graumann et al., 2003). In accordance, we also did not find significant differences in the astrocytic morphology between the NAWM of EAE animals and non-induced controls.

Altogether, in this work we propose that, in response to EAE, astrocytes showed an increased expression of enzymes of the glycolysis and TCA cycle suggesting a metabolic shift to oxidative phosphorylation. Those alterations are concomitant with the development of an A1 neurotoxic phenotype. Hence, we hypothesize that TCA cycle upregulation in MS astrocytes is contributing to exacerbate brain inflammation, leading to myelin damage, which needs further investigation.

Acknowledgments

The authors would like to acknowledge Sara Duarte-Silva (ICVS) for sharing primers; Claudia Nobrega (ICVS) for help with the AutoMACS Pro Separator equipment.

Funding

This work was supported by Foundation for Science and Technology (FCT) and COMPETE through the project EXPL/NEU-OSD/2196/2013 and by The Clinical Academic Center (2CA-Braga) through the project EXPL/001/2016. The work at ICVS/3B's has been developed under the scope of the project NORTE-01-0145-FEDER-000013, supported by the Northern Portugal Regional Operational Programme (NORTE 2020), under the Portugal 2020 Partnership Agreement, through the European Regional Development Fund (FEDER), and funded by FEDER funds through the Competitiveness Factors Operational Programme (COMPETE), and by National funds, through the Foundation for Science and Technology (FCT), under the scope of the project POCI-01-0145-FEDER-007038. FM is an assistant researcher and recipient of an FCT Investigator grant with the reference CEECIND/01084/2017. SN is a recipient of a Ph.D. fellowship with the reference PD/BD/114120/2015 from MCTES national funds.

Author contributions

SN performed the experimental procedures, statistical analysis and wrote the manuscript; FG, JD and GC produced the RNAseq data results; JC, NS, JP an JC critically revised the manuscript; FM supervised the study and edited the manuscript.

Conflict of interest

The authors declare that the research was conducted in the absence of any commercial or financial relationship that could be construed as a potential conflict of interest.

References

Abbott NJ, Ronnback L, Hansson E. Astrocyte-endothelial interactions at the blood-brain barrier. Nature Reviews Neuroscience. 2006;7:41-53.

Allen IV, McKeown SR. A histological, histochemical and biochemical study of the macroscopically normal white matter in multiple sclerosis. Journal of the Neurological Sciences. 1979;41:81-91.

Allen NJ, Barres BA. Neuroscience: Glia - more than just brain glue. Nature. 2009;457:675-677.

Aquino DA, Shafit-Zagardo B, Brosnan CF, Norton WT. Expression of glial fibrillary acidic protein and neurofilament mRNA in gliosis induced by experimental autoimmune encephalomyelitis. Journal of Neurochemistry. 1990;54:1398-1404.

Batiuk MY, de Vin F, Duque SI, Li C, Saito T, Saido T, et al. An immunoaffinity-based method for isolating ultrapure adult astrocytes based on ATP1B2 targeting by the ACSA-2 antibody. Journal of Biological Chemistry. 2017;292:8874-8891.

Chao CC, Gutierrez-Vazquez C, Rothhammer V, Mayo L, Wheeler MA, Tjon EC, et al. Metabolic control of astrocyte pathogenic activity via cPLA2-MAVS. Cell. 2019;179:1483-1498 e1422.

Correale J, Farez MF. The role of astrocytes in multiple sclerosis progression. Frontiers in neurology. 2015;6:180.

das Neves SP, Serre-Miranda C, Nobrega C, Roque S, Cerqueira JJ, Correia-Neves M, et al. Immune thymic profile of the MOG-induced experimental autoimmune encephalomyelitis mouse model. Frontiers in Immunology. 2018;9:2335.

Du XF, Liu J, Hua QF, Wu YJ. Relapsing-remitting multiple sclerosis is associated with regional brain activity deficits in motor- and cognitive-related brain areas. Frontiers in neurology. 2019;10:1136.

Frohman EM, Racke MK, Raine CS. Multiple sclerosis–the plaque and its pathogenesis. The New England Journal of Medicine. 2006;354:942-955.

Galvan-Pena S, O'Neill LA. Metabolic reprograming in macrophage polarization. Frontiers in Immunology. 2014;5:420.

Graumann U, Reynolds R, Steck AJ, Schaeren-Wiemers N. Molecular changes in normal appearing white matter in multiple sclerosis are characteristic of neuroprotective mechanisms against hypoxic insult. Brain Pathology. 2003;13:554-573.

Hofstetter HH, Shive CL, Forsthuber TG. Pertussis toxin modulates the immune response to neuroantigens injected in incomplete Freund's adjuvant: induction of Th1 cells and experimental autoimmune encephalomyelitis in the presence of high frequencies of Th2 cells. Journal of Immunology. 2002;169:117-125.

Holt LM, Olsen ML. Novel applications of magnetic cell sorting to analyze cell-type specific gene and protein expression in the central nervous system. PloS One. 2016;11:e0150290.

Itoh N, Itoh Y, Tassoni A, Ren E, Kaito M, Ohno A, et al. Cell-specific and region-specific transcriptomics in the multiple sclerosis model: Focus on astrocytes. Proceedings of the National Academy of Sciences of the United States of America. 2018;115:E302-E309.

Kamburov A, Pentchev K, Galicka H, Wierling C, Lehrach H, Herwig R. ConsensusPathDB: toward a more complete picture of cell biology. Nucleic Acids Research. 2011;39:D712-717.

Kamburov A, Wierling C, Lehrach H, Herwig R. ConsensusPathDB–a database for integrating human functional interaction networks. Nucleic Acids Research. 2009;37:D623-628.

Kantzer CG, Boutin C, Herzig ID, Wittwer C, Reiss S, Tiveron MC, et al. Anti-ACSA-2 defines a novel monoclonal antibody for prospective isolation of living neonatal and adult astrocytes. Glia. 2017;65:990-1004.

Lakens D. Calculating and reporting effect sizes to facilitate cumulative science: a practical primer for t-tests and ANOVAs. Frontiers in Psychology. 2013;4:863.

Liddelow SA, Guttenplan KA, Clarke LE, Bennett FC, Bohlen CJ, Schirmer L, et al. Neurotoxic reactive astrocytes are induced by activated microglia. Nature. 2017;541:481-487.

Longair MH, Baker DA, Armstrong JD. Simple Neurite Tracer: open source software for reconstruction, visualization and analysis of neuronal processes. Bioinformatics. 2011;27:2453-2454.

Luo J, Ho P, Steinman L, Wyss-Coray T. Bioluminescence in vivo imaging of autoimmune encephalomyelitis predicts disease. Journal of Neuroinflammation. 2008;5:6.

MacKenzie-Graham A, Tinsley MR, Shah KP, Aguilar C, Strickland LV, Boline J, et al. Cerebellar cortical atrophy in experimental autoimmune encephalomyelitis. Neuroimage. 2006;32:1016-1023.

Mayo L, Trauger SA, Blain M, Nadeau M, Patel B, Alvarez JI, et al. Regulation of astrocyte activation by glycolipids drives chronic CNS inflammation. Nature Medicine. 2014;20:1147-1156.

Mueller AM, Pedre X, Stempfl T, Kleiter I, Couillard-Despres S, Aigner L, et al. Novel role for SLPI in MOG-induced EAE revealed by spinal cord expression analysis. Journal of Neuroinflammation. 2008;5:20.

Negrotto L, Correale J. Amino acid catabolism in multiple sclerosis affects immune homeostasis. Journal of Immunology. 2017;198:1900-1909.

Noseworthy JH. Progress in determining the causes and treatment of multiple sclerosis. Nature. 1999;399:A40-47.

Noseworthy JH, Lucchinetti C, Rodriguez M, Weinshenker BG. Multiple sclerosis. The New England Journal of Medicine. 2000;343:938-952.

Orihuela R, McPherson CA, Harry GJ. Microglial M1/M2 polarization and metabolic states. British Journal of Pharmacology and Chemotherapy. 2016;173:649-665.

Robb JL, Hammad NA, Weightman Potter PG, Chilton JK, Beall C, Ellacott KLJ. The metabolic response to inflammation in astrocytes is regulated by nuclear factor-kappa B signaling. Glia. 2020.

Saab CY, Craner MJ, Kataoka Y, Waxman SG. Abnormal Purkinje cell activity in vivo in experimental allergic encephalomyelitis. Experimental Brain Research. 2004;158:1-8.

Schindelin J, Arganda-Carreras I, Frise E, Kaynig V, Longair M, Pietzsch T, et al. Fiji: an open-source platform for biological-image analysis. Nature Methods. 2012;9:676-682.

Schreck L, Ryan S, Monaghan P. Cerebellum and cognition in multiple sclerosis. Journal of Neurophysiology. 2018;120:2707-2709.

Sevastou I, Pryce G, Baker D, Selwood DL. Characterisation of transcriptional changes in the spinal cord of the progressive experimental autoimmune encephalomyelitis Biozzi ABH mouse model by RNA sequencing. PloS One. 2016;11:e0157754.

Smith ME, Eng LF. Glial fibrillary acidic protein in chronic relapsing experimental allergic encephalomyelitis in SJL/J mice. Journal of Neuroscience Research. 1987;18:203-208.

Smith ME, Somera FP, Eng LF. Immunocytochemical staining for glial fibrillary acidic protein and the metabolism of cytoskeletal proteins in experimental allergic encephalomyelitis. Brain Research. 1983;264:241-253.

Sofroniew MV. Astrogliosis. Cold Spring Harbor Perspectives in Biology. 2014;7:a020420.

Tani M, Glabinski AR, Tuohy VK, Stoler MH, Estes ML, Ransohoff RM. In situ hybridization analysis of glial fibrillary acidic protein mRNA reveals evidence of biphasic astrocyte activation during acute experimental autoimmune encephalomyelitis. The American Journal of Pathology. 1996;148:889-896.

Tassoni A, Farkhondeh V, Itoh Y, Itoh N, Sofroniew MV, Voskuhl RR. The astrocyte transcriptome in EAE optic neuritis shows complement activation and reveals a sex difference in astrocytic C3 expression. Scientific Reports. 2019;9:10010.

Tavares G, Martins M, Correia JS, Sardinha VM, Guerra-Gomes S, das Neves SP, et al. Employing an open-source tool to assess astrocyte tridimensional structure. Brain Structure and Function. 2017;222:1989-1999.

Turley DM, Miller SD. Peripheral tolerance induction using ethylenecarbodiimide-fixed APCs uses both direct and indirect mechanisms of antigen presentation for prevention of experimental autoimmune encephalomyelitis. Journal of Immunology. 2007;178:2212-2220.

Williams A, Piaton G, Lubetzki C. Astrocytes–friends or foes in multiple sclerosis? Glia. 2007;55:1300-1312.

Wu GF, Alvarez E. The immunopathophysiology of multiple sclerosis. Neurologic Clinics. 2011;29:257-278.

Supplementary material

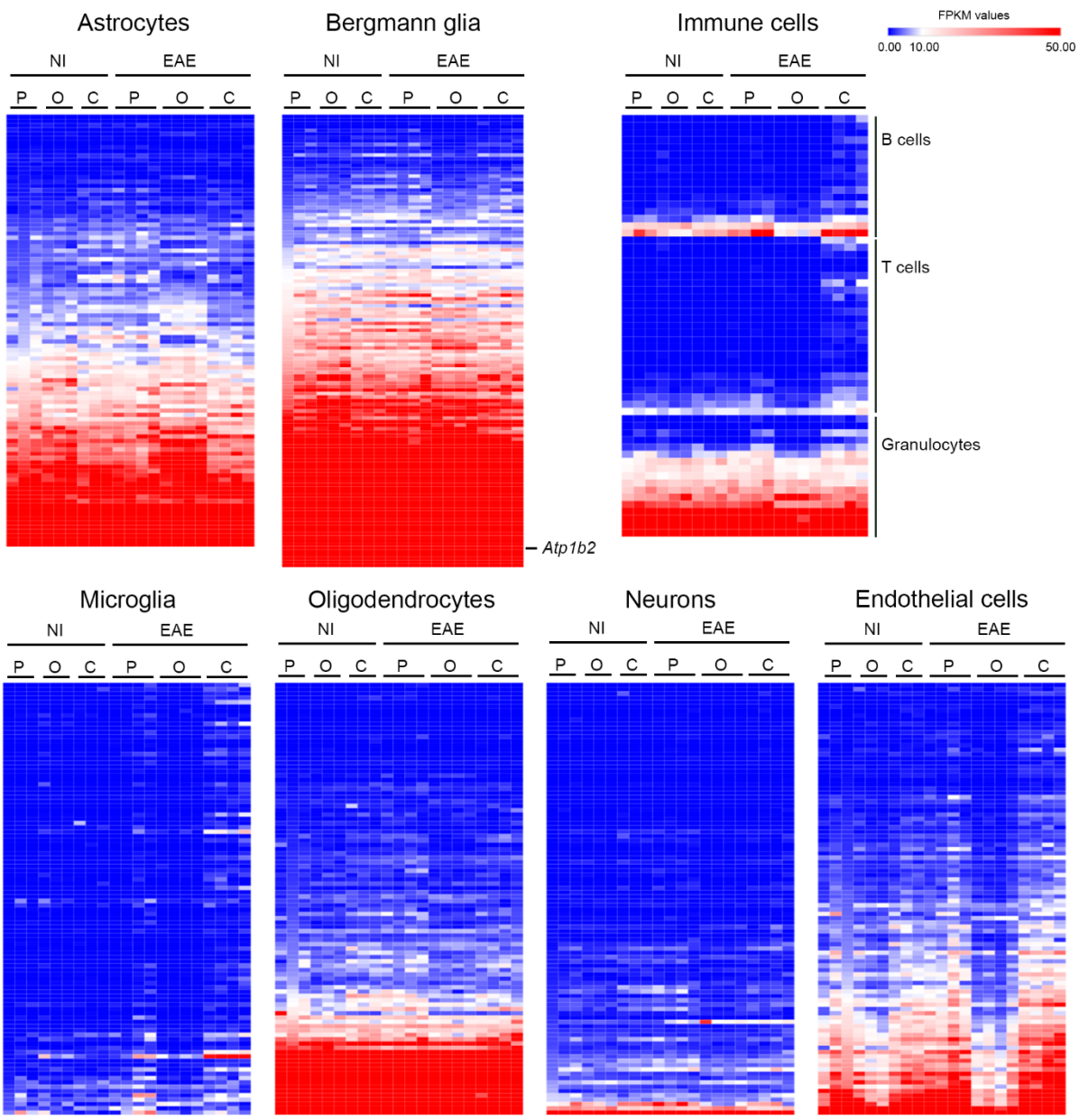

Supplementary figure 2. 1 – Expression levels of cell-type specific markers.

Expression levels of genes associated with CNS cells (astrocytes, Bergmann glia, microglia, oligodendrocytes and neurons), with endothelial cells and different immune cell populations (B cells, T cells and granulocytes). The expression levels of *Atp1b2*, which was identified as the ACSA-2 epitope, used in the MACS technique to isolate the astrocytes, is highlighted. Heatmaps obtained using the Morpheus APP tool of CLUE. C – chronic time point; FPKM – fragments per kilobase of exon per million fragments mapped; NI – non-induced; O – onset time point; P – pre-symptomatic time point.

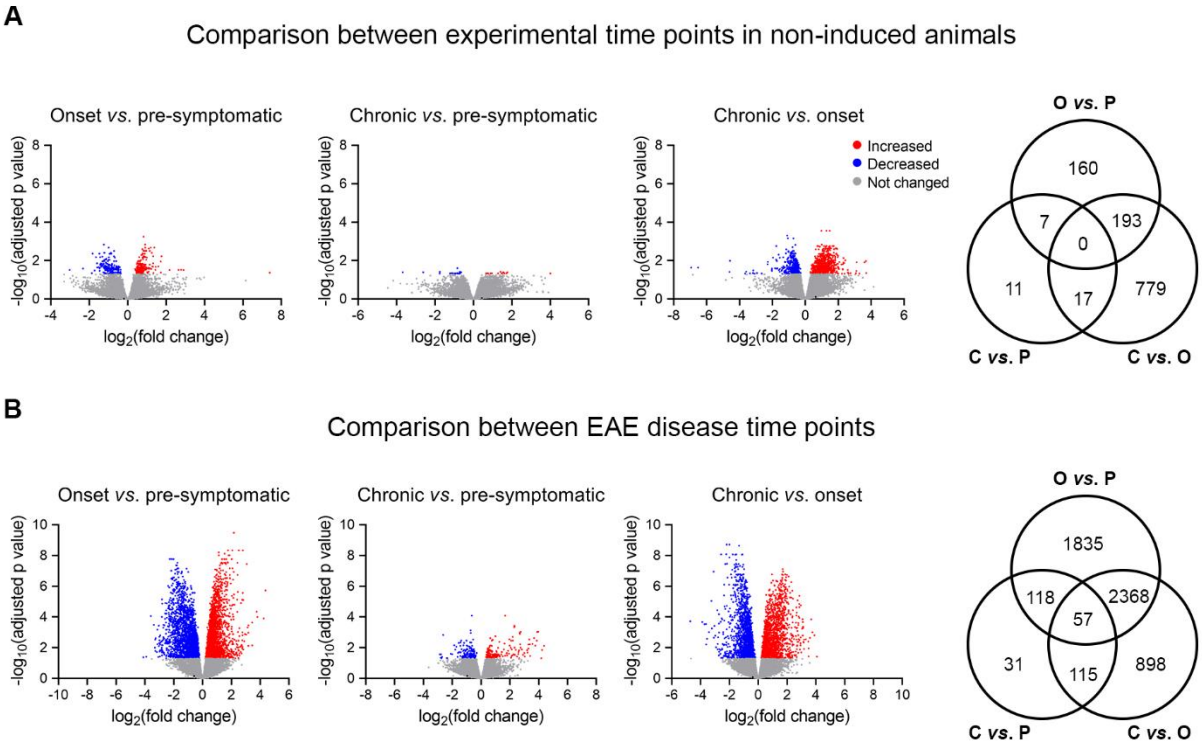

Supplementary figure 2. 2 – Volcano plots of differentially expressed genes.

(A) Differentially expressed astrocytic genes for the comparisons between experimental time points in non-induced animals. (B) Differentially expressed genes for the comparisons between disease time points in EAE animals, before normalization to the respective non-induced group. Genes whose expression was not altered are represented in gray; significant underexpessed genes are represented in blue; significant overexpressed genes are represented in red. C – chronic time point; O – onset time point; P – pre-symptomatic time point.

Supplementary table 2. 1 – Primers sequence and annealing temperature.

Gene	Primer sequence (5'→3')	Annealing temperature (ºC)
Amigo2	Fw: GAGGCGACCATAATGTCGTT Rv: GCATCCAACAGTCCGATTCT	60
Fbln5	Fw: CTTCAGATGCAAGCAACAA Rv: AGGCAGTGTCAGAGGCCTTA	58
Fkbp5	Fw: TATGCTTATGGCTCGGCTGG Rv: CAGCCTTCCAGGTGGACTTT	60
Atp5b	Fw: GGCCAAGATGTCCTGCTGTT Rv: GCTGGTAGCCTACAGCAGAAGG	60
Hspcb	Fw: GCTGGCTGAGGACAAGGAGA Rv: CGTCGGTTAGTGGAATCTTCATG	60
Tbp	Fw: GGGAGAATCATGGACCAGAA Rv: TTGCTGCTGCTGTCTTTGTT	55
Idh3g	Fw: GGCAATGCTCAAGCCAACTC Rv: TGGAGGAATTGTTTGTTGTGAGG	60
Aldoc	Fw: GCCTGTTTGGTTAGGAGAGGA Rv: CATGCTGCCTACGGACTCAT	60
Sdha	Fw: TGATGCTGTGGTTGTAGGCG Rv: GATACCTCCCTGTGCTGCAA	60
Pfkm	Fw: GGTTTGGAAGCCTCTCCTCC Rv: GGGTCATGATCCACTCTTGTAGT	60

Supplementary table 2. 2 – List of genes specifically associated with CNS cells (astrocytes, Bergmann glia, microglia, oligodendrocytes and neurons), endothelial cells and different immune cell populations (B cells, T cells and granulocytes).

Cell type	Associated markers
Astrocytes	2610034M16Rik, Myom3, Sctr, Fam181a, Pla2g3, Chrdl1, Hgf, Fzd10, 2900052N01Rik, Ttll8, Gcnt4, Ptx3, 2900005J15Rik, Vnn1, Ppp1r3g, Crb2, Tmem82, Celsr1, Prdm16, Grhl1, Cybrd1, P4ha3, Fzd2, Aqp9, Pipox, Itga7, Gm266, Ccdc37, Slc15a2, Ccdc80, Glis3, Entpd2, Frem2, Pamr1, Cyp4f15, Sypl2, Gdpd2, Slc14a2, Kcnn3, Cth, Pm20d1, Sorcs2, Ephx2, Gli2, Adhfe1, Plcd4, Ranbp3l, Gli1, Slc25a34, Nat8, Gli3, Gm973, Fmo1, St6galnac5, Ttpa, Mamdc2, Lgr6, Abcd2, Gm5089, Trim9, Phkg1, Tnc, Egfr, Slc7a11, Rgs20, Aifm3, Paqr6, Slc30a10, Rorb, Notch3, Atp13a4, Daam2, Slc6a11, AI464131, Vcam1, Cbs, Slc7a10, Bmpr1b, Aldh1l1, Fam20a, Fgfr3, Slc39a12, Cldn10, 1700084C01Rik, Slc7a2, Grm3, Sox9, Itih3, Ppp1r3c, Dio2, Lrig1, Slc14a1, Elovl2, A2m, Nwd1, Gja1, Mlc1, Aqp4, Slc4a4, Slc1a3
Bergmann glia	Rasgef1c, 1110032F04Rik, Dusp5, Slitrk6, 1700086L19Rik, 5830416P10Rik, Fhod1, Col4a6, Dbpht2, 6530402F18Rik, Phf19, Cdk6, Chrm4, Otof, Sema3a, Lmcd1, Mboat1, Hs3st1, Tbc1d4, Col5a3, Vwa5b1, Ntng2, Sec14l2, Cpne8, Wnt5a, Nfatc1, Rhbdf1, Pdlim3, Prss23, Plekha2, Brinp3, Nedd9, Etv4, 2810459M11Rik, Ppp1r14c, Gas2l3, Trhde, Pcdh20, Pld1, Arhgef4, Carhsp1, Rab3gap2, Abcb9, F730043M19Rik, Gpr89, Pde3a, Selenbp1, Lpin2, Arhgap26, Cd44, St5, Gper1, Klf15, Gpc4, Cdh7, Slitrk2, Idh1, Slc12a4, Car8, Dmd, Lifr, Ddr1, Fam181b, Rhoj, Stom, Hnmt, Ttyh2, Sox8, Gm7694, Gsap, Rasa3, Gabra4, Fam81a, Spred2, Cyp51, Hmgcs1, Fgfr1, Add1, Sat1, Mt3, Tubb2a, Smpdl3a, Ugp2, Ecm2, Slc9a3r1, Etv5, Tubb2b, Gucy1a3, Tagln2, Fbxo2, Nkain4, Lgi4, Shisa9, Gabrb1, Mcc, Cpne2, Tril, Grid2, Prex1, Mybpc1, Cacng5, Lxn, Acsbg1, Abat, Fabp7, Ddah1, Hopx, Serpine2, Gdf10, Luzp2, Kcnj10, Ptn, Pea15a, Ptprz1, Metrn, Timp4, Pla2g7, Paqr8, Cst3, Atp1a2, Gstm1, S100b, Slc1a2, Atp1b2, Mt2, Dbi, Sparcl1, Fam107a, Gpm6b
Microglia	Bcl2a1d, Ccl3, Tnf, Ccl4, Bcl2a1b, P2ry6, Gdf15, Tmem119, Ccl9, Ccr7, Ptafr, Slc15a3, Selplg, Cd300a, C5ar1, Gpr183, Irf8, Hck, Sash3, Tlr9, Slamf8, Ncf4, Abcc3, Cd37, H2-Oa, Il10ra, Lag3, Rasal3, Rhoh, Vav1, Il1b, Snx20, Ltc4s, Cd68, Cd52, Csf3r, Itgb2, Cbr2, Nlrp3, Blnk, Myo1g, Pik3ap1, Fcgr3, Il21r, Rac2, Alox5ap, Tnfaip8l2, Nfkbid, Myo1f, Parvg, Ccl7, Fcer1g, Slamf9, Siglech, Psd4, Pik3r5, Cx3cr1, H2-DMb1, Was, Ccdc88b, Gpr157, Nckap1l, Nfam1, Kcnk6, Csf1r, Ncf1, Ccr5, Ptpn6, Irf5, Angptl7, Hmha1, Pld4, Tbxas1, Hk3, Cxcl16, C1qb, Card9, Csf2rb, Slc11a1, Asb2, Tlr2, Cd83, Lyz2, C1qc, Ncf2, Laptm5, Cd74, Fermt3, Arhgap9, Tyrobp, Slfn2, Ch25h, Plau, Olfml3, Pla2g15, Cd14, Ccrl2, Fcgr2b, Ang, Ccl2

(Continues)

Supplementary table 2. 2 (Continued).

Cell type		Associated markers
Oligodendrocytes		Slc5a11, Pkd2l1, Cldn14, Sh3gl3, Mog, Carns1, Tmem151a, D7Ertd443e, S1pr5, Mag, Gjc2, Galnt6, Nkain2, Adssl1, Fa2h, Ldb3, Slc45a3, Ermn, Anln, Rab37, Phospho1, Lgi3, Fam178b, Tmem117, Ccdc13, Ppap2c, Cntn2, Gpr62, Arsg, Smtnl2, Dbil5, Stmn4, Nkain1, Glra4, Pigz, Ppp1r14a, Rftn1, Mobp, Synj2, Srd5a1, Adamtsl4, Itgb4, Plekhh1, Cldn11, Padi2, Tprn, Tmeff2, Larp6, Dock5, Aspa, Wnt3, Phlda3, Cdc42ep2, Bace2, Tmem88b, Acy3, Prr5l, Gss, Nol3, B3galt5, Slain1, Car14, Prr18, Inf2, Gsn, Gamt, Josd2, Nkx6-2, Gng13, Pdlim2, Gpr37, Hist1h4h, Fbxo36, Tmod1, Rhou, Slco3a1, Mbp, Qdpr, Mal, Slc48a1, Ctnna3, Ndrg1, Dbndd2, Tppp3, Trak2, Efhd1, Pla2g16, Adi1, Lpar1, Cryab, Aplp1, Cnp, Scd1, Trp53inp2, Cmtm5, Kif5a, Trf, Sept4, Apod, Plekhb1
Neurons		Nhlh2, 5330417C22Rik, Mrap2, Gdf5, Slc10a4, Pnoc, Grem2, Kcnj5, Lhx1, Hcn4, Npas4, Pcsk1, Lhx6, P2rx5, Nxph3, Hs6st3, Samd3, Fam131c, E330013P04Rik, Kcnb2, Stk32b, Slc17a8, Trank1, Trim66, Bcl11b, Galntl6, Islr2, Abcc8, Kcnh7, Col25a1, Ripk4, Nell1, Igfbpl1, Casz1, Mme, Plek2, Synpr, Kctd8, Igsf9, Bcl11a, Barhl2, Ccbe1, Celsr3, Kcnc2, Cacng2, Slc32a1, Ebf3, Penk, Tmem130, Cdh8, L1cam, Necab1, Elavl2, Srrm4, Clstn2, Vmn2r1, Amy1, Kcnk9, Nos1, Mab21l1, Meg3, Ajap1, Dync1i1, Dpysl5, Trp73, Nppc, Cpne4, Nxph4, Gad2, Crmp1, Scube3, St8sia2, Tubb3, Rian, Bhlhe22, March4, Ankrd35, Mirg, Cd274, Ina, Snhg11, Syt1, Reln, Syt4, Sphkap, Calb2, Celf4, BC005764, Cacna2d2, Bmp5, Fibin, Neurod1, Robo2, Myt1l, Gap43, Rgs8, Stmn2, Fam183b, Ndrg4, Npy
Endothelial cells		Fgfbp1, Adamtsl2, Aplnr, Ly6c2, Adh1, Myct1, Sigirr, Kcnq1, Abcc6, Dll4, Mmp25, 4930578C19Rik, Stap2, Asb4, Pcdh12, Gimap4, Gm694, Fam124b, Igsf5, Ctsw, Ly75, Hmcn1, Sema3g, Cd40, Megf6, Ushbp1, Clec14a, Tie1, Sox17, Gimap8, Rnf125, Akr1c14, AU021092, Ptgis, Fam129a, Mecom, Scarf1, Mfsd7c, Icam2, Trim16, Robo4, Nos3, Slc19a3, Flt4, Foxq1, Angpt2, She, 8430408G22Rik, C130074G19Rik, Mmrn2, Erg, Wfdc1, Slc39a8, Scgb3a1, Hmgcs2, Slc16a4, Stra6, Nostrin, Adcy4, Slc38a5, Csrp2, Kdr, Ctla2a, Cyyr1, Serpinb6b, Tek, Itga4, Cdh5, Lsr, Egfl7, Hrct1, Cd93, Slfn5, Cd34, Ptprb, Foxf2, Rassf9, Cgnl1, Ocln, Pecam1, Cldn5, Abcb1a, Emcn, Eltd1, Apold1, Pglyrp1, Gpr116, Gja4, Slco1a4, Slc22a8, Fn1, Flt1, Itm2a, Esam, Ly6c1, Car4, Higd1b, Tm4sf1, Ly6a, Igfbp7
Immune cells	**B cells**	H2-DMb2, Cd19, Igj, Cd79a, Btk, Cd79b, Cd22, Spib, Cd86, Syk, Irf4, Cebpb, H2-DMa, Cd72, Stat6, Lyn, Cd200
	T cells	Cd3e, Cd3g, Cd3d, Cd8a, Cd8b1, Cd4, Cd2, Cd28, Lat, Cd6, Stat4, Gata3, Lck, Cd5, Klrg1, Klrc1, Cst7, Zap70, Prf1, Fyb, Runx2, Pim1, Tcf7, Lef1, Satb1
	Granulocytes	Mnda, Il1rn, Ctss, Il1r2, Ctsc, Il13ra1, Rgs2, Taldo1, Gnb2, Gca, Fcgrt, Bcl6, Sod2, Rassf2, Ifitm2, Ctsb, Itm2b

Data obtained from (Cahoy et al., 2008; Heng et al., 2017; Koirala and Corfas, 2010; Palmer et al., 2006; Zhang et al., 2014).

Supplementary table 2. 3 – Pathways significantly altered in the comparison between EAE and non-induced animals at the pre-symptomatic phase.

p-value	q-value	Pathway
2.41E-09	2.05E-06	XPodNet - protein-protein interactions in the podocyte expanded by STRING
6.75E-09	2.88E-06	Extracellular matrix organization
5.22E-08	1.48E-05	ECM-receptor interaction - Mus musculus (mouse)
1.50E-07	3.19E-05	Neuronal system
4.67E-06	0.000795	Focal adhesion - Mus musculus (mouse)
6.19E-06	0.000879	PodNet- protein-protein interactions in the podocyte
7.56E-06	0.00092	Phospholipase D signaling pathway - Mus musculus (mouse)
1.38E-05	0.001468	Focal adhesion
1.90E-05	0.0018	Calcium signaling pathway - Mus musculus (mouse)
3.29E-05	0.0028	ECM proteoglycans
4.38E-05	0.003391	Transmission across chemical synapses
6.36E-05	0.004033	Adherens junction - Mus musculus (mouse)
6.39E-05	0.004033	Signaling by receptor tyrosine kinases
6.63E-05	0.004033	Insulin secretion - Mus musculus (mouse)
8.52E-05	0.004688	Laminin interactions
9.35E-05	0.004688	GABAergic synapse - Mus musculus (mouse)
9.35E-05	0.004688	Dilated cardiomyopathy (DCM) - Mus musculus (mouse)
0.000132	0.006006	Dopaminergic synapse - Mus musculus (mouse)
0.000145	0.006006	Morphine addiction - Mus musculus (mouse)
0.000147	0.006006	Collagen biosynthesis and modifying enzymes
0.000148	0.006006	Regulation of actin cytoskeleton - Mus musculus (mouse)
0.000167	0.006454	Protein-protein interactions at synapses
0.000198	0.007324	GABA receptor activation
0.000294	0.010434	RHO GTPases activate PAKs
0.000316	0.010768	Neurotransmitter receptors and postsynaptic signal transmission
0.000329	0.010768	Adenylate cyclase activating pathway
0.000416	0.013117	Estrogen signaling pathway - Mus musculus (mouse)
0.000456	0.01386	Retrograde endocannabinoid signaling - Mus musculus (mouse)
0.000596	0.017496	Nicotine addiction - Mus musculus (mouse)
0.000681	0.01933	Pathways in cancer - Mus musculus (mouse)
0.000803	0.022063	Huntington disease - Mus musculus (mouse)
0.001047	0.027863	Human papillomavirus infection - Mus musculus (mouse)
0.001131	0.028556	cAMP signaling pathway - Mus musculus (mouse)

(Continues)

Supplementary table 2.3 (Continued).

p-value	q-value	Pathway
0.00114	0.028556	Thyroid hormone signaling pathway - Mus musculus (mouse)
0.001175	0.028611	Collagen formation
0.001316	0.030945	Arrhythmogenic right ventricular cardiomyopathy (ARVC) - Mus musculus (mouse)
0.001391	0.030945	Adenylate cyclase inhibitory pathway
0.001391	0.030945	Inhibition of adenylate cyclase pathway
0.001421	0.030945	Signaling by MET
0.001453	0.030945	Thyroid hormone synthesis - Mus musculus (mouse)
0.001558	0.03172	Axon guidance
0.001601	0.03172	Gastric acid secretion - Mus musculus (mouse)
0.001601	0.03172	Bacterial invasion of epithelial cells - Mus musculus (mouse)
0.001752	0.033931	Amoebiasis - Mus musculus (mouse)
0.0019	0.035982	Post-translational protein phosphorylation
0.001975	0.036022	VEGFR2 mediated vascular permeability
0.002008	0.036022	Endocytosis - Mus musculus (mouse)
0.002029	0.036022	Rap1 signaling pathway - Mus musculus (mouse)
0.002107	0.03663	Regulation of Insulin-like Growth Factor (IGF) transport and uptake by Insulin-like Growth Factor Binding Proteins (IGFBPs)
0.002319	0.039515	Salivary secretion - Mus musculus (mouse)
0.002372	0.039619	MET promotes cell motility
0.00254	0.041615	MAP2K and MAPK activation
0.002909	0.046004	Signaling by EGFR
0.002916	0.046004	Signaling by PDGF
0.00314	0.047911	Cholinergic synapse - Mus musculus (mouse)
0.003154	0.047911	MAPK family signaling cascades
0.003318	0.047911	Activation of GABAB receptors
0.003318	0.047911	GABA B receptor activation
0.003318	0.047911	Signaling by SCF-KIT
0.003392	0.048167	Circadian entrainment - Mus musculus (mouse)
0.003553	0.049625	VEGFA-VEGFR2 Pathway
0.003767	0.05177	Kinesins
0.003852	0.052097	Hypertrophic cardiomyopathy (HCM) - Mus musculus (mouse)
0.003927	0.052276	Melanogenesis - Mus musculus (mouse)
0.004106	0.053815	Membrane trafficking

(Continues)

Supplementary table 2.3 (Continued).

p-value	q-value	Pathway
0.004225	0.054537	Focal adhesion-PI3K-Akt-mTOR-signaling pathway
0.004651	0.059142	Recycling pathway of L1
0.004978	0.061858	Factors involved in megakaryocyte development and platelet production
0.00501	0.061858	γ-glutamyl cycle
0.005261	0.064039	Neurexins and neuroligins
0.005814	0.069767	MAPK1/MAPK3 signaling
0.005962	0.07055	MAPK signaling pathway
0.006538	0.075113	Signaling by VEGF
0.006538	0.075113	G Protein Signaling Pathways
0.0067	0.075113	Crosslinking of collagen fibrils
0.0067	0.075113	Interleukin-6 signaling
0.006917	0.076536	CD28 co-stimulation
0.007722	0.078732	Calcium regulation in the cardiac cell
0.007811	0.078732	Integrin cell surface interactions
0.007811	0.078732	Longevity regulating pathway - multiple species - Mus musculus (mouse)
0.007811	0.078732	Costimulation by the CD28 family
0.007811	0.078732	Synaptic vesicle cycle - Mus musculus (mouse)
0.00784	0.078732	ATP sensitive Potassium channels
0.007868	0.078732	NCAM signaling for neurite out-growth
0.00804	0.078732	Calmodulin induced events
0.00804	0.078732	CaM pathway
0.00804	0.078732	GP generic
0.00814	0.078811	Adrenergic signaling in cardiomyocytes - Mus musculus (mouse)
0.00849	0.081275	Vascular smooth muscle contraction - Mus musculus (mouse)
0.008906	0.083838	EPHB-mediated forward signaling
0.008955	0.083838	Platelet activation, signaling and aggregation
0.009094	0.084217	Proteoglycans in cancer - Mus musculus (mouse)
0.009196	0.08425	Vesicle-mediated transport
0.009452	0.085673	DAG and IP3 signaling
0.009779	0.086793	Leukocyte transendothelial migration - Mus musculus (mouse)
0.009779	0.086793	Glutamatergic synapse - Mus musculus (mouse)
0.009994	0.087543	Regulation of actin cytoskeleton

Supplementary table 2. 4 – Pathways significantly altered in the comparison between EAE and non-induced animals at the onset phase.

p-value	q-value	Pathway
2.70E-10	1.87E-07	Metabolism
5.33E-08	1.85E-05	Cholesterol metabolism (includes both Bloch and Kandutsch-Russell pathways)
1.78E-07	4.12E-05	Cholesterol biosynthesis III (via desmosterol)
3.24E-07	4.83E-05	Superpathway of cholesterol biosynthesis
3.48E-07	4.83E-05	Cholesterol biosynthesis I
5.84E-07	6.75E-05	Adar1 editing defficiency immune response
1.08E-06	0.000107	Omega-9 FA synthesis
1.76E-06	0.000152	Cholesterol biosynthesis
3.15E-06	0.000243	Metabolism of amino acids and derivatives
4.93E-06	0.000329	Cholesterol biosynthesis
5.22E-06	0.000329	Metabolism of lipids
8.66E-06	0.000501	Steroid biosynthesis - Mus musculus (mouse)
1.90E-05	0.001013	Oleate biosynthesis II (animals)
2.22E-05	0.001101	Branched-chain amino acid catabolism
3.71E-05	0.001644	Cholesterol biosynthesis II (via 24,25-dihydrolanosterol)
3.79E-05	0.001644	Valine degradation
7.46E-05	0.003045	HSP90 chaperone cycle for steroid hormone receptors (SHR)
8.20E-05	0.003162	Phosphatidylinositol signaling system - Mus musculus (mouse)
0.000128	0.00467	Gap junction - Mus musculus (mouse)
0.000143	0.004947	Valine, leucine and isoleucine degradation - Mus musculus (mouse)
0.000213	0.007052	Biosynthesis of unsaturated fatty acids - Mus musculus (mouse)
0.000398	0.012568	Fatty acid metabolism
0.000444	0.013396	AGE-RAGE signaling pathway in diabetic complications - Mus musculus (mouse)
0.00056	0.01554	Antigen processing and presentation - Mus musculus (mouse)
0.00056	0.01554	PPAR signaling pathway - Mus musculus (mouse)
0.000606	0.015635	Human cytomegalovirus infection - Mus musculus (mouse)
0.000621	0.015635	Omega-3-Omega-6 FA synthesis
0.000653	0.015635	Antigen processing-Cross presentation
0.000653	0.015635	Platelet activation - Mus musculus (mouse)
0.000699	0.016098	AMPK signaling pathway - Mus musculus (mouse)
0.00075	0.016098	Signaling by SCF-KIT
0.000763	0.016098	NOD-like receptor signaling pathway - Mus musculus (mouse)
0.000765	0.016098	Epoxysqualene biosynthesis

(Continues)

Supplementary table 2.4 (continued).

p-value	q-value	Pathway
0.001065	0.02173	Valine degradation I
0.001169	0.022541	Estrogen signaling pathway - Mus musculus (mouse)
0.001169	0.022541	Adipogenesis genes
0.001243	0.023315	Dopaminergic synapse - Mus musculus (mouse)
0.001327	0.02423	Thyroid hormone signaling pathway - Mus musculus (mouse)
0.001389	0.024696	Salivary secretion - Mus musculus (mouse)
0.001423	0.024696	Long-term depression - Mus musculus (mouse)
0.001564	0.025896	Acetylcholine regulates insulin secretion
0.001567	0.025896	Endochondral ossification
0.001773	0.028622	PPAR signaling pathway
0.001988	0.031282	Type II interferon signaling (IFNG)
0.002066	0.031282	Glucagon signaling pathway - Mus musculus (mouse)
0.002073	0.031282	VEGFA-VEGFR2 Pathway
0.002254	0.032592	Metallothioneins bind metals
0.002254	0.032592	Response to metal ions
0.002463	0.034891	Long-term potentiation - Mus musculus (mouse)
0.002599	0.036077	Antigen presentation: folding, assembly and peptide loading of class I MHC
0.002853	0.038077	Synthesis of IP3 and IP4 in the cytosol
0.002853	0.038077	Fatty acid biosynthesis
0.002948	0.038605	The role of GTSE1 in G2/M progression after G2 checkpoint
0.003429	0.044072	Adipocytokine signaling pathway - Mus musculus (mouse)
0.003693	0.046411	Signaling by VEGF
0.003756	0.046411	Mitochondrial fatty acid Beta-oxidation
0.003851	0.046411	Leucine catabolism
0.004009	0.046411	Inositol phosphate metabolism - Mus musculus (mouse)
0.004325	0.046411	Gastric acid secretion - Mus musculus (mouse)
0.004426	0.046411	Valine, leucine and isoleucine biosynthesis - Mus musculus (mouse)
0.004426	0.046411	Astrocytic glutamate-glutamine uptake and metabolism
0.004426	0.046411	Neurotransmitter uptake and metabolism in glial cells
0.004426	0.046411	Lysine degradation II
0.004426	0.046411	γ-linolenate biosynthesis II (animals)
0.004426	0.046411	Cholesterol biosynthesis via desmosterol
0.004426	0.046411	Cholesterol biosynthesis via lathosterol
0.004515	0.046411	Proteoglycans in cancer - Mus musculus (mouse)

(Continues)

Supplementary table 2.4 (continued).

p-value	q-value	Pathway
0.004547	0.046411	Apoptosis - Mus musculus (mouse)
0.005523	0.055241	Herpes simplex infection - Mus musculus (mouse)
0.005572	0.055241	Insulin signaling pathway - Mus musculus (mouse)
0.005817	0.056861	Inositol phosphate metabolism
0.00614	0.058494	Fatty acid β-oxidation I
0.006153	0.058494	Choline metabolism in cancer - Mus musculus (mouse)
0.006399	0.060011	Platelet activation, signaling and aggregation
0.007241	0.063615	Activation of RAS in B cells
0.007241	0.063615	Sodium-coupled phosphate cotransporters
0.007241	0.063615	The fatty acid cycling model
0.007241	0.063615	The proton buffering model
0.007241	0.063615	Mitochondrial Uncoupling Proteins
0.007489	0.064161	Isoleucine degradation
0.007489	0.064161	Syndecan interactions
0.007594	0.064273	SLC-mediated transmembrane transport
0.008984	0.075118	Circadian rhythm - Mus musculus (mouse)
0.009326	0.077051	Epstein-Barr virus infection - Mus musculus (mouse)
0.009742	0.079211	Collagen biosynthesis and modifying enzymes
0.009816	0.079211	Extracellular matrix organization
0.009942	0.079305	Necroptosis - Mus musculus (mouse)

Supplementary table 2. 5 – Pathways significantly altered in the comparison between EAE and non-induced animals at the chronic phase.

p-value	q-value	Pathway
1.29E-12	7.84E-10	Adar1 editing deficiency immune response
4.83E-11	1.47E-08	Epstein-Barr virus infection - Mus musculus (mouse)
4.66E-10	7.96E-08	Th17 cell differentiation - Mus musculus (mouse)
5.24E-10	7.96E-08	Cell adhesion molecules (CAMs) - Mus musculus (mouse)
2.20E-09	2.68E-07	Antigen processing and presentation - Mus musculus (mouse)
2.71E-09	2.74E-07	Immune System
6.28E-09	5.44E-07	Human T-cell leukemia virus 1 infection - Mus musculus (mouse)
1.01E-08	7.67E-07	Viral myocarditis - Mus musculus (mouse)
3.14E-08	2.10E-06	NOD-like receptor signaling pathway - Mus musculus (mouse)
3.47E-08	2.10E-06	Influenza A - Mus musculus (mouse)
6.42E-08	3.54E-06	Toxoplasmosis - Mus musculus (mouse)
7.19E-08	3.64E-06	Type II interferon signaling (IFNG)
8.24E-08	3.85E-06	TNF signaling pathway - Mus musculus (mouse)
2.05E-07	8.88E-06	Th1 and Th2 cell differentiation - Mus musculus (mouse)
2.46E-07	9.95E-06	Herpes simplex infection - Mus musculus (mouse)
2.64E-07	1.00E-05	TCR signaling
5.81E-07	2.07E-05	Apoptosis
1.25E-06	4.23E-05	Kaposi sarcoma-associated herpesvirus infection - Mus musculus (mouse)
1.38E-06	4.40E-05	TYROBP Causal Network
2.31E-06	7.02E-05	Osteoclast differentiation - Mus musculus (mouse)
6.22E-06	0.000175	Translocation of ZAP-70 to Immunological synapse
6.34E-06	0.000175	Measles - Mus musculus (mouse)
7.34E-06	0.000194	Staphylococcus aureus infection - Mus musculus (mouse)
8.33E-06	0.000211	Tuberculosis - Mus musculus (mouse)
9.94E-06	0.000241	Allograft rejection - Mus musculus (mouse)
1.06E-05	0.000248	Downstream TCR signaling
1.33E-05	0.000288	Inflammatory bowel disease (IBD) - Mus musculus (mouse)
1.33E-05	0.000288	Graft-versus-host disease - Mus musculus (mouse)
1.50E-05	0.000305	Human cytomegalovirus infection - Mus musculus (mouse)
1.51E-05	0.000305	Phosphorylation of CD3 and TCR zeta chains
1.56E-05	0.000306	Generation of second messenger molecules
1.71E-05	0.000323	Death Receptor Signalling
2.02E-05	0.000372	Human immunodeficiency virus 1 infection - Mus musculus (mouse)

(Continues)

Supplementary table 2.5 (continued).

p-value	q-value	Pathway
2.10E-05	0.000374	C-type lectin receptor signaling pathway - Mus musculus (mouse)
2.30E-05	0.000398	Natural killer cell mediated cytotoxicity - Mus musculus (mouse)
2.61E-05	0.000441	Type I diabetes mellitus - Mus musculus (mouse)
2.99E-05	0.000491	NF-kappa B signaling pathway - Mus musculus (mouse)
3.16E-05	0.000505	PD-1 signaling
3.32E-05	0.000511	B Cell Receptor Signaling Pathway
3.36E-05	0.000511	Leishmaniasis - Mus musculus (mouse)
4.28E-05	0.000633	Innate immune system
5.87E-05	0.000848	Adaptive immune system
6.79E-05	0.000959	Autoimmune thyroid disease - Mus musculus (mouse)
9.10E-05	0.001255	Regulation of actin cytoskeleton - Mus musculus (mouse)
0.000115	0.001546	Adipogenesis genes
0.000133	0.001755	Endosomal/Vacuolar pathway
0.000142	0.001832	Apoptosis - Mus musculus (mouse)
0.000145	0.001838	TRAIL signaling
0.000158	0.001961	Osteoclast
0.000166	0.001992	Cytokine signaling in immune system
0.000169	0.001992	Downstream signaling events of B cell receptor (BCR)
0.000174	0.001992	XPodNet - protein-protein interactions in the podocyte expanded by STRING
0.000174	0.001992	Hepatitis C - Mus musculus (mouse)
0.000188	0.002117	Rheumatoid arthritis - Mus musculus (mouse)
0.000198	0.002187	T cell receptor signaling pathway - Mus musculus (mouse)
0.000287	0.003111	Neutrophil degranulation
0.000396	0.004118	Phagosome - Mus musculus (mouse)
0.000407	0.004118	RIPK1-mediated regulated necrosis
0.000407	0.004118	Regulated necrosis
0.000407	0.004118	Interleukin-4 and 13 signaling
0.000468	0.004653	T cell receptor signaling pathway
0.000492	0.004821	Viral carcinogenesis - Mus musculus (mouse)
0.000546	0.005264	Intestinal immune network for IgA production - Mus musculus (mouse)
0.000568	0.005389	IL-2 signaling pathway
0.000608	0.005676	Chemokine signaling pathway
0.000674	0.006092	TNF-alpha NF-κB Signaling Pathway
0.000677	0.006092	Salmonella infection - Mus musculus (mouse)

(Continues)

Supplementary table 2.5 (continued).

p-value	q-value	Pathway
0.000682	0.006092	Activation of NF-kappaB in B cells
0.000719	0.006324	Pathways in cancer - Mus musculus (mouse)
0.000744	0.006407	MHC class II antigen presentation
0.000749	0.006407	JAK-STAT signaling pathway - Mus musculus (mouse)
0.000776	0.006539	Inflammatory response pathway
0.00082	0.006622	Cytokine-cytokine receptor interaction - Mus musculus (mouse)
0.000821	0.006622	Costimulation by the CD28 family
0.000829	0.006622	AGE-RAGE signaling pathway in diabetic complications - Mus musculus (mouse)
0.000829	0.006622	Immunoregulatory interactions between a lymphoid and a non-lymphoid cell
0.001001	0.007888	Chemokine signaling pathway - Mus musculus (mouse)
0.001053	0.008191	Apoptosis - multiple species - Mus musculus (mouse)
0.001273	0.00978	Regulation of actin cytoskeleton
0.001397	0.010598	CLEC7A (Dectin-1) signaling
0.001461	0.010945	Necroptosis - Mus musculus (mouse)
0.00159	0.011271	CASP8 activity is inhibited
0.00159	0.011271	Regulation of necroptotic cell death
0.00159	0.011271	Dimerization of procaspase-8
0.00159	0.011271	Regulation by c-FLIP
0.001597	0.011271	Antigen presentation: folding, assembly and peptide loading of class I MHC
0.001724	0.012027	C-type lectin receptors (CLRs)
0.001838	0.012536	B cell receptor signaling pathway - Mus musculus (mouse)
0.001838	0.012536	Adipocytokine signaling pathway - Mus musculus (mouse)
0.001994	0.013451	Hematopoietic cell lineage - Mus musculus (mouse)
0.002091	0.013949	Leukocyte transendothelial migration - Mus musculus (mouse)
0.002531	0.016701	Interferon signaling
0.002613	0.016982	Antigen processing-cross presentation
0.002658	0.016982	Asthma - Mus musculus (mouse)
0.002658	0.016982	Interleukin-6 family signaling
0.002809	0.017764	TNFR1-induced proapoptotic signaling
0.002963	0.018543	Hepatitis B - Mus musculus (mouse)
0.003266	0.020232	Nucleotide-binding domain, leucine rich repeat containing receptor (NLR) signaling pathways
0.003365	0.020629	IL-3 Signaling Pathway
0.003555	0.020992	TFs Regulate miRNAs related to cardiac hypertrophy

(Continues)

Supplementary table 2.5 (continued).

p-value	q-value	Pathway
0.003555	0.020992	CLEC7A/inflammasome pathway
0.003577	0.020992	Chagas disease (American trypanosomiasis) - Mus musculus (mouse)
0.003597	0.020992	Novel Jun-Dmp1 Pathway
0.003597	0.020992	TNFR1-induced NFkappaB signaling pathway
0.003905	0.022576	IL-4 signaling Pathway
0.004141	0.023713	NOD1/2 Signaling Pathway
0.004457	0.025282	IL-7 signaling pathway
0.005252	0.02952	Cellular senescence - Mus musculus (mouse)
0.005499	0.030624	Ligand-dependent caspase activation
0.006101	0.032953	DAP12 signaling
0.006101	0.032953	Interferon alpha/beta signaling
0.006101	0.032953	Amine compound SLC transporters
0.006135	0.032953	Platelet degranulation
0.006485	0.03453	TNFR2 non-canonical NF-κB pathway
0.006645	0.034591	EDA Signalling in Hair Follicle Development
0.006667	0.034591	IL-5 signaling pathway
0.006667	0.034591	RIG-I-like receptor signaling pathway - Mus musculus (mouse)
0.007746	0.039844	Response to elevated platelet cytosolic Ca2+
0.007923	0.040078	Complement activation, classical pathway
0.007923	0.040078	RHO GTPases activate PAKs
0.008596	0.043124	Toll like receptor signaling
0.009086	0.045208	Chemokine receptors bind chemokines

Supplementary table 2. 6 – Pathways significantly altered in the comparison between EAE animals at the onset and pre-symptomatic phases, after normalization for the respective non-induced group.

p-value	q-value	Pathway
6.46E-08	4.69E-05	Extracellular matrix organization
1.30E-07	4.74E-05	Metabolism
1.19E-06	0.000279	Metabolism of amino acids and derivatives
1.53E-06	0.000279	ECM-receptor interaction - Mus musculus (mouse)
8.06E-06	0.001172	HSP90 chaperone cycle for steroid hormone receptors (SHR)
3.18E-05	0.003851	Laminin interactions
4.26E-05	0.00442	Branched-chain amino acid catabolism
6.58E-05	0.005499	Valine degradation
6.81E-05	0.005499	Proteoglycans in cancer - Mus musculus (mouse)
8.16E-05	0.00558	Thyroid hormone synthesis - Mus musculus (mouse)
8.44E-05	0.00558	ECM proteoglycans
0.000134	0.008114	PodNet- protein-protein interactions in the podocyte
0.000177	0.009913	XPodNet - protein-protein interactions in the podocyte expanded by STRING
0.000215	0.011175	Long-term potentiation - Mus musculus (mouse)
0.000241	0.011697	Amphetamine addiction - Mus musculus (mouse)
0.000295	0.013128	PPAR signaling pathway - Mus musculus (mouse)
0.000313	0.013128	Valine, leucine and isoleucine degradation - Mus musculus (mouse)
0.000325	0.013128	Gap junction - Mus musculus (mouse)
0.000374	0.013698	Leucine catabolism
0.000382	0.013698	Non-integrin membrane-ECM interactions
0.000397	0.013698	Fatty acid Beta-oxidation (streamlined)
0.000415	0.013698	Amoebiasis - Mus musculus (mouse)
0.000451	0.013918	Focal Adhesion-PI3K-Akt-mTOR-signaling pathway
0.000459	0.013918	Gastric acid secretion - Mus musculus (mouse)
0.000563	0.016364	Focal adhesion
0.00068	0.018331	Salivary secretion - Mus musculus (mouse)
0.000683	0.018331	Vascular smooth muscle contraction - Mus musculus (mouse)
0.000706	0.018331	Calcium signaling pathway - Mus musculus (mouse)
0.000896	0.019522	PPAR signaling pathway
0.000896	0.019522	Estrogen signaling pathway - Mus musculus (mouse)
0.000958	0.019522	Dopaminergic synapse - Mus musculus (mouse)
0.000958	0.019522	Syndecan interactions
0.000965	0.019522	Cysteine formation from homocysteine

(Continues)

Supplementary table 2.6 (continued).

p-value	q-value	Pathway
0.000965	0.019522	Cysteine biosynthesis/homocysteine degradation
0.000965	0.019522	Cysteine biosynthesis II
0.000967	0.019522	Collagen biosynthesis and modifying enzymes
0.001032	0.020268	Cellular responses to external stimuli
0.001082	0.020268	Melanogenesis - Mus musculus (mouse)
0.001087	0.020268	A tetrasaccharide linker sequence is required for GAG synthesis
0.001246	0.022343	Mitochondrial LC-fatty acid Beta-oxidation
0.00126	0.022343	Glucagon signaling pathway - Mus musculus (mouse)
0.001311	0.0227	MAPK signaling pathway
0.001404	0.023513	Focal adhesion - Mus musculus (mouse)
0.00146	0.023513	Post-translational protein phosphorylation
0.001488	0.023513	Leucine degradation I
0.001488	0.023513	Valine degradation I
0.001563	0.024169	Cellular responses to stress
0.001749	0.026351	PI3K-Akt signaling pathway - Mus musculus (mouse)
0.001776	0.026351	Inflammatory mediator regulation of TRP channels - Mus musculus (mouse)
0.002127	0.030928	Inflammatory response pathway
0.00218	0.031081	Acetylcholine regulates insulin secretion
0.002261	0.031612	Histidine, lysine, phenylalanine, tyrosine, proline and tryptophan catabolism
0.00274	0.036155	Long-term depression - Mus musculus (mouse)
0.002835	0.036155	Metallothioneins bind metals
0.002835	0.036155	Response to metal ions
0.002835	0.036155	Fatty acid β-oxidation III (unsaturated, odd number)
0.002835	0.036155	Inositol transporters
0.003005	0.03767	Chondroitin sulfate biosynthesis
0.003313	0.040827	Signaling by receptor tyrosine kinases
0.003752	0.044715	Fatty acid Beta-oxidation
0.003752	0.044715	COPI-independent Golgi-to-ER retrograde traffic
0.004089	0.046348	The role of GTSE1 in G2/M progression after G2 checkpoint
0.004089	0.046348	Dermatan sulfate biosynthesis
0.0043	0.046348	Regulation of Insulin-like Growth Factor (IGF) transport and uptake by Insulin-like Growth Factor Binding Proteins (IGFBPs)
0.00432	0.046348	Triacylglyceride synthesis
0.004355	0.046348	Chondroitin sulfate/dermatan sulfate metabolism

(Continues)

Supplementary table 2.6 (continued).

p-value	q-value	Pathway
0.004355	0.046348	Fatty acid degradation - Mus musculus (mouse)
0.004355	0.046348	Arginine and proline metabolism - Mus musculus (mouse)
0.004399	0.046348	Pathways in cancer - Mus musculus (mouse)
0.004526	0.047001	Peroxisome - Mus musculus (mouse)
0.004864	0.049804	Insulin secretion - Mus musculus (mouse)
0.004943	0.049907	Protein processing in endoplasmic reticulum - Mus musculus (mouse)
0.005044	0.050232	Fluid shear stress and atherosclerosis - Mus musculus (mouse)
0.005297	0.051637	One carbon metabolism and related pathways
0.005327	0.051637	CDP-diacylglycerol biosynthesis II
0.005553	0.053116	Valine, leucine and isoleucine biosynthesis - Mus musculus (mouse)
0.005982	0.056482	MAPK signaling pathway
0.006116	0.057002	Mitochondrial fatty acid Beta-oxidation
0.006413	0.059019	Primary focal segmental glomerulosclerosis FSGS
0.006767	0.059995	Phosphatidylglycerol biosynthesis I (plastidic)
0.006767	0.059995	CDP-diacylglycerol biosynthesis I
0.006767	0.059995	Regulation of KIT signaling
0.006855	0.060047	GnRH signaling pathway - Mus musculus (mouse)
0.007805	0.067547	Small cell lung cancer - Mus musculus (mouse)
0.008416	0.071147	Phosphatidylglycerol biosynthesis II (non-plastidic)
0.008416	0.071147	Omega-9 FA synthesis
0.008618	0.072013	Fatty acid metabolism
0.009065	0.072417	Disinhibition of SNARE formation
0.009065	0.072417	The fatty acid cycling model
0.009065	0.072417	The proton buffering model
0.009065	0.072417	Mitochondrial uncoupling proteins
0.009174	0.072496	Fatty acid Beta-oxidation I

Supplementary table 2. 7 – Pathways significantly altered in the comparison between EAE animals at the chronic and pre-symptomatic phases, after normalization for the respective non-induced group.

p-value	q-value	Pathway
0.000164	0.028341	Cilium assembly
0.000384	0.033188	Organelle biogenesis and maintenance
0.001049	0.056976	Cell junction organization
0.001634	0.056976	Adherens junctions interactions
0.002353	0.056976	Acyl-CoA hydrolysis
0.002811	0.056976	Translocation of ZAP-70 to Immunological synapse
0.002811	0.056976	TNFR1-induced proapoptotic signaling
0.002868	0.056976	Cell-cell communication
0.002964	0.056976	Intraflagellar transport
0.003594	0.060421	Cell-cell junction organization
0.003842	0.060421	Phosphorylation of CD3 and TCR zeta chains
0.006249	0.089271	Phagosome - Mus musculus (mouse)
0.006708	0.089271	Tuberculosis - Mus musculus (mouse)
0.009364	0.108426	Huntington disease - Mus musculus (mouse)

Supplementary table 2. 8 – Pathways significantly altered in the comparison between EAE animals at the chronic and onset phases, after normalization for the respective non-induced group.

p-value	q-value	Pathway
7.33E-13	4.43E-10	Metabolism
7.32E-07	0.000221	Metabolism of amino acids and derivatives
1.32E-06	0.000266	Translocation of ZAP-70 to Immunological synapse
2.28E-06	0.00028	Fatty acid metabolism
2.66E-06	0.00028	AMPK signaling pathway - Mus musculus (mouse)
2.93E-06	0.00028	PPAR signaling pathway - Mus musculus (mouse)
3.24E-06	0.00028	Phosphorylation of CD3 and TCR zeta chains
7.53E-06	0.000569	Cell adhesion molecules (CAMs) - Mus musculus (mouse)
1.48E-05	0.000997	PPAR signaling pathway
1.98E-05	0.001199	Metabolism of lipids
2.73E-05	0.001503	Insulin resistance - Mus musculus (mouse)
3.78E-05	0.001908	Fatty acid biosynthesis
6.54E-05	0.003044	Estrogen metabolism
0.000109	0.00473	MHC class II antigen presentation
0.00016	0.006434	PD-1 signaling
0.000193	0.007311	Oleate biosynthesis II (animals)
0.000206	0.007319	Serotonin and anxiety
0.00025	0.008393	Fatty acid Beta-oxidation (streamlined)
0.000268	0.008546	Fluid shear stress and atherosclerosis - Mus musculus (mouse)
0.000286	0.008662	Adipocytokine signaling pathway - Mus musculus (mouse)
0.000336	0.00969	Proteoglycans in cancer - Mus musculus (mouse)
0.000499	0.013712	Valine, leucine and isoleucine degradation - Mus musculus (mouse)
0.000643	0.01691	Viral myocarditis - Mus musculus (mouse)
0.000703	0.017715	Generation of second messenger molecules
0.000745	0.018019	VEGFA-VEGFR2 Pathway
0.000859	0.019359	Antigen processing and presentation - Mus musculus (mouse)
0.000864	0.019359	Serotonin and anxiety-related events
0.000964	0.020118	Metallothioneins bind metals
0.000964	0.020118	Response to metal ions
0.001135	0.02289	Thyroid hormone signaling pathway - Mus musculus (mouse)
0.001285	0.024883	Signaling by VEGF
0.001316	0.024883	Fatty acid Beta-oxidation I
0.001458	0.02673	Import of palmitoyl-CoA into the mitochondrial matrix

(Continues)

Supplementary table 2.8 (continued).

p-value	q-value	Pathway
0.001659	0.028823	Post-translational protein phosphorylation
0.001745	0.028823	Chemokine signaling pathway
0.001757	0.028823	Primary Focal Segmental Glomerulosclerosis FSGS
0.001831	0.028823	Omega-9 FA synthesis
0.001843	0.028823	TCR signaling
0.001906	0.028823	γ-linolenate biosynthesis II (animals)
0.001906	0.028823	Amine oxidase reactions
0.002019	0.029077	Fatty acid degradation - Mus musculus (mouse)
0.002019	0.029077	Arginine and proline metabolism - Mus musculus (mouse)
0.00223	0.031053	Amino acid synthesis and interconversion (transamination)
0.002258	0.031053	Valine degradation
0.002482	0.032349	Glucagon signaling pathway - Mus musculus (mouse)
0.002513	0.032349	Downstream TCR signaling
0.002513	0.032349	Citrate cycle (TCA cycle) - Mus musculus (mouse)
0.002584	0.03257	Chemokine signaling pathway - Mus musculus (mouse)
0.002743	0.033445	Mitochondrial LC-Fatty Acid Beta-Oxidation
0.002853	0.033445	Adipogenesis genes
0.003081	0.033445	Signaling by FGFR1
0.003138	0.033445	Activation of RAS in B cells
0.003138	0.033445	The fatty acid cycling model
0.003138	0.033445	The proton buffering model
0.003138	0.033445	Mitochondrial Uncoupling Proteins
0.003151	0.033445	Fatty acid Beta-oxidation
0.003151	0.033445	Metabolism of polyamines
0.003338	0.034818	MAPK signaling pathway
0.003407	0.034824	Biological oxidations
0.003508	0.034824	Glycolysis
0.003511	0.034824	Pathways in cancer - Mus musculus (mouse)
0.003578	0.034916	The citric acid (TCA) cycle and respiratory electron transport
0.003891	0.036351	Fatty acyl-CoA biosynthesis
0.003905	0.036351	Regulation of Insulin-like Growth Factor (IGF) transport and uptake by Insulin-like Growth Factor Binding Proteins (IGFBPs)
0.003905	0.036351	Insulin signaling pathway - Mus musculus (mouse)
0.004109	0.037667	Peroxisome - Mus musculus (mouse)

(Continues)

Supplementary table 2.8 (continued).

p-value	q-value	Pathway
0.004651	0.040783	Regulation of ornithine decarboxylase (ODC)
0.004651	0.040783	AMPK inhibits chREBP transcriptional activation activity
0.004741	0.040976	Mitochondrial fatty acid Beta-oxidation
0.005177	0.043772	Costimulation by the CD28 family
0.005209	0.043772	Downstream signaling of activated FGFR1
0.00575	0.047522	Regulation of actin cytoskeleton - Mus musculus (mouse)
0.005813	0.047522	Human cytomegalovirus infection - Mus musculus (mouse)
0.006095	0.049167	Non-integrin membrane-ECM interactions
0.006236	0.049646	Bladder cancer - Mus musculus (mouse)
0.006632	0.052018	Oxytocin signaling pathway - Mus musculus (mouse)
0.006797	0.052018	Intestinal immune network for IgA production - Mus musculus (mouse)
0.006964	0.052018	Downstream signaling events of B Cell Receptor (BCR)
0.006964	0.052018	Branched-chain amino acid catabolism
0.006964	0.052018	GP generic
0.008016	0.059143	Mineral absorption - Mus musculus (mouse)
0.008478	0.061795	Dopamine degradation
0.008914	0.064202	Asthma - Mus musculus (mouse)
0.009507	0.067665	AGE-RAGE signaling pathway in diabetic complications - Mus musculus (mouse)

Supplementary material references

Cahoy JD, Emery B, Kaushal A, Foo LC, Zamanian JL, Christopherson KS, et al. A transcriptome database for astrocytes, neurons, and oligodendrocytes: a new resource for understanding brain development and function. Journal of Neuroscience. 2008;28:264-278.

Heng X, Guo Q, Leung AW, Li JY. Analogous mechanism regulating formation of neocortical basal radial glia and cerebellar Bergmann glia. eLife. 2017;6.

Koirala S, Corfas G. Identification of novel glial genes by single-cell transcriptional profiling of Bergmann glial cells from mouse cerebellum. PloS One. 2010;5:e9198.

Palmer C, Diehn M, Alizadeh AA, Brown PO. Cell-type specific gene expression profiles of leukocytes in human peripheral blood. BMC Genomics. 2006;7:115.

Zhang Y, Chen K, Sloan SA, Bennett ML, Scholze AR, O'Keeffe S, et al. An RNA-sequencing transcriptome and splicing database of glia, neurons, and vascular cells of the cerebral cortex. Journal of Neuroscience. 2014;34:11929-11947.

CHAPTER 3

Sofia Pereira das Neves, Sónia Guerra-Gomes, João José Cerqueira, João Filipe Oliveira, Fernanda Marques

Experimental autoimmune encephalomyelitis induction in a model of astrocytic global calcium signaling impairment

(Manuscript in preparation)

(2020)

Title

Experimental autoimmune encephalomyelitis induction in a model of astrocytic global calcium signaling impairment

Authors

Sofia Pereira das Neves [a,b], Sónia Guerra-Gomes [a,b], João José Cerqueira [a,b,c], Nuno Sousa [a,b,c], João Filipe Oliveira [a,b,d], Fernanda Marques [a,b]

Affiliations

[a] Life and Health Sciences Research Institute (ICVS), School of Medicine, University of Minho, Campus Gualtar, 4710-057 Braga, Portugal.

[b] ICVS/3B's – PT Government Associate Laboratory, Braga/Guimarães, Portugal.

[c] Clinical Academic Center - Braga, Braga, Portugal.

[d] IPCA-EST-2Ai, Applied Artificial Intelligence Laboratory, Polytechnic Institute of Cávado and Ave, Campus of IPCA, Barcelos, Portugal.

Corresponding author

Fernanda Marques (PhD), Life and Health Sciences Research Institute (ICVS), School of Medicine, University of Minho, Campus Gualtar, 4710-057 Braga, Portugal.

Phone number: +351 253 604 839

E-mail: fmarques@med.uminho.pt

Abstract

Growing evidence suggest that peripheral inflammatory cells alone cannot explain the neurodegenerative processes observed in multiple sclerosis (MS). Rather, evidence suggests that disease progression and disability is better correlated with the maintenance of a low-grade persistent inflammation inside the CNS, driven by local glial cells, such as astrocytes. Considering that the modulation of intracellular Ca^{2+} levels is the major modulator of astrocyte signaling, in this work we explored the role of astrocytic calcium signaling in MS. To do so, we induced EAE in type 2 inositol 1,4,5-triphosphate receptor (IP_3R2)-null animals, whose astrocytes present minimal Ca^{2+} elevations in the soma and main processes. No differences were observed regarding disease progression, as evaluated by the clinical score, however IP_3R2-null animals presented a decreased lesion burden in the cerebellum, compared to Wt littermates. Also, astrocytes from IP_3R2-null animals had increased length and complexity near lesions, compared to the non-lesioned areas. We hypothesize that in IP_3R2-null animals, at a more inflammatory phase of the disease, astrocytes become more reactive near the lesions, and so are able to control better immune cell infiltration, resulting in smaller lesions.

Introduction

Multiple sclerosis (MS) is characterized by an autoimmune reaction against the myelin sheath that surrounds central nervous system (CNS) axons, leading to demyelination and, consequently, to axonal and neuronal damage (Sospedra and Martin, 2005). However, growing evidence suggest that T cell-mediated inflammatory mechanisms alone cannot explain the neurodegenerative processes observed. In this regard, it was proposed that the innate immune response of resident CNS cells, including microglia and astrocytes, also plays a role in oligodendrocyte injury and axonal degeneration (Correale and Farez, 2015). Regarding astrocytes, in the disease context, they become hypertrophied and upregulate GFAP and vimentin, and gliosis is a characteristic feature of demyelinated plaques (Williams et al., 2007). Moreover, astrocytes may contribute for leukocyte migration to the CNS by secreting both cytokines and metalloproteinases (Brosnan and Raine, 2013). On the other hand, astrocytes may also play a beneficial role in MS by secreting factors involved in lesion repair (Voskuhl et al., 2009).

Alterations in intracellular calcium (Ca^{2+}) levels ($[Ca^{2+}]_i$) are the major modulator of astrocyte signaling (Guerra-Gomes et al., 2017; Petravicz et al., 2008; Strokin et al., 2011). Appropriate Ca^{2+} signaling is important for several astrocytic functions, including regulation of gene expression, gliotransmitter release, local blood flow and morphological plasticity of astrocytic processes (Strokin et al., 2011; Wu et al., 2019). The most widely accepted mechanism for astrocytic Ca^{2+} increase is the phospholipase C (PLC)/inositol 1,4,5-triphosphate (IP_3) pathway. In response to G_q G protein-coupled receptor activation, PLC hydrolyses phosphatidylinositol 4,5-biphosphate to diacylglycerol and IP_3, which is going to activate IP_3 receptors (IP_3Rs) and result in Ca^{2+} release from the endoplasmic reticulum (Agulhon et al., 2008; Petravicz et al., 2008; Vardjan and Zorec, 2015). Immunohistochemistry and transcriptomic analysis showed that, in the CNS, type 2 IP_3R (IP_3R2) is mainly expressed in astrocytes (Hertle and Yeckel, 2007; Sharp et al., 1999). In addition, previous *in vitro* and *in vivo* studies showed that genetic deletion of IP_3R2 resulted in complete loss of spontaneous and agonist-evoked IP_3R-dependent Ca^{2+} increases in astrocytes (Agulhon et al., 2008; Petravicz et al., 2008). Of interest, Staats and colleagues (2016) observed an overexpression of the *Itpr2* gene in the spinal cord of experimental autoimmune encephalomyelitis (EAE) animals (Staats et al., 2016), and our transcriptomic results also demonstrated an increased astrocytic expression of this gene, in the cerebellum of EAE animals, at the onset phase of disease (unpublished results).

Thus, considering that EAE animals overexpress *Itpr2* in regions affected by the disease and that proper Ca^{2+} signaling in astrocytes is crucial for their function, in this work we studied the functional outcome of "silencing" astrocytes in the EAE mice model.

Methods

Animals and EAE induction

All experiments were reviewed and approved by the Portuguese national authority for animal experimentation, *Direção Geral de Veterinária* (ID: DGV9458). Animals were housed and handled in accordance with the guidelines for the care and handling of laboratory animals in the Directive 2010/63/EU of the European Parliament and the Council.

Animals were housed and maintained in a specific pathogen free environment at 22-24°C and 55% humidity, on 12 hours (h) light/dark cycles (lights on from 8 a.m. to 8 p.m.) and fed with regular chow and tap water *ad libitum*. Paper towels were used as environmental enrichment. Paralyzed mice, with clinical scores above 3, were offered easier access to food and water.

IP_3R2-null mice were kindly given by Prof. Alfonso Araque (University of Minnesota, USA) (Navarrete et al., 2012), under agreement with Prof. Ju Chen (University of San Diego, USA) (Li et al., 2005). Mice were backcrossed to C57BL/6 for at least five generations in our lab. IP_3R2-null and wild-type (Wt) littermates were obtained in our lab by crossing $IP_3R2^{+/-}$ mice. Toe clipping was performed on P6-P7 pups for genotyping and identification.

IP_3R2-null female mice and Wt littermates, with 9-15 weeks of age (18.1-26.0 g) were induced with EAE using a commercially available kit (EK-2110; Hooke Laboratories, USA). Briefly, animals were immunized subcutaneously with 200 µg of myelin oligodendrocyte glycoprotein 35-55 (MOG_{35-55}), emulsified in complete Freund's adjuvant (lot# 0114 and #0126 for experiments 1 and 2, respectively), at the upper and lower back. Pertussis toxin (PTX) in phosphate buffered saline (PBS) was administered intraperitoneally 2 and 24h after immunization (227 ng of PTX from lot# 1001 and 90.8 ng per injection from lot#1007, for experiments 1 and 2 respectively).

Animals were daily weighted and monitored for clinical symptoms of disease. Disease severity was evaluated as previously described (das Neves et al., 2018), in a blind manner regarding the animals' genotype. Only one animal, an IP_3R2-null, died during the experiment, at day 17 post-induction, and was excluded from all analysis.

Tissue sample collection

For biological sample collection, EAE animals were sacrificed at the light phase of the diurnal cycle, at day 16 (active phase of disease, onset phase, experiment 1) and 30 (chronic phase, experiment 2) post-disease induction. Animals were anesthetized with an intraperitoneal injection of ketamine hydrochloride (150 mg/kg, Imalgene 1000; Merial, USA) plus medetomidine hydrochloride (0.3 mg/kg, Dorben Vet;

Pfizer, USA). Under deep anesthesia, mice were transcardially perfused with cold 0.9% saline solution, and the brain and spinal cord were dissected. For histological analysis, the brain was immediately embedded in Tissue-Tek O.C.T. compound (Sakura Finetek, Japan), snap-frozen and kept frozen until further sectioning.

Luxol Fast Blue staining

Serial 20 µm sections of frozen cerebellum were cut in the cryostat and collected to SuperFrost Plus slides (ThermoFisher Scientific, USA), and were posteriorly stained with Luxol Fast Blue as reported previously (das Neves et al., 2018). The quantification of the total lesioned area was done in 5 non-consecutive sections per animal, representative of the entire cerebellum, in a blind manner regarding the animals' genotype. The sections were visualized with an Olympus BX51 stereological microscope, and the quantification of the areas was performed with the Visiopharm integrator system software (version 2.12.3.0, Hoersholm, Denmark). The total white matter area was drawn using a 4x objective, and the lesion areas using the 10x objective. The percentage of lesioned area, for each section, was calculated by dividing the sum of the lesioned areas by the total white matter area. Statistical analysis was performed using the average of all sections of the animal.

GFAP immunofluorescence and 3-dimensional reconstruction of astrocytes

Serial 20 µm sections of cerebellum (coronal sections) were stained for GFAP. Sections were fixed in 4% paraformaldehyde (PFA) in PBS for 30 minutes (min) at room temperature (RT). After antigen retrieval, with pre-heated citrate buffer (Sigma-Aldrich) in the microwave for 20 min, tissue slices were permeabilized with PBS-triton 0.3%, for 10 min, and subsequently blocked with 10% fetal bovine serum in PBS-triton 0.3%, for 30 min. Sections were incubated over-night with rabbit anti-mouse GFAP antibody in blocking solution (1:200; Dako), and, afterwards, with Alexa Fluor 594 goat anti-rabbit diluted in PBS-triton 0.3% (1:500; Fisher Technologies, Thermo Fisher Scientific), for 2 hours. After incubation with 4′,6-diamidino-2-phenylindole (DAPI; 1:200; Invitrogen, Thermo Fisher Scientific), for 10 min, slides were coversliped with Immumount (Fisher Scientific, Thermo Fisher Scientific). All steps were performed at RT, except for antigen retrieval, and were followed by a washing step using PBS or PBS-triton 0.3%.

To perform the 3-dimensional reconstruction of astrocytes, 2-4 photographs per animal were taken from the cerebellum white matter, near lesion regions and in normal appearing white matter (NAWM) regions, using a confocal microscope (FV1000, Olympus) and the following parameters: 40x objective, 1024x1024 resolution, 1 µm increment. The confocal images were then used to performe the

morphological reconstruction using the Fiji plugin "Simple Neurite Tracer" (Longair et al., 2011; Schindelin et al., 2012), as previously described (Tavares et al., 2017). For Sholl analysis, concentric circles were superimposed on astrocytes, with origin in the cell soma and with 4 µm distance from each other. 5-6 astrocytes were reconstructed per animal, and their average was used for statistical analysis.

Statistical analysis

Statistical analysis was performed using SPSS software (version 23, IBM, USA). Sample normality was assessed using the Shapiro-Wilk normality test. EAE animals of both genotypes were compared using a two-tailed unpaired t-test or the Mann-Whitney U test, respectively, for samples with and without a normal distribution. For the percentage of lesioned area, comparison between genotypes and disease time points was performed with a two-way ANOVA. The repeated measures ANOVA was used to analyze the results of the weight, clinical score, total astrocytic length and astrocytic Sholl analysis. The Bonferroni's multiple comparison test was used as post-hoc test. The partial eta squared value (η_p^2) was calculated as a measure of effect size.

Results are presented as mean ± standard error of the mean (SEM) for parametric statistical tests, or median ± interquartile range (IQR) for non-parametric statistical tests. For Sholl analysis, results are presented only as mean. The number of biological replicates (n) are specified in the legend of each figure. Statistical significance was considered for $p < 0.05$ (*), $p < 0.01$ (**), $p < 0.001$ (***), $p < 0.0001$ (****).

Results

Similar disease development in IP$_3$R2-null animals and Wt littermates

IP$_3$R2-null animals and Wt littermates immunized with MOG$_{35-55}$ developed disease in a similar fashion (Figure 3. 1A. Time factor: $F_{(30,540)} = 92.033$, $p < 0.0001$, $\eta_p^2 = 0.836$; genotype factor: $F_{(1,18)} = 1.036$, $p = 0.3222$; interaction: $F_{(30,540)} = 0.459$, $p = 0.9945$). The animals reached the peak of disease by days 15-16 post-induction, and this average clinical score was maintained until the end of the experiment, at day 30 post-induction. The weight of both genotypes was also similar along disease development. As expected, we observed a weight loss in the days following symptoms appearance (Figure 3. 1B. Time factor: $F_{(30,510)} = 41.698$, $p < 0.0001$, $\eta_p^2 = 0.710$; genotype factor: $F_{(1,17)} = 0.859$, $p = 0.3669$; interaction: $F_{(30,510)} = 0.730$, $p = 0.8528$).

On average, IP$_3$R2-null and Wt littermates presented the first clinical symptoms of disease at the same day post-induction (Figure 3. 1C. $t_{(18)} = 0.521$, $p = 0.6088$), and they also progressed similarly to a score of 3 (paralysis of both hind paws) (Figure 3. 1D. $U = 32.50$, $p = 0.5016$). Moreover, both genotypes presented similar clinical scores on the first day of disease (Figure 3. 1E. $U = 48.00$, $p = 0.8703$).

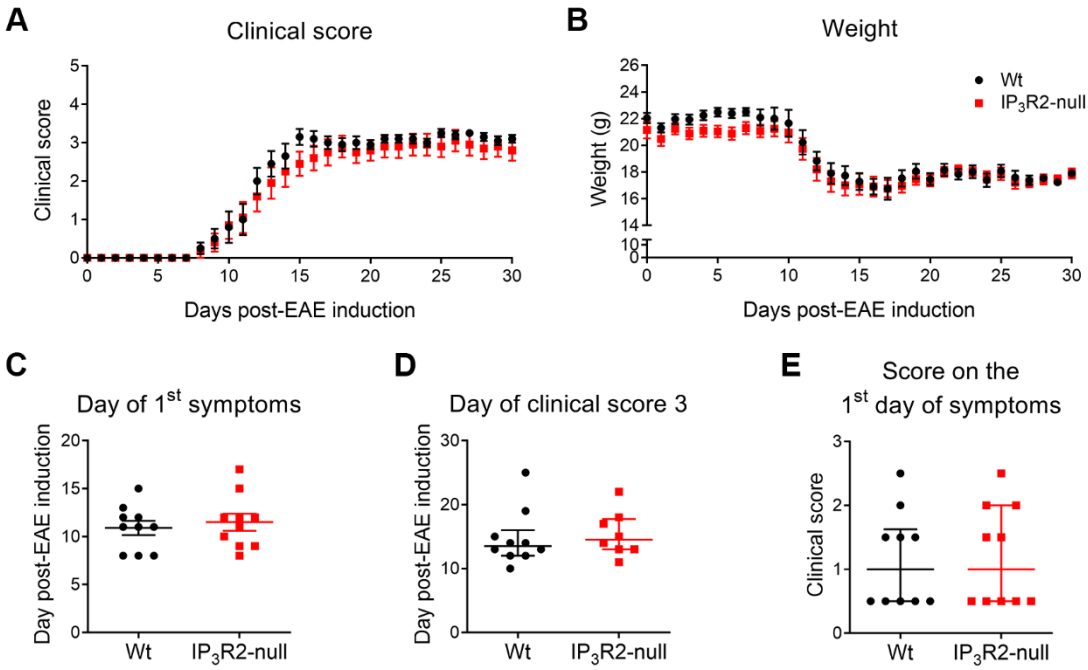

Figure 3. 1 – IP$_3$R2-null EAE animals presented a disease course similar to their Wt EAE littermates. (A) IP$_3$R2-null and Wt littermates developed EAE in a similar way until the end of the experiment (day 30), presenting no differences regarding the clinical score. (B) Also, the weight variation was similar between genotypes, having both groups lost weight after the appearance of clinical symptoms of disease. (C) IP$_3$R2-null and Wt littermates presented the first symptoms of disease and (D) reached a clinical score of 3 on average on the same day. (E) The

(Continues)

score given on the first day of disease was similar between genotypes. Data from one representative experiment is presented as mean ± SEM or median ± IQR. n_{Wt} = 10, $n_{IP3R2\text{-}null}$ = 8 in (D); n_{Wt} = 10, $n_{IP3R2\text{-}null}$ = 10 for remaining graphs.

Decreased lesion burden in the cerebellum of IP$_3$R2-null animals at the onset phase of disease

Even though no differences were observed between genotypes regarding their clinical score, which is mainly dependent on lesion burden at the spinal cord, we next wanted to evaluate if the lesion burden was altered in the cerebellum, which is also affected in EAE and MS. To do so, we quantified the percentage of lesioned area in the cerebellum white matter (Figure 3. 2A), at a more active phase of the disease, the onset phase (day 16), and later at the chronic phase (day 30). As previously published by our group (das Neves et al., 2018), we found a decreased percentage of lesioned area at the chronic phase of disease compared to the onset phase. Interestingly, at the onset phase, the IP$_3$R2-null animals showed a significant decrease in lesion burden compared to their Wt littermates (Figure 3. 2B. Time point factor: $F_{(1,23)}$ = 54.259, p < 0.0001 , η_p^2 = 0.702; genotype factor: $F_{(1,23)}$ = 10.636, p = 0.0034, η_p^2 = 0.316; interaction: $F_{(1,23)}$ = 20.308, p = 0.0002, η_p^2 = 0.469).

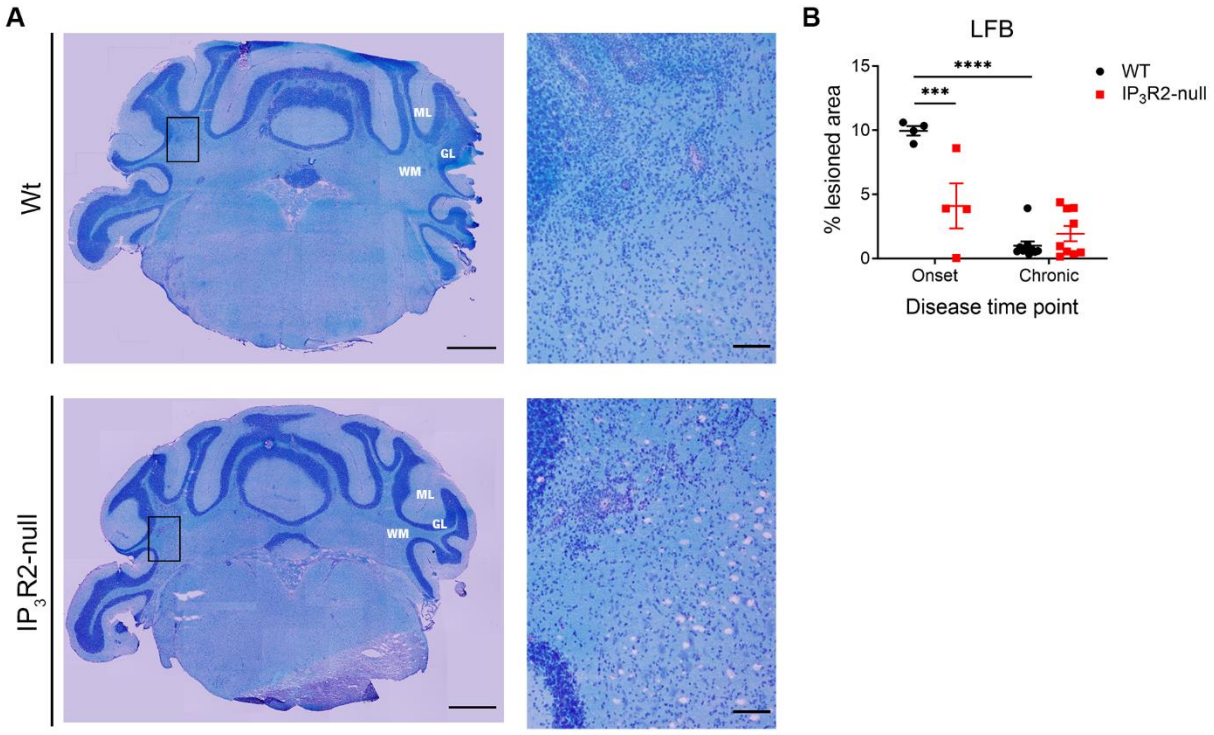

Figure 3. 2 – IP$_3$R2-null presented a decreased percentage of lesion area compared to Wt animals, at the onset phase of disease.

(A) Both groups of EAE animals presented lesioned areas, characterized by inflammatory infiltrates and paler blue staining with LFB [scale bars indicate 1 mm for lower magnification (left) and 100 µm for higher magnification

(Continues)

(right)]. (B) The percentage of white matter area occupied by these lesions was decreased in IP_3R2-null animals compared to Wt littermates, at the onset phase of disease. Data presented as mean ± SEM. $n_{Wt\ onset} = 4$; $n_{IP3R2\text{-}null\ onset} = 4$; $n_{Wt\ chronic} = 10$; $n_{IP3R2\text{-}null\ chronic} = 9$. *** $p < 0.001$, **** $p < 0.0001$. GL – granular layer; LFB – Luxol Fast Blue; ML – molecular layer; WM – white matter.

Increased astrocytic complexity near lesion regions in IP_3R2-null animals

Since we observed differences between genotypes regarding the total white matter area occupied by lesions, at the onset phase of disease, we next reconstructed astrocytes near these lesion regions and compared with astrocytes from regions where the white matter appeared normal (NAWM) (Figure 3. 3A). Representative images of the astrocytes reconstructed are presented in Figure 3. 3B. Regarding the total astrocytic length, we observed that astrocytes located near lesion regions were significantly longer than astrocytes from the NAWM, but this was only significant for the IP_3R2-null animals (Figure 3. 3C. Region factor: $F_{(1,6)} = 11.820$, $p = 0.0138$, $\eta_p^2 = 0.663$; genotype factor: $F_{(1,6)} = 0.657$, $p = 0.4485$; interaction: $F_{(1,6)} = 7.682$, $p = 0.0324$, $\eta_p^2 = 0.561$). Moreover, IP_3R2-null astrocytes were also more complex, presenting more ramifications, near lesion regions compared to NAWM regions (Figure 3. 3D. Region factor: $F_{(1,6)} = 17.413$, $p = 0.0059$, $\eta_p^2 = 0.744$; genotype factor: $F_{(1,6)} = 0.192$, $p = 0.6765$; radius factor: $F_{(18,108)} = 261.762$, $p < 0.0001$, $\eta_p^2 = 0.978$; region*genotype interaction: $F_{(1,6)} = 9.401$, $p = 0.0221$, $\eta_p^2 = 0.610$; radius*genotype interaction: $F_{(18,108)} = 1.049$, $p = 0.4129$; region*radius interaction: $F_{(18,108)} = 0.814$, $p = 0.6799$; region*radius*genotype interaction: $F_{(18,108)} = 0.521$, $p = 0.9429$).

At the chronic phase of disease, no differences were observed between genotypes or cerebellum regions (Supplementary figure 3. 1. Total length: region factor: $F_{(1,6)} = 3.914$, $p = 0.0952$; genotype factor: $F_{(1,6)} = 1.037$, $p = 0.3478$; interaction: $F_{(1,6)} = 1.942$, $p = 0.2129$. Sholl analysis: Region factor: $F_{(1,6)} = 2.643$, $p = 0.1551$; genotype factor: $F_{(1,6)} = 0.673$, $p = 0.4434$; radius factor: $F_{(23,138)} = 251.819$, $p < 0.0001$, $\eta_p^2 = 0.977$; region*genotype interaction: $F_{(1,6)} = 1.510$, $p = 0.2651$; radius*genotype interaction: $F_{(23,138)} = 0.566$, $p = 0.9436$; region*radius interaction: $F_{(23,138)} = 1.647$, $p = 0.0419$, $\eta_p^2 = 0.215$; region*radius*genotype interaction: $F_{(23,138)} = 0.700$, $p = 0.8392$).

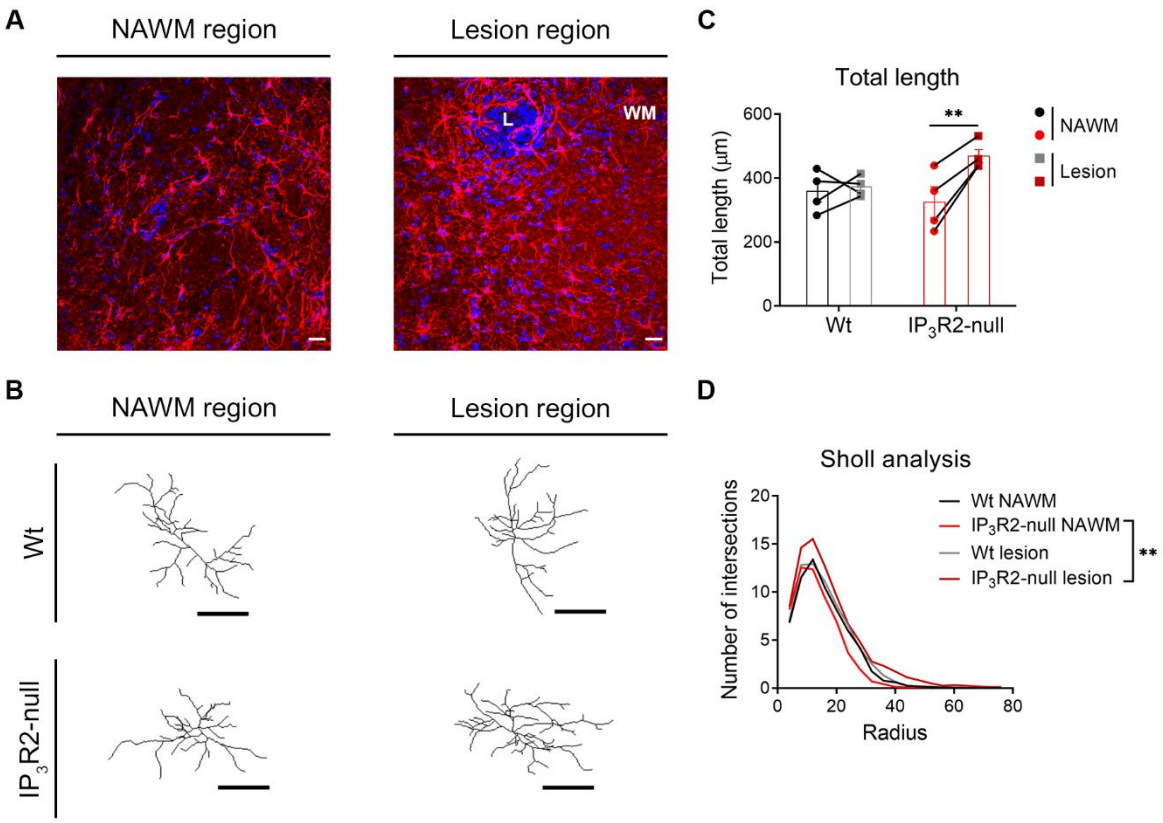

Figure 3. 3 – At the onset phase of disease, astrocytes from IP_3R2-null animals were more complex near lesion regions.

(A) Representative images of cerebellum sections immunostained for GFAP (scale bar represents 20 μm). (B) Representative drawings of astrocytes reconstructed using the Simple Neurite Tracer plugin of Fiji (scale bar represents 20 μm). (C) At the onset phase of disease, IP_3R2-null mice presented longer astrocytes near lesion regions compared to NAWM regions, while Wt animals' astrocytes were similar in both regions. (D) IP_3R2-null animals also presented astrocytes more complex near lesion regions, compared to NAWM regions, as evaluated by the Sholl analysis. Data presented as mean ± SEM for total length and as mean for Sholl analysis. n = 4 per experimental group, 5-6 astrocytes reconstructed per animal. ** $p < 0.01$. L – lesion, NAWM – normal appearing white matter, WM – white matter.

Discussion

It is well known that astrocytes play diverse and important roles both in physiological and pathological conditions. In this regard, astrocytic intracellular Ca^{2+} signaling has gained increased attention since these cells are electrically not excitable, but present robust spontaneous and stimulus-induced Ca^{2+} transients (Okubo et al., 2019; Shigetomi et al., 2016). In fact, alterations in glial Ca^{2+} signaling were suggested to be associated with different neuropathologies (Nedergaard et al., 2010; Shigetomi et al., 2016). In stroke, the propagation of the infarction was associated with aberrant astroglial Ca^{2+} waves, which in turn induced waves of astroglial glutamate release that resulted in distant excitotoxicity (Nedergaard et al., 2010). *In vivo* imaging studies have also suggested that astrocytic Ca^{2+} homeostasis and signaling is altered in an Alzheimer's disease mice model, particularly in astrocytes surrounding amyloid beta plaques (Kuchibhotla et al., 2009; Nedergaard et al., 2010; Shigetomi et al., 2016).

In this work we sought to explore the role of astrocytic Ca^{2+} signaling in MS. To do so, we induced EAE in IP_3R2-null animals, which present "silent" astrocytes, with minimal Ca^{2+} elevations in the soma and main processes. Regarding the clinical score of the animals, we did not find differences between genotypes, however IP_3R2-null animals presented a decreased lesion burden in the cerebellum, compared to Wt littermates. In the IP_3R2-null animals, this was accompanied by a significant increase in astrocytic length and complexity near lesions, compared to the NAWM. We hypothesize that in IP_3R2-null animals, at a more active phase of the disease, astrocytes become more reactive near the lesions, and so are able to control better cell infiltration, resulting in smaller lesions.

Our results go along with studies performed in other disease models, which have shown a phenotype improvement after IP_3R2 ablation. In particular, IP_3R2 ablation in the APPPS1 mice model of Alzheimer's disease ($Appps1^{+/-}$ x $IP_3R2^{-/-}$) was able to improve spatial memory deficits, in comparison with diseased animals presenting functional astrocytic Ca^{2+} signaling ($Appps1^{+/-}$ x $IP_3R2^{+/+}$) (Reichenbach et al., 2018). In another study, using a model of brain ischemia, IP_3R2-null animals exhibited reduced brain damage, neuronal death and tissue loss, compared to Wt mice, which resulted in improved functional behavioral. However, in this study the authors refer an attenuation of the reactive astrogliosis, characterized by a decreased density of GFAP positive cells (Li et al., 2015), while we suggest that the decrease in the lesioned area observed in IP_3R2-null animals is accompanied by an increased astrocytic reactivity. It is conceivable that different pathologies present differences in the inflammatory mediators produced, resulting in different states of astrocytic reactivity, and also that the same activation state could be beneficial in the context of a disease, but deleterious in another. Even in the context of EAE model, different results were observed after targeting astrogliosis. In one study, EAE mice treated with MW01-5-

188WH, a drug that targets glial activation, for 30 days, starting on the day of induction, presented an amelioration of the clinical score, accompanied by a partial rescue of oligodendrocytes from cell death (Guo et al., 2007). In another study, GFAP-thymidine kinase mice induced with EAE and treated with ganciclovir, since day 7 post-immunization, to ablate proliferating reactive astrocytes, exhibited a rapid acute EAE course that was significantly more severe (Voskuhl et al., 2009).

Herein, after EAE induction, we showed that IP_3R2-null animals presented decreased lesion burden in the cerebellum in comparison with Wt littermates and this was probably associated with increased astrocytic length and complexity near lesion regions.

Acknowledgements

The authors are grateful to Prof. Alfonso Araque and Prof. Ju Chen for sharing the mice line.

Funding

This work was supported by Foundation for Science and Technology (FCT) and COMPETE through the project EXPL/NEU-OSD/2196/2013 and by The Clinical Academic Center (2CA-Braga) through the project EXPL/001/2016. The work at ICVS/3B's has been developed under the scope of the project NORTE-01-0145-FEDER-000013, supported by the Northern Portugal Regional Operational Programme (NORTE 2020), under the Portugal 2020 Partnership Agreement, through the European Regional Development Fund (FEDER), and funded by FEDER funds through the Competitiveness Factors Operational Programme (COMPETE), and by National funds, through the Foundation for Science and Technology (FCT), under the scope of the project POCI-01-0145-FEDER-007038. FM is an assistant researcher and recipient of an FCT Investigator grant with the reference CEECIND/01084/2017. JO is a recipient of an FCT Investigator grant with the reference IF/00328/2015, and Bial Foundation grants with the references 207/14 and 037/18. SG and SN are recipients of Ph.D. fellowships with the references SFRH/BD/101298/2014 and PD/BD/114120/2015, respectively, from MCTES national funds.

Author contributions

SN and SG performed the experiments; SN performed the data analysis and wrote the manuscript; JC and JO critically revised the manuscript; FM designed and supervised the study and edited the manuscript.

Conflict of interest

The authors declare that the research was conducted in the absence of any commercial o financial relationship that could be construed as a potential conflict of interest.

References

Agulhon C, Petravicz J, McMullen AB, Sweger EJ, Minton SK, Taves SR, et al. What is the role of astrocyte calcium in neurophysiology? Neuron. 2008;59:932-946.

Brosnan CF, Raine CS. The astrocyte in multiple sclerosis revisited. Glia. 2013;61:453-465.

Correale J, Farez MF. The role of astrocytes in multiple sclerosis progression. Frontiers in neurology. 2015;6:180.

das Neves SP, Serre-Miranda C, Nobrega C, Roque S, Cerqueira JJ, Correia-Neves M, et al. Immune thymic profile of the MOG-induced experimental autoimmune encephalomyelitis mouse model. Frontiers in Immunology. 2018;9:2335.

Guerra-Gomes S, Sousa N, Pinto L, Oliveira JF. Functional roles of astrocyte calcium elevations: from synapses to behavior. Frontiers in Cellular Neuroscience. 2017;11:427.

Guo X, Nakamura K, Kohyama K, Harada C, Behanna HA, Watterson DM, et al. Inhibition of glial cell activation ameliorates the severity of experimental autoimmune encephalomyelitis. Neuroscience Research. 2007;59:457-466.

Hertle DN, Yeckel MF. Distribution of inositol-1,4,5-trisphosphate receptor isotypes and ryanodine receptor isotypes during maturation of the rat hippocampus. Neuroscience. 2007;150:625-638.

Kuchibhotla KV, Lattarulo CR, Hyman BT, Bacskai BJ. Synchronous hyperactivity and intercellular calcium waves in astrocytes in Alzheimer mice. Science. 2009;323:1211-1215.

Li H, Xie Y, Zhang N, Yu Y, Zhang Q, Ding S. Disruption of IP(3)R2-mediated Ca(2)(+) signaling pathway in astrocytes ameliorates neuronal death and brain damage while reducing behavioral deficits after focal ischemic stroke. Cell Calcium. 2015;58:565-576.

Li X, Zima AV, Sheikh F, Blatter LA, Chen J. Endothelin-1-induced arrhythmogenic Ca2+ signaling is abolished in atrial myocytes of inositol-1,4,5-trisphosphate(IP3)-receptor type 2-deficient mice. Circulation Research. 2005;96:1274-1281.

Longair MH, Baker DA, Armstrong JD. Simple Neurite Tracer: open source software for reconstruction, visualization and analysis of neuronal processes. Bioinformatics. 2011;27:2453-2454.

Navarrete M, Perea G, Fernandez de Sevilla D, Gomez-Gonzalo M, Nunez A, Martin ED, et al. Astrocytes mediate in vivo cholinergic-induced synaptic plasticity. PLoS Biology. 2012;10:e1001259.

Nedergaard M, Rodriguez JJ, Verkhratsky A. Glial calcium and diseases of the nervous system. Cell Calcium. 2010;47:140-149.

Okubo Y, Kanemaru K, Suzuki J, Kobayashi K, Hirose K, Iino M. Inositol 1,4,5-trisphosphate receptor type 2-independent Ca(2+) release from the endoplasmic reticulum in astrocytes. Glia. 2019;67:113-124.

Petravicz J, Fiacco TA, McCarthy KD. Loss of IP3 receptor-dependent Ca2+ increases in hippocampal astrocytes does not affect baseline CA1 pyramidal neuron synaptic activity. Journal of Neuroscience. 2008;28:4967-4973.

Reichenbach N, Delekate A, Breithausen B, Keppler K, Poll S, Schulte T, et al. P2Y1 receptor blockade normalizes network dysfunction and cognition in an Alzheimer's disease model. Journal of Experimental Medicine. 2018;215:1649-1663.

Schindelin J, Arganda-Carreras I, Frise E, Kaynig V, Longair M, Pietzsch T, et al. Fiji: an open-source platform for biological-image analysis. Nature Methods. 2012;9:676-682.

Sharp AH, Nucifora FC, Jr., Blondel O, Sheppard CA, Zhang C, Snyder SH, et al. Differential cellular expression of isoforms of inositol 1,4,5-triphosphate receptors in neurons and glia in brain. Journal of Comparative Neurology. 1999;406:207-220.

Shigetomi E, Patel S, Khakh BS. Probing the complexities of astrocyte calcium signaling. Trends in Cell Biology. 2016;26:300-312.

Sospedra M, Martin R. Immunology of multiple sclerosis. Annu Rev Immunol. 2005;23:683-747.

Staats KA, Humblet-Baron S, Bento-Abreu A, Scheveneels W, Nikolaou A, Deckers K, et al. Genetic ablation of IP3 receptor 2 increases cytokines and decreases survival of SOD1G93A mice. Human Molecular Genetics. 2016;25:3491-3499.

Strokin M, Sergeeva M, Reiser G. Proinflammatory treatment of astrocytes with lipopolysaccharide results in augmented Ca2+ signaling through increased expression of via phospholipase A2 (iPLA2). American Journal of Physiology-Cell Physiology. 2011;300:C542-549.

Tavares G, Martins M, Correia JS, Sardinha VM, Guerra-Gomes S, das Neves SP, et al. Employing an open-source tool to assess astrocyte tridimensional structure. Brain Structure and Function. 2017;222:1989-1999.

Vardjan N, Zorec R. Excitable astrocytes: Ca(2+)- and cAMP-regulated exocytosis. Neurochemical Research. 2015;40:2414-2424.

Voskuhl RR, Peterson RS, Song B, Ao Y, Morales LB, Tiwari-Woodruff S, et al. Reactive astrocytes form scar-like perivascular barriers to leukocytes during adaptive immune inflammation of the CNS. Journal of Neuroscience. 2009;29:11511-11522.

Williams A, Piaton G, Lubetzki C. Astrocytes–friends or foes in multiple sclerosis? Glia. 2007;55:1300-1312.

Wu YW, Gordleeva S, Tang X, Shih PY, Dembitskaya Y, Semyanov A. Morphological profile determines the frequency of spontaneous calcium events in astrocytic processes. Glia. 2019;67:246-262.

Supplementary material

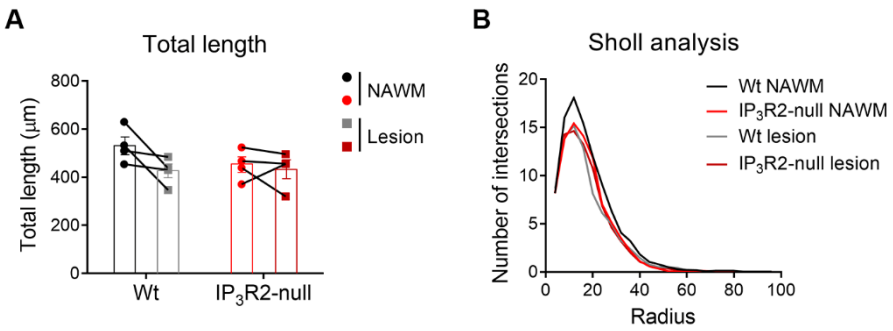

Supplementary figure 3. 1 – At the chronic phase of disease, astrocytes from both genotypes and white matter sub-regions were similar.

(A) Total length and (B) Sholl analysis of astrocytes reconstructed from IP_3R2-null animals and Wt littermates, near lesions or at NAWM regions. Data presented as mean ± SEM for total length and as mean for Sholl analysis. n= 4 per experimental group, 5-6 astrocytes reconstructed per animal.

CHAPTER 4

Sofia Pereira das Neves, Gisela Santos, Catarina Barros, Diana Rodrigues Pereira, Ricardo Ferreira, Cristina Mota, Susana Monteiro, Adelaide Fernandes, Fernanda Marques, João José Cerqueira

Enhanced cognitive performance in experimental autoimmune encephalomyelitis mice treated with dimethyl fumarate after the appearance of disease symptoms

Journal of neuroinflammation. doi.org/10.1016/j.jneuroim.2020.577163

(2020)

Journal of Neuroimmunology 340 (2020) 577163

Contents lists available at ScienceDirect

Journal of Neuroimmunology

journal homepage: www.elsevier.com/locate/jneuroim

Enhanced cognitive performance in experimental autoimmune encephalomyelitis mice treated with dimethyl fumarate after the appearance of disease symptoms

Sofia P. das Neves[a,b], Gisela Santos[c], Catarina Barros[c], Diana Rodrigues Pereira[a,b], Ricardo Ferreira[a,b], Cristina Mota[a,b], Susana Monteiro[a,b], Adelaide Fernandes[c,d], Fernanda Marques[a,b], João José Cerqueira[a,b,e,*]

[a] Life and Health Sciences Research Institute (ICVS), School of Medicine, University of Minho, Campus Gualtar, 4710-057 Braga, Portugal
[b] ICVS/3B's – PT Government Associate Laboratory, Braga/Guimarães, Portugal
[c] Neuron-Glia Biology in Health and Disease, Research Institute for Medicines (iMed.ULisboa), Faculty of Pharmacy, Universidade de Lisboa, Portugal
[d] Department of Biochemistry and Human Biology, Faculty of Pharmacy, Universidade de Lisboa, Portugal
[e] 2CA, Clinical Academic Center – Braga, Braga, Portugal

ARTICLE INFO

Keywords:
Autoimmunity
Multiple sclerosis
Rodent
Experimental autoimmune encephalomyelitis
Dimethyl fumarate
Cognition

ABSTRACT

In multiple sclerosis (MS), cognitive dysfunction is common but difficult to treat. We analyzed the impact of dimethyl fumarate, an MS drug with neuroprotective properties, in spatial memory performance in a mouse model of MS and looked for structural correlates in the hippocampus. Treated mice presented better cognitive performance which was not associated with structural hippocampal damage but with decreased demyelination in the fimbria. Dimethyl fumarate, even if initiated after hindlimb paralysis, ameliorated memory deficits in the MS mouse model due, at least in part, to its positive impact in the demyelination of the main hippocampal output pathway.

1. Introduction

Multiple sclerosis (MS) is a chronic immune-mediated demyelinating disease of the central nervous system (CNS) (Compston and Coles, 2008; Noseworthy et al., 2000; Steinman, 2001). In developed countries it is the second cause of neurological disability in young adults, with high burden for the patient and his family, and also for the health system (Borreani et al., 2014; Kobelt et al., 2017). MS patients present a strong immune response directed against the myelin sheath of CNS axons (Compston and Coles, 2008), and the hallmarks of the disease are focal demyelination, inflammation, glial scar formation and axonal damage (Lucchinetti et al., 2005). Lesion plaques are widespread in the patients' brain, consequently leading to a wide range of clinical symptoms, including motor, cognitive and neuropsychiatric problems (Chiaravalloti and DeLuca, 2008).

Cognitive impairments have a great negative influence on the daily life and employment of MS patients, constituting a heavy burden not only for the patient, but also for the family and healthcare and social welfare systems (Muckschel et al., 2016; Rao et al., 1991). Several studies have reported cognitive impairments in early phases of MS, and even in patients with clinically isolated syndrome (CIS) (reviewed in (Muckschel et al., 2016)). Different cognitive functions were found to be affected, such as attention, information processing efficiency, executive functioning, processing speed and long-term memory (reviewed in (Chiaravalloti and DeLuca, 2008) and (Guimaraes and Sa, 2012)). Moreover, deficits in spatial memory are commonly found. Some of these deficits are likely caused by damage to the hippocampus, a critical structure for learning and memory (Roosendaal et al., 2010).

Studies suggest that cognitive deficits could be better explained by irreversible demyelination and consequent neuronal damage, than by acute inflammatory activity (Geurts and Barkhof, 2008). Therefore, drugs able to confer neuroprotection in addition to modulating the immune response, could present better results in the prevention and improvement of cognitive deficits. One of these drugs is dimethyl fumarate (DMF), which was found to interfere with the cellular redox system and to exert a neuroprotective role (Linker et al., 2011).

In the MS animal model of experimental autoimmune encephalomyelitis (EAE), it was shown that the neuroprotective role of DMF in later stages of the disease is dependent on the function of nuclear factor erythroid-related factor 2 (*Nrf2*) (Linker et al., 2011). The

* Corresponding author at: Life and Health Sciences Research Institute (ICVS), School of Medicine, University of Minho, Campus Gualtar, 4710-057 Braga, Portugal.
E-mail address: jcerqueira@med.uminho.pt (J.J. Cerqueira).

https://doi.org/10.1016/j.jneuroim.2020.577163
Received 21 August 2019; Received in revised form 2 January 2020; Accepted 10 January 2020

Nrf2 pathway is involved in the regulation of the oxidative and metabolic stress response (Burness and Deeks, 2014). Moreover, a recent study has also found that DMF can present clinical and immunological benefits independently of *Nrf2*, in an earlier and more inflammatory phase of EAE (Schulze-Topphoff et al., 2016).

Considering the possible association between cognitive impairment and neurodegeneration, and the neuroprotective role of DMF, the main objective of this work was to evaluate the effect of DMF on cognitive performance in the EAE mouse model. We used a spatial reference memory task to evaluate the cognitive performance of animals, and then performed several analyses on the structure of the dorsal hippocampus, to correlate with the behavioral performance. More specifically, we estimated hippocampal volume and cell density, reconstructed neurons from the granular and pyramidal layers, assessed cell proliferation in the subgranular zone (SGZ) and evaluated the myelination of the main output tract (the fimbria). In addition, we also assessed astrocytic and microglial activation.

We concluded that, when compared with no treatment, DMF resulted in better spatial reference memory performance of EAE mice. Intriguingly, we could only correlate this with decreased demyelination of the fimbria, as we did not observe differences in the hippocampal volume, in hippocampal neuronal morphology, pyramidal and granular cell numbers, or in hippocampal cell progenitor proliferation.

2. Materials and methods

2.1. Animals

All experiments were conducted in accordance with the Portuguese national authority for animal experimentation, *Direcção Geral de Veterinária* (ID: DGV9457). Animals were housed and handled in accordance with the guidelines for the care and handling of laboratory animals in the Directive 2010/63/EU of the European Parliament and Council.

Animals were acquired from Charles River (Barcelona, Spain), housed and maintained in an SPF facility at 22–24 °C and 55% humidity, on 12 h' light/dark cycles (lights on at 8 a.m.), and fed with regular rodent's chow and tap water *ad libitum*.

2.2. EAE induction and experimental groups

Female C57BL/6J wild-type mice were used to induce EAE. Disease induction was performed at 9–11 weeks of age, using a commercial kit (EK-2110; Hooke Laboratories, Lawrence, MA, USA), according to the manufacturer's instructions. This experiment was repeated twice. Briefly, animals were immunized subcutaneously with 200 μg of myelin oligodendrocyte glycoprotein 35–55 ($MOG_{35–55}$), emulsified in complete Freund's adjuvant (CFA), at the upper and lower back (100 μL of emulsion per site of injection). Pertussis toxin (PTX) in phosphate buffered saline (PBS) was administered intraperitoneally after 2 and 24 h of immunization (227 ng of PTX per injection). Non-induced age-matched female littermates were used as controls. Non-induced animals were injected subcutaneously with an emulsion of PBS in CFA (Difco Laboratories, Detroit, USA), and were injected with PTX at the same concentration and timepoints as the EAE animals.

Animals were daily weighted and monitored for clinical symptoms of disease, and the evaluation of the clinical disease score was performed with the experimenter blinded to the treatment group. Animals were treated by oral gavage, two times per day, starting on day 18, accordingly to Linker et al. (2011) (Linker et al., 2011). On day 18, animals were scored and weighted, and EAE animals were divided in two groups of equal size (DMF-treated and vehicle-treated). Animal division ensured that both treatment groups had the same average clinical score and weight, on the first day of treatment. EAE animals were treated with vehicle solution, 0.8% hypromellose (Sigma-Aldrich, St. Louis, Missouri, USA), or with 15 μg/g of DMF (Sigma-Aldrich) in 0.8% hypromellose. Non-induced animals were treated with vehicle solution and followed the same treatment timeline.

Disease severity was assessed as previously described (Stromnes and Goverman, 2006), with few changes, as follows: 0 – no clinical symptoms; 0.5 – partially limp tail; 1 – paralyzed tail; 1.5 – at least one hind limb falls through consistently when the animal is placed on a wire rack; 2 – loss in coordinated movement, wobbly walk; 2.5 – dragging of hind limbs; 3 – paralysis of both hind limbs; 3.5 – hind limbs paralyzed and weakness of forelimbs; 4 – complete hind limbs paralysis and partial forelimbs paralysis; 4.5 – animal is not alert, no movement; 5 – moribund state or death. Paralyzed mice were offered easier access to food and water.

Three animals were excluded from all analyses because they did not present clinical symptoms of EAE throughout the entire experiment. Another three animals had to be sacrificed taking into account humane endpoints, not disease-related, and were also excluded from all analyses.

2.3. Cognitive behavioral assessment – Morris water maze (MWM)

The cognitive behavioral assessment was performed during the mice-resting period (between 8 a.m. and 8 p.m.). Before behavioral assessment, mice were transported to the testing room and left for habituation to room conditions for 30 min. Behavioral data analysis was performed with the experimenter blinded to the treatment group, and only animals with a clinical score equal or inferior to 2.5 performed the behavioral task.

To assess spatial reference memory, mice were tested in a circular pool (116 cm diameter) filled with water (24–25 °C) placed in a dimly lit room. Titanium oxide (IV) (Sigma-Aldrich) was added to the water to give it a white color, to allow the tracking system to distinguish mice from the background. The pool was divided in four imaginary quadrants, and a spatial cue was placed in the wall near each quadrant (square, stripes, triangle and a cross). A platform with 11 cm of diameter was hidden in one of the quadrants (stripes). Data was collected using a fixed camera placed in the ceiling and connected to a video-tracking system (Viewpoint, Champagne-au-Mont-d'or, France).

Mice had to learn the position of the hidden platform over a period of four days. Each day, mice were placed facing the wall of the pool for a total of 4 trials per day. In each trial, the mice started from a different quadrant, and the sequence of quadrants was different every day. Each trial was completed whenever the mouse reached the platform or when 60 s elapsed. Latency to reach the platform (latency to platform) and the distance swam until reaching the platform (distance to platform) was recorded for each trial during the four days. On the fifth day, the platform was removed and a trial of 30 + 30 s was performed (probe trial). During the probe trial, the percentage of time and of distance that each mouse swam in each quadrant was recorded to confirm the acquisition of platform location through reference memory.

2.4. Animals sacrifice

Non-induced, vehicle- and DMF-treated EAE animals were sacrificed at the light phase of the diurnal cycle, at days 40–41 post-EAE induction. Animals were anesthetized with an intraperitoneal injection of ketamine hydrochloride (150 mg/kg, Imalgene 1000) plus medetomidine hydrochloride (0.3 mg/kg, Dorben).

For stereology and Golgi analysis, mice were transcardially perfused with cold 0.9% saline solution, and the brains were removed. For stereology analysis, one brain hemisphere was posteriorly fixed in 4% paraformaldehyde (PFA), with constant agitation for at least 24 h, and kept in 4% PFA until further processing. For Golgi analysis, the other brain hemisphere was immersed in Golgi-Cox solution for 21 days and then was transferred to a 30% sucrose solution until further processing.

For histological analysis, mice were transcardially perfused with cold 0.9% saline solution, followed by perfusion with 4% PFA. The

brains were then collected, left in 4% PFA for 24 h, and switched to a 30% sucrose solution for 24 h. The brains were then embedded in Tissue-Tek O.C.T. compound (Sakura Finetek, Japan), snap-frozen and kept frozen until further sectioning.

The brains of the animals that were able to perform the MWM were processed for stereology and Golgi analysis, while the brains of those that did not perform the behavioral task were processed for histological analysis.

2.5. Stereology analysis

Brains were processed for stereology according to the method described previously (Keuker et al., 2001). Briefly, brains were embedded in glycomethacrylate (Tecnovit, 7100; Heraeus Kulzer, Werheim, Germany) and 30 μm-thick sections were obtained using a microtome. Every other section was collected into non-coated glass slides, were stained with Giemsa and cover-slipped using Entellan (Merck, Darmstadt, Germany). Each brain was coded to keep the experiment blind to the experimental group. The hippocampal formation was analyzed according to its main anatomical divisions: dentate gyrus (DG) (molecular layer, granular layer and hilus), cornu ammonis (CA) 3 and CA1 (*strata oriens*, *pyramidale* and *radiatum*). Volumes of the different hippocampal subregions were determined using the Cavalieri's principle (Gundersen et al., 1988). Briefly, every eighth section was used and its' cross-sectional area was estimated by point counting. For this, we randomly superimposed onto each area a test point grid in which the interpoint distance, at a tissue level, was 150 μm for the DG and 200 μm for CA3 and CA1 regions. The volume of the region of interest was calculated from the number of points that felt within its boundaries and the distance between the systematically samples sections. Average neuronal cell density numbers were estimated using the optical fractionator method (West et al., 1991). Briefly, using the same sections drawn before, a grid of virtual three-dimensional boxes for granule cell layer of the DG (20x20x15) and for pyramidal cell layer of CA1 and CA3 regions (40x40x15) was superimposed onto each section and neurons were counted whenever their nucleus (identified by size, shape and a prominent nucleoli) came into focus within the counting box. Volume and neuronal number estimations were performed using Stereo Investigator software (MBF Bioscience, Williston, VT, USA) and a motorized microscope (Olympus, Hamburg, Germany).

2.6. Hippocampal neurons morphology

To assess the three-dimensional (3D) dendritic morphology of hippocampal neurons we used the Golgi-Cox method. Coronal sections 200 μm-thick were cut on a vibratome, were collected in 6% sucrose and blotted dry onto gelatin-coated microscope slides. They were subsequently alkalinized in 18.7% ammonia, developed in Dektol (Kodak, Rochester, NY, USA), fixed in Kodak Rapid Fix, dehydrated, xylene cleared, mounted and coverslipped with Entellan (Merck). All incubation steps were performed in a dark room. Five to eight Golgi-impregnated neurons, from the DG and CA1, were reconstructed, and the average of each animal was used for statistical analysis. The following criteria were used to select the neurons to reconstruct: (1) full Golgi-impregnation along the dendritic tree; (2) complete dendrites without truncated branches; and (3) relative isolation from neighboring impregnated neurons, astrocytes or blood vessels to avoid interference with the analysis. Slides containing the region of interest were randomly searched and the first five to eight neurons fulfilling the criteria (maximum of 3 neurons per section) were selected. For each selected neuron, all branches of the dendritic tree were reconstructed using the x100 (immersion oil) objective of a motorized microscope (Axioplan 2, Carl Zeiss, Germany) and using the Neurolucida software (MicroBright Field, Williston, VT, USA). A 3D analysis of the reconstructed neurons was performed using the NeuroExplorer software (MicroBright Field). Dendritic morphology was examined by the total dendritic length and arrangement of dendritic material using a 3D version of sholl analysis (Sholl, 1956) of intersections. The number of dendritic intersections with concentric spheres positioned at radial intervals of 10 μm from the soma was registered.

2.7. Immunofluorescence

Hippocampal coronal slices were double stained for Ki67 and doublecortin (DCX) to evaluate cell proliferation. Briefly, the slides were permeabilized with PBS-triton 0.3% for 10 min. After washing with PBS, the slides were transferred to pre-heated citrate buffer (Sigma-Aldrich), left in the microwave for 20 min, and then washed with PBS. Blocking was performed with 10% fetal bovine serum (FBS) in PBS-triton for 30 min. Slides were then incubated over-night, at room temperature (RT), with the primary antibodies rabbit anti-Ki67 (1:300; Millipore, Billerica, MA, USA) and goat anti-DCX (1:300; Dako, Glostrup, Denmark). After washing with PBS-triton, slides were incubated with the secondary antibodies donkey anti-goat 488 (1:500, Invitrogen, Life Technologies, Carlsbad, CA, USA) and donkey anti-rabbit 594 (1:500, Invitrogen), for 2 h at RT. After washing with PBS-triton, the nuclei were stained with DAPI (1:1000, Invitrogen) for 10 min at RT. Slides were washed with PBS and mounted with Immumount (Fisher Scientific, Thermo Fisher Scientific, Waltham, MA, USA).

Proliferation densities were estimated in the SGZ of the DG as a ratio between the total number of immunostained cells and the area of the SGZ. For each animal, a minimum of three sections were analyzed, including both the right and left brain hemispheres. The SGZ area was evaluated using an Olympus BX51 optical microscope (Olympus) and Stereo Investigator software (MBF Bioscience). The double staining was evaluated using a confocal microscope (FV1000 Olympus) and the FV10-ASW software (Olympus). Ki67 positive and double stained cells were counted for each section, by an observer naïve to the animals' experimental group, and the average of each animal was used for statistical analysis.

To evaluate astrocytic and microglial activation, coronal brain slices were stained for glial fibrillary acidic protein (GFAP) (mouse, 1:200, Novocastra, Wetzlar, Germany) and calcium-binding adapter molecule 1 (Iba1) staining (rabbit, 1:250, Wako Chemicals, VA, USA). After fixation in 4% PFA, sections were incubated with blocking solution (1 nM HEPES, 2% heat-inactivated horse serum, 10% heat-inactivated FBS, 1% BSA and 0.25% Triton X-100 in HBSS) for 1 h at RT. Slices were then incubated with primary antibodies diluted in blocking solution for 24 h, at 4 °C, following incubation with the secondary antibodies goat anti-mouse 594 (1:1000, Invitrogen) and goat anti-rabbit 488 (1:1000, Invitrogen). To identify the total number of cells, nuclei were stained with Hoechst 33258 dye (1:1000). Fluorescent images were acquired using a confocal microscope (Confocal Point Scanning Microscope Zeiss LSM 710 META, Carl Zeiss) using a 20/1.2 (zoom). Binary masks were defined using a cut-off intensity threshold value for each region of interest, which corresponds to a minimum intensity due to specific staining above background values. The number of Iba1 and GFAP positive cells were counted in sections from different animals, by an observer naïve to the animals' experimental group. The number of cells was normalized to the area of interest, the fimbria, and the average of each animal was used for statistical analysis.

2.8. Assessment of myelination

Hippocampal coronal slices (intercalated with the ones used for immunostaining) were stained for Luxol Fast Blue (LFB) and visualized by light microscopy to assess the degree of demyelination. Slides were allowed to dry overnight (approximately 16 h) at RT. Then, they were incubated with 0.1% LFB solution in 96% ethanol and 10% acetic acid overnight at 56 °C. The excess of dye was removed by washing with distilled water. Tissue differentiation was performed using 0.05%

lithium carbonate solution followed by 70% ethanol, and these steps were repeated until the white and gray matter were distinguishable. The slices were then rinsed with distilled water and counterstained with hematoxylin (Merck) for 10 min at RT, and rinsed with tap water for 5 min. Hydrochloric acid was used to differentiate the slices followed by water one last time for 5 min. Finally, the slides were allowed to dry on air, and were mounted with Entellan (Merck). The images were taken using an optical microscope, Leica DC 100 camera (Leica, Wetzlar, Germany) using the x10 objective under a bright field. Then the level of myelination was quantitatively evaluated by determining the percentage of brain area that was stained with LFB, using the Fiji software (Schindelin et al., 2012).

2.9. Statistical analysis

Results are presented as mean ± standard error of mean (SEM), for parametric statistical tests, or median and interquartile range (IQR), for non-parametric statistical tests, and as the average of the two independent experiments performed (Supplementary tables 1 and 2). The number of biological replicates (n) of the representative independent experiments is specified in the legend of each figure. Sample normality distribution was tested using the Shapiro-Wilk normality test. Data from the reference memory and sholl analysis was analyzed using a two-way repeated measures ANOVA, and differences between groups compared with the *post hoc* Tukey's test. The remaining data was analyzed using a parametric one-way ANOVA with the *post hoc* Tukey's test, or the non-parametric Kruskal-Wallis test with Dunn's multiple comparison test, when at least one of the groups did not present a normal distribution. To quantify the strength of the differences, the partial eta-squared (η_p^2) (0.02 was considered a small-, 0.13 a medium- and 0.26 a large-effect size) or the eta-squared (η^2) (0.01 was considered a small-, 0.06 a medium- and 0.14 a large-effect size) were calculated as a measure of effect size. Partial eta-squared values were calculated with the SPSS v24 (SPSS Inc., Chicago, Illinois, USA), and eta-squared values were calculated according to Tomczak and Tomczak (2014) (Tomczak and Tomczak, 2014). Statistical significance was considered for $p < 0.05$ (*), $p < 0.01$ (**), $p < 0.001$ (***), $p < 0.0001$ (****). Statistical analyses were performed with the GraphPad Prism 6.01 (GraphPad Software, Inc., La Jolla, San Diego, CA, USA) and the SPSS.

3. Results

3.1. C57Bl/6J mice immunized with $MOG_{35–55}$ developed a chronic disease course

Non-induced animals maintained a similar weight until the end of the experiment (Fig. 1A). On the other hand, EAE animals started losing weight by day 11 post-EAE induction (Fig. 1A), when they started presenting the first clinical symptoms of disease (Fig. 1B). By day 17, EAE animals had lost around 15% of their initial weight, and maintained that weight until the end of the experiment (Fig. 1A). Considering that only animals with a clinical score equal or inferior to 2.5 were able to perform the MWM task, we verified if there were differences in the clinical score between the vehicle- and DMF-treated animals during the testing days, and found no significant differences (Fig. 1C).

3.2. DMF treatment improved the cognitive performance of EAE animals

Non-induced and EAE animals of both treatment groups performed a reference memory task after 18 days of treatment. During the first 4 days of MWM, animals had to learn the location of a hidden platform in a swimming pool. In each day, four trials were performed, and the average of the four trials was used for statistical comparison between groups, to compare the learning curve of each group. In the fifth day, a probe trial was performed, to evaluate the animals' recollection of the platform location. As mentioned before, during the five days of testing the clinical scores were not different between the two EAE groups (Fig. 1C).

Throughout the four days of reference memory task, EAE animals treated with DMF presented a learning curve similar to the non-induced animals (Fig. 2A). On the other hand, EAE animals treated with vehicle were not able to learn the location of the platform (Fig. 2A) (two-way repeated measures ANOVA, time factor – $F_{(3,93)} = 8.249$, $p < 0.0001$, $\eta_p^2 = 0.210$; group factor – $F_{(2,31)} = 3.727$, $p = 0.0354$, $\eta_p^2 = 0.194$; interaction – $F_{(6,93)} = 1.553$, $p = 0.1699$).

In addition, non-induced animals significantly reduced the distance swam to reach the platform, indicating that they took shorter paths from day to day (Fig. 2B). EAE animals from both treatment groups did not present such a significant decrease in the distance swam until reaching the platform, throughout the days (Fig. 2B) (two-way repeated measures ANOVA, time factor – $F_{(3,93)} = 15.554$, $p < 0.0001$, $\eta_p^2 = 0.334$; group factor – $F_{(2,31)} = 4.715$, $p = 0.0163$, $\eta_p^2 = 0.233$; interaction – $F_{(6,93)} = 2.560$, $p = 0.0244$, $\eta_p^2 = 0.142$). Considering that EAE animals treated with vehicle took longer to reach the platform but swam distances similar to DMF-treated EAE mice, we concluded that this group swam without purpose for longer periods of time compared to the animals treated with DMF. In line with this, the average swimming speed was not different between both EAE groups but, as expected, significantly decreased when compared with non-induced animals (Fig. 2C) (two-way repeated measures ANOVA, time factor – $F_{(3,93)} = 1.534$, $p = 0.211$; group factor – $F_{(2,31)} = 13.943$, $p < 0.0001$, $\eta_p^2 = 0.474$; interaction – $F_{(6,93)} = 1.853$, $p = 0.0973$).

In the probe trial, vehicle-treated EAE animals spent significantly less time, and swam less distance, in the platform quadrant, *i.e.*, in the stripes quadrant, while the DMF-treated EAE animals spent almost the same time as non-induced animals (Fig. 2D and E) (percentage of time – one-way ANOVA, $F_{(2,31)} = 4.270$, $p = 0.023$, $\eta^2 = 0.216$; percentage of distance –Kruskal-Wallis, $\chi^2_{(2)} = 5.849$, $p = 0.0537$). Interestingly, and also in the probe trial, EAE animals treated with vehicle spent more time in the quadrant from where they were dropped, compared to the other two groups (Fig. 2F) (cross quadrant – Kruskal-Wallis test, $\chi^2_{(2)} = 3.766$, $p = 0.1522$; square quadrant – Kruskal-Wallis test, $\chi^2_{(2)} = 6.236$, $p = 0.0443$, $\eta^2 = 0.125$; triangle quadrant – one-way ANOVA, $F_{(2,34)} = 0.5050$, $p = 0.608$).

Overall, these results suggest that animals treated with DMF do not show the spatial learning deficits revealed by their non-treated EAE counterparts.

3.3. EAE induction and DMF treatment did not affect the dorsal hippocampal volume nor the dendritic arborization of dorsal hippocampal neurons

To evaluate the cognitive performance of the animals we performed a reference memory task, which is mostly dependent on the dorsal hippocampus. For that reason, after sacrificing the animals, at days 40–41 post-EAE induction, we studied the dorsal hippocampus structure and neuronal morphology. At the sacrifice, one brain hemisphere was processed for Golgi staining and the other hemisphere for Giemsa staining.

For the 3D morphological reconstruction of neurons, a minimum of 5 neurons per animal was drawn in each region, and the average measures for each animal were used for statistical comparison. Due to technical difficulties, we were not able to reconstruct CA3 neurons. Representative images of the reconstructed DG and CA1 neurons are presented in Fig. 3C and H. The total dendritic length and the ramification of DG granular neurons were similar between the three groups analyzed (Fig. 3A and B) (length - one-way ANOVA, $F_{(2,19)} = 0.872$, $p = 0.434$; sholl analysis - two-way repeated measures ANOVA, radius factor – $F_{(27,513)} = 304.9$, $p < 0.0001$, $\eta_p^2 = 0.941$; group factor – $F_{(2,19)} = 0.7625$, $p = 0.4803$; interaction – $F_{(54,513)} = 0.4829$, $p = 0.9993$). Likewise, the total length and ramification of both the basal

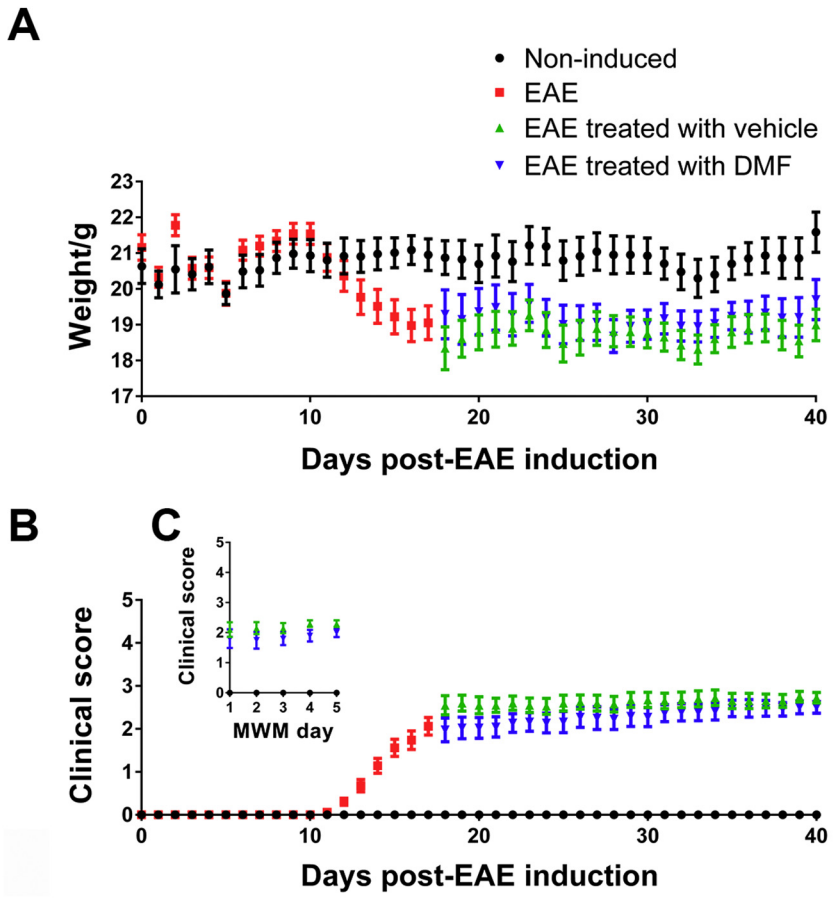

Fig. 1. – EAE animals treated with vehicle or DMF presented a similar disease course. EAE animals started losing weight around day 11 (A), when the first clinical symptoms of disease began (B). Diseased animals presented a chronic disease course, characterized by an increase in the clinical score until around day 17, and maintaining a similar clinical score for the remaining time of the experiment (B). Treatment with DMF or vehicle solution started at day 18 post-EAE induction, and both treatment groups presented a similar disease course until the end of the experiment (B). Only animals with clinical scores equal or inferior to 2.5 performed the MWM, and the average clinical score of both treatment groups was similar during the testing days (C) ($n_{non\text{-}induced} = 14$, $n_{EAE} = 42$, $n_{EAE\ treated\ with\ vehicle} = 20$ in (B) and 10 in (C), $n_{EAE\ treated\ with\ DMF} = 22$ in (B) and 10 in (C). Data presented as mean ± SEM).

and apical CA1 dendrites did not differ significantly between experimental groups (Fig. 3D-G) (CA1 basal length – one-way ANOVA, $F_{(2,18)} = 0.4459$, $p = 0.6471$; CA1 basal sholl analysis – two-way repeated measures ANOVA, radius factor – $F_{(23,414)} = 327.9$, $p < 0.0001$, $\eta_p^2 = 0.948$; group factor – $F_{(2,18)} = 0.4257$, $p = 0.6598$; interaction – $F_{(46,414)} = 0.5601$, $p = 0.9913$; CA1 apical length – one-way ANOVA, $F_{(2,18)} = 0.664$, $p = 0.5271$; CA1 apical sholl analysis – two-way repeated measures ANOVA, radius factor – $F_{(48,864)} = 243.3$, $p < 0.0001$, $\eta_p^2 = 0.931$; group factor – $F_{(2,18)} = 0.5804$, $p = 0.5698$; interaction – $F_{(98,864)} = 0.9119$, $p = 0.7115$). These results suggest that EAE induction and DMF treatment do not induce dendrite remodeling in DG and CA1 neurons.

For the hippocampal structural analysis, the hippocampus was divided in DG, CA1 and CA3, and each region was sub-divided in three other regions. The DG was sub-divided in granular, molecular and hilus layers (Fig. 4A). The CA1 and CA3 were sub-divided in *pyramidale*, *radiatum* and *oriens* layers (Fig. 4A). We did not find differences between the volumes of these sub-regions in the three experimental groups, for that reason, the results for each region – DG, CA1 and CA3 – are presented as the sum of the volume of their respective sub-divisions. All three groups presented similar DG, CA1 and CA3 volumes, indicating that neither EAE induction nor DMF treatment altered hippocampal volume (Fig. 4B) (DG – one-way ANOVA, $F_{(2,19)} = 0.634$, $p = 0.541$; CA1 – one-way ANOVA, $F_{(2,19)} = 1.403$, $p = 0.270$; CA3 – one-way ANOVA, $F_{(2,19)} = 1.342$, $p = 0.285$).

Likewise, non-induced animals and EAE animals treated with vehicle or DMF presented similar total neuronal cell numbers in the granular layer of the DG, and in the *pyramidale* layers of the CA1 and CA3, indicating that total neuronal cell number in dorsal hippocampus was not affected by EAE induction or DMF treatment (Fig. 4C) (DG – one-way ANOVA, $F_{(2,19)} = 0.424$, $p = 0.660$; CA1 – Kruskal-Wallis test, $\chi^2_{(2)} = 3.317$, $p = 0.194$; CA3 – one-way ANOVA, $F_{(2,19)} = 1.199$, $p = 0.323$).

3.4. Hippocampal progenitor cell proliferation was similar between EAE animals treated with vehicle and DMF and non-induced animals

Besides studying the hippocampal structure and neuronal morphology, we also looked at the SGZ of the DG, a brain region in which adult neurogenesis occurs. To quantify the number of proliferating cells in the SGZ we used the Ki67 marker, and to specifically evaluate immature neurons we stained for DCX (Fig. 5A). We found that EAE animals, of both treatment groups, and non-induced animals, presented similar numbers of Ki67 positive cells (Fig. 5B) and double stained cells (Fig. 5C) per area unit (number Ki67 + /area – Kruskal-Wallis test, $\chi^2_{(2)} = 0.442$, $p = 0.819$; number Ki67 + DCX + /area – Kruskal-Wallis test, $\chi^2_{(2)} = 0.709$, $p = 0.731$). Moreover, all experimental groups presented similar percentages of DCX positive cells within the total Ki67 positive population (Fig. 5D) (Kruskal-Wallis test, $\chi^2_{(2)} = 0.733$, $p = 0.715$).

3.5. DMF treated animals have less demyelination in the fimbria

Finally, we also assessed both demyelination and glial activation in the fimbria, the main white matter tract out of the dorsal hippocampus. To evaluate demyelination, hippocampal sections were stained with LFB (Fig. 6A-B). We found that vehicle-treated EAE animals had significantly more demyelination (decreased percentage of LFB stained area) than both DMF-treated EAE mice and non-induced animals, which did not differ (Fig. 6C) (one-way ANOVA, $F_{(2,18)} = 11.650$, $p = 0.0006$, $\eta^2 = 0.5642$).

Furthermore, we observed an increased astrocyte activation in the fimbria of vehicle-treated animals, as evaluated by an increased number of GFAP positive cells per area unit, which was reverted to control

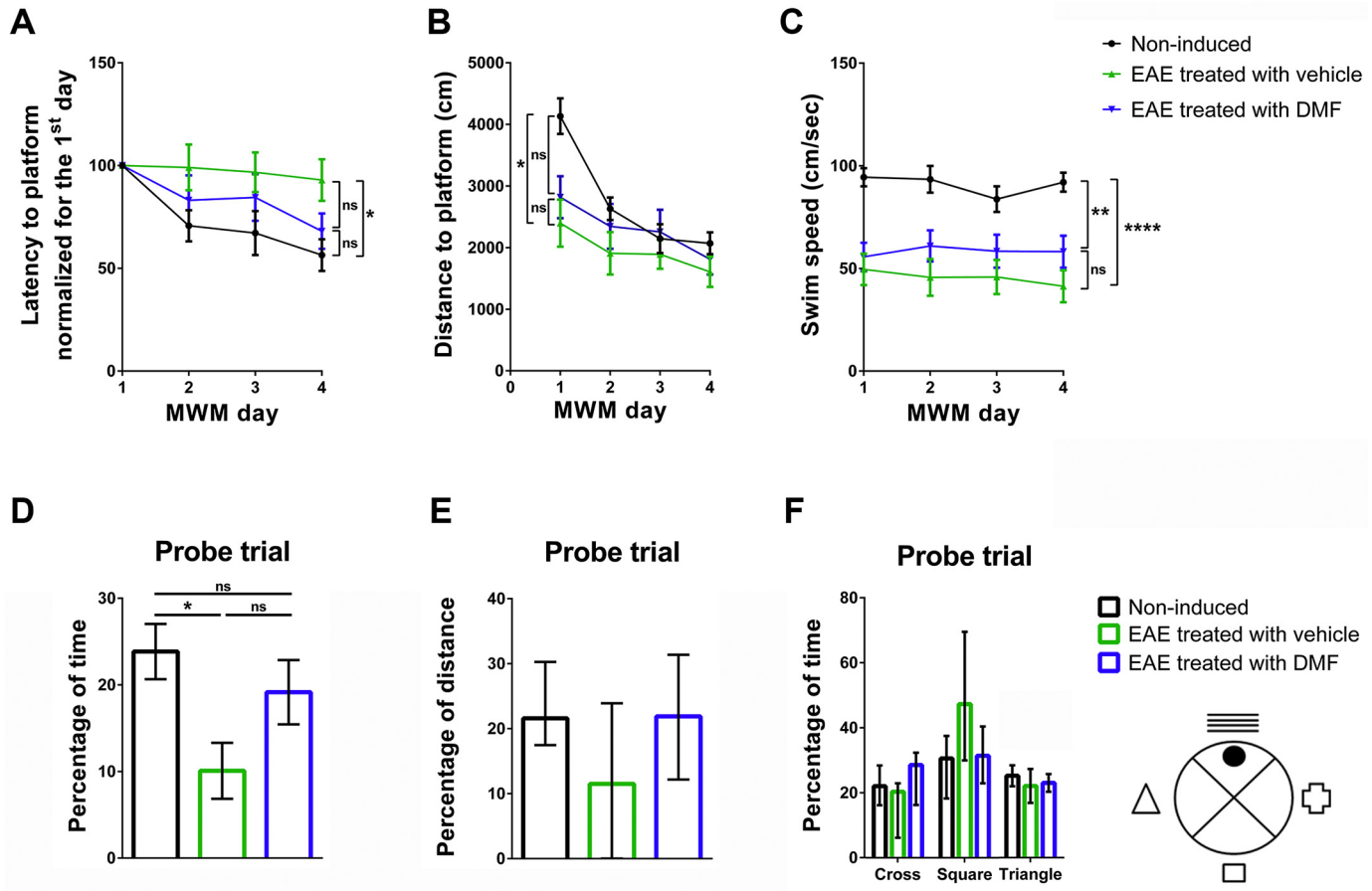

Fig. 2. – DMF treatment improved the cognitive performance of EAE animals. In the spatial learning task, and similarly to non-induced animals, EAE animals treated with DMF were able to learn the task and find the platform, as assessed by a decrease in the latency time to platform (A). EAE animals from both treatment groups presented locomotion problems, observed as a less accentuated decrease in the distance swam until reaching the platform (B) and a decreased velocity (C), compared to non-induced animals. At the probe trial, DMF-treated animals presented similar percentages of time (D) and distance swam (E) in the platform quadrant to non-induced animals, while the EAE animals treated with vehicle spent less time in the platform quadrant. Regarding the percentage of time spent on the other pool quadrants, EAE animals treated with vehicle spent more time in the square quadrant (F), which was the quadrant from where they were dropped ($n_{non\text{-}induced} = 14$, $n_{EAE\ treated\ with\ vehicle} = 10$, $n_{EAE\ treated\ with\ DMF} = 10$. Data presented as mean ± SEM, for parametric statistical analysis, or median ± IQR, for non-parametric statistical analysis. * $p < 0.05$, ** $p < 0.01$, **** $p < 0.0001$).

levels after DMF treatment (Fig. 6D-E) (one-way ANOVA, $F_{(2,19)} = 8.837$, $p = 0.0019$, $\eta^2 = 0.4819$).

Regarding microglial activation, we observed an increased number of Iba1 positive cells after EAE induction, that further increased by DMF treatment (Fig. 6F-G) (one-way ANOVA, $F_{(2,13)} = 31.860$, $p < 0.0001$, $\eta^2 = 0.8306$).

4. Discussion

Previous studies have shown that DMF was able to modulate EAE progression (Linker et al., 2011; Schilling et al., 2006; Schulze-Topphoff et al., 2016), however the exact mechanism of action is not fully elucidated. Some authors suggest that the neuroprotective effects of DMF are dependent on Nrf2 mediated anti-oxidative pathways (Linker et al., 2011), while others have shown beneficial effects independent of Nrf2 (Schulze-Topphoff et al., 2016). Nevertheless, it is accepted that DMF improves the clinical course of EAE and exerts a neuroprotective role. Moreover, studies performed in MS patients showed that DMF treatment was associated with continuously low clinical and magnetic resonance imaging (MRI) disease activity in relapse-remitting patients (Gold et al., 2017).

Considering the potential neuroprotective role of DMF, this could be a good candidate drug to improve cognitive deficits in MS patients. For that reason, in this work, we intended to evaluate the effects of DMF on the cognitive performance of an MS animal model, the EAE model. To do so, we induced EAE in C57BL/6J females, using a commercial kit and $MOG_{35–55}$ as an encephalitogenic peptide. MOG-induced C57BL/6 mice presented a chronic disease course, characterized by a gradual worsening of the clinical score, which never showed a full score reduction, as already reported (McCarthy et al., 2012). The DMF treatment timeline and dosage were chosen according to a published work by Linker et al. (2011). These authors observed beneficial effects in the clinical score of the animals 10 days after treatment initiation, on day 28 post-EAE induction (Linker et al., 2011). Contrary to their results, we did not observe a significant improvement in the clinical score of our DMF-treated animals, and even after 18 days of treatment the clinical scores of EAE animals from the vehicle- and the DMF-treated groups did not differ significantly. So, even though we used similar induction and treatment protocols, our animals showed a different disease course. At the time of treatment initiation, our group of EAE animals presented hind limb paralysis – average clinical score of 3 in a scale from 0 to 5 –, while in the previous work animals only presented with gait ataxia – average clinical score of 4 in a scale from 0 to 10. This could indicate that, in our experiment, EAE was more severe and the extension and degree of damage were greater and already installed when treatment was started, thus explaining the puzzling findings regarding the impact of DMF treatment on the clinical score.

In a hippocampal-dependent task, the MWM, EAE animals treated

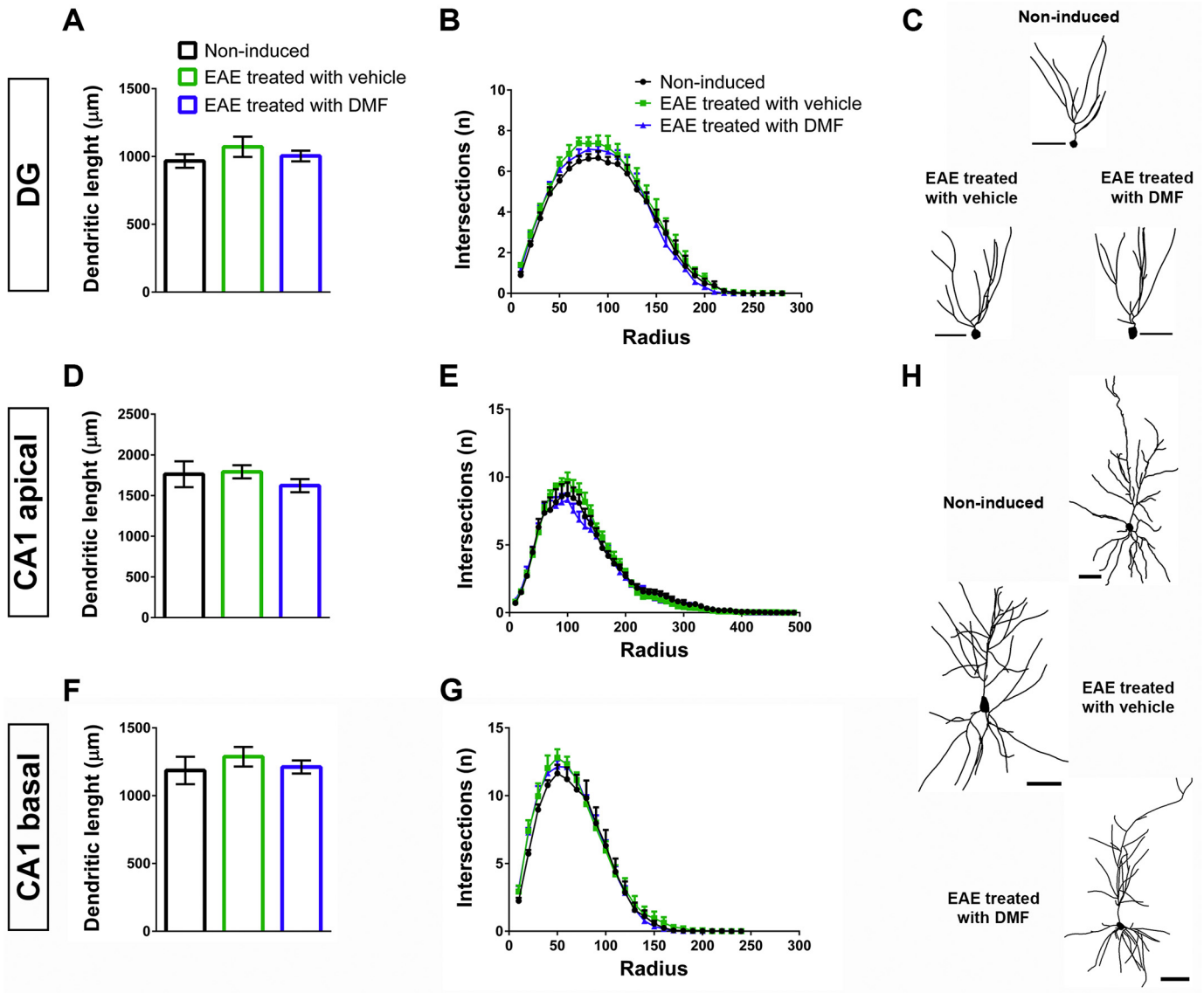

Fig. 3. – DG and CA1 hippocampal neurons of EAE animals were similar to non-induced animals. The total dendritic length (A) and differential dendritic rearrangement (B) of DG neurons was similar between non-induced animals and EAE animals treated with either vehicle or DMF. Computer assisted 3D reconstructions of representative granular neurons (C). The total dendritic length (D and F) and differential dendritic rearrangement (E and G) of CA1 pyramidal neurons was similar between non-induced animals and EAE animals of both treatment groups. Computer assisted 3D reconstructions of representative CA1 pyramidal neurons (H) (Scale bar = 50 µm. (A) to (B) $n_{non\text{-}induced} = 7$, $n_{EAE\ treated\ with\ vehicle} = 7$, $n_{EAE\ treated\ with\ DMF} = 8$; (D) to (G) $n_{non\text{-}induced} = 7$, $n_{EAE\ treated\ with\ vehicle} = 6$, $n_{EAE\ treated\ with\ DMF} = 8$. Data presented as mean ± SEM).

with vehicle solution presented a worst performance than non-induced animals and were not able to learn the location of the platform, as evaluated in the probe trial. These results are similar to previously published works, in which EAE mice also showed cognitive deficits in hippocampal-dependent tasks (Dutra et al., 2013; Kim et al., 2012; Ziehn et al., 2010). Interestingly, DMF treatment was able to revert the cognitive deficits of EAE animals, which presented a behavioral performance similar to non-induced animals.

It is important to point out the difficulties associated to cognitive assessment in the EAE mice model, since the most widely used cognitive tests are all dependent on some kind of motor behavior. MOG-immunized animals develop a chronic disease course, and most of them become paralyzed, making it difficult for them to perform the behavioral tasks. The test used in this work, the MWM, is no exception. For that reason, we had to exclude animals *a priori* solely based on their clinical score, making it impossible to evaluate the cognitive performance of animals in most advanced stages of the disease. Hence, it is important to keep developing new behavioral tasks, which allow cognitive assessment in animals with motor deficits, like the one published by Novkovic et al. (2015) (Novkovic et al., 2015).

We further studied the hippocampus of the animals to explore possible alterations which could explain the cognitive improvement observed. We analyzed the hippocampus for differences in volume, cell density, dendritic morphology, and altered proliferation rate of neuronal precursors. A Golgi staining protocol was used in hippocampal slices, and the 3D morphology of neurons was posteriorly reconstructed using the Neurolucida software. DG and CA1 neurons presented similar dendritic lengths and ramifications, between both EAE groups and non-induced animals. This indicates that neurons from these hippocampal regions did not alter their morphology in response to EAE induction. Additionally, this also suggests that the behavioral cognitive improvements shown by the DMF-treated EAE group are not a result of hippocampal dendritic remodeling. In a previous work by Planche and co-workers (2017), the total dendritic length and the complexity of the

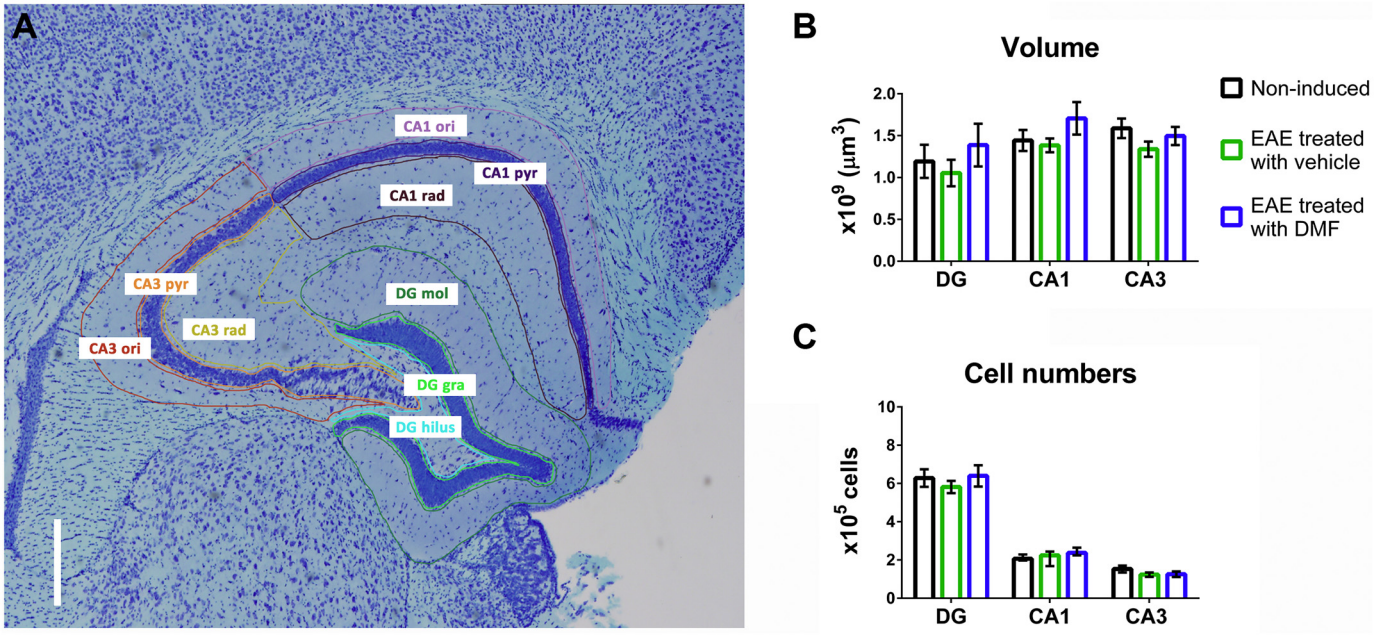

Fig. 4. – EAE animals presented hippocampal volumes, and granular and *pyramidale* cell numbers similar to non-induced animals. Schematic representation of the anatomical divisions of the hippocampus (A). Stereological estimations of volumes from DG, CA1 and CA3 revealed similar volumes between non-induced animals and both EAE groups (B). The total volume of the DG, CA1 and CA3 was calculated as the sum of the respective 3 sub-regions. Stereological estimations of the total cell numbers in the granular layer of the DG and the *pyramidale* layers of the CA1 and CA3 subregions showed similar cell numbers in non-induced animals and EAE animals from both treatment groups (C) (Scale bar = 300 µm. rad: *radiatum*; pyr: *pyramidale*; ori: *oriens*; mol: molecular; gra: granular; $n_{non\text{-}induced} = 7$, $n_{EAE\ treated\ with\ vehicle} = 7$, $n_{EAE\ treated\ with\ DMF} = 8$. Data presented as mean ± SEM, for parametric statistical analysis, or median ± IQR, for non-parametric statistical analysis).

dendritic arbor of DG neurons were found decreased in EAE mice, compared to non-induced animals. In this study, animals were sacrificed at day 20 post-induction and, even though the reconstruction software used was also Neurolucida, neurons were immunostained for anti-neurofilament H non-phosphorylated (SMI-32) and they used the x40 objective for reconstruction (Planche et al., 2017), which could have contributed for differences observed in the results. Using an unbiased stereological approach to estimate the hippocampal volume of mice, we observed that EAE animals, treated with vehicle or DMF, and non-induced animals presented similar DG, CA1 and CA3 volumes. Additionally, all groups presented similar cell numbers in the granular layer of the DG, and *pyramidale* layers of CA1 and CA3. These results suggest that the cognitive improvement observed in the EAE animals treated with DMF was not due to hippocampal structural alterations. Previous studies both in the EAE animal model (Hamilton et al., 2019; Kim et al., 2012; Ziehn et al., 2010) and in MS patients (Papadopoulos et al., 2009; Sicotte et al., 2008) showed hippocampal atrophy in the disease context. It is important to refer that in all these studies, except for one (Ziehn et al., 2010), the hippocampal volume was estimated using MRI acquisitions, while in our study we performed an unbiased stereology estimation using the Stereo Investigator software. Ziehn et al. (2010) also performed an unbiased stereology approach, but using the Fiji software, and they studied males instead of females (Ziehn et al., 2010). Interestingly, a recent work by Hamilton et al. (2019) showed that in later stages of the disease, after day 66 post-induction, only EAE animals with high scores (full hind limb paralysis with some weakness in the forelimbs) presented hippocampal atrophy. On the other hand, EAE animals with low scores (tail paralysis, hindlimb weakness and some limb dragging) were similar to both naïve and non-induced animals. In fact, they found a negative correlation between the volume of some brain regions, including the hippocampus, and the cumulative long-term clinical disease score (Hamilton et al., 2019). As previously mentioned, only the animals with clinical scores equal or below 2.5 performed the MWM, and the brains of these animals were processed for stereological analysis. So the hippocampal volume was estimated only in animals with lower clinical scores, which might explain the absence of hippocampal atrophy.

It is widely accepted that the formation of new neurons is involved in almost all of the known hippocampal functions, including learning and memory (Opendak and Gould, 2015). Hence, we next quantified the percentage of neuronal progenitor cells proliferating in the SGZ of the DG. Previous studies which assessed neurogenesis in the EAE model, using BrdU or IddU staining, show contradictory results, with some defending an increase in neurogenesis (Giannakopoulou et al., 2013), and others a decrease (Guo et al., 2010; Pluchino et al., 2008). In this study, we did not observe differences in the number of Ki67+ proliferating cells in the SGZ of EAE mice, nor in the numbers of neuronal progenitors (Ki67 + DCX+). Moreover, DMF treatment also did not affect neurogenesis. Our results are in accordance with those by Giannakopolou and co-workers (2017) (Giannakopoulou et al., 2017), which previously found that at the chronic phase of EAE, on day 30 post-disease induction, the proliferative capacity of neural precursor cells, evaluated by Ki67 immunohistochemistry staining, was almost the same between EAE and controls. Also in accordance, Planche et al. (2017) did not found significant differences in the number of DCX+ cells in the SGZ, between EAE and non-induced animals (Planche et al., 2017).

Finally, we also assessed myelination of the most important white matter pathway from the hippocampus, the fimbria, which is highly myelinated. Our data showed that DMF treatment was associated with an almost complete preservation of fimbria myelin content, which could, in our opinion, be enough to explain the behavioral effects of DMF herein described. Importantly, and in line with this hypothesis, lesions of the fimbria are sufficient to induce cognitive deficits similar to those associated with hippocampal damage (Galani et al., 2002). However, this interpretation must be taken with caution, since, due to the way the experiments were programmed, we could not correlate individual behavioral performances with the individual degree of fimbria demyelination. In addition, other factors such as alterations in the oxidative state of hippocampal cells ((Di Filippo et al., 2016b). Erratum

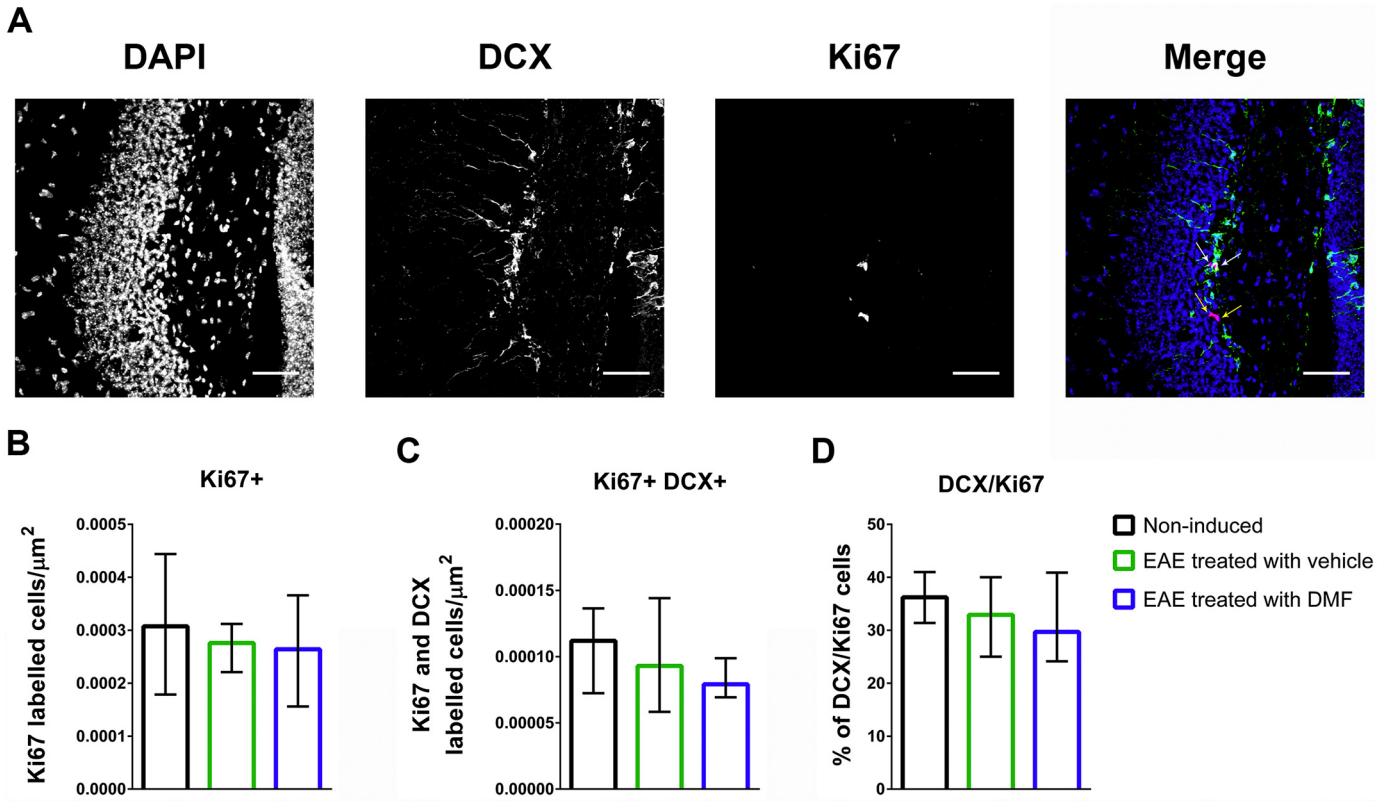

Fig. 5. – Vehicle- and DMF-treated EAE animals presented similar numbers of hippocampal progenitor cells. Hippocampal slices were double stained with Ki67 (red), to quantify the number of proliferating cells in the SGZ, and with DCX (green), to evaluate specifically the number of immature neurons in this area. Cell nuclei were stained with DAPI (blue). Double stained cells are evidenced by white arrows and Ki67 single stained cells by yellow arrows (A). The total number of Ki67 positive cells (B) and double stained cells (C) per area unit were similar in both EAE treated with vehicle or DMF, and the non-induced group. The three experimental groups also presented a similar percentage of DCX cells within the Ki67 positive cell population (D) (Scale bar = 50 µm. $n_{non\text{-}induced} = 4$, $n_{EAE\ treated\ with\ vehicle} = 7$, $n_{EAE\ treated\ with\ DMF} = 7$. Data presented as median ± IQR). (For interpretation of the references to color in this figure legend, the reader is referred to the web version of this article.)

in (Di Filippo et al., 2016a)) could also play a role in the observed behavioral effects of DMF.

Several studies have shown the presence of reactive astrocytes in different regions of the CNS of EAE models (Aquino et al., 1990; Luo et al., 2008; Smith and Eng, 1987; Tani et al., 1996). Here, we also found an increased astrocytic reactivity in the fimbria of EAE animals, characterized by an increased number of GFAP positive cells in this region. Interestingly, this increase was reverted to control levels by DMF treatment, indicating a beneficial effect of this drug on astrocyte reactivity.

In addition, microglial reactivity was described to be present in the hippocampus of both EAE mice (Planche et al., 2017) and MS patients (Colasanti et al., 2016), along with increased expression levels of microglial activation markers such as Iba1, CD11b and CD68 (Planche et al., 2017). More so, reactive microglial cells are able to modulate synaptic plasticity, for example through the production of pro-inflammatory cytokines that can influence both synaptic transmission and long-term potentiation, which is important for the storage of information (Di Filippo et al., 2018). In accordance, we have found an increased number of Iba1 positive cells in the animals' fimbria after EAE induction. However, contrary to astrocyte activation, DMF treatment was not able to revert microglial activation. In fact, the number of Iba1 positive cells was significantly higher in the DMF-treated animals compared with both non-induced and vehicle-treated animals. This was also true for the number of Iba1 positive cells in the hippocampus (data not shown). Without further characterization, that would be relevant in future studies, it is not possible to say if the microglia in the two EAE experimental groups presents a different inflammatory profile, that could also be contributing to symptoms amelioration. Interestingly, Parodi et al. (2015) observed that the *in vitro* treatment of microglia with MMF (active metabolite of DMF) reverted the LPS-induced expression of pro-inflammatory cytokines, like *tumor necrosis factor alfa* and *interleukin-1 beta*, and stress response molecules, like *heme oxygenase-1* and *inducible nitric oxide synthase*. Concomitantly, they observed the overexpression of genes associated with an alternative activation phenotype, like *insulin growth factor 1* and *arginase 1*. This could indicate that MMF could induce a switch from a classically pro-inflammatory activated phenotype to an alternative activated microglial state, that could be neuroprotective (Parodi et al., 2015).

In conclusion, the present study showed that DMF treatment after the disease was well established was able to ameliorate both the hippocampal-dependent cognitive abilities as well as the myelination and astrocytic reactivity of the main hippocampal output tract in a chronic MS mice model. By doing so, it provided new insights into the pathophysiology of cognitive deficits and new avenues for the preclinical testing of novel treatment possibilities.

Acknowledgments

The authors would like to acknowledge Ana Luísa Sousa and Pedro Moreira for comments and scientific discussion; Ana Lima and Mónica Dias from the histology services for Golgi-impregnated and Giemsa-staining tissue processing; Lucília Goreti Pinto for acquiring confocal images (all from the ICVS/3B's – PT Government Associate Laboratory).

Funding

This work was funded by an investigator initiated grant from Biogen

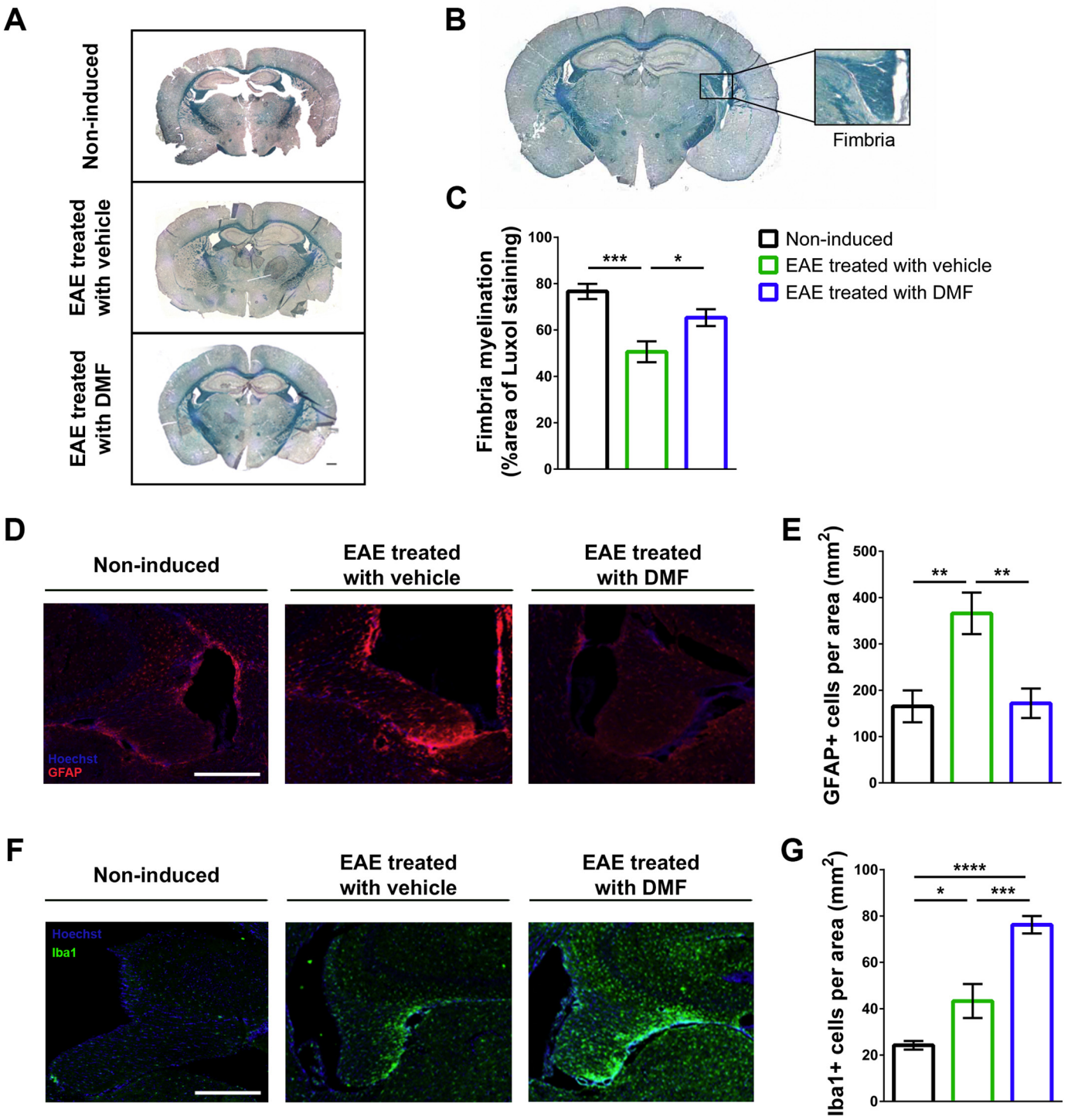

Fig. 6. – DMF treatment reduced the demyelination of the fimbria. Hippocampal slices were stained with LFB (A) (Scale bar = 400 μm) and the percentage of myelinated (stained) area in the fimbria (B) was quantified (C). Vehicle-treated EAE animals had significantly less myelinated area compared with both EAE DMF-treated and non-induced mice ($n_{non\text{-}induced}$ = 7, $n_{EAE\ treated\ with\ vehicle}$ = 7, $n_{EAE\ treated\ with\ DMF}$ = 7). Brain slices containing the fimbria/hippocampus were stained with GFAP (D) (Scale bar = 500 μm). The number of GFAP positive astrocytes increased in the fimbria of EAE animals, but DMF treatment was able to reverse this increase to control levels (E) ($n_{non\text{-}induced}$ = 8, $n_{EAE\ treated\ with\ vehicle}$ = 6, $n_{EAE\ treated\ with\ DMF}$ = 8). Brain slices containing the fimbria/hippocampus stained with Iba1 (F) (Scale bar = 500 μm). The number of Iba1 positive microglia was increased in the fimbria of vehicle-treated EAE group, compared to the non-induced animals, and further increased in the DMF-treated group (G) ($n_{non\text{-}induced}$ = 5, $n_{EAE\ treated\ with\ vehicle}$ = 5, $n_{EAE\ treated\ with\ DMF}$ = 6). Data presented as mean ± SEM. * $p < 0.05$, ** $p < 0.01$, *** $p < 0.001$, **** $P < 0.0001$).

Idec, USA, to João J. Cerqueira (PRT-BGT-13-10438), and by project DoIT – Desenvolvimento e Operacionalização da Investigação de Translação (Project number 13853), funded by European Regional Development Fund (FEDER) through Programa Operacional Fatores de Competitividade (POFC), "MyHealth" – My Data Module. The work at ICVS/3B's has been developed under the scope of the project NORTE-01-0145-FEDER-000013, supported by the Northern Portugal Regional Operational Programme (NORTE 2020), under the Portugal 2020

Partnership Agreement, through the FEDER, and funded by FEDER funds through the Competitiveness Factors Operational Programme (COMPETE), and by National funds, through the FCT, under the scope of the project POCI-01-0145-FEDER-007038. The work at iMed.ULisboa was funded by FCT UID/DTP/04138/2013. F.M. is an assistant researcher and recipient of an FCT Investigator grant with the reference IF/00231/2013. S.N. is a recipient of a PhD fellowship with the reference PD/BD/114120/2015, from MCTES national funds.

Declaration of Competing Interest

This work was funded by an investigator initiated grant from Biogen to João J. Cerqueira (PRT-BGT-13-10438).

Appendix A. Supplementary data

Supplementary data to this article can be found online at https://doi.org/10.1016/j.jneuroim.2020.577163.

References

Aquino, D.A., Shafit-Zagardo, B., Brosnan, C.F., Norton, W.T., 1990. Expression of glial fibrillary acidic protein and neurofilament mRNA in gliosis induced by experimental autoimmune encephalomyelitis. J. Neurochem. 54, 1398–1404.
Borreani, C., Bianchi, E., Pietrolongo, E., Rossi, I., Cilia, S., Giuntoli, M., et al., 2014. Unmet needs of people with severe multiple sclerosis and their carers: qualitative findings for a home-based intervention. PLoS One 9, e109679.
Burness, C.B., Deeks, E.D., 2014. Dimethyl fumarate: a review of its use in patients with relapsing-remitting multiple sclerosis. CNS drugs. 28, 373–387.
Chiaravalloti, N.D., DeLuca, J., 2008. Cognitive impairment in multiple sclerosis. Lancet Neurol. 7, 1139–1151.
Colasanti, A., Guo, Q., Giannetti, P., Wall, M.B., Newbould, R.D., Bishop, C., et al., 2016. Hippocampal neuroinflammation, functional connectivity, and depressive symptoms in multiple sclerosis. Biol. Psychiatry 80, 62–72.
Compston, A., Coles, A., 2008. Multiple sclerosis. Lancet. 372, 1502–1517.
Di Filippo, M., de Iure, A., Giampa, C., Chiasserini, D., Tozzi, A., Orvietani, P.L., et al., 2016a. Erratum: persistent activation of microglia and NADPH oxidase drive hippocampal dysfunction in experimental multiple sclerosis. Sci. Rep. 6, 23855.
Di Filippo, M., de Iure, A., Giampa, C., Chiasserini, D., Tozzi, A., Orvietani, P.L., et al., 2016b. Persistent activation of microglia and NADPH oxidase [corrected] drive hippocampal dysfunction in experimental multiple sclerosis. Sci. Rep. 6, 20926.
Di Filippo, M., Portaccio, E., Mancini, A., Calabresi, P., 2018. Multiple sclerosis and cognition: synaptic failure and network dysfunction. Nat. Rev. Neurosci. 19, 599–609.
Dutra, R.C., Moreira, E.L., Alberti, T.B., Marcon, R., Prediger, R.D., Calixto, J.B., 2013. Spatial reference memory deficits precede motor dysfunction in an experimental autoimmune encephalomyelitis model: the role of kallikrein-kinin system. Brain Behav. Immun. 33, 90–101.
Galani, R., Obis, S., Coutureau, E., Jarrard, L., Cassel, J.C., 2002. A comparison of the effects of fimbria-fornix, hippocampal, or entorhinal cortex lesions on spatial reference and working memory in rats: short versus long postsurgical recovery period. Neurobiol. Learn. Mem. 77, 1–16.
Geurts, J.J., Barkhof, F., 2008. Grey matter pathology in multiple sclerosis. Lancet Neurol. 7, 841–851.
Giannakopoulou, A., Grigoriadis, N., Bekiari, C., Lourbopoulos, A., Dori, I., Tsingotjidou, A.S., et al., 2013. Acute inflammation alters adult hippocampal neurogenesis in a multiple sclerosis mouse model. J. Neurosci. Res. 91, 890–900.
Giannakopoulou, A., Lyras, G.A., Grigoriadis, N., 2017. Long-term effects of autoimmune CNS inflammation on adult hippocampal neurogenesis. J. Neurosci. Res. 95, 1446–1458.
Gold, R., Arnold, D.L., Bar-Or, A., Hutchinson, M., Kappos, L., Havrdova, E., et al., 2017. Long-term effects of delayed-release dimethyl fumarate in multiple sclerosis: interim analysis of ENDORSE, a randomized extension study. Mult. Scler. 23, 253–265.
Guimaraes, J., Sa, M.J., 2012. Cognitive dysfunction in multiple sclerosis. Front. Neurol. 3, 74.
Gundersen, H.J., Bendtsen, T.F., Korbo, L., Marcussen, N., Moller, A., Nielsen, K., et al., 1988. Some new, simple and efficient stereological methods and their use in pathological research and diagnosis. APMIS 96, 379–394.
Guo, J., Li, H., Yu, C., Liu, F., Meng, Y., Gong, W., et al., 2010. Decreased neural stem/progenitor cell proliferation in mice with chronic/nonremitting experimental autoimmune encephalomyelitis. Neurosignals. 18, 1–8.
Hamilton, A.M., Forkert, N.D., Yang, R., Wu, Y., Rogers, J.A., Yong, V.W., et al., 2019. Central nervous system targeted autoimmunity causes regional atrophy: a 9.4T MRI study of the EAE mouse model of multiple sclerosis. Sci. Rep. 9, 8488.
Keuker, J.I., Vollmann-Honsdorf, G.K., Fuchs, E., 2001. How to use the optical fractionator: an example based on the estimation of neurons in the hippocampal CA1 and CA3 regions of tree shrews. Brain Res Brain Res Protoc. 7, 211–221.
Kim, D.Y., Hao, J., Liu, R., Turner, G., Shi, F.D., Rho, J.M., 2012. Inflammation-mediated memory dysfunction and effects of a ketogenic diet in a murine model of multiple sclerosis. PLoS One 7, e35476.
Kobelt, G., Thompson, A., Berg, J., Gannedahl, M., Eriksson, J., Group MS, et al., 2017. New insights into the burden and costs of multiple sclerosis in Europe. Mult. Scler. 23, 1123–1136.
Linker, R.A., Lee, D.H., Ryan, S., van Dam, A.M., Conrad, R., Bista, P., et al., 2011. Fumaric acid esters exert neuroprotective effects in neuroinflammation via activation of the Nrf2 antioxidant pathway. Brain 134, 678–692.
Lucchinetti, C.F., Parisi, J., Bruck, W., 2005. The pathology of multiple sclerosis. Neurol. Clin. 23, 77–105 (vi).
Luo, J., Ho, P., Steinman, L., Wyss-Coray, T., 2008. Bioluminescence in vivo imaging of autoimmune encephalomyelitis predicts disease. J. Neuroinflammation 5, 6.
McCarthy, D.P., Richards, M.H., Miller, S.D., 2012. Mouse models of multiple sclerosis: experimental autoimmune encephalomyelitis and Theiler's virus-induced demyelinating disease. Methods Mol. Biol. 900, 381–401.
Muckschel, M., Beste, C., Ziemssen, T., 2016. Immunomodulatory treatments and cognition in MS. Acta Neurol. Scand. 134 (Suppl. 200), 55–59.
Noseworthy, J.H., Lucchinetti, C., Rodriguez, M., Weinshenker, B.G., 2000. Multiple sclerosis. N. Engl. J. Med. 343, 938–952.
Novkovic, T., Shchyglo, O., Gold, R., Manahan-Vaughan, D., 2015. Hippocampal function is compromised in an animal model of multiple sclerosis. Neuroscience. 309, 100–112.
Opendak, M., Gould, E., 2015. Adult neurogenesis: a substrate for experience-dependent change. Trends Cogn. Sci. 19, 151–161.
Papadopoulos, D., Dukes, S., Patel, R., Nicholas, R., Vora, A., Reynolds, R., 2009. Substantial archaeocortical atrophy and neuronal loss in multiple sclerosis. Brain Pathol. 19, 238–253.
Parodi, B., Rossi, S., Morando, S., Cordano, C., Bragoni, A., Motta, C., et al., 2015. Fumarates modulate microglia activation through a novel HCAR2 signaling pathway and rescue synaptic dysregulation in inflamed CNS. Acta Neuropathol. 130, 279–295.
Planche, V., Panatier, A., Hiba, B., Ducourneau, E.G., Raffard, G., Dubourdieu, N., et al., 2017. Selective dentate gyrus disruption causes memory impairment at the early stage of experimental multiple sclerosis. Brain Behav. Immun. 60, 240–254.
Pluchino, S., Muzio, L., Imitola, J., Deleidi, M., Alfaro-Cervello, C., Salani, G., et al., 2008. Persistent inflammation alters the function of the endogenous brain stem cell compartment. Brain 131, 2564–2578.
Rao, S.M., Leo, G.J., Ellington, L., Nauertz, T., Bernardin, L., Unverzagt, F., 1991. Cognitive dysfunction in multiple sclerosis. II. Impact on employment and social functioning. Neurology. 41, 692–696.
Roosendaal, S.D., Hulst, H.E., Vrenken, H., Feenstra, H.E., Castelijns, J.A., Pouwels, P.J., et al., 2010. Structural and functional hippocampal changes in multiple sclerosis patients with intact memory function. Radiology. 255, 595–604.
Schilling, S., Goelz, S., Linker, R., Luehder, F., Gold, R., 2006. Fumaric acid esters are effective in chronic experimental autoimmune encephalomyelitis and suppress macrophage infiltration. Clin. Exp. Immunol. 145, 101–107.
Schindelin, J., Arganda-Carreras, I., Frise, E., Kaynig, V., Longair, M., Pietzsch, T., et al., 2012. Fiji: an open-source platform for biological-image analysis. Nat. Methods 9, 676–682.
Schulze-Topphoff, U., Varrin-Doyer, M., Pekarek, K., Spencer, C.M., Shetty, A., Sagan, S.A., et al., 2016. Dimethyl fumarate treatment induces adaptive and innate immune modulation independent of Nrf2. Proc. Natl. Acad. Sci. U. S. A. 113, 4777–4782.
Sholl, D.A., 1956. The measurable parameters of the cerebral cortex and their significance in its organization. Prog. Neurobiol. 324–333.
Sicotte, N.L., Kern, K.C., Giesser, B.S., Arshanapalli, A., Schultz, A., Montag, M., et al., 2008. Regional hippocampal atrophy in multiple sclerosis. Brain. 131, 1134–1141.
Smith, M.E., Eng, L.F., 1987. Glial fibrillary acidic protein in chronic relapsing experimental allergic encephalomyelitis in SJL/J mice. J. Neurosci. Res. 18, 203–208.
Steinman, L., 2001. Multiple sclerosis: a two-stage disease. Nat. Immunol. 2, 762–764.
Stromnes, I.M., Goverman, J.M., 2006. Active induction of experimental allergic encephalomyelitis. Nat. Protoc. 1, 1810–1819.
Tani, M., Glabinski, A.R., Tuohy, V.K., Stoler, M.H., Estes, M.L., Ransohoff, R.M., 1996. In situ hybridization analysis of glial fibrillary acidic protein mRNA reveals evidence of biphasic astrocyte activation during acute experimental autoimmune encephalomyelitis. Am. J. Pathol. 148, 889–896.
Tomczak, M., Tomczak, E., 2014. The need to report effect size estimates revisited. An overview of some recommended measures of effect size. Trends in sport. Sciences. 1, 19–25.
West, M.J., Slomianka, L., Gundersen, H.J., 1991. Unbiased stereological estimation of the total number of neurons in thesubdivisions of the rat hippocampus using the optical fractionator. Anat. Rec. 231, 482–497.
Ziehn, M.O., Avedisian, A.A., Tiwari-Woodruff, S., Voskuhl, R.R., 2010. Hippocampal CA1 atrophy and synaptic loss during experimental autoimmune encephalomyelitis, EAE. Lab. Investig. 90, 774–786.

Supplementary Table 1 – Mean ± SEM of data compared using the parametric two-tailed one-way ANOVA with Tukey's multiple comparison post-hoc test

Data	Group	Mean ± SEM
Percentage of time in platform quadrant (%)	Non-induced	23.85 ± 3.194
	EAE treated with vehicle	10.08 ± 3.228
	EAE treated with DMF	19.15 ± 3.718
Percentage of time in triangle quadrant (%)	Non-induced	25.23 ± 3.228
	EAE treated with vehicle	20.46 ± 4.068
	EAE treated with DMF	23.02 ± 2.730
Total dendritic length of DG neurons (μm)	Non-induced	967.0 ± 49.86
	EAE treated with vehicle	1071.0 ± 74.95
	EAE treated with DMF	1004.0 ± 39.52
Total basal dendritic length of CA1 neurons (μm)	Non-induced	1186.0 ± 101.20
	EAE treated with vehicle	1287.0 ± 72.21
	EAE treated with DMF	1211.0 ± 48.12
Total apical dendritic length of CA1 neurons (μm)	Non-induced	1762.0 ± 159.40
	EAE treated with vehicle	1792.0 ± 81.29
	EAE treated with DMF	1622.0 ± 80.69
DG volume x 10^9 (μm^3)	Non-induced	1.19 ± 0.197
	EAE treated with vehicle	1.05 ± 0.159
	EAE treated with DMF	1.39 ± 0.255
CA1 volume x 10^9 (μm^3)	Non-induced	1.44 ± 0.125
	EAE treated with vehicle	1.38 ± 0.082
	EAE treated with DMF	1.71 ± 0.194
CA3 volume x 10^9 (μm^3)	Non-induced	1.59 ± 0.116
	EAE treated with vehicle	1.34 ± 0.092
	EAE treated with DMF	1.50 ± 0.108
Total cell number in granular layer of DG x 10^5	Non-induced	6.28 ± 0.461
	EAE treated with vehicle	5.81 ± 0.322
	EAE treated with DMF	6.40 ± 0.559
Total cell number in *pyramidale* layer of CA3 x 10^5	Non-induced	1.53 ± 0.181
	EAE treated with vehicle	1.23 ± 0.110
	EAE treated with DMF	1.26 ± 0.141
Percentage of myelination in the fimbria (%)	Non-induced	76.61 ± 3.272
	EAE treated with vehicle	50.59 ± 4.474
	EAE treated with DMF	65.33 ± 3.621
GFAP+ cells per area (mm^2)	Non-induced	165.2 ± 34.35
	EAE treated with vehicle	365.9 ± 44.81
	EAE treated with DMF	171.8 ± 31.80
Iba1+ cells per area (mm^2)	Non-induced	24.2 ± 1.84
	EAE treated with vehicle	43.3 ± 7.33
	EAE treated with DMF	76.2 ± 3.76

Supplementary Table 2 – Median ± IQR of data compared using the non-parametric two-tailed Kruskal-Wallis with Dunn's multiple comparison post-hoc test

Data	Group	Median	IQR
Percentage of distance in platform quadrant (%)	Non-induced	21.59	[17.48, 30.27]
	EAE treated with vehicle	11.5	[0.00, 23.92]
	EAE treated with DMF	21.89	[12.17, 31.37]
Percentage of time in cross quadrant (%)	Non-induced	22.09	[16.17, 28.42]
	EAE treated with vehicle	16.92	[4.50, 22.50]
	EAE treated with DMF	28.59	[16.25, 32.37]
Percentage of time in square quadrant (%)	Non-induced	30.58	[18.25, 37.54]
	EAE treated with vehicle	47.33	[30.00, 69.58]
	EAE treated with DMF	31.42	[22.92, 40.42]
Total cell number in *pyramidale* layer of CA1 x 10^5	Non-induced	2.068	[1.97, 2.29]
	EAE treated with vehicle	2.24	[1.68, 2.44]
	EAE treated with DMF	2.37	[2.25, 2.65]
Number Ki67+ cells/area (cells/μm^2)	Non-induced	0.00031	[0.000179, 0.000444]
	EAE treated with vehicle	0.00028	[0.000221, 0.000312]
	EAE treated with DMF	0.00026	[0.000156, 0.000366]
Number Ki67+DCX+ cells/area (cells/μm^2)	Non-induced	0.000112	[0.0000724, 0.0001364]
	EAE treated with vehicle	0.000093	[0.0000583, 0.0001441]
	EAE treated with DMF	0.000079	[0.0000693, 0.0000988]
Percentage DCX+ cells/total Ki67+ cells (%)	Non-induced	36.2	[31.38, 40.99]
	EAE treated with vehicle	32.9	[25.00, 40.00]
	EAE treated with DMF	29.7	[24.14, 40.88]

CHAPTER 5

Sofia Pereira das Neves, Cláudia Serre-Miranda, João Carlos Sousa, Patrício Costa, Nuno Sousa, João José Cerqueira, Fernanda Marques

Higher Lipocalin-2 CSF levels could to be associated with faster MS progression

(Part of manuscript in preparation)

(2020)

Title

Higher Lipocalin-2 CSF levels could be associated with faster MS progression

Authors

Sofia Pereira das Neves [a,b], Cláudia Serre-Miranda [a,b], João Carlos Sousa [a,b], Patrício Costa [a,b], Nuno Sousa [a,b,c], João José Cerqueira [a,b,c,d,*], Fernanda Marques [a,b,d,*]

Affiliations

[a] Life and Health Sciences Research Institute (ICVS), School of Medicine, University of Minho, Campus Gualtar, 4710-057 Braga, Portugal.

[b] ICVS/3B's – PT Government Associate Laboratory, Braga/Guimarães, Portugal.

[c] Clinical Academic Center - Braga, Braga, Portugal.

* These authors share co-authorship

Corresponding author

Fernanda Marques (PhD), Life and Health Sciences Research Institute (ICVS), School of Medicine, University of Minho, Campus Gualtar, 4710-057 Braga, Portugal.

Phone number: +351 253 604 839

E-mail: fmarques@med.uminho.pt or jcerqueira@med.uminho.pt

Abstract

Lipocalin-2 (LCN2) is an acute phase protein that was found to be overexpressed by astrocytes in the active phase of the relapsing-remitting model of multiple sclerosis (MS). Moreover, both experimental autoimmune encephalomyelitis (EAE) animals and MS patients presented increased cerebrospinal (CSF) levels of LCN2. In this work, we explored the prognostic value of LCN2 in MS. For that, we collected CSF, for LCN2 quantification, and clinical data from a group of relapsing-remitting MS (RRMS) patients. We observed that RRMS patients with higher LCN2 levels at the time of lumbar puncture took less time to reach an expanded disability status scale (EDSS) of 3, hence presenting a faster disease progression. Moreover, a higher age, at lumbar puncture, was also associated with faster disease progression, while no significant association was found for disease progression and presence/absence of oligoclonal bands. After performing a regression analysis for time until EDSS of 3 including these three parameters, only age remained statistically significant. However, the confidence intervals do not rule out the possibility of LCN2 concentration being one of the factors contributing for disease progression. Future studies, with increased number of patients and a longer follow-up period should be performed to elucidate the prognostic value of LCN2 in MS.

Introduction

Multiple sclerosis (MS) is a chronic inflammatory disease of the central nervous system (CNS) (Lassmann and van Horssen, 2011), characterized by an increased migration of autoreactive lymphocytes across the blood-brain barrier (Compston and Coles, 2008). In the brain parenchyma, autoreactive T cells react against myelin peptides, inducing inflammation, demyelination, astrocytosis, and axonal and neuronal degeneration (Nakahara et al., 2010; Noseworthy et al., 2000).

Initial reports in mice have described lipocalin-2 (LCN2) as an acute phase protein (Liu and Nilsen-Hamilton, 1995), involved in the response to bacterial infection (Flo et al., 2004), inflammatory (Marques et al., 2008) and stressful stimuli (Mucha et al., 2011). Further studies have also implicated LCN2 in the pathophysiology of several CNS disorders like Alzheimer's disease (Choi et al., 2011; Naude et al., 2012), pain (Jha et al., 2014), and also MS (Al Nimer et al., 2016; Berard et al., 2012; Khalil et al., 2016; Marques et al., 2012; Nam et al., 2014).

Specifically for MS, most studies report an increase in serum and cerebrospinal fluid (CSF) LCN2 levels, compared to control groups (Al Nimer et al., 2016; Berard et al., 2012; Marques et al., 2012), while one study reported decreased levels in the serum and CSF of MS patients (Khalil et al., 2016). Regarding the experimental autoimmune encephalomyelitis (EAE) animal model, which is used to study MS, we previously found that *Lcn2* was the most significantly upregulated gene in the choroid plexus of a relapse-remitting EAE mice model, during the active phases of disease (onset and relapse phases). Moreover, during these active phases of disease, LCN2 was increased in astrocytes of lesioned areas and in the animals' CSF. Of interest, LCN2 was described as a pan-reactive astrocytic gene (general marker of activation induced by neuroinflammation or ischemia) (Liddelow et al., 2017). Furthermore, the increase of LCN2 in the CSF and its astrocytic production was reverted by natalizumab treatment (Marques et al., 2012). LCN2-null animals induced with EAE presented a significant decrease in disease severity (Nam et al., 2014), accompanied by reduced inflammatory infiltration, inflammatory cytokine production, glial activation and demyelination (das Neves, 2015; Nam et al., 2014), suggesting that LCN2 plays a detrimental role in the context of MS. Contrarily, another study has reported that LCN2-null mice presented a more severe EAE phenotype and pro-inflammatory response, compared to wild-type animals (Berard et al., 2012). To further complement these studies, here we addressed the question of whether LCN2 levels in MS patients could be used as a predictor of disease progression.

Methods

Human samples

CSF samples were obtained according to standardized protocols from patients admitted for lumbar puncture (LP) in Hospital de Braga since 2009. Patients were referred to the Neuroimmunology Clinic, Hospital de Braga, Portugal and underwent diagnostic program including magnetic resonance imaging scan and LP. LP was performed within 30 days of symptom debut, thus in the active phase of disease. Patients included in the study were diagnosed with clinically definite relapsing remitting multiple sclerosis (RRMS), according to the MacDonald 2017 criteria (Thompson et al., 2018). The studies with human samples were approved by the ethical committee of Hospital de Braga and all patients signed an informed consent.

LCN2 protein quantification by ELISA

The primary monoclonal antibody rat anti-human LCN2 (1:200 in phosphate buffered saline (PBS); MAB17571, R&D Systems, Minneapolis, MN, USA) was incubated over-night at room temperature (RT) in 96 well plates (MaxiSorpTM, VWR International, Radnor, PA, USA). The blocking was performed with 1% bovine serum albumin in PBS for 2 h at RT. CSF samples (1:2) and standards were diluted in blocking solution and incubated for 2 h at RT. All samples and standards were analyzed in duplicates. The secondary polyclonal antibody goat anti-human LCN2 (1:700 in blocking solution; BAF1757, R&D Systems) was incubated for 2 h at RT. Streptavidin-peroxidase (1:2000 in PBS; S2438, Sigma-Aldrich) was incubated for 30 min in the dark. All the previous steps were followed by a washing step with PBS-Tween 20 0.05%. Next, the 3,3',5,5'-tetramethylbenzidine (Sigma Aldrich) substrate was incubated for 30 min in the dark. The reaction was stopped by adding sulfuric acid (2 M), and the absorbance was read in a multiplate reader (BioRad Laboratories) at 450 nm, using the 570 nm as reference. The standard curve was modeled using a four-parameter logistic curve, and the Microplate Manager Software version 5.2.1 (BioRad Laboratories) was used to calculate the LCN2 concentration in samples.

Statistical analysis

Statistical analysis of the results was performed using GraphPad Prism version 6.01 (GraphPad software Inc., La Jolla, CA, USA) and IBM® SPSS® version 23. The Mann-Whitney U test was used to compare the LCN2 concentration of patients with presence/absence of oligoclonal bands (OCBs), after confirming the sample did not present a normal distribution, using the Shapiro-Wilk normality test. The Kaplan-Meier survival curve was used to evaluate disease progression until expanded disability status scale (EDSS) 3

in patients, after dividing them according to LCN2 concentration (above or below group median) or presence/absence of OCBs. A Cox proportional hazard regression analysis was used to evaluate the effect of LCN2 concentration, age at LP and presence/absence of oligoclonal bands for EDSS progression (until EDSS of 3). Information regarding presence/absence of OCBs was not available for 6 MS patients.

Results are presented as mean ± standard error of mean (SEM). The statistical significance and number of biological replicates (n) is specified in the legend of each figure.

Results

Increased LCN2 CSF levels in MS patients could be associated with faster disease progression

Previous studies from our group (das Neves, 2015) and others (Nam et al., 2014) have shown that LCN2 absence is associated with a decrease disease burden, in the chronic EAE model. To explore the possible clinical relevance of such findings in the MS context, we assessed if LCN2 CSF levels were associated with the disease progression rate. Table 5. 1 presents the demographic characteristics of the RRMS patients included in the study. LCN2 concentration was quantified in CSF samples of patients, that were subsequently divided in two sub-groups (high and low LCN2), according to the median value of the whole group (0.9557 ng/mL). The sub-group of patients with higher LCN2 levels presented a significantly faster disease progression, taking less time to reach an EDSS of 3 (Figure 5. 1A; median survival $_{\text{below median}}$ = 389.0, median survival $_{\text{above median}}$ = 141.0, Log rank = 4.499, p = 0.0339). Considering that the presence of OCBs is commonly used as part of the diagnosis for MS, we next evaluated if disease progression was different according to the presence/absence of OCBs. In our sample, we did not find significant differences in disease progression when dividing the patients according to the presence/absence of OCBs (Figure 5. 1B; median survival $_{\text{no}}$ = 389.0, median survival $_{\text{yes}}$ = 152.0, Log rank = 1.876, p = 0.171). LCN2 concentration was significantly increased in the group positive for OCBs, compared to the group without OCBs (Figure 5. 1C; U = 138.0, p = 0.0275). Considering this difference, and the fact that patients' age was significantly different between the high and low LCN2 concentration groups, we used these three variables to perform a Cox regression analysis (Table 5. 2). We observed that higher LCN2 concentration was significantly associated with faster disease progression until EDSS 3, however this was no longer statistically significant after adjusting for age at LP and OCBs presence/absence. Increased age at LP was also associated with faster disease progression and remained significant after adjustment. In addition, no significant associations were found between LCN2 CSF concentration and the number of Barkhof criteria or the presence of active lesions at the time of LP (data not shown).

Table 5. 1 – Sample demographic information.

	Total patient sample Mean ± SD	Below LCN2 median Mean ± SD	Above LCN2 median Mean ± SD
Number of patients	49	25	24
Female:Male number	32:17	17:8	15:9
Age at LP (years)	34.84 ± 10.357	32.04 ± 10.269 ‡	37.75 ± 9.821‡
Age at diagnosis (years)*	35.48 ± 10.294	32.68 ± 10.282 †	38.52 ± 9.615 †
LCN2 concentration in CSF (ng/mL)	1.079 ± 0.3565	0.819 ± 0.0982 #	1.350 ± 0.3240 #
LCN2 median (ng/mL)	0.9557	–	–

* Information regarding date of diagnosis was not available for 1 patient; ‡ $t_{(47)} = -1.988$, $p = 0.053$; † $t_{(46)} = -2.028$, $p = 0.048$; # $t_{(27.037)} = -7.698$, $p < 0.0001$. CSF – cerebrospinal fluid; LP – lumbar puncture; SD – standard deviation.

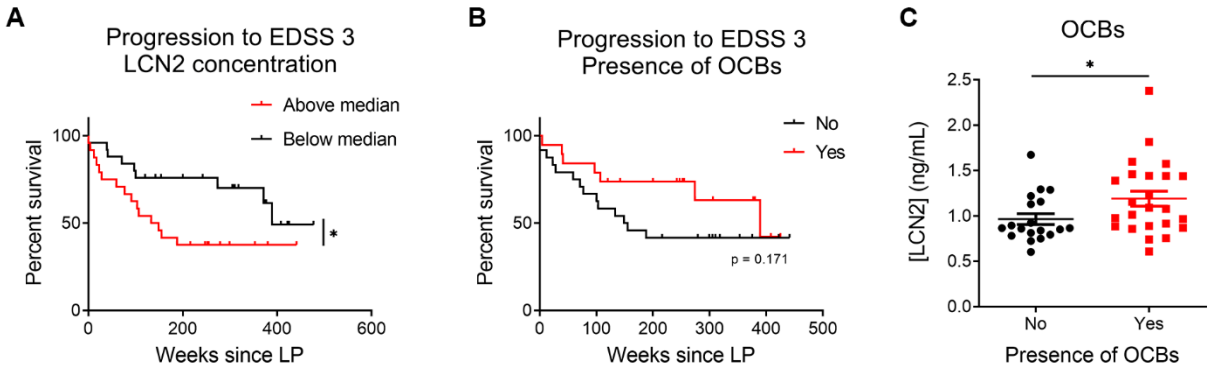

Figure 5. 1 – Patients with higher LCN2 levels seem to progress faster in the disease.

(A) Progression to EDSS 3 in patients with LCN2 levels above and below group median ($n_{below\ median} = 25$, $n_{above\ median} = 24$). (B) Progression to EDSS 3 in patients with presence or absence of OCBs ($n_{no} = 19$, $n_{yes} = 24$). (C) LCN2 concentration in RRMS patients with presence or absence of OCBs ($n_{no} = 19$, $n_{yes} = 24$). Data presented as mean ± SEM. * $p < 0.05$. EDSS – expanded disability status scale; LP – lumbar puncture; OCBs – oligoclonal bands.

Table 5. 2 – Cox regression analysis of time for progression until EDSS 3.

	p	Crude HR	95%CI
LCN2 concentration*	**0.041**	2.956	1.048-8.340
Presence/absence of OCBs‡	0.178	1.868	0.752-4.638
Age at LP	**< 0.0001**	1.108	1.056-1.162
	p	**Adjusted HR**	**95%CI**
LCN2 concentration*	0.706	1.259	0.381-4.158
Presence/absence of OCBs‡	0.289	1.663	0.649-4.262
Age at LP	**0.0002**	1.105	1.049-1.163

* The Cox regression analysis was performed using the LCN2 concentration values; ‡ Information regarding presence/absence of OCBs was not available for 6 patients. CI – confidence interval; HR – hazard ratio; LP – lumbar puncture.

Discussion

Partially in accordance with the data obtained in the LCN2-null EAE mice (das Neves, 2015), in the human disease we found that higher LCN2 levels were associated with a faster disease progression, assessed by the EDSS. However, this association was lost after controlling for the presence of OCBs and for age at LP (adjusted hazard ratio = 1.259, 95% confidence interval = 0.381-4.158). Nonetheless, the confidence interval does not rule out the possibility of LCN2 concentration being one of the factors contributing for disease progression. Further studies that include larger sample sizes and longer follow-up periods are needed to verify this. Of interest, it was previously shown in clinically isolated syndrome (CIS) patients that high LCN2 CSF levels were an independent predictive factor for conversion to clinically definite MS, during the study follow-up period (Khalil et al., 2016). However, increased LCN2 levels were also reported in other conditions (Choi et al., 2011; Chun et al., 2015; Parmar et al., 2018), suggesting its increase is not specific for MS. Thus, the integration of LCN2 CSF values in a broader biomarker panel, instead of being used alone, could be helpful to predict disease progression and eventually also aid in therapeutic decisions.

Several studies have found that the presence of OCBs in the CSF of MS patients was associated with faster disease progression and with conversion from CIS to clinically definite MS [meta-analysis performed by (Dobson et al., 2013)]. In our sample, patients with positive OCBs in the CSF seemed to progress faster to an EDSS of 3, but this did not reach statistical significance.

In this cohort of RRMS patients, those with older ages reached an EDSS of 3 faster than younger patients which is in accordance with previously published studies (Guillemin et al., 2017; Leray et al., 2010). Interestingly, this seems to be true only until patients reach a certain threshold of disability, i.e., above an EDSS of 3 disability progresses at the same rate, independently of age at onset (Leray et al., 2010).

This study presents some drawbacks, including low patient number, a small follow-up period (2-10 years) and absence of information for OCBs in some patients.

In conclusion, our results suggest that LCN2 could play a detrimental role in the MS context. This is based on the previous results obtained by our lab and others that LCN2-null EAE animals presented a decreased inflammatory response in the CNS when compared to wild-type EAE animals (das Neves, 2015), and also to the fact that, in this study, a faster disease progression in MS patients seems to be associated with higher LCN2 CSF levels.

Funding

This work was supported by Foundation for Science and Technology (FCT) and COMPETE through the project EXPL/NEU-OSD/2196/2013 and by The Clinical Academic Center (2CA-Braga) through the project EXPL/001/2016. The work at ICVS/3B's has been developed under the scope of the project NORTE-01-0145-FEDER-000013, supported by the Northern Portugal Regional Operational Programme (NORTE 2020), under the Portugal 2020 Partnership Agreement, through the European Regional Development Fund (FEDER), and funded by FEDER funds through the Competitiveness Factors Operational Programme (COMPETE), and by National funds, through the Foundation for Science and Technology (FCT), under the scope of the project POCI-01-0145-FEDER-007038. F.M. is an assistant researcher and recipient of an FCT Investigator grant with the reference CEECIND/01084/2017. CM and SN are recipients of PhD fellowships with the references SFRH/BD/112494/2015 and PD/BD/114120/2015, respectively, from MCTES national funds.

Author contributions

SN and CM performed the experiments; SN and PC performed the statistical analysis; SN performed the data analysis and wrote the manuscript; JC collected the human samples; JC, NS and JC critically revised the manuscript; FM designed and supervised the study and edited the manuscript.

Conflict of interest

The authors have no conflicting financial interest to declare.

References

Al Nimer F, Elliott C, Bergman J, Khademi M, Dring AM, Aeinehband S, et al. Lipocalin-2 is increased in progressive multiple sclerosis and inhibits remyelination. Neurology: Neuroimmunology and NeuroInflammation. 2016;3:e191.

Berard JL, Zarruk JG, Arbour N, Prat A, Yong VW, Jacques FH, et al. Lipocalin 2 is a novel immune mediator of experimental autoimmune encephalomyelitis pathogenesis and is modulated in multiple sclerosis. Glia. 2012;60:1145-1159.

Choi J, Lee HW, Suk K. Increased plasma levels of lipocalin 2 in mild cognitive impairment. Journal of the Neurological Sciences. 2011;305:28-33.

Chun BY, Kim JH, Nam Y, Huh MI, Han S, Suk K. Pathological involvement of astrocyte-derived lipocalin-2 in the demyelinating optic neuritis. Investigative Ophthalmology and Visual Science. 2015;56:3691-3698.

Compston A, Coles A. Multiple sclerosis. Lancet. 2008;372:1502-1517.

das Neves SP (2015). Studying the role of lipocalin-2 in the pathophysiology of multiple sclerosis: looking beyond the brain (Master dissertation University of Minho, Braga, Portugal). Retrived from http://hdl.handle.net/1822/47233.

Dobson R, Ramagopalan S, Davis A, Giovannoni G. Cerebrospinal fluid oligoclonal bands in multiple sclerosis and clinically isolated syndromes: a meta-analysis of prevalence, prognosis and effect of latitude. Journal of Neurology, Neurosurgery and Psychiatry. 2013;84:909-914.

Flo TH, Smith KD, Sato S, Rodriguez DJ, Holmes MA, Strong RK, et al. Lipocalin 2 mediates an innate immune response to bacterial infection by sequestrating iron. Nature. 2004;432:917-921.

Guillemin F, Baumann C, Epstein J, Kerschen P, Garot T, Mathey G, et al. Older age at multiple sclerosis onset is an independent factor of poor prognosis: a population-based cohort study. Neuroepidemiology. 2017;48:179-187.

Jha MK, Jeon S, Jin M, Ock J, Kim JH, Lee WH, et al. The pivotal role played by lipocalin-2 in chronic inflammatory pain. Experimental Neurology. 2014;254:41-53.

Khalil M, Renner A, Langkammer C, Enzinger C, Ropele S, Stojakovic T, et al. Cerebrospinal fluid lipocalin 2 in patients with clinically isolated syndromes and early multiple sclerosis. Multiple Sclerosis. 2016;22:1560-1568.

Lassmann H, van Horssen J. The molecular basis of neurodegeneration in multiple sclerosis. FEBS Letters. 2011;585:3715-3723.

Leray E, Yaouanq J, Le Page E, Coustans M, Laplaud D, Oger J, et al. Evidence for a two-stage disability progression in multiple sclerosis. Brain. 2010;133:1900-1913.

Liddelow SA, Guttenplan KA, Clarke LE, Bennett FC, Bohlen CJ, Schirmer L, et al. Neurotoxic reactive astrocytes are induced by activated microglia. Nature. 2017;541:481-487.

Liu Q, Nilsen-Hamilton M. Identification of a new acute phase protein. Journal of Biological Chemistry. 1995;270:22565-22570.

Marques F, Mesquita SD, Sousa JC, Coppola G, Gao F, Geschwind DH, et al. Lipocalin 2 is present in the EAE brain and is modulated by natalizumab. Frontiers in Cellular Neuroscience. 2012;6:33.

Marques F, Rodrigues AJ, Sousa JC, Coppola G, Geschwind DH, Sousa N, et al. Lipocalin 2 is a choroid plexus acute-phase protein. Journal of Cerebral Blood Flow and Metabolism. 2008;28:450-455.

Mucha M, Skrzypiec AE, Schiavon E, Attwood BK, Kucerova E, Pawlak R. Lipocalin-2 controls neuronal excitability and anxiety by regulating dendritic spine formation and maturation. Proceedings of the National Academy of Sciences of the United States of America. 2011;108:18436-18441.

Nakahara J, Aiso S, Suzuki N. Autoimmune versus oligodendrogliopathy: the pathogenesis of multiple sclerosis. Archivum Immunologiae et Therapiae Experimentalis. 2010;58:325-333.

Nam Y, Kim JH, Seo M, Kim JH, Jin M, Jeon S, et al. Lipocalin-2 protein deficiency ameliorates experimental autoimmune encephalomyelitis: the pathogenic role of lipocalin-2 in the central nervous system and peripheral lymphoid tissues. Journal of Biological Chemistry. 2014;289:16773-16789.

Naude PJ, Nyakas C, Eiden LE, Ait-Ali D, van der Heide R, Engelborghs S, et al. Lipocalin 2: novel component of proinflammatory signaling in Alzheimer's disease. FASEB Journal. 2012;26:2811-2823.

Noseworthy JH, Lucchinetti C, Rodriguez M, Weinshenker BG. Multiple sclerosis. The New England Journal of Medicine. 2000;343:938-952.

Parmar T, Parmar VM, Perusek L, Georges A, Takahashi M, Crabb JW, et al. Lipocalin 2 plays an important role in regulating inflammation in retinal degeneration. Journal of Immunology. 2018;200:3128-3141.

Thompson AJ, Banwell BL, Barkhof F, Carroll WM, Coetzee T, Comi G, et al. Diagnosis of multiple sclerosis: 2017 revisions of the McDonald criteria. Lancet Neurology. 2018;17:162-173.

CHAPTER 6

General discussion and future perspectives

Metabolic reprogramming seems to occur in astrocytes during EAE

Recently, a classification of reactive astrocytes in A1 and A2 was proposed, in analogy to the M1/M2 macrophage nomenclature. A1 and A2 astrocytes are induced by neuroinflammation and ischemia, respectively. Interestingly, we observed that the astrocytes from EAE animals presented an A1 phenotype, while the A2 specific genes did not present major alterations. Moreover, our transcriptomic analysis revealed that important metabolic alterations occurred in astrocytes of EAE animals. Thus, we hypothesized that astrocytes, similarly to macrophages, could also undergo metabolic reprogramming during EAE. In fact, previous studies have demonstrated not only that pro-inflammatory stimuli are able to modulate the metabolism of astrocytes (Chao et al., 2019; Hamby et al., 2012; Motori et al., 2013), but also that sphingolipid metabolism, particularly lactosylceramide biosynthesis, is able to control astrocyte responses that are relevant to the pathogenesis of MS (Chao et al., 2019; Mayo et al., 2014). Furthermore, previous studies have observed the downregulation of cholesterol biosynthesis pathways in EAE animals (Itoh et al., 2018; Mueller et al., 2008; Sevastou et al., 2016; Tassoni et al., 2019).

Regarding the alterations in sphingolipid metabolism, Chao and colleagues (2019) reported increased astrocytic expression levels of genes related with this metabolic pathway, specifically in *beta-1,4-galactosyltransferase 6* (*B4galt6*) and *ceramide synthase (Cers) 6*, during the progressive phase of EAE (Chao et al., 2019). In addition, Mayo et al. (2014) had previously demonstrated upregulation of *B4galt6* in astrocytes and increased lactosylceramide levels in the CNS of EAE animals (Mayo et al., 2014). From the analysis of our transcriptomic data, it seems that the LacCer biosynthesis pathway is also upregulated in EAE animals compared to non-induced controls. Namely, *Cers4* expression was upregulated at the chronic phase, *UDP-glucose ceramide glucosyltransferase* was upregulated at the pre-symptomatic phase, while the *B4galt6* and *Cers6* expression seemed to be increased at the onset and pre-symptomatic phases of disease, respectively, but this did not reach statistical significance.

As for alterations occurring in cholesterol biosynthesis, Itoh and co-workers (2018) described that several genes involved in this pathway were downregulated by astrocytes at day 45-50 post-EAE induction, but not at day 21 (Itoh et al., 2018). In our study, we also observed a downregulation of genes involved in this pathway, namely *3-hydroxy-3-methylglutaryl-CoA synthase 1*, *farnesyl diphosphate synthase* and *farnesyl-diphosphate farnesyltransferase 1*, at the onset phase of disease (days 9-12 post-induction). However, when looking at the three non-induced groups of animals, we detected that the onset group overexpressed these genes in comparison to the remaining two non-induced time points. Thus, at least in our animals, it seems that at the onset time point the cholesterol synthesis is upregulated in non-induced animals, and not downregulated in the EAE group. Even though our results are not in accordance

to the ones obtained previously, here we performed a cross-sectional analysis of the disease, while the remaining works have studied only one disease time point [day 45 p.i. in (Itoh et al., 2018), day 50 p.i. in (Tassoni et al., 2019), post-relapsing chronic phase in (Sevastou et al., 2016)] or merged the different time points to obtain a value representing the average expression in EAE [expression values for the acute, recovery and relapsing phases merged in the work by (Mueller et al., 2008)]. Moreover, the other studies used only one control group of healthy animals for EAE comparison, while we included a non-induced control for each time point, who were also injected with CFA and PTX. These differences could, at least partially, explain the distinct results.

All together, these data suggests that metabolic pathways in astrocytes are possible therapeutic targets in MS, particularly in progressive phases of disease, that present limited treatment options (Correale et al., 2017; Faissner et al., 2019) and during which astrocytes seem to play a relevant role (Correale and Farez, 2015; Nylander and Hafler, 2012; Wheeler and Quintana, 2019). In this regard, Chao and colleagues (2019) demonstrated that Miglustat treatment, which is able to reduce lactosylceramide levels, could reduce the clinical scores of EAE animals, accompanied by a reduction in axonal loss, demyelination and recruitment of pro-inflammatory monocytes to the CNS (Chao et al., 2019). The specific inhibition of B4GALT5/6, with D-threo-1-phenyl-2-decanoylamino-3-morpholino-1-propanol, also decreased the lactosylceramide levels and suppressed EAE progression in terms of clinical score, demyelination and axonal loss (Mayo et al., 2014). In addition, the treatment of EAE animals with CS-6253 was able to increase the expression levels of genes involved in cholesterol synthesis, particularly in astrocytes, resulting in an improvement of the animals' clinical score and motor function (Itoh et al., 2018). The overexpression of glycolysis and TCA cycle genes observed in this study suggest these pathways are also possible therapeutic targets in astrocytes. Of relevance, glycolysis inhibition in LPS-stimulated cultured astrocytes, by pre-treatment with the non-metabolizable glucose analogue 2-deoxyglucose, significantly decreased the LPS-induced release of TNFα and IL-6 (Robb et al., 2020). Moreover, previous studies have demonstrated that itaconate treatment is able to modulate the TCA cycle, thus inducing immune paralysis. Namely, macrophage/monocyte treatment with itaconate inhibited succinate dehydrogenase activity, which lead to succinate accumulation and, consequently, to decreased TCA cycle activity (Dominguez-Andres et al., 2019; Lampropoulou et al., 2016). Similarly, dimethyl itaconate was also able to suppress microglia activation (Kuo et al., 2020). Remarkably, the Nrf2-mediated response was also shown to be induced by itaconate treatment, in macrophages and microglia (Bambouskova et al., 2018; Kuo et al., 2020). Thus, itaconate could have a dual beneficial effect on astrocytes, by inducing immune paralysis on one hand, and by increasing its anti-oxidative effects on the other. Of relevance, a recent

study has demonstrated that dimethyl itaconate treatment was able to reduce the clinical symptoms of EAE animals, that presented a decrease in BBB permeability and in MMPs production, resulting in decreased Th1 and Th17 infiltration in the CNS, and suppressed microglial activation, compared to vehicle-treated animals (Kuo et al., 2020). However, these authors have not performed any analysis on astrocytes.

It is important to highlight that, even tough we observed metabolic alterations in astrocytes similar to the ones reported before, our results do not exactly replicate those studies. One of the factors that could also contribute to variability among studies, other than the ones already mentioned, is the protocol used to isolate astrocytes. While we specifically isolated ACSA-2/Atp1b2 positive astrocytes using MACS, the previously mentioned studies have used fluorescence-activated cell sorting or astrocyte RiboTag mice to isolate these cells (Chao et al., 2019; Itoh et al., 2018; Tassoni et al., 2019). So, we cannot exclude the hypothesis that different astrocytic populations, that could differentially respond to disease, are being analyzed in the different studies, leading to the distinct results in gene expression.

In addition to metabolic alterations, other relevant astrocytic functions were observed to be altered in our EAE animals, namely, several pathways involved in the modulation of the ECM, particularly at the pre-symptomatic phase. Interestingly, the great majority of significantly altered genes were upregulated in EAE animals, including genes encoding for collagen and laminin proteins. In accordance, previous works have reported alterations in the expression levels of ECM genes and proteins both in EAE and MS (Gresle et al., 2014; Han et al., 2008; Ibrahim et al., 2001; Kroksveen et al., 2017; Satoh et al., 2009). Astrocytes are major producers of ECM proteins in the CNS, and particularly in glial scars, the production of fibronectin, hyaluronan and CSPGs by reactive astrocyte is detrimental for remyelination (Lau et al., 2013; Stoffels et al., 2013). Thus, the modulation of the astrocytes capacity for producing ECM proteins also presents as a possible therapeutic target. It is important to mention that we cannot exclude that the upregulation of these ECM-related genes originates from endothelial cells, and not astrocytes, considering that we also found increased expression levels of some endothelial markers in our samples, and that these cells present high expression levels of most of the genes found altered (Zhang et al., 2014). In fact, Munji and colleagues (2019) have reported alterations in ECM-related pathways in endothelial cells during EAE (Munji et al., 2019). Future studies using laser capture microdissection followed by gene expression profiling (Nichterwitz et al., 2018) or spatial transcriptomics (Vickovic et al., 2019) would be important to further explore the alterations occurring in each cell type during EAE, and specifically pinpoint the astrocytic-specific changes.

Besides performing a transcriptomic characterization of astrocytes, we also performed a morphological study of astrocytes throughout disease development. The 3D morphology reconstruction was performed after GFAP staining. One of the drawbacks of using GFAP for morphology reconstruction is that not all astrocytes are positive for GFAP (Walz and Lang, 1998; Zhang et al., 2019), and GFAP immunohistochemistry only labels the main cellular branches, being absent in fine processes (Bushong et al., 2002; Herrmann et al., 2008; Sofroniew and Vinters, 2010). Thus, our analysis is biased towards this specific astrocytic sub-population and does not cover the entire morphological alterations that could be occurring in astrocytes during disease. Another disadvantage is the thickness of the sections used, which do not allow the visualization of the entire astrocytic structure. Nevertheless, we were able to confirm an increased astrocytic reactivity near lesion regions of EAE animals, characterized by increased total length and number of processes. In future studies, double staining protocols would be useful in the characterization of the morphological alterations occurring specifically in A1 and A2 astrocytes.

When it comes to the NAWM of EAE animals, no significant differences were observed, in comparison to non-induced animals. Interestingly, astrocytes from the NAWM of EAE animals presented high variability, which could be associated with the presence of increased BBB permeability in some of these animals, for example. In fact, already at the pre-symptomatic phase there seems to exist two groups of animals, and the higher astrocyte reactivity in some of them could be preceding the appearance of clinical symptoms. To confirm this hypothesis, it would be of relevance to evaluate astrocytic reactivity in live animals throughout disease development. This could be performed using two-photon Ca^{2+} imaging, since changes in intracellular Ca^{2+} levels could be a good indicator for alterations in astrocytic physiology.

Decreased lesion burden in IP_3R2-null EAE mice

Intracellular Ca^{2+} transients represent a form of astrocytic excitability (Scemes and Giaume, 2006; Sofroniew and Vinters, 2010) and are important for several astrocytic functions, like the release of vasoactive metabolites, that regulate cerebral blood flow and energy supply, and gliotransmitters, that generate a wide range of effects on neurons (Bazargani and Attwell, 2016). Moreover, alterations in intracellular Ca^{2+} transients have been reported to occur in models of neurological diseases, like Alzheimer's disease and Huntington's disease (Ding et al., 2007; Jiang et al., 2016; Kuchibhotla et al., 2009; Reichenbach et al., 2018), however the astrocytic Ca^{2+} signaling pattern remains to be explored in EAE. Future studies using two-photon microscopy would allow the study of Ca^{2+} waves in live animals, throughout disease progression, to evaluate if these are also altered in the EAE context.

Interestingly, the astrocytic hyperactivity observed in a model of Alzheimer's disease (Kuchibhotla et al., 2009; Reichenbach et al., 2018), along with the cognitive deficits presented in this model, were reverted by the deletion of IP_3R2 (Reichenbach et al., 2018). IP_3R activation in astrocytes is involved in the release of Ca^{2+} from the endoplasmic reticulum (Agulhon et al., 2008; Petravicz et al., 2008; Vardjan and Zorec, 2015), and the type 2 receptor was reported to be expressed mainly in astrocytes, in the CNS (Hertle and Yeckel, 2007; Sharp et al., 1999). As already mentioned, the profile of astrocytic Ca^{2+} signaling is not known in EAE, however, the *Itpr2* gene, that encodes for the IP_3R2, was reported to be increased in this model (Staats et al., 2016), and IP_3-dependent Ca^{2+} signaling seems to be involved in the astrocytic response to injury (Kanemaru et al., 2013). Taking all this into account, we decided to study the consequences of ablating IP_3-dependent Ca^{2+} signaling in the EAE model. While no differences were observed between genotypes regarding the clinical score, we did detect a decrease in the percentage of lesioned area in the cerebellum of IP_3R2-null mice, compared to Wt littermates, at the onset phase of disease. In addition, the IP_3R2-null mice astrocytes were more reactive (higher length and number of processes) near lesion regions, than in the NAWM, which was not observed in Wt animals. This suggests that in IP_3R2-null mice astrocytes could be more effective at containing the inflammatory infiltrates than Wt astrocytes. These results are contradictory to what was expected, since previous studies have found that IP_3-dependent Ca^{2+} signaling is important for the astrocytic response to injury. This way, in the absence of this signaling pathway astrocytes should become less reactive and present a decreased capacity for containing inflammatory infiltration. In fact, Kanemaru and colleagues (2013) observed decreased astrocytic reactivity and increased number of infiltrating leukocytes in the CNS of IP_3R2-null mice, after a stab wound injury (Kanemaru et al., 2013). Nevertheless, the two disease models used are very different. In EAE, there is an autoimmune reaction against myelin antigens, BBB leakage allows the entry of the autoreactive cells into the CNS, and lesions occur scattered throughout the entire CNS. On the other hand, the stab wound injury is an acute model of damage, that triggers reactive gliosis and glial scar formation at a specific location, followed by tissue remodeling (Allahyari and Garcia, 2015). Moreover, leukocyte infiltration into the CNS is associated with the damage to the blood vessels, caused by the stab injury. It is possible that IP_3R2-independent mechanisms contribute to astrocyte reactivity, and further confinement of inflammatory infiltration, during EAE but not in the stab wound injury model.

The genetic ablation of IP_3R2 was also shown to be detrimental for neuronal survival in a model of amyotrophic lateral sclerosis (ALS) (Staats et al., 2016). Interestingly, in this study, the authors observed that IP_3R2-null mice present an increased propensity to inflammation, since these animals had an increase in the relative number of monocytes, in the spleen and blood, and in the IFNγ serum levels.

Previous studies using different EAE animal models have demonstrated that IFNγ plays a protective role in EAE, particularly during early phases of disease (Billiau et al., 1988; Heremans et al., 1996). So, the protective effects observed in IP_3R2-null mice could also be related with increased peripheral levels of IFNγ. In future studies, it would be relevant to specifically ablate IP_3R2 in astrocytes, for example by crossing GFAP-Cre or Aldh1l1-Cre with $IP_3R2^{fl/fl}$ mice, and evaluate Ca^{2+} signaling after EAE induction. This way, it would be possible to study the response of knock-out astrocytes during disease development, while avoiding the confounding effects of both peripheral IP_3R2 ablation and increased IFNγ levels.

DMF is a good therapeutic drug to improve cognitive deficits and it impacts astrocytic activation

On the last part of this work, we studied the effects of DMF on the cognitive performance of EAE animals, since its immunomodulatory and neuroprotective actions supported a possible beneficial role on the cognitive function. In fact, our work has shown that DMF treatment, starting at the symptomatic phase of disease, is able to rescue the cognitive deficits observed in vehicle-treated EAE animals. However, these conclusions can only be applied to animals that present a less severe disease, i.e. animals with clinical scores below 3, because mice with hind paw paralysis were not able to perform the Morris water maze (MWM) cognitive task. In fact, cognitive evaluation is difficult in the symptomatic phase of EAE, since EAE animals present severe motor deficits, and most cognitive tasks rely on motor function. To overcome this limitation, it is important to develop new tasks for cognitive evaluation, that rely less on motor function. Moreover, the induction of a less severe disease phenotype, for example by modulating the concentrations of MOG and PTX (Dias et al., 2015; Hooke Laboratories; Nam et al., 2014), would allow the cognitive evaluation of an increased number of animals. Finally, future studies using MS patients treated with DMF will be essential to confirm the effects of this drug on cognitive performance.

Associated with cognitive rescue, DMF-treated animals also presented a decrease in demyelination and astrocyte numbers in the fimbria. In the recent work of Wheeler and colleagues (2020), *Nfe2l2*, which encodes the Nrf2 transcription factor, was identified as a possible transcriptional regulator of gene expression in astrocytic subpopulations expanded in EAE animals. Namely, these subpopulations of astrocytes presented decreased expression of Nrf2 target genes. In addition, the *Nfe2l2* inactivation, by lentivirus, specifically in astrocytes worsened the clinical score of EAE animals, associated with an activation of pro-inflammatory pathways in astrocytes. Overall, these data suggested that Nrf2 signaling decreases the transcriptional responses in astrocytes that promote the pathogenesis of EAE (Wheeler et

al., 2020). Accordingly, in our work DMF could be inducing Nrf2 activation in astrocytes, contributing for decreased astrocytic reactivity. Astrocyte isolation from animals induced with EAE and treated with DMF would allow to confirm if this decrease in reactivity is associated with Nrf2 activation in astrocytes. Moreover, it would be interesting to induce EAE in a model of Nrf2-targeted ablation in astrocytes, and further treat these animals with DMF, to verify if the beneficial effects of DMF are loss.

LCN2 is a possible prognostic biomarker in MS

Currently there are no specific biomarkers for MS, and, even though MRI and OCBs are used in the clinics to aid in disease diagnosis, the alterations observed in MS patients are not specific of this disease. More specifically, MRI abnormalities, similar to the ones observed in MS, and the presence of CSF OCBs occur in several other diseases (Petzold, 2013; Rolak and Fleming, 2007). Several works have tried to identify new disease biomarkers, being LCN2 one of them. LCN2 levels were reported to be increased in MS patients' samples by different groups, including ours (Al Nimer et al., 2016; Berard et al., 2012; Marques et al., 2012). In this work, we intended to evaluate the prognostic value of LCN2 for MS disease progression. The Kaplan-Meyer survival curve analysis revealed that increased LCN2 CSF levels were associated with faster disease progression. However, the association found between LCN2 and disease progression was lost after controlling for the age of the patients. In fact, previous studies had already reported that older patients present a faster disease progression, at least until reaching a certain EDSS (Guillemin et al., 2017; Leray et al., 2010), and our results support these findings.

Nevertheless, the confidence intervals obtained in the Cox regression analysis do not rule out a possible contribution of LCN2 for disease progression. Of relevance, a previous study, using a sample size similar to ours, has found that high CSF levels of this protein were an independent predictive factor for CIS conversion to clinically definite MS (Khalil et al., 2016). Thus, we propose that this study should be repeated using a larger sample size and longer follow-up periods. Moreover, considering that increased LCN2 levels were also observed in other conditions (Choi et al., 2011; Llorens et al., 2020; Mike et al., 2019), future studies should also quantify other possible biomarkers, like the ones already referred in the introduction section, in parallel to LCN2, to try to establish a panel of biomarkers that are specific for MS diagnosis and prognosis.

Concluding remarks

With the work developed in this thesis we tackled the astrocytic response during EAE using different strategies. At first, we performed a wide transcriptomic approach to identify genes significantly altered throughout disease development, by looking at three disease time points. From this analysis we identified that astrocytes could be undergoing metabolic reprograming and are currently testing this hypothesis using primary astrocyte cultures. Following this, we used a model of global astrocytic Ca^{2+} signaling impairment, and studied the consequences for EAE progression of "silencing" astrocytes. Here, we observed that astrocytes with impaired Ca^{2+} signaling remain reactive and seem to control inflammatory infiltration in the cerebellum more efficiently than Wt astrocytes. Then, we studied the effects of a drug currently used in the clinics to treat MS, DMF, on cognitive performance and astrocytic reactivity, and observed positive effects on both measurements. Finally, we moved to human samples and focused our attention in one molecule already known to be produced by astrocytes in the context of MS and EAE, LCN2, and found that it could present prognostic value in MS.

To summarize, the main conclusions of this work are:

- During EAE, particularly at the onset phase of disease, astrocytes seem to undergo metabolic reprogramming, acquiring a neurotoxic (A1) phenotype associated with increased glycolytic rate and TCA cycle activity;
- Ablation of the IP_3-dependent Ca^{2+} signaling decreases the percentage of lesioned area in the cerebellum, even tough it is not sufficient to improve the animals' clinical score;
- DMF is able to improve the cognitive performance of EAE animals and this is associated with decreased demyelination and astrocytic reactivity;
- LCN2 is a possible prognostic marker for MS progression.

References

Agulhon C, Petravicz J, McMullen AB, Sweger EJ, Minton SK, Taves SR, et al. What is the role of astrocyte calcium in neurophysiology? Neuron. 2008;59:932-946.

Al Nimer F, Elliott C, Bergman J, Khademi M, Dring AM, Aeinehband S, et al. Lipocalin-2 is increased in progressive multiple sclerosis and inhibits remyelination. Neurology: Neuroimmunology and NeuroInflammation. 2016;3:e191.

Allahyari RV, Garcia AD. Triggering reactive gliosis in vivo by a forebrain stab injury. J Vis Exp. 2015:e52825.

Bambouskova M, Gorvel L, Lampropoulou V, Sergushichev A, Loginicheva E, Johnson K, et al. Electrophilic properties of itaconate and derivatives regulate the IkappaBzeta-ATF3 inflammatory axis. Nature. 2018;556:501-504.

Bazargani N, Attwell D. Astrocyte calcium signaling: the third wave. Nature Neuroscience. 2016;19:182-189.

Berard JL, Zarruk JG, Arbour N, Prat A, Yong VW, Jacques FH, et al. Lipocalin 2 is a novel immune mediator of experimental autoimmune encephalomyelitis pathogenesis and is modulated in multiple sclerosis. Glia. 2012;60:1145-1159.

Billiau A, Heremans H, Vandekerckhove F, Dijkmans R, Sobis H, Meulepas E, et al. Enhancement of experimental allergic encephalomyelitis in mice by antibodies against IFN-gamma. Journal of Immunology. 1988;140:1506-1510.

Bushong EA, Martone ME, Jones YZ, Ellisman MH. Protoplasmic astrocytes in CA1 stratum radiatum occupy separate anatomical domains. Journal of Neuroscience. 2002;22:183-192.

Chao CC, Gutierrez-Vazquez C, Rothhammer V, Mayo L, Wheeler MA, Tjon EC, et al. Metabolic control of astrocyte pathogenic activity via cPLA2-MAVS. Cell. 2019;179:1483-1498 e1422.

Choi J, Lee HW, Suk K. Increased plasma levels of lipocalin 2 in mild cognitive impairment. Journal of the Neurological Sciences. 2011;305:28-33.

Correale J, Farez MF. The role of astrocytes in multiple sclerosis progression. Frontiers in neurology. 2015;6:180.

Correale J, Gaitan MI, Ysrraelit MC, Fiol MP. Progressive multiple sclerosis: from pathogenic mechanisms to treatment. Brain. 2017;140:527-546.

Dias AT, De Castro SB, Alves CC, Mesquita FP, De Figueiredo NS, Evangelista MG, et al. Different MOG(35-55) concentrations induce distinguishable inflammation through early regulatory response by IL-

10 and TGF-beta in mice CNS despite unchanged clinical course. Cellular Immunology. 2015;293:87-94.

Ding S, Fellin T, Zhu Y, Lee SY, Auberson YP, Meaney DF, et al. Enhanced astrocytic Ca2+ signals contribute to neuronal excitotoxicity after status epilepticus. Journal of Neuroscience. 2007;27:10674-10684.

Dominguez-Andres J, Novakovic B, Li Y, Scicluna BP, Gresnigt MS, Arts RJW, et al. The itaconate pathway is a central regulatory node linking innate immune tolerance and trained immunity. Cell Metabolism. 2019;29:211-220 e215.

Faissner S, Plemel JR, Gold R, Yong VW. Progressive multiple sclerosis: from pathophysiology to therapeutic strategies. Nature Reviews: Drug Discovery. 2019;18:905-922.

Gresle MM, Schulz K, Jonas A, Perreau VM, Cipriani T, Baxter AG, et al. Ceruloplasmin gene-deficient mice with experimental autoimmune encephalomyelitis show attenuated early disease evolution. Journal of Neuroscience Research. 2014;92:732-742.

Guillemin F, Baumann C, Epstein J, Kerschen P, Garot T, Mathey G, et al. Older age at multiple sclerosis onset is an independent factor of poor prognosis: a population-based cohort study. Neuroepidemiology. 2017;48:179-187.

Hamby ME, Coppola G, Ao Y, Geschwind DH, Khakh BS, Sofroniew MV. Inflammatory mediators alter the astrocyte transcriptome and calcium signaling elicited by multiple G-protein-coupled receptors. Journal of Neuroscience. 2012;32:14489-14510.

Han MH, Hwang SI, Roy DB, Lundgren DH, Price JV, Ousman SS, et al. Proteomic analysis of active multiple sclerosis lesions reveals therapeutic targets. Nature. 2008;451:1076-1081.

Heremans H, Dillen C, Groenen M, Martens E, Billiau A. Chronic relapsing experimental autoimmune encephalomyelitis (CREAE) in mice: enhancement by monoclonal antibodies against interferon-gamma. European Journal of Immunology. 1996;26:2393-2398.

Herrmann JE, Imura T, Song B, Qi J, Ao Y, Nguyen TK, et al. STAT3 is a critical regulator of astrogliosis and scar formation after spinal cord injury. Journal of Neuroscience. 2008;28:7231-7243.

Hertle DN, Yeckel MF. Distribution of inositol-1,4,5-trisphosphate receptor isotypes and ryanodine receptor isotypes during maturation of the rat hippocampus. Neuroscience. 2007;150:625-638.

Hooke Laboratories. EAE Induction by Active Immunization in C57BL/6 Mice. 04/04/2020. https://hookelabs.com/protocols/eaeAI_C57BL6.html.

Ibrahim SM, Mix E, Bottcher T, Koczan D, Gold R, Rolfs A, et al. Gene expression profiling of the nervous system in murine experimental autoimmune encephalomyelitis. Brain. 2001;124:1927-1938.

Itoh N, Itoh Y, Tassoni A, Ren E, Kaito M, Ohno A, et al. Cell-specific and region-specific transcriptomics in the multiple sclerosis model: Focus on astrocytes. Proceedings of the National Academy of Sciences of the United States of America. 2018;115:E302-E309.

Jiang R, Diaz-Castro B, Looger LL, Khakh BS. Dysfunctional calcium and glutamate signaling in striatal astrocytes from Huntington's disease model mice. Journal of Neuroscience. 2016;36:3453-3470.

Kanemaru K, Kubota J, Sekiya H, Hirose K, Okubo Y, Iino M. Calcium-dependent N-cadherin up-regulation mediates reactive astrogliosis and neuroprotection after brain injury. Proceedings of the National Academy of Sciences of the United States of America. 2013;110:11612-11617.

Khalil M, Renner A, Langkammer C, Enzinger C, Ropele S, Stojakovic T, et al. Cerebrospinal fluid lipocalin 2 in patients with clinically isolated syndromes and early multiple sclerosis. Multiple Sclerosis. 2016;22:1560-1568.

Kroksveen AC, Guldbrandsen A, Vaudel M, Lereim RR, Barsnes H, Myhr KM, et al. In-depth cerebrospinal fluid quantitative proteome and deglycoproteome analysis: presenting a comprehensive picture of pathways and processes affected by multiple sclerosis. Journal of Proteome Research. 2017;16:179-194.

Kuchibhotla KV, Lattarulo CR, Hyman BT, Bacskai BJ. Synchronous hyperactivity and intercellular calcium waves in astrocytes in Alzheimer mice. Science. 2009;323:1211-1215.

Kuo PC, Weng WT, Scofield BA, Paraiso HC, Brown DA, Wang PY, et al. Dimethyl itaconate, an itaconate derivative, exhibits immunomodulatory effects on neuroinflammation in experimental autoimmune encephalomyelitis. Journal of Neuroinflammation. 2020;17:138.

Lampropoulou V, Sergushichev A, Bambouskova M, Nair S, Vincent EE, Loginicheva E, et al. Itaconate links inhibition of succinate dehydrogenase with macrophage metabolic remodeling and regulation of inflammation. Cell Metabolism. 2016;24:158-166.

Lau LW, Cua R, Keough MB, Haylock-Jacobs S, Yong VW. Pathophysiology of the brain extracellular matrix: a new target for remyelination. Nature Reviews Neuroscience. 2013;14:722-729.

Leray E, Yaouanq J, Le Page E, Coustans M, Laplaud D, Oger J, et al. Evidence for a two-stage disability progression in multiple sclerosis. Brain. 2010;133:1900-1913.

Llorens F, Hermann P, Villar-Pique A, Diaz-Lucena D, Nagga K, Hansson O, et al. Cerebrospinal fluid lipocalin 2 as a novel biomarker for the differential diagnosis of vascular dementia. Nature Communications. 2020;11:619.

Marques F, Mesquita SD, Sousa JC, Coppola G, Gao F, Geschwind DH, et al. Lipocalin 2 is present in the EAE brain and is modulated by natalizumab. Frontiers in Cellular Neuroscience. 2012;6:33.

Mayo L, Trauger SA, Blain M, Nadeau M, Patel B, Alvarez JI, et al. Regulation of astrocyte activation by glycolipids drives chronic CNS inflammation. Nature Medicine. 2014;20:1147-1156.

Mike EV, Makinde HM, Gulinello M, Vanarsa K, Herlitz L, Gadhvi G, et al. Lipocalin-2 is a pathogenic determinant and biomarker of neuropsychiatric lupus. Journal of Autoimmunity. 2019;96:59-73.

Motori E, Puyal J, Toni N, Ghanem A, Angeloni C, Malaguti M, et al. Inflammation-induced alteration of astrocyte mitochondrial dynamics requires autophagy for mitochondrial network maintenance. Cell Metabolism. 2013;18:844-859.

Mueller AM, Pedre X, Stempfl T, Kleiter I, Couillard-Despres S, Aigner L, et al. Novel role for SLPI in MOG-induced EAE revealed by spinal cord expression analysis. Journal of Neuroinflammation. 2008;5:20.

Munji RN, Soung AL, Weiner GA, Sohet F, Semple BD, Trivedi A, et al. Profiling the mouse brain endothelial transcriptome in health and disease models reveals a core blood-brain barrier dysfunction module. Nature Neuroscience. 2019;22:1892-1902.

Nam Y, Kim JH, Seo M, Kim JH, Jin M, Jeon S, et al. Lipocalin-2 protein deficiency ameliorates experimental autoimmune encephalomyelitis: the pathogenic role of lipocalin-2 in the central nervous system and peripheral lymphoid tissues. Journal of Biological Chemistry. 2014;289:16773-16789.

Nichterwitz S, Benitez JA, Hoogstraaten R, Deng Q, Hedlund E. LCM-Seq: a method for spatial transcriptomic profiling using laser capture microdissection coupled with PolyA-based RNA sequencing. Methods in Molecular Biology. 2018;1649:95-110.

Nylander A, Hafler DA. Multiple sclerosis. Journal of Clinical Investigation. 2012;122:1180-1188.

Petravicz J, Fiacco TA, McCarthy KD. Loss of IP3 receptor-dependent Ca2+ increases in hippocampal astrocytes does not affect baseline CA1 pyramidal neuron synaptic activity. Journal of Neuroscience. 2008;28:4967-4973.

Petzold A. Intrathecal oligoclonal IgG synthesis in multiple sclerosis. Journal of Neuroimmunology. 2013;262:1-10.

Reichenbach N, Delekate A, Breithausen B, Keppler K, Poll S, Schulte T, et al. P2Y1 receptor blockade normalizes network dysfunction and cognition in an Alzheimer's disease model. Journal of Experimental Medicine. 2018;215:1649-1663.

Robb JL, Hammad NA, Weightman Potter PG, Chilton JK, Beall C, Ellacott KLJ. The metabolic response to inflammation in astrocytes is regulated by nuclear factor-kappa B signaling. Glia. 2020.

Rolak LA, Fleming JO. The differential diagnosis of multiple sclerosis. Neurologist. 2007;13:57-72.

Satoh JI, Tabunoki H, Yamamura T. Molecular network of the comprehensive multiple sclerosis brain-lesion proteome. Multiple Sclerosis. 2009;15:531-541.

Scemes E, Giaume C. Astrocyte calcium waves: what they are and what they do. Glia. 2006;54:716-725.

Sevastou I, Pryce G, Baker D, Selwood DL. Characterisation of transcriptional changes in the spinal cord of the progressive experimental autoimmune encephalomyelitis Biozzi ABH mouse model by RNA sequencing. PloS One. 2016;11:e0157754.

Sharp AH, Nucifora FC, Jr., Blondel O, Sheppard CA, Zhang C, Snyder SH, et al. Differential cellular expression of isoforms of inositol 1,4,5-triphosphate receptors in neurons and glia in brain. Journal of Comparative Neurology. 1999;406:207-220.

Sofroniew MV, Vinters HV. Astrocytes: biology and pathology. Acta Neuropathologica. 2010;119:7-35.

Staats KA, Humblet-Baron S, Bento-Abreu A, Scheveneels W, Nikolaou A, Deckers K, et al. Genetic ablation of IP3 receptor 2 increases cytokines and decreases survival of SOD1G93A mice. Human Molecular Genetics. 2016;25:3491-3499.

Stoffels JM, de Jonge JC, Stancic M, Nomden A, van Strien ME, Ma D, et al. Fibronectin aggregation in multiple sclerosis lesions impairs remyelination. Brain. 2013;136:116-131.

Tassoni A, Farkhondeh V, Itoh Y, Itoh N, Sofroniew MV, Voskuhl RR. The astrocyte transcriptome in EAE optic neuritis shows complement activation and reveals a sex difference in astrocytic C3 expression. Scientific Reports. 2019;9:10010.

Vardjan N, Zorec R. Excitable astrocytes: Ca(2+)- and cAMP-regulated exocytosis. Neurochemical Research. 2015;40:2414-2424.

Vickovic S, Eraslan G, Salmen F, Klughammer J, Stenbeck L, Schapiro D, et al. High-definition spatial transcriptomics for in situ tissue profiling. Nature Methods. 2019;16:987-990.

Walz W, Lang MK. Immunocytochemical evidence for a distinct GFAP-negative subpopulation of astrocytes in the adult rat hippocampus. Neuroscience Letters. 1998;257:127-130.

Wheeler MA, Clark IC, Tjon EC, Li Z, Zandee SEJ, Couturier CP, et al. MAFG-driven astrocytes promote CNS inflammation. Nature. 2020;578:593-599.

Wheeler MA, Quintana FJ. Regulation of astrocyte functions in multiple sclerosis. Cold Spring Harbor Perspectives in Medicine. 2019;9.

Zhang Y, Chen K, Sloan SA, Bennett ML, Scholze AR, O'Keeffe S, et al. An RNA-sequencing transcriptome and splicing database of glia, neurons, and vascular cells of the cerebral cortex. Journal of Neuroscience. 2014;34:11929-11947.

Zhang Z, Ma Z, Zou W, Guo H, Liu M, Ma Y, et al. The appropriate marker for astrocytes: comparing the distribution and expression of three astrocytic markers in different mouse cerebral regions. Biomed Res Int. 2019;2019:9605265.

ANNEX 1

Sofia Pereira das Neves, João José Cerqueira, Fernanda Marques

Targeting astrocytes in the treatment of multiple sclerosis

(Review manuscript in preparation)

(2020)

Title

Targeting astrocytes in the treatment of multiple sclerosis.

Authors

Sofia Pereira das Neves [a,b], João José Cerqueira [a,b,c], Fernanda Marques [a,b]

Affiliations

[a] Life and Health Sciences Research Institute (ICVS), School of Medicine, University of Minho, Campus Gualtar, 4710-057 Braga, Portugal.

[b] ICVS/3B's – PT Government Associate Laboratory, Braga/Guimarães, Portugal.

[c] Clinical Academic Center - Braga, Braga, Portugal.

Corresponding author

Fernanda Marques (PhD), Life and Health Sciences Research Institute (ICVS), School of Medicine, University of Minho, Campus Gualtar, 4710-057 Braga, Portugal.

Phone number: +351 253 604 839

E-mail: fmarques@med.uminho.pt

Abstract

Astrocytes are fundamental cells for the maintenance of brain homeostasis. In physiological conditions they are involved in neuronal support and maintenance of blood-brain barrier integrity, among other important functions. During pathological conditions, like in multiple sclerosis (MS), astrocytes play both detrimental and protective roles. Considering that currently there is no cure for MS, and that the immunomodulatory drugs being used have poor efficacy in the progressive forms of disease, in which astrocytes are believed to play a relevant role, these cells are possible therapeutic targets. In this review, we explored the astrocytic response to several therapeutic agents that are not in use in the clinics, and then we reviewed the astrocytic response to currently approved MS drugs that are already in use in patients.

Introduction

In physiological conditions, astrocytes play several important roles, like the support of neural transmission and maintenance of blood-brain barrier (BBB) permeability (Abbott et al., 2006; Allen and Barres, 2009). However, during inflammatory processes astrocytes become reactive, they proliferate and upregulate the expression of glial fibrillary acid protein (GFAP), in a process called astrogliosis (Adams and Gallo, 2018; Anderson et al., 2014). Moreover, in diseases like multiple sclerosis (MS), they acquire several deleterious functions, like pro-inflammatory cytokine and chemokine production, which contribute to the recruitment of peripheral immune cells (Yi et al., 2019). Thus, targeting inflammatory pathways in astrocytes, without interfering with their protective roles, is highly relevant in the context of MS (Yan et al., 2012). In this manuscript we will review the impact of several therapeutic agents in the modulation of astrocytic function and activation, after treatment of MS animal models, like the experimental autoimmune encephalomyelitis (EAE) and cuprizone models, or astrocytic cell cultures. In addition, we will also explore the effects of currently approved MS drugs on astrocytes.

1. Role of therapeutic agents not used in the clinics in astrocytic function

1.1. Production of inflammatory mediators

Astrocytes, along with macrophages and microglia, are major producers of inflammatory mediators, like cytokines, chemokines and nitric oxide (NO). In pathological circumstances, NO and pro-inflammatory cytokine production, like interleukin (IL)-1β, IL-17, and interferon gamma (IFNγ), by these cells can induce the expression of inducible nitric oxide synthase (iNOS) in astrocytes, increasing even more NO concentration (Yi et al., 2019). *In vitro* studies suggest that glial-cells derived NO can lead to the death of oligodendrocytes (Merrill et al., 1993), which could be a potential therapeutic target in MS.

In astrocytes, NO signaling via cyclic guanosine monophosphate was shown to be involved in the upregulation of GFAP (Brahmachari et al., 2006) and in the rearrangement of actin and GFAP filaments, influencing astrocyte stellation and motility (Boran and Garcia, 2007). These results suggest a role for this pathway in the regulation of the reactive phenotype in astrocytes. Pifarre and co-workers (2011) used Sildenafil, a phosphodiesterase type 5 inhibitor, to decrease the activation of this pathway. Sub-cutaneous treatment with Sildenafil, starting 18 days post-immunization, was able to improve the clinical score of EAE animals. Regarding astrocytic effects, no differences were observed in the overall GFAP staining intensity, but in the spinal cord of Sildenafil-treated animals there was a tendency for the formation of scar-like structures around confined infiltrates, what might suggest a role in controlling the spreading of infiltration (Pifarre et al., 2011).

Another drug that is able to inhibit iNOS and pro-inflammatory cytokine expression in activated astrocytes and microglia in culture is lovastatin, a 3-hidroxi-3-methyl-glutaril-CoA reductase (Pahan et al., 1997). The treatment of EAE rats with Lovastatin, since the first day of immunization, delayed the onset of symptoms and decreased disease severity. Besides, it was observed a decreased iNOS expression in GFAP positive astrocytes and ED1 positive macrophages/microglia (Stanislaus et al., 1999). Also, the treatment of EAE animals with 1,25-dihydroxyvitamin-D_3 (1,25-D3), by peripheral injection, at the symptomatic phase of disease, was able to decreased the expression of iNOS in both central nervous system (CNS)-infiltrating and resident cells, including microglia and astrocytes, and exerted beneficial effects on clinical symptoms (Garcion et al., 1997; Garcion et al., 2003). On the other hand, the administration of 1,25-D3 in the diet of the animals had no effect on *Inos* expression or severity of symptoms (Spach et al., 2004), which suggest that different forms of drug delivery have an important role and must be considered.

Moreover, the production of NO and IL-6 was significantly ablated by treatment with CD200Fc, an agonist of the CD200 receptor, in primary cultures of astrocytes activated with IFNγ plus tumor necrosis factor (TNF) α. In the EAE mouse model, both CD200 and CD200R are upregulated on astrocytes, while the treatment with CD200Fc reduced the activation state of these cells, besides significantly reducing EAE severity, when used at the post-symptomatic phase (Liu et al., 2010). In addition, the glia inhibitor MW01-5-188WH was previously shown to inhibit the overproduction of pro-inflammatory cytokines, namely IL-1β and TNFα, in glial cells (Ralay Ranaivo et al., 2006). Oral treatment with this compound improved the symptoms of myelin oligodendrocyte glycoprotein (MOG)-induced EAE mice and seemed to reduce oligodendrocyte death, at least partly, through the attenuation of microglia and astrocyte activation (Guo et al., 2007).

The *in vitro* treatment with Geldanamycin, that belongs to the family of antibiotic benzoquinones, was shown to reduce nitrite production in C6 glioma cells and primary astrocytic cultures, via inhibition of iNOS (Murphy et al., 2002). The related analogue 17-allylamino-17-demehtoxygeldanamycin (17-AAG) exhibited similar inhibition of iNOS activity in primary astrocyte cultures, with the advantage of presenting reduced toxicity (Dello Russo et al., 2006; Murphy et al., 2002). However, both *in vivo* preventive and therapeutic treatments with 17-AAG presented little or no effect on glial cell activation, even tough there was an amelioration of the animals' clinical score (Dello Russo et al., 2006).

1.2. Glutamate excitotoxicity

Glutamate excitotoxicity has been pointed out as a potential mechanism involved in the pathogenesis of MS (Kostic et al., 2013; Stojanovic et al., 2014), and astrocytes play an important role in the removal of

excessive glutamate from the extracellular space. However, it was shown that the astrocytic glutamate removal capacity is impaired in EAE (Hardin-Pouzet et al., 1997; Ohgoh et al., 2002). Ceftriaxone is a β-lactam antibiotic which was described to upregulate the expression of *GLT-1*, which is the astrocytic transporter for glutamate clearance from the synaptic cleft (Rothstein et al., 2005). To explore its role in the EAE model, Ramos and colleagues (2010) immunized rats with MOG and treated them intrathecally with Ceftriaxone, starting on the first day of clinical symptoms. Ceftriaxone treatment was able to improve the motor deficit scores of the animals and to revert the decrease in protein expression of membrane-bound dimerized GLT-1, in the animals' spinal cord. Astrocyte activation in the spinal cord was also prevented, as assessed by GFAP protein expression (Ramos et al., 2010).

1.3. Modulation of immune cells capacity to infiltrate the brain parenchyma

Charles F. Barlow (1956) first described that the BBB integrity was compromised in animals induced with experimental encephalomyelitis, by injecting animals with trypan blue in the periphery and observing staining in the brain parenchyma, in lesion areas (Barlow, 1956). However, he also described the presence of abnormal vessels, in regions without lesions, that were not permeable to the dye. This way, Barlow suggested that dye diffusion was more related with the characteristics of the brain parenchyma, probably the perivascular glia, than with the alterations of vascular endothelium (Barlow, 1956). It is known that astrocytic endfeet are closely associated with parenchymal vessels and it was shown that astrocytes participate in the maintenance of physical (modulation of tight junctions strength), transport and also metabolic barriers (expression and polarized location of transporters, like glucose transporter 1, and of specialized enzymes) (Abbott et al., 2006). Furthermore, proteolysis by matrix metalloproteinases (MMPs) contribute to the inflammatory damage caused to the BBB and myelin (Rosenberg, 2005), and astrocytes are a major source of extracellular matrix (ECM) degrading proteases, like MMPs (Ogier et al., 2006). Hence, by targeting astrocytes in MS, it may be possible to prevent or decrease the BBB permeability observed in MS and reduce immune infiltration, consequently improving the clinical symptoms.

When analyzing the BBB at the ultra-structural level, EAE animals were shown to present opened tight junctions and edema of astrocytes, among other alterations. A reversion of these alterations was observed in animals treated orally with spinal cord proteins hydrolysate, which was suggested to induce oral tolerance to myelin peptides (Kwiatkowska-Patzer et al., 2003). In an EAE mice model treated with RG-13577, a heparin-mimicking compound, the reduction in CNS inflammation and amelioration of

symptoms was suggested to be in part associated with a reduction in heparanase (ECM degrading enzyme) expression by astrocytes (Irony-Tur-Sinai et al., 2003).

Additionally, MMP inhibitors were used to treat a chronic relapsing EAE model, which presented improved clinical score and a reduction in demyelination and glial scarring. The differences in gliosis were observed by electron microscopy and by decreased GFAP levels in western blot analysis (Liedtke et al., 1998). Besides synthetic inhibitors, the proteolytic activity of MMPs can also be opposed by members of the tissue inhibitor of MMPs (TIMPs) family. In accordance, EAE animals treated with Darbepoetin alpha (synthetic analogue of recombinant human erythropoietin, which presents a longer *in vivo* half-life) presented increased expression of TIMP-1 in astrocytes and decreased mean clinical scores, at day 21 post-induction (Thorne et al., 2009).

In addition to the alterations in the ECM, other important aspect for immune cell infiltration is the production of chemoattractant molecules, such as chemokines. Chemokine (C-C motif) ligand (CCL) 2 is mainly expressed by reactive astrocytes and drives myeloid cell recruitment to sites of injury via its receptor chemokine (C-C motif) receptor (CCR) 2 (Giraud et al., 2010; Kim et al., 2014). *In vitro* studies demonstrated that huperzine A, which is a potent, selective and reversible inhibitor of acetylcholinesterase, could revert the lipopolysaccharide (LPS)-induced secretion of CCL2 in astrocytes, while having no effect on the production of other pro-inflammatory cytokines, like TNFα, IL-6 or IL-1β. In addition, transwell migration assays showed that supernatant from huperzine A-treated astrocytes could suppress peripheral blood mononuclear cell (PBMC) migration, compared to LPS-treated astrocyte supernatant. Moreover, CD200Fc treatment ablated CCL2 production, in primary cultures of astrocytes activated with IFNγ plus TNFα (Liu et al., 2010). As for *in vivo* studies, huperzine A treatment of EAE animals was able to revert CCL2 overexpression, decrease inflammation, demyelination and axonal injury, improving disease severity (Tian et al., 2013). The post-symptomatic treatment of EAE animals with 17β-estradiol was also shown to decrease the clinical score of mice and reduce both the CCL2 protein and mRNA levels, mainly by targeting the estrogen receptors in astrocytes (Giraud et al., 2010).

In vitro studies suggest that Fasudil, a Rho-kinase inhibitor, is able to decrease the ability of astrocytes to attract immune cells from the periphery. Astrocytes cultured in a transwell system with mononuclear cells from the spleen, and stimulated with LPS or IFNγ, promoted the migration of these cells (Guo et al., 2014). Fasudil treatment significantly decreased this migration, while decreasing the production of TNFα, IL-6, NO and also chemotactic factors, like CCL5, macrophage inflammatory protein 1 α and CCL2, in astrocytes (Guo et al., 2014). In accordance, EAE animals treated with Fasudil, starting at the pre-symptomatic phase, presented a decrease in the number of CCL20 double positive astrocytes. This might

have prevented the infiltration of inflammatory cells into the CNS and contributed to the amelioration observed in the clinical score of Fasudil-treated animals (Guo et al., 2014).

Besides the aforementioned studies, there were several others in which the main therapeutic target was not related with specific astrocytic functions altered in MS disease, but in which a beneficial effect was observed in terms of astrocytic reactivity, alongside with clinical score improvement. Table S1. 1 resumes the findings of these studies.

Table S1. 1 – Summary of effects observed in astrocytes of different animal models after treatment with therapeutic agents.

Therapeutic agent	Administration protocol	Model used	Outcome observed in astrocytes*	Reference
Recombinant human erythropoietin	Daily i.p. injections, starting on day 3 p.i.	Female Lewis rats, 6-8 weeks of age, immunized with guinea pig MBP, sacrificed at day 12 p.i.	Decreased GFAP immunostaining	(Agnello et al., 2002)
	Daily i.v. injections, starting 36-48 hours after the onset of neurological impairment (clinical score 1-2)	Female C57BL/6, 8-14 weeks of age, immunized with $MOG_{35-55,}$ sacrificed at day 30 p.i.	Decreased MHC II immunostaining in astrocytes	(Li et al., 2004)
Batroxobin	I.p. injection every other day, starting on the day of immunization or after the appearance of clinical manifestations	Female C57BL/6 mice, 12 weeks of age, immunized with $MOG_{35-55,}$ sacrificed at days 30, 40 and 60 p.i.	Deceased GFAP immunostaining intensity	(Yang et al., 2011)
Platelet-rich plasma	Intrathecal administration at score equal to 1 (days 10-14 p.i.)	Female C57BL/6J mice, with 10 weeks of age, immunized with MOG_{35-55}, sacrificed at day 28 p.i.	Decreased *Gfap* mRNA levels	(Borhani-Haghighi and Mohamadi, 2019)
Opioid growth factor	Daily i.p. injections, starting on the day of immunization	Female C57BL/6 mice, 7-10 weeks of age, immunized with MOG_{35-55}, sacrificed at day 20 p.i.	Decreased number of reactive astrocytes per area unit	(Zagon et al., 2010)
	Daily i.p. injections, starting on the day of immunization	Female SJL/JOrlCRL mice, immunized with $PLP_{139-151}$, sacrificed at days 14 and 55 p.i.	Decreased number of GFAP positive astrocytes per field	(Hammer et al., 2013)
	Daily i.p. injections, starting on the second consecutive day of clinical disease score	Female SJL/JOrlCRL mice, 6-8 weeks of age, immunized with $PLP_{139-151}$, sacrificed at days 5, 14 and 40 of treatment	Decreased number of GFAP single positive and GFAP/Ki67 double positive astrocytes per field	(Hammer et al., 2015)
Opioid growth factor or low dose naltrexone	Daily i.p. injections, starting on the day of immunization	Female C57BL/6 mice, 7-10 weeks of age, immunized with MOG_{35-55}, sacrificed at days 10 and 30 p.i.	Decreased number of reactive astrocytes per field	(Rahn et al., 2011)
Progesterone and 17β-estradiol	One subcutaneous pellet for each hormone, 1 week before EAE induction	Female C57BL/6 mice, 9-11 weeks of age, immunized with MOG_{40-54}, sacrificed at day 16 p.i.	Decreased number of GFAP positive astrocytes per area unit	(Garay et al., 2010)
Indazole chloride	Subcutaneous daily injection, starting on the day of immunization	Male and female PLP_EGFP C57BL/6 mice, 8 weeks of age, immunized with MOG_{35-55}, sacrificed at day 40 p.i.	Reduced GFAP immunostaining intensity	(Moore et al., 2014)
L-DOPS	Subcutaneous injection three times per week, starting on day 30 p.i.	Female C57BL/6 mice, 6-8 weeks of age, immunized with MOG_{35-55}, sacrificed at day 19 after treatment initiation	Decreased GFAP immunostaining	(Simonini et al., 2010)
Idazoxan	Daily i.p. injections from days 0-10 p.i.	Female Wistar rats, 5-6 weeks of age, immunized with GPSCH, sacrifice at day 18 p.i.	Increased number of GFAP positive astrocytes	(Wang et al., 2009)

(Continues)

Table S1. 1 (Continued).

Therapeutic agent	Administration protocol	Model used	Outcome observed in astrocytes*	Reference
Ribavirin	Daily i.p. injections, starting on the day of immunization	Female Dark Agouti rats, 8 weeks of age, immunized with emulsified rat spinal cord homogenate, sacrificed at day 15 p.i.	Decreased GFAP immunostaining intensity (5-point grading scale) and mRNA expression levels	(Lavrnja et al., 2012)
P110	Daily i.p. injection, starting on the day of immunization	Female C57BL/6J mice, 10 weeks of age, immunized with $MOG_{35-55,}$ sacrificed at day 29 p.i.	Decreased number of GFAP positive astrocytes per area unit	(Luo et al., 2017)
2-PMPA	I.p. injection, twice a week, since the day of immunization	Female C57BL/6 mice, 6-7 weeks of age, immunized with MOG_{35-55}, sacrificed at day 25 p.i.	Reduced GFAP protein levels	(Ha et al., 2016)
GluA2-G-Gpep	Daily i.p. injection starting on day 10 p.i.	Female C57BL/6 mice, 8-12 weeks of age, immunized with $MOG_{35-55,}$ sacrificed at day 28 p.i.	Decreased number of GFAP positive cells, GFAP immunostaining intensity and positive area, and GFAP protein levels	(Lee et al., 2018)
Epimedium flavonoids	Intragastrical daily treatment using two different concentrations, starting on the day of immunization	Female Lewis rats, 7-8 weeks of age, immunized with partially purified MBP, sacrificed at day 14 p.i.	Reduced GFAP immunoreactivity	(Yin et al., 2012)
Astragaloside IV	Daily i.p. injection, starting one day before immunization, for 2 weeks	Female C57BL/6 mice, 6 weeks of age, immunized with MOG_{35-55}, sacrificed at day 20 p.i.	Reduced GFAP immunoreactivity, *Gfap* mRNA expression and GFAP protein expression	(He et al., 2013)
Hyungbangpaedok-san	Daily oral administration starting on days 6-8 p.i.	Female C57BL/6 mice, 8-9 weeks of age, immunized with MOG_{35-55}, sacrificed at days 20-22 p.i.	Reduced GFAP immunoreactivity, *Gfap* mRNA expression and GFAP protein expression	(Choi et al., 2015)
Piperlongumine	I.p. injection every other day, starting on day 2 p.i.	Female C57BL/6 mice, 10 weeks of age, immunized with MOG_{35-55}, sacrificed at day 28 p.i.	Reduced GFAP immunoreactivity and protein levels	(Gu et al., 2017)
Matrine	Daily i.p. injection, starting on day 13 p.i.	Female C57BL/6 mice, 8-10 weeks of age, immunized with MOG_{35-55}, sacrificed at day 23 p.i.	Increased number of GFAP/NT3 double positive cells	(Zhang et al., 2017)
Inosine	I.p. injection twice a day, starting on the day of immunization	Female C57BL/6 mice, 6-12 weeks of age, immunized with MOG_{35-55}, sacrificed at day 40 p.i.	Reduced GFAP immunostaining intensity	(Junqueira et al., 2017)
Reg-2 or C16+Ang-1 or Reg-2+C16+Ang-1	Reg-2: intrathecal administration via osmotic pumps; C16 and angiopoietin-1: daily i.v. injection; for 2 weeks, starting on the day of immunization	Male Lewis rats, weighing 250-300 g, immunized with GPSCH, sacrificed at 8 weeks p.i.	Decreased GFAP positive area	(Tian et al., 2017)

(Continues)

Table S1. 1 (Continued).

Therapeutic agent	Administration protocol	Model used	Outcome observed in astrocytes*	Reference
Methotrexate	Daily i.v. administration in the 3rd ventricle, starting on the first day of cuprizone-feeding	C57BL/6 mice, 8 weeks of age, fed with 0.2% cuprizone mixed into ground standard chow, sacrificed after 28 days of cuprizone-feeding	Decreased number of astrocytes accumulated in the corpus callosum	(Mueller et al., 2013)
Orexin A	I.p. administration, for five consecutive days, starting at score equal to 1.5	Female C57BL/6Rj mice, 9-12 weeks of age, immunized with MOG_{35-55}, sacrificed at day 21 p.i.	Decreased GFAP positive area	(Becquet et al., 2019)
Gallic acid	I.p. injection for 10 days, starting one day before immunization	Female C57BL/6 mice, 6-8 weeks of age, immunized with MOG_{35-55}, sacrificed at day 18 p.i.	Reduction in mRNA expression of *Ccl2* in astrocytes	(Abdullah et al., 2019)
MR16-1	I.p. injection on days 0 or 3 p.i.	Female C57BL/6J mice, 7 weeks of age, immunized with $MOG_{35-55,}$ sacrifice at day 20 p.i.	Decreased GFAP immunostaining	(Serizawa et al., 2018)
ACDT	Daily i.p. injection, starting at the day of immunization	Female C57BL/6 mice, 7-9 weeks of age, immunized with $MOG_{35-55,}$ sacrificed at day 30 p.i.	Decreased expression of A1 astrocyte specific genes (*Ggta1*, *H2-D1* and *Serping1*)	(Kuo et al., 2018)
Quetiapine	Daily oral administration, starting on day 16 p.i.	Female C57BL/6 mice, 8 weeks of age, immunized with MOG_{35-55}, sacrificed at day 30 p.i.	Decreased GFAP immunostaining intensity	(Mei et al., 2012)
Sevoflurane	Exposure to inhaled anaesthetic for 2 hours on day 17 p.i.	Female C57BL/6 mice, 6-8 weeks of age, immunized with MOG_{35-55}, sacrificed 4 weeks after treatment initiation	Decreased percentage of GFAP positive area	(Polak et al., 2012)
AAV8 vector carrying the coding sequence of soluble IL-23	Vector injected i.v. at day 18 before immunization	Female C57BL/6J mice, with 8-10 weeks of age, immunized with MOG_{40-55}, sacrifice at day 14 p.i..	Decreased GFAP immunostaining intensity	(Miralles et al., 2017)
Transcranial magnetic stimulation	EL-EMF applied for 2 h in the morning, every day, five days a week, starting on day 14 p.i.	Male Dark Agouti rats, 8 weeks of age, immunized with MOG_{35-55}, sacrificed at day 35 p.i.	Decreased number of GFAP positive astrocytes	(Medina-Fernandez et al., 2017)

* In comparison with non-treated- or vehicle-treated EAE group.

2-PMPA - 2-(phosphonomethyl)-pentapedioic acid; AAV – Adeno-associated virus; ACDT – 5-Amino-3-thioxo-*3H*-(1,2)dithiole-4-carboxylic acid ethyl ester; Ang-1 – Angiopoietin-1; EGFP – Enhanced green fluorescent protein; EL-EMF – Extremely low-frequency electromagnetic field stimulation; GFAP – glial fibrillary acid protein; GPSCH – guinea pig spinal cord homogenate; i.p. – Intraperitoneal; i.v. – Intravenous; L-DOPS - L-threo-3,4-dihydroxyphenylserine; MBP – Myelin basic protein; MHC – Major histocompatibility complex; MOG – Myelin oligodendrocyte glycoprotein; NT3 – Neurotrophin 3; p.i. – Post-immunization; PLP – Myelin proteolipid protein; Reg-2 – Regeneration gene protein 2.

2. Impact of cell-based therapies in astrocytes

The transplantation of stem cells has been used to try to enhance neuroprotective mechanisms and induce neuroregeneration (Cuascut and Hutton, 2019). The peripheral injection of EAE-induced animals (chronic and relapsing-remitting models) with bone marrow derived human mesenchymal stem cells (BM-hMSCs), after the establishment of clinical symptoms of disease, was able to induce clinical recovery. Even though this recovery was related with a decrease in the number of infiltrating cells and in the extent of demyelination, and with the protection or recruitment of oligodendrocytes, it was also possible to observe a decrease in astrogliosis, in the spinal cord of the animals (Bai et al., 2009). Mesenchymal stem cells (MSCs) derived from human periodontal ligament also improved the clinical score of EAE animals, and significantly decreased the degree of GFAP positive staining (Trubiani et al., 2016).

BM-hMSCs therapy was also tested in combination with the antibiotic minocycline, but in this case the treatment started 2 days before the appearance of clinical signs of disease (Hou et al., 2013). The combinatorial treatment significantly ameliorated the clinical severity and improved functional recovery of EAE mice, in comparison with both isolated treatments. In this study, the isolated treatments were able to decrease the number of infiltrating cells, the lesion area, the GFAP positive area and Iba1 positive cell number in the spinal cord, while increasing the myelin basic protein (MBP) positive area and the number of NeuN positive cells. Furthermore, the combinatorial treatment presented an even higher effect on all these parameters, presenting a higher therapeutic effect (Hou et al., 2013).

Interestingly, several studies identified the presence of transplanted cells in the brain parenchyma, mostly associated with lesions or inflammatory infiltrates (Bai et al., 2009; Gerdoni et al., 2007), which indicates that they are able to cross the BBB at regions of increased permeability.

Besides MSCs transplantation, cultured astrocytes transplantation was also used as therapeutic approach, however no differences were observed between astrocyte-transplanted and vehicle-transplanted groups, probably because of their inability to migrate from the ventricular space, where they were injected, into lesion sites at the brain parenchyma (Einstein et al., 2006; Einstein et al., 2003).

3. Therapeutic agents that specifically target astrocytes

Some therapeutic agents already tested in MS animal models are highly specific for astrocytes, since their targets are mainly expressed in these cells. Sulfonylurea receptor 1 (SUR1)-transient receptor potential melastatin 4 channels were showed to be upregulated in EAE mice, and these channels are expressed predominantly by reactive astrocytes, in regions that present a significant inflammatory burden (Makar et al., 2015). Moreover, post-mortem analysis of human MS samples revealed SUR1 expression

predominantly in astrocytes, evaluated by co-labelling with GFAP and S100 calcium-binding protein β (S100β) (Gerzanich et al., 2017). Taking this into account, Glibenclamide, which is a pharmacological inhibitor of SUR1, could be used to specifically target reactive astrocytes, reducing their expression of pro-inflammatory cytokines, chemokines and neurotoxic factors. In fact, Glibenclamide symptomatic treatment was shown to improve the clinical score of EAE animals, while decreasing reactive astrocytosis and astrocytic expression of TNF, B-cell activating factor, CCL2 and iNOS (Gerzanich et al., 2017).

During adulthood, astrocytes are the main CNS cells producing cholesterols, which is then transported via ApoE to neurons and oligodendrocytes, for membrane and synapse or myelin synthesis, respectively (Saher and Stumpf, 2015). Transcriptomic analysis of astrocytes isolated from different CNS regions, including spinal cord and cerebellum, after EAE induction, revealed a downregulation of cholesterol synthesis pathways (Itoh et al., 2018), suggesting astrocytic cholesterol homeostasis as a possible therapeutic target. More so, considering that reduced cholesterol synthesis in astrocytes during EAE could lead to reduced cholesterol transport to oligodendrocytes, and consequently, decreased myelin synthesis. To test this hypothesis, EAE animals were treated with CS-6253, an agonist for ATP-binding cassette transporter A1 that increases the efflux of cholesterol. CS-6253 was administered daily to EAE animals, starting 4 days before immunization, until day 40 post-immunization, inducing a significant amelioration of the animals' clinical score. Gene expression and immunohistochemistry analysis of spinal cord astrocytes revealed a significant restoration to control levels in enzymes involved in the cholesterol synthesis pathway in CS-6253-treated animals (Itoh et al., 2018).

Additionally, genetic approaches have been used to specifically target astrocytes, and these have been focused primarily on reducing the inflammatory status of astrocytes. Namely, the downregulation of *actin related gene 1* (*Act1*), which is involved in IL-17 signaling, in astrocytes was able to improve the clinical symptoms of EAE animals (Yan et al., 2012). Furthermore, knocking-down *Act1* expression in cultured astrocytes reduced the transmigration of MOG-stimulated splenocytes of 2D2 mice (Yan et al., 2012).

4. Role of currently approved MS drugs on astrocytes

In the clinics, for the management of clinical relapses, MS patients are usually treated with corticosteroids, such as methylprednisolone, in an attempt to fasten recovery (Noseworthy et al., 2000). Lee and co-workers (2014) used a liposomal encapsulated formula of methylprednisolone to treat EAE mice, after the appearance of clinical symptoms. A low dose of methylprednisolone was encapsulated in liposomes, and their efficacy was compared with the efficacy of low and high doses of free drug. They observed an amelioration of the clinical score in the groups treated with low dose liposomal methylprednisolone and

high dose free methylprednisolone, in comparison with low dose free methylprednisolone and vehicle-treated animals. In addition, liposomal encapsulated methylprednisolone significantly reduced the number of GFAP positive astrocytes, in spinal cord lesions, similarly to the high dose free methylprednisolone (Lee et al., 2014). Regarding the effects of methylprednisolone in human astrocytes the knowledge is still very scarce.

Another drug that is used as an anti-symptomatic treatment for MS is 4-aminopyridine (4-AP), which is a potent inhibitor of voltage gated K^+ channels. However, its efficacy in improving the clinical symptoms of EAE animals was dependent on the model used (Moriguchi et al., 2018). Pre-symptomatic treatment, since the day of immunization, was able to improve disease severity in the RR EAE model (SJL/J females immunized with $PLP_{139-151}$) but not in the chronic EAE model (C57BL/6 females immunized with MOG_{35-55}). Moreover, in the SJL/J EAE mice, 4-AP was able to downregulate GFAP expression (Moriguchi et al., 2018).

Regarding disease modifying drugs, interferons (IFNs), GA, laquinimod and DMF are among the first line treatments used in MS patients. The mechanism of action of IFNs in MS is not fully understood, but they present several immune-mediating activities, and several clinical trials demonstrated that IFNβ1b treatment reduces the frequency of relapses (Noseworthy et al., 2000). Even tough with different biological activities, IFNβ demonstrated a good efficacy in long-term RRMS therapy, and also, to some extent, in SPMS therapy (Lubina-Dabrowska et al., 2017). Regarding animal model results, the pre-symptomatic treatment of EAE Lewis female rats with both IFNβ1a and IFNβ1b presented beneficial effects on the animals' clinical score, and a reduction in GFAP protein levels in the animals' cortex, when compared to non-treated animals (Lubina-Dabrowska et al., 2017). To improve the therapeutic effects of IFNs, Mastronardi and colleagues (2004) combined IFNβ therapy with vitamin B_{12} cyanocobalamin, since previous works had demonstrated beneficial effects of vitamin B_{12} treatment in reversing demyelination. The combinatorial treatment was able to reduce clinical disease and cell infiltration to near normal levels. Moreover, the amount of GFAP in whole brain homogenates was reduced to the levels of untreated mice, indicating a reduction in astrocytic activation (Mastronardi et al., 2004).

GA is a mixture of synthetic polypeptides resembling MBP, and composed of alanine, lysine, glutamic acid and tyrosine (Ure and Rodriguez, 2002). These types of polypeptides were initially used to simulate the ability of MBP to induce EAE, however they were not able to induce disease, and several of them were even shown to suppress EAE. Moreover, this suppressive capacity was independent of species, disease type or encephalitogen used for EAE induction (Ziemssen and Schrempf, 2007). In the Lewis rat EAE

model, subcutaneous injections of GA, starting on the day of immunization, besides decreasing the clinical symptoms of disease, reduced GFAP immunofluorescence labelling in the spinal cord, compared to placebo-treated rats (Marques et al., 2009). Furthermore, GA treatment was able to revert the alterations occurring in the astrocyte association with cortical blood vessels and neuronal synapses. Under physiological conditions, the astrocytes' cell bodies are located close to penetrating blood vessels. However, in EAE animals, astrocytes presented an activated morphology, with retracted un-branched processes, and extensive decrease in the perivascular end-feet coverage as well as number of processes pointing towards neurons. In GA-treated animals, after preventive or suppressive treatment, most of the astroglial cell bodies were lined along the blood vessels and their morphology resembled pre-inflammatory appearance with multiple astrocyte-blood vessels and astrocyte-neuronal contacts (Eilam et al., 2018). GA was also shown to modulate astrocytic reactivity *in vitro*. Namely, the IL-1β- and TNFα-induced production of CCL5 was inhibited by GA pre-treatment, in astrocytoma cell lines (Li and Bever, 2001; Li et al., 2001).

DMF treatment in astrocyte cultures, or microglia/astrocyte co-cultures, was shown to attenuate the LPS-induced increase of *Il-1b*, *Il-6* and *Tnfa* expression (Wierinckx et al., 2005; Wilms et al., 2010) and the IL-1β-induced increase of *Il-6*, *Cxcl10* and *Ccl2* (Galloway et al., 2017). However, no effect was observed regarding *Inos* expression (Wilms et al., 2010). Contrarily to these results, in the work by Lin and colleagues (2011), DMF treatment was able to suppress the LPS- and IFNγ-induced nitrite production, both in primary astrocyte cultures and rat C6 glioma cells (Lin et al., 2011). Both *in vitro* and *in vivo* studies have observed an increased expression of Nrf2 in astrocytes, after treatment with DMF or MMF (Brennan et al., 2015; Brennan et al., 2017; Linker et al., 2011).

A redox analogue of DMF, ethyl pyruvate (EP), was also tested in an EAE rat model. The intraperitoneal treatment with EP, starting on the day before appearance of clinical symptoms, significantly reduced the animals clinical score and seemed to reduce astrocyte activation at day 12 post-immunization (Djedovic et al., 2017). When tested *in vitro*, both DMF and EP suppressed IL-6 release and NF-κB activation in IFNγ- and IL-17-stimulated astrocytes (Miljkovic et al., 2015). Taking all this into account, both DMF and EP could target astrocytes and play a direct antioxidative protection in the context of EAE and MS.

Regarding second line treatments, natalizumab and fingolimod are widely used. Natalizumab is a humanized mouse monoclonal antibody against the integrin VLA-4 on leukocytes, which prevents leukocyte entry into the CNS. Previous work from our lab has shown that natalizumab treatment, after the appearance of clinical symptoms of disease, was able to improve the clinical manifestations of disease of a RR model of EAE (Marques et al., 2012). Moreover, treated animals presented a decrease in the CSF

LCN2 levels and in the number of LCN2 GFAP double positive cells in the cerebellum (Marques et al., 2012). Hence, it seems that natalizumab treatment is able to reduce astrocyte activation, since LCN2 in the brain is described to occur mainly in astrocytes and in response to an injury or inflammatory stimulus (Ferreira et al., 2015). Still, it is possible that this improvement in astrocytic reactivity might just be related with natalizumab's ability to prevent immune cell infiltration into the brain (Marques et al., 2012).

The main immunomodulatory mechanism of action of fingolimod is related with its effects on lymphocyte homing. Fingolimod decreases immune cell trafficking out of secondary lymphoid organs, such as lymph nodes, by acting on sphingosine-1-phosphate (S1P) receptors. Therefore, fingolimod prevents immune cell migration into the CNS (Colombo et al., 2014; Huwiler and Zangemeister-Wittke, 2018). Importantly, reactive astrocytes represent a direct target of fingolimod, since they overexpress sphingosine-1-phosphate (S1P) receptors and this drug is able to cross the BBB (Colombo et al., 2014; Van Doorn et al., 2010). Hence, several *in vitro* and *in vivo* studies have explored the effects of fingolimod on astrocytes. In what concerns the *in vitro* studies, fingolimod was shown to modulate the expression of genes associated with migratory pathways, antigen presentation, inflammasome activation, axonal guidance and fatty acid α-oxidation, when added to a primary astrocytic human culture (Rothhammer et al., 2017). Van Doorn and co-workers (2010) observed a decrease in TNFα-induced CCL2 release, in primary cultures of human astrocytes, in a concentration-dependent fashion, after fingolimod pre-treatment (Van Doorn et al., 2010). Furthermore, it was shown that the astrocyte-conditioned medium (ACM) of cells cultured in the presence of IL-1, IL-17 or S1P induced *in vitro* neuronal degeneration. However, when neurons were exposed to the same ACM in the presence of fingolimod, or to the ACM of astrocytes cultured in the presence of fingolimod, neurodegeneration was hampered or reduced (Colombo et al., 2014; Rothhammer et al., 2017). Further neuroprotective effects of fingolimod were shown by its ability to induce *leukemia inhibitory factor*, *IL-11* and *heparin-binding EGF-like growth factor (HBEGF)* expression in human astrocyte cell cultures, both in the presence and absence of the inflammatory cytokine TNF (Hoffmann et al., 2015).

As for the *in vivo* studies, C57BL/6 EAE animals treated with fingolimod, after the appearance of clinical signs of disease, presented clinical recovery at later time points (Colombo et al., 2014; Smith et al., 2018). Moreover, fingolimod-treated animals presented decreased astrocytic activation (Colombo et al., 2014; Smith et al., 2018) and reduced iNOS levels (Colombo et al., 2014). In another study, fingolimod was used to treat nonobese diabetic EAE mice, instead of using the chronic EAE model, since this resembles several aspects of secondary progressive MS (Rothhammer et al., 2017). In this case, treatment started at day 40 post-immunization, already at the chronic progressive phase of disease, and

after the initial acute neurological event, followed by recovery. After 80 days of treatment, fingolimod-treated animals presented a decrease in the average clinical score, compared to vehicle-treated animals (Rothhammer et al., 2017). In what concerns astrocytes, fingolimod treatment downregulated the expression of pro-inflammatory cytokines and chemokines, including *Il-6*, *Ccl2*, *Ccl20*, *Ifng*, *Il-23a*, *Cxcl10* and *Il-1b*, and of neurotoxic factors, like *Inos* (Rothhammer et al., 2017). In addition, the conditional deletion of the $S1P_1$ receptor subtype in GFAP-expressing astrocytes, but not in synapsin-expressing neurons, ameliorated the clinical severity of EAE (Choi et al., 2011). Despite $S1P_1$ signaling in astrocytes being a key mediator of fingolimod efficacy, conflicting results regarding $S1P_1$ signaling have been shown in the sense that both $S1P_1$ deletion in astrocytes and exposure to $S1P_1$ agonists, like fingolimod, ameliorate EAE (Choi et al., 2011). Other studies have targeted $S1P_1$ receptors using a different agonist, namely CYM-5442 (2-(4-(5-(3,4-diethoxyphenyl)-1,2,4-oxadiazol-3-yl)-2,3-dihydro-1H-inden-1-yl amino) ethanol). The treatment of MOG_{35-55}-induced EAE mice with this agonist, after the appearance of clinical symptoms, resulted in a significant attenuation of clinical signs and weight loss and astrogliosis inhibition, as evaluated by decreased GFAP immunostaining (Gonzalez-Cabrera et al., 2012).

In the cuprizone model, which is a T cell independent experimental model of toxic CNS demyelination, fingolimod treatment significantly suppressed the accumulation of reactive astrocytes, but only when treatment was initiated soon after the beginning of cuprizone diet (3 days later) (Kim et al., 2018), and not after demyelination was already established (Alme et al., 2015).

Concluding remarks

MS is a disease with a complex pathophysiology, which involves both immunological and neurodegenerative processes, and presently there is no cure for this disease. Most treatments currently used are immunomodulatory, presenting beneficial effects in speeding recovery from attacks, preventing relapses, and managing symptoms. However, they are not so effective in the treatment of symptoms more related with neurodegeneration and for progressive forms of the disease. To tackle this, new drugs or combinatorial approaches should continue to be tested, and astrocytes seem to be a good therapeutic target, due to their location, close to the BBB, and also to the different roles they perform in the CNS. Importantly, the molecular pathways regulating distinct aspects of reactive astrogliosis need to the better understood, in order to develop therapeutic strategies that prevent the detrimental effects of astrocytes, but still permit or even potentiate their beneficial effects. In addition, these therapies should be disease-specific since certain reactive astrocyte responses may be beneficial in one context and detrimental in another.

Funding

This work was supported by Foundation for Science and Technology (FCT) and COMPETE through the project EXPL/NEU-OSD/2196/2013 and by The Clinical Academic Center (2CA-Braga) through the project EXPL/001/2016. The work at ICVS/3B's has been developed under the scope of the project NORTE-01-0145-FEDER-000013, supported by the Northern Portugal Regional Operational Programme (NORTE 2020), under the Portugal 2020 Partnership Agreement, through the European Regional Development Fund (FEDER), and funded by FEDER funds through the Competitiveness Factors Operational Programme (COMPETE), and by National funds, through the Foundation for Science and Technology (FCT), under the scope of the project POCI-01-0145-FEDER-007038. F.M. is an assistant researcher and recipient of an FCT Investigator grant with the reference CEECIND/01084/2017. S.N. is a recipient of a PhD fellowship with the reference PD/BD/114120/2015, from MCTES national funds.

References

Abbott NJ, Ronnback L, Hansson E. Astrocyte-endothelial interactions at the blood-brain barrier. Nature Reviews Neuroscience. 2006;7:41-53.

Abdullah A, Maged M, Hairul-Islam MI, Osama IA, Maha H, Manal A, et al. Activation of aryl hydrocarbon receptor signaling by a novel agonist ameliorates autoimmune encephalomyelitis. PloS One. 2019;14:e0215981.

Adams KL, Gallo V. The diversity and disparity of the glial scar. Nature Neuroscience. 2018;21:9-15.

Agnello D, Bigini P, Villa P, Mennini T, Cerami A, Brines ML, et al. Erythropoietin exerts an anti-inflammatory effect on the CNS in a model of experimental autoimmune encephalomyelitis. Brain Research. 2002;952:128-134.

Allen NJ, Barres BA. Neuroscience: Glia - more than just brain glue. Nature. 2009;457:675-677.

Alme MN, Nystad AE, Bo L, Myhr KM, Vedeler CA, Wergeland S, et al. Fingolimod does not enhance cerebellar remyelination in the cuprizone model. Journal of Neuroimmunology. 2015;285:180-186.

Anderson MA, Ao Y, Sofroniew MV. Heterogeneity of reactive astrocytes. Neuroscience Letters. 2014;565:23-29.

Bai L, Lennon DP, Eaton V, Maier K, Caplan AI, Miller SD, et al. Human bone marrow-derived mesenchymal stem cells induce Th2-polarized immune response and promote endogenous repair in animal models of multiple sclerosis. Glia. 2009;57:1192-1203.

Barlow CF. A study of abnormal blood-brain permeability in experimental allergic encephalomyelitis. Journal of Neuropathology and Experimental Neurology. 1956;15:196-207.

Becquet L, Abad C, Leclercq M, Miel C, Jean L, Riou G, et al. Systemic administration of orexin A ameliorates established experimental autoimmune encephalomyelitis by diminishing neuroinflammation. Journal of Neuroinflammation. 2019;16:64.

Boran MS, Garcia A. The cyclic GMP-protein kinase G pathway regulates cytoskeleton dynamics and motility in astrocytes. Journal of Neurochemistry. 2007;102:216-230.

Borhani-Haghighi M, Mohamadi Y. The therapeutic effect of platelet-rich plasma on the experimental autoimmune encephalomyelitis mice. Journal of Neuroimmunology. 2019;333:476958.

Brahmachari S, Fung YK, Pahan K. Induction of glial fibrillary acidic protein expression in astrocytes by nitric oxide. Journal of Neuroscience. 2006;26:4930-4939.

Brennan MS, Matos MF, Li B, Hronowski X, Gao B, Juhasz P, et al. Dimethyl fumarate and monoethyl fumarate exhibit differential effects on KEAP1, NRF2 activation, and glutathione depletion in vitro. PloS One. 2015;10:e0120254.

Brennan MS, Matos MF, Richter KE, Li B, Scannevin RH. The NRF2 transcriptional target, OSGIN1, contributes to monomethyl fumarate-mediated cytoprotection in human astrocytes. Scientific Reports. 2017;7:42054.

Choi JH, Lee MJ, Jang M, Kim EJ, Shim I, Kim HJ, et al. An oriental medicine, Hyungbangpaedok-San attenuates motor paralysis in an experimental model of multiple sclerosis by regulating the T cell response. PloS One. 2015;10:e0138592.

Choi JW, Gardell SE, Herr DR, Rivera R, Lee CW, Noguchi K, et al. FTY720 (fingolimod) efficacy in an animal model of multiple sclerosis requires astrocyte sphingosine 1-phosphate receptor 1 (S1P1) modulation. Proceedings of the National Academy of Sciences of the United States of America. 2011;108:751-756.

Colombo E, Di Dario M, Capitolo E, Chaabane L, Newcombe J, Martino G, et al. Fingolimod may support neuroprotection via blockade of astrocyte nitric oxide. Annals of Neurology. 2014;76:325-337.

Cuascut FX, Hutton GJ. Stem cell-based therapies for multiple sclerosis: current perspectives. Biomedicines. 2019;7.

Dello Russo C, Polak PE, Mercado PR, Spagnolo A, Sharp A, Murphy P, et al. The heat-shock protein 90 inhibitor 17-allylamino-17-demethoxygeldanamycin suppresses glial inflammatory responses and ameliorates experimental autoimmune encephalomyelitis. Journal of Neurochemistry. 2006;99:1351-1362.

Djedovic N, Stanisavljevic S, Jevtic B, Momcilovic M, Lavrnja I, Miljkovic D. Anti-encephalitogenic effects of ethyl pyruvate are reflected in the central nervous system and the gut. Biomedicine and Pharmacotherapy. 2017;96:78-85.

Eilam R, Segal M, Malach R, Sela M, Arnon R, Aharoni R. Astrocyte disruption of neurovascular communication is linked to cortical damage in an animal model of multiple sclerosis. Glia. 2018;66:1098-1117.

Einstein O, Grigoriadis N, Mizrachi-Kol R, Reinhartz E, Polyzoidou E, Lavon I, et al. Transplanted neural precursor cells reduce brain inflammation to attenuate chronic experimental autoimmune encephalomyelitis. Experimental Neurology. 2006;198:275-284.

Einstein O, Karussis D, Grigoriadis N, Mizrachi-Kol R, Reinhartz E, Abramsky O, et al. Intraventricular transplantation of neural precursor cell spheres attenuates acute experimental allergic encephalomyelitis. Molecular and Cellular Neurosciences. 2003;24:1074-1082.

Ferreira AC, Da Mesquita S, Sousa JC, Correia-Neves M, Sousa N, Palha JA, et al. From the periphery to the brain: lipocalin-2, a friend or foe? Progress in Neurobiology. 2015;131:120-136.

Galloway DA, Williams JB, Moore CS. Effects of fumarates on inflammatory human astrocyte responses and oligodendrocyte differentiation. Annals of Clinical and Translational Neurology. 2017;4:381-391.

Garay L, Gonzalez Deniselle MC, Gierman L, Lima A, Roig P, De Nicola AF. Pharmacotherapy with 17beta-estradiol and progesterone prevents development of mouse experimental autoimmune encephalomyelitis. Hormone Molecular Biology and Clinical Investigation. 2010;1:43-51.

Garcion E, Nataf S, Berod A, Darcy F, Brachet P. 1,25-Dihydroxyvitamin D3 inhibits the expression of inducible nitric oxide synthase in rat central nervous system during experimental allergic encephalomyelitis. Brain Research: Molecular Brain Research. 1997;45:255-267.

Garcion E, Sindji L, Nataf S, Brachet P, Darcy F, Montero-Menei CN. Treatment of experimental autoimmune encephalomyelitis in rat by 1,25-dihydroxyvitamin D3 leads to early effects within the central nervous system. Acta Neuropathologica. 2003;105:438-448.

Gerdoni E, Gallo B, Casazza S, Musio S, Bonanni I, Pedemonte E, et al. Mesenchymal stem cells effectively modulate pathogenic immune response in experimental autoimmune encephalomyelitis. Annals of Neurology. 2007;61:219-227.

Gerzanich V, Makar TK, Guda PR, Kwon MS, Stokum JA, Woo SK, et al. Salutary effects of glibenclamide during the chronic phase of murine experimental autoimmune encephalomyelitis. Journal of Neuroinflammation. 2017;14:177.

Giraud SN, Caron CM, Pham-Dinh D, Kitabgi P, Nicot AB. Estradiol inhibits ongoing autoimmune neuroinflammation and NFkappaB-dependent CCL2 expression in reactive astrocytes. Proceedings of the National Academy of Sciences of the United States of America. 2010;107:8416-8421.

Gonzalez-Cabrera PJ, Cahalan SM, Nguyen N, Sarkisyan G, Leaf NB, Cameron MD, et al. S1P(1) receptor modulation with cyclical recovery from lymphopenia ameliorates mouse model of multiple sclerosis. Molecular Pharmacology. 2012;81:166-174.

Gu SM, Yun J, Son DJ, Kim HY, Nam KT, Kim HD, et al. Piperlongumine attenuates experimental autoimmune encephalomyelitis through inhibition of NF-kappaB activity. Free Radical Biology and Medicine. 2017;103:133-145.

Guo MF, Meng J, Li YH, Yu JZ, Liu CY, Feng L, et al. The inhibition of Rho kinase blocks cell migration and accumulation possibly by challenging inflammatory cytokines and chemokines on astrocytes. Journal of the Neurological Sciences. 2014;343:69-75.

Guo X, Nakamura K, Kohyama K, Harada C, Behanna HA, Watterson DM, et al. Inhibition of glial cell activation ameliorates the severity of experimental autoimmune encephalomyelitis. Neuroscience Research. 2007;59:457-466.

Ha D, Bing SJ, Ahn G, Kim J, Cho J, Kim A, et al. Blocking glutamate carboxypeptidase II inhibits glutamate excitotoxicity and regulates immune responses in experimental autoimmune encephalomyelitis. FEBS Journal. 2016;283:3438-3456.

Hammer LA, Zagon IS, McLaughlin PJ. Treatment of a relapse-remitting model of multiple sclerosis with opioid growth factor. Brain Research Bulletin. 2013;98:122-131.

Hammer LA, Zagon IS, McLaughlin PJ. Improved clinical behavior of established relapsing-remitting experimental autoimmune encephalomyelitis following treatment with endogenous opioids: implications for the treatment of multiple sclerosis. Brain Research Bulletin. 2015;112:42-51.

Hardin-Pouzet H, Krakowski M, Bourbonniere L, Didier-Bazes M, Tran E, Owens T. Glutamate metabolism is down-regulated in astrocytes during experimental allergic encephalomyelitis. Glia. 1997;20:79-85.

He Y, Du M, Gao Y, Liu H, Wang H, Wu X, et al. Astragaloside IV attenuates experimental autoimmune encephalomyelitis of mice by counteracting oxidative stress at multiple levels. PloS One. 2013;8:e76495.

Hoffmann FS, Hofereiter J, Rubsamen H, Melms J, Schwarz S, Faber H, et al. Fingolimod induces neuroprotective factors in human astrocytes. Journal of Neuroinflammation. 2015;12:184.

Hou Y, Ryu CH, Park KY, Kim SM, Jeong CH, Jeun SS. Effective combination of human bone marrow mesenchymal stem cells and minocycline in experimental autoimmune encephalomyelitis mice. Stem Cell Research and Therapy. 2013;4:77.

Huwiler A, Zangemeister-Wittke U. The sphingosine 1-phosphate receptor modulator fingolimod as a therapeutic agent: recent findings and new perspectives. Pharmacology and Therapeutics. 2018;185:34-49.

Irony-Tur-Sinai M, Vlodavsky I, Ben-Sasson SA, Pinto F, Sicsic C, Brenner T. A synthetic heparin-mimicking polyanionic compound inhibits central nervous system inflammation. Journal of the Neurological Sciences. 2003;206:49-57.

Itoh N, Itoh Y, Tassoni A, Ren E, Kaito M, Ohno A, et al. Cell-specific and region-specific transcriptomics in the multiple sclerosis model: Focus on astrocytes. Proceedings of the National Academy of Sciences of the United States of America. 2018;115:E302-E309.

Junqueira SC, Dos Santos Coelho I, Lieberknecht V, Cunha MP, Calixto JB, Rodrigues ALS, et al. Inosine, an endogenous purine nucleoside, suppresses immune responses and protects mice from

experimental autoimmune encephalomyelitis: a role for A2A adenosine receptor. Molecular Neurobiology. 2017;54:3271-3285.

Kim RY, Hoffman AS, Itoh N, Ao Y, Spence R, Sofroniew MV, et al. Astrocyte CCL2 sustains immune cell infiltration in chronic experimental autoimmune encephalomyelitis. Journal of Neuroimmunology. 2014;274:53-61.

Kim S, Bielawski J, Yang H, Kong Y, Zhou B, Li J. Functional antagonism of sphingosine-1-phosphate receptor 1 prevents cuprizone-induced demyelination. Glia. 2018;66:654-669.

Kostic M, Zivkovic N, Stojanovic I. Multiple sclerosis and glutamate excitotoxicity. Reviews in the Neurosciences. 2013;24:71-88.

Kuo PC, Brown DA, Scofield BA, Paraiso HC, Wang PY, Yu IC, et al. Dithiolethione ACDT suppresses neuroinflammation and ameliorates disease severity in experimental autoimmune encephalomyelitis. Brain, Behavior, and Immunity. 2018;70:76-87.

Kwiatkowska-Patzer B, Baranowska B, Walski M, Lipkowski AW. Influence of spinal cord protein hydrolysate upon the blood brain barrier changes due to experimental allergic encephalomyelitis in Lewis rats. Ultrastructural study. Folia Neuropathologica. 2003;41:29-34.

Lavrnja I, Savic D, Bjelobaba I, Dacic S, Bozic I, Parabucki A, et al. The effect of ribavirin on reactive astrogliosis in experimental autoimmune encephalomyelitis. Journal of Pharmacological Sciences. 2012;119:221-232.

Lee DH, Rotger C, Appeldoorn CC, Reijerkerk A, Gladdines W, Gaillard PJ, et al. Glutathione PEGylated liposomal methylprednisolone (2B3-201) attenuates CNS inflammation and degeneration in murine myelin oligodendrocyte glycoprotein induced experimental autoimmune encephalomyelitis. Journal of Neuroimmunology. 2014;274:96-101.

Lee FHF, Zhang H, Jiang A, Zai CC, Liu F. Specific alterations in astrocyte properties via the GluA2-GAPDH complex associated with multiple sclerosis. Scientific Reports. 2018;8:12856.

Li QQ, Bever CT. Glatiramer acetate blocks interleukin-1-dependent nuclear factor-kappaB activation and RANTES expression in human U-251 MG astroglial cells. Brain Research: Molecular Brain Research. 2001;87:48-60.

Li QQ, Burt DR, Bever CT. Glatiramer acetate inhibition of tumor necrosis factor-alpha-induced RANTES expression and release from U-251 MG human astrocytic cells. Journal of Neurochemistry. 2001;77:1208-1217.

Li W, Maeda Y, Yuan RR, Elkabes S, Cook S, Dowling P. Beneficial effect of erythropoietin on experimental allergic encephalomyelitis. Annals of Neurology. 2004;56:767-777.

Liedtke W, Cannella B, Mazzaccaro RJ, Clements JM, Miller KM, Wucherpfennig KW, et al. Effective treatment of models of multiple sclerosis by matrix metalloproteinase inhibitors. Annals of Neurology. 1998;44:35-46.

Lin SX, Lisi L, Dello Russo C, Polak PE, Sharp A, Weinberg G, et al. The anti-inflammatory effects of dimethyl fumarate in astrocytes involve glutathione and haem oxygenase-1. ASN Neuro. 2011;3.

Linker RA, Lee DH, Ryan S, van Dam AM, Conrad R, Bista P, et al. Fumaric acid esters exert neuroprotective effects in neuroinflammation via activation of the Nrf2 antioxidant pathway. Brain. 2011;134:678-692.

Liu Y, Bando Y, Vargas-Lowy D, Elyaman W, Khoury SJ, Huang T, et al. CD200R1 agonist attenuates mechanisms of chronic disease in a murine model of multiple sclerosis. Journal of Neuroscience. 2010;30:2025-2038.

Lubina-Dabrowska N, Stepien A, Sulkowski G, Dabrowska-Bouta B, Langfort J, Chalimoniuk M. Effects of IFN-beta1a and IFN-beta1b treatment on the expression of cytokines, inducible NOS (NOS type II), and myelin proteins in animal model of multiple sclerosis. Archivum Immunologiae et Therapiae Experimentalis. 2017;65:325-338.

Luo F, Herrup K, Qi X, Yang Y. Inhibition of Drp1 hyper-activation is protective in animal models of experimental multiple sclerosis. Experimental Neurology. 2017;292:21-34.

Makar TK, Gerzanich V, Nimmagadda VK, Jain R, Lam K, Mubariz F, et al. Silencing of Abcc8 or inhibition of newly upregulated Sur1-Trpm4 reduce inflammation and disease progression in experimental autoimmune encephalomyelitis. Journal of Neuroinflammation. 2015;12:210.

Marques F, Mesquita SD, Sousa JC, Coppola G, Gao F, Geschwind DH, et al. Lipocalin 2 is present in the EAE brain and is modulated by natalizumab. Frontiers in Cellular Neuroscience. 2012;6:33.

Marques KB, Scorisa JM, Zanon R, Freria CM, Santos LM, Damasceno BP, et al. The immunomodulator glatiramer acetate influences spinal motoneuron plasticity during the course of multiple sclerosis in an animal model. Brazilian Journal of Medical and Biological Research. 2009;42:179-188.

Mastronardi FG, Min W, Wang H, Winer S, Dosch M, Boggs JM, et al. Attenuation of experimental autoimmune encephalomyelitis and nonimmune demyelination by IFN-beta plus vitamin B12: treatment to modify notch-1/sonic hedgehog balance. Journal of Immunology. 2004;172:6418-6426.

Medina-Fernandez FJ, Luque E, Aguilar-Luque M, Aguera E, Feijoo M, Garcia-Maceira FI, et al. Transcranial magnetic stimulation modifies astrocytosis, cell density and lipopolysaccharide levels in experimental autoimmune encephalomyelitis. Life Sciences. 2017;169:20-26.

Mei F, Guo S, He Y, Wang L, Wang H, Niu J, et al. Quetiapine, an atypical antipsychotic, is protective against autoimmune-mediated demyelination by inhibiting effector T cell proliferation. PloS One. 2012;7:e42746.

Merrill JE, Ignarro LJ, Sherman MP, Melinek J, Lane TE. Microglial cell cytotoxicity of oligodendrocytes is mediated through nitric oxide. Journal of Immunology. 1993;151:2132-2141.

Miljkovic D, Blazevski J, Petkovic F, Djedovic N, Momcilovic M, Stanisavljevic S, et al. A comparative analysis of multiple sclerosis-relevant anti-inflammatory properties of ethyl pyruvate and dimethyl fumarate. Journal of Immunology. 2015;194:2493-2503.

Miralles M, Eixarch H, Tejero M, Costa C, Hirota K, Castano AR, et al. Clinical and histopathological amelioration of experimental autoimmune encephalomyelitis by AAV vectors expressing a soluble interleukin-23 receptor. Neurotherapeutics. 2017;14:1095-1106.

Moore SM, Khalaj AJ, Kumar S, Winchester Z, Yoon J, Yoo T, et al. Multiple functional therapeutic effects of the estrogen receptor beta agonist indazole-Cl in a mouse model of multiple sclerosis. Proceedings of the National Academy of Sciences of the United States of America. 2014;111:18061-18066.

Moriguchi K, Miyamoto K, Fukumoto Y, Kusunoki S. 4-Aminopyridine ameliorates relapsing remitting experimental autoimmune encephalomyelitis in SJL/J mice. Journal of Neuroimmunology. 2018;323:131-135.

Mueller AM, Nassery A, Conlon H, Liu X, Jun E, Yoon BH, et al. Effects of intraventricular methotrexate administration on Cuprizone-induced demyelination in mice. Frontiers in Molecular Neuroscience. 2013;6:34.

Murphy P, Sharp A, Shin J, Gavrilyuk V, Dello Russo C, Weinberg G, et al. Suppressive effects of ansamycins on inducible nitric oxide synthase expression and the development of experimental autoimmune encephalomyelitis. Journal of Neuroscience Research. 2002;67:461-470.

Noseworthy JH, Lucchinetti C, Rodriguez M, Weinshenker BG. Multiple sclerosis. The New England Journal of Medicine. 2000;343:938-952.

Ogier C, Bernard A, Chollet AM, T LED, Hanessian S, Charton G, et al. Matrix metalloproteinase-2 (MMP-2) regulates astrocyte motility in connection with the actin cytoskeleton and integrins. Glia. 2006;54:272-284.

Ohgoh M, Hanada T, Smith T, Hashimoto T, Ueno M, Yamanishi Y, et al. Altered expression of glutamate transporters in experimental autoimmune encephalomyelitis. Journal of Neuroimmunology. 2002;125:170-178.

Pahan K, Sheikh FG, Namboodiri AM, Singh I. Lovastatin and phenylacetate inhibit the induction of nitric oxide synthase and cytokines in rat primary astrocytes, microglia, and macrophages. Journal of Clinical Investigation. 1997;100:2671-2679.

Pifarre P, Prado J, Baltrons MA, Giralt M, Gabarro P, Feinstein DL, et al. Sildenafil (Viagra) ameliorates clinical symptoms and neuropathology in a mouse model of multiple sclerosis. Acta Neuropathologica. 2011;121:499-508.

Polak PE, Dull RO, Kalinin S, Sharp AJ, Ripper R, Weinberg G, et al. Sevoflurane reduces clinical disease in a mouse model of multiple sclerosis. Journal of Neuroinflammation. 2012;9:272.

Rahn KA, McLaughlin PJ, Zagon IS. Prevention and diminished expression of experimental autoimmune encephalomyelitis by low dose naltrexone (LDN) or opioid growth factor (OGF) for an extended period: Therapeutic implications for multiple sclerosis. Brain Research. 2011;1381:243-253.

Ralay Ranaivo H, Craft JM, Hu W, Guo L, Wing LK, Van Eldik LJ, et al. Glia as a therapeutic target: selective suppression of human amyloid-beta-induced upregulation of brain proinflammatory cytokine production attenuates neurodegeneration. Journal of Neuroscience. 2006;26:662-670.

Ramos KM, Lewis MT, Morgan KN, Crysdale NY, Kroll JL, Taylor FR, et al. Spinal upregulation of glutamate transporter GLT-1 by ceftriaxone: therapeutic efficacy in a range of experimental nervous system disorders. Neuroscience. 2010;169:1888-1900.

Rosenberg GA. Matrix metalloproteinases biomarkers in multiple sclerosis. Lancet. 2005;365:1291-1293.

Rothhammer V, Kenison JE, Tjon E, Takenaka MC, de Lima KA, Borucki DM, et al. Sphingosine 1-phosphate receptor modulation suppresses pathogenic astrocyte activation and chronic progressive CNS inflammation. Proceedings of the National Academy of Sciences of the United States of America. 2017;114:2012-2017.

Rothstein JD, Patel S, Regan MR, Haenggeli C, Huang YH, Bergles DE, et al. Beta-lactam antibiotics offer neuroprotection by increasing glutamate transporter expression. Nature. 2005;433:73-77.

Saher G, Stumpf SK. Cholesterol in myelin biogenesis and hypomyelinating disorders. Biochimica et Biophysica Acta. 2015;1851:1083-1094.

Serizawa K, Tomizawa-Shinohara H, Magi M, Yogo K, Matsumoto Y. Anti-IL-6 receptor antibody improves pain symptoms in mice with experimental autoimmune encephalomyelitis. Journal of Neuroimmunology. 2018;319:71-79.

Simonini MV, Polak PE, Sharp A, McGuire S, Galea E, Feinstein DL. Increasing CNS noradrenaline reduces EAE severity. Journal of Neuroimmune Pharmacology. 2010;5:252-259.

Smith PA, Schmid C, Zurbruegg S, Jivkov M, Doelemeyer A, Theil D, et al. Fingolimod inhibits brain atrophy and promotes brain-derived neurotrophic factor in an animal model of multiple sclerosis. Journal of Neuroimmunology. 2018;318:103-113.

Spach KM, Pedersen LB, Nashold FE, Kayo T, Yandell BS, Prolla TA, et al. Gene expression analysis suggests that 1,25-dihydroxyvitamin D3 reverses experimental autoimmune encephalomyelitis by stimulating inflammatory cell apoptosis. Physiological Genomics. 2004;18:141-151.

Stanislaus R, Pahan K, Singh AK, Singh I. Amelioration of experimental allergic encephalomyelitis in Lewis rats by lovastatin. Neuroscience Letters. 1999;269:71-74.

Stojanovic IR, Kostic M, Ljubisavljevic S. The role of glutamate and its receptors in multiple sclerosis. Journal of Neural Transmission. 2014;121:945-955.

Thorne M, Moore CS, Robertson GS. Lack of TIMP-1 increases severity of experimental autoimmune encephalomyelitis: effects of darbepoetin alfa on TIMP-1 null and wild-type mice. Journal of Neuroimmunology. 2009;211:92-100.

Tian GX, Zhu XQ, Chen Y, Wu GC, Wang J. Huperzine A inhibits CCL2 production in experimental autoimmune encephalomyelitis mice and in cultured astrocyte. International Journal of Immunopathology and Pharmacology. 2013;26:757-764.

Tian KW, Zhang F, Jiang H, Wang B, Han S. Role of C16, angiopoietin-1 and regeneration gene protein 2 in attenuating inflammation in an experimental rat model of autoimmune encephalomyelitis. Journal of Anatomy. 2017;230:30-46.

Trubiani O, Giacoppo S, Ballerini P, Diomede F, Piattelli A, Bramanti P, et al. Alternative source of stem cells derived from human periodontal ligament: a new treatment for experimental autoimmune encephalomyelitis. Stem Cell Research and Therapy. 2016;7:1.

Ure DR, Rodriguez M. Polyreactive antibodies to glatiramer acetate promote myelin repair in murine model of demyelinating disease. FASEB Journal. 2002;16:1260-1262.

Van Doorn R, Van Horssen J, Verzijl D, Witte M, Ronken E, Van Het Hof B, et al. Sphingosine 1-phosphate receptor 1 and 3 are upregulated in multiple sclerosis lesions. Glia. 2010;58:1465-1476.

Wang XS, Chen YY, Shang XF, Zhu ZG, Chen GQ, Han Z, et al. Idazoxan attenuates spinal cord injury by enhanced astrocytic activation and reduced microglial activation in rat experimental autoimmune encephalomyelitis. Brain Research. 2009;1253:198-209.

Wierinckx A, Breve J, Mercier D, Schultzberg M, Drukarch B, Van Dam AM. Detoxication enzyme inducers modify cytokine production in rat mixed glial cells. Journal of Neuroimmunology. 2005;166:132-143.

Wilms H, Sievers J, Rickert U, Rostami-Yazdi M, Mrowietz U, Lucius R. Dimethylfumarate inhibits microglial and astrocytic inflammation by suppressing the synthesis of nitric oxide, IL-1beta, TNF-alpha and IL-6 in an in-vitro model of brain inflammation. Journal of Neuroinflammation. 2010;7:30.

Yan Y, Ding X, Li K, Ciric B, Wu S, Xu H, et al. CNS-specific therapy for ongoing EAE by silencing IL-17 pathway in astrocytes. Molecular Therapy. 2012;20:1338-1348.

Yang Y, Tian SJ, Wu L, Huang DH, Wu WP. Fibrinogen depleting agent batroxobin has a beneficial effect on experimental autoimmune encephalomyelitis. Cellular and Molecular Neurobiology. 2011;31:437-448.

Yi W, Schluter D, Wang X. Astrocytes in multiple sclerosis and experimental autoimmune encephalomyelitis: Star-shaped cells illuminating the darkness of CNS autoimmunity. Brain, Behavior, and Immunity. 2019;80:10-24.

Yin LL, Lin LL, Zhang L, Li L. Epimedium flavonoids ameliorate experimental autoimmune encephalomyelitis in rats by modulating neuroinflammatory and neurotrophic responses. Neuropharmacology. 2012;63:851-862.

Zagon IS, Rahn KA, Bonneau RH, Turel AP, McLaughlin PJ. Opioid growth factor suppresses expression of experimental autoimmune encephalomyelitis. Brain Research. 2010;1310:154-161.

Zhang ML, Zhang XJ, Kang J, Zhang HJ, Chen XL, Liu N, et al. Matrine promotes NT3 expression in CNS cells in experimental autoimmune encephalomyelitis. Neuroscience Letters. 2017;649:100-106.

Ziemssen T, Schrempf W. Glatiramer acetate: mechanisms of action in multiple sclerosis. International Review of Neurobiology. 2007;79:537-570.